Does Night-time Chemistry of Isoprene Impact Urban Air Quality in Polluted Environments?

Alfred W. Mayhew

Doctor of Philosophy

University of York

Chemistry

March 2023

Abstract

Isoprene is a small organic compound that is predominantly emitted into the atmosphere by trees. It is the most emitted non-methane volatile organic hydrocarbon globally, meaning its chemistry is highly consequential for human health and climate around the world. Isoprene organonitrates are species which can be formed from the oxidation of isoprene by the hydroxyl (OH) or nitrate (NO_3) radicals, and are of interest due to their potential to impact the chemical cycles that form HO_x, NO_x, and O_3, as well as their ability to contribute to secondary organic aerosol (SOA). This thesis presents the results from a collection of modelling and experimental studies that investigate the oxidation of isoprene by NO_3 and the chemistry of isoprene organonitrates. This work identifies crucial differences between the formation of some groups of organonitrates in existing chemical mechanisms; explores the importance of response factors in the analysis of isoprene organonitrates by Iodide Chemical Ionisation Mass Spectrometry (I^--CIMS); investigates the impacts of changing NO_x and O_3 concentrations on the production of different organonitrates; highlights the importance of a small number of low-concentration high-volatility species for SOA formation; provides experimental evidence for the role of daytime NO_3 chemistry under polluted conditions; presents measurements of nitrated epoxides from the NO_3-initiated oxidation of isoprene; and describes measurements of several particle-phase isoprene oxidation products. These findings reveal the impact that isoprene nitrate chemistry can have on polluted environments, and provide direction for future investigations into isoprene chemistry and measurement of the resulting products.

Table of Contents

List of Figures

11

List of Tables

List of Abbreviations

AMS − aerosol mass spectrometer

APHH − Atmospheric Pollution and Human Health in a Chinese Megacity

BVOC − Biogenic volatile organic compound

C_{sat} − Saturation vapour concentration

DC-GC-FID − Dual-channel gas chromatography with flame ionization detection

EUPHORE − EUropean PHOtoREactor

FIGAERO − Filter inlet for gases and aerosols

FTIR − Fourier-transform infra-red

FZJ − Forschungszentrum Jülich

HESI − heated electrospray ionisation

HMML − Hydroxymethyl-methyl-α-lactone

HOM − Highly oxidised molecule

HO_x − Sum of OH and HO2

HPALD − Hydroperoxy aldehyde

I⁻-CIMS − Iodide chemical ionisation mass spectrometry

ICN − isoprene carbonyl nitrate

IDN − isoprene dinitrate

IDNE − isoprene dinitrooxy epoxide

IEPOX − Isoprene epoxydiol

IHN − isoprene hydroxy nitrate

INCE − isoprene nitrooxycarbonyl epoxide

INHE − isoprene nitrooxyhydroxy epoxide

INHL − Isoprenenitrooxy hydroxy-α-lactone

INO − isoprene alkoxy nitrate

INO$_2$ – isoprene peroxy nitrate

INPE – isoprene nitrooxyhydroperoxy epoxide

IPN – isoprene hydroperoxy nitrate

ISOPOOH – Isoprene hydroxyhydroperoxide

k$_{NO3}$ – NO3 reactivity

k$_{OH}$ – OH reactivity

LIF – Laser-induced fluorescence

MACR – Methacrolein

MCM – Master chemical mechanism

MVK – Methyl vinyl ketone

m/z – Mass-to-charge ratio

ncps – Normalised counts per second

NMVOC – Non-methane volatile organic compound

NO$_x$ – Sum of NO and NO2

NPF – New particle formation

OA – Organic aerosol

PM – Particulate matter

PTR-MS – Proton transfer reaction mass spectrometer

RH – Relative humidity

RO – Alkoxy radical

RO$_2$ – Peroxy radical

RONO$_2$ – Organonitrate

RT – Retention Time

sCI – stabilised Criegee intermediate

SIFT-MS – Selected ion flow mass spectrometry

SMPS – Scanning mobility particle sizer

SOA – Secondary organic aerosol

UHPLC-MS – Ultra-high-performance liquid chromatography mass-spectrometry

VOC – Volatile organic compound

$\Sigma C_4H_7NO_5$ – C4H7NO5 species derived from isoprene or other VOCs.

ΣICN – isoprene carbonyl nitrate and isomeric species (i.e. compounds with the formula C5H7NO4)

ΣIHN – isoprene hydroxy nitrate and isomeric species (i.e. compounds with the formula C5H9NO4)

ΣIPN – isoprene hydroperoxy nitrate and isomeric species (i.e. compounds with the formula C5H9NO5). Synonymous with ΣIPN+INHE.

ΣIPN+INHE – isoprene hydroperoxy nitrate, isoprene nitrooxyhydroxy epoxide, and isomeric species (i.e. compounds with the formula C5H9NO5). Synonymous with ΣIPN.

Acknowledgements

The work presented in this thesis would not have been possible without the help and support of a wide range of collaborators, friends, and family. Below I would like to give thanks to many of the people who have supported me over the past few years, though I am aware that there are countless other people that I am unable to name who have enabled me to reach this point.

Firstly, thanks to Jacqui Hamilton and Pete Edwards for supervising this project and offering advice and support throughout my undergraduate and postgraduate studies and enabling my development from a naïve student into a confidently naïve researcher. I'd also like to thank the entire staff at WACL who have provided help and expertise throughout my studies, particularly Mat Evans for his consistently helpful contributions in TAP meetings and Andrew Rickard for his sustained assistance with, and enthusiasm for, my work. I would also specifically like to thank my entire PhD cohort for their help and support as well as Killian Murphy, Daniel Bryant, Marvin Shaw, Mike Newland, Beth Nelson, Rhianna Evans, and Sari Budisulistiorini.

Next, I would like to thank all of my external collaborators from around the world for their contributions to the work presented in this thesis. I would particularly like to thank all of the staff at EUPHORE for their hard work that allowed the chamber experiments to go ahead, despite the difficulties of COVID travel restrictions. This effort from Amalia Muñoz, Rubén Soler, Teresa Vera, Milagros Ródenas, and Esther Borrás is greatly appreciated. My belated trip to Valencia is certainly a highlight of my PhD experience, along with hosting Rubén here in York, so I am immensely grateful.

I'd like to give thanks to all of those who have supported my education throughout the years that has led me to this point, including an army of teachers and lecturers who have fostered my curiosity and interest in science from an early age. A huge thanks to my friends and family, especially my Mum and Dad who have always been the best role models, encouraged me to follow my interests, and provided me with the perfect environment to learn and grow. Finally, a special thank you goes to Amelia who has loved and supported me as we have both gone through this journey together. We have shared so many good times over the past few years, in spite of the world ending around us, but I know that there are many more adventures to come.

Author's Declaration

I declare that this thesis is a presentation of original work and I am the sole author. This work has not previously been presented for a degree or other qualification at this University or elsewhere. All sources are acknowledged as references. Some of the presented work is reproduced from peer-reviewed publications in which I am the lead author. References for these works are presented below:

- Mayhew, A. W. *et al.* Evaluation of isoprene nitrate chemistry in detailed chemical mechanisms. Atmospheric Chemistry and Physics 22, 14783-14798 (2022). https://doi.org:10.5194/acp-22-14783-2022

- Mayhew, A. W. *et al.* Daytime Isoprene Nitrates Under Changing NO_x and O_3. Atmospheric Chemistry and Physics, 2023. *Under review.* https://doi.org/10.5194/egusphere-2023-226

Chapter 1

Introduction to the Atmospheric Chemistry of Isoprene

1.1 Isoprene in the Atmosphere

Isoprene is a small organic compound with the molecular formula C_5H_8, illustrated in Figure 1.1. The primary sources of isoprene to the atmosphere are plants, hence isoprene is referred to as a Biogenic Volatile Organic Compound (BVOC).[1] Isoprene is the most emitted non-methane volatile organic compound (NMVOC) globally, and accounts for around 70% of global BVOC emissions.[2-5] The high emissions of isoprene into the atmosphere mean that it can have large impacts on global atmospheric chemistry, even as the result of processes that only affect a small proportion of the total isoprene.

Though there is some debate as to the function of isoprene within plants, it is thought to assist in the organisms' tolerance against environmental stresses such as high temperatures, and exposure to O_3 and other reactive oxygen species.[6-8] Isoprene emissions have been observed to increase during heatwave events that lead to moderate drought.[9]
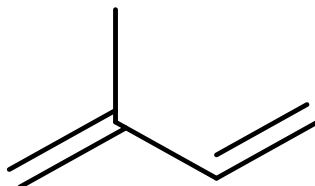
Figure 1.1. Chemical structure of isoprene.

The emission of isoprene by plants means that isoprene concentrations are generally highest closest to the ground, due to its emission from ground-based sources and its relatively high reactivity.[10,11] This profile may be modulated during the night as isoprene emissions are minimal and stratification of the atmosphere can form a poorly mixed residual layer in which isoprene will react throughout the night.[12]

Isoprene emissions by plants are also strongly dependent on solar irradiation and temperature, meaning that isoprene concentrations in the atmosphere generally peak at around mid-day and are usually lower during the night.[13,14] However, this diurnal concentration profile can be modified by meteorological effects such as wind speed. For example, a measurement campaign in the United States regularly detected peaks of isoprene at around 21:00 local time, resulting from low wind speeds producing an accumulation of isoprene below the forest canopy.[15] Additionally, since vegetative emissions of isoprene are lower in non-summer months, the concentration diurnal may be much flatter and night-time concentrations may be marginally higher,[16,17] as was shown in long-term measurements from a site in Beijing.[18]

In some locations, vehicle exhaust can act as an anthropogenic source of isoprene, though this is only significant in highly polluted environments.[19-24] Kashyap *et al.* estimated that between 19.90%

and 60.97% of isoprene at traffic sites in Delhi came from anthropogenic sources.[25] Wang *et al.*[16] presented measurements from traffic and background urban sites in Taipei and showed that while the roadside isoprene was dominated by anthropogenic emissions, biogenic emissions accounted for 97% of summer day-time isoprene at the urban site. The fraction of anthropogenic isoprene at urban sites normally increases at night and in autumn time, when biogenic concentrations decrease.[23] Humans have also been shown to directly emit low concentrations of isoprene in exhaled breath, leading Wagner *et al.* to propose large crowds in the city of Essen, Germany, as the cause of elevated winter-time isoprene concentrations.[24]

Although isoprene concentrations are generally highest during the day, the night-time oxidation of isoprene has been shown to be important in a range of environments.[12] For example, a box model based on observations made in Crete, Greece estimated that isoprene supressed night-time NO_3 by 25% in midsummer as well as similar magnitude impacts on OH, HO_2, and RO_x.[26]

Once emitted into the atmosphere, isoprene will undergo oxidation, with a typical atmospheric lifetime on the order of hours.[27] This chapter aims to outline the fundamental aspects of VOC oxidation in the atmosphere and apply them to isoprene in order to demonstrate its widespread importance when studying atmospheric chemistry.

1.2 Isoprene Oxidation

The oxidation of isoprene generally proceeds via reaction with one of three common atmospheric oxidants: OH, O_3, or NO_3. Table 1.1 shows the calculated atmospheric lifetime of isoprene under typical atmospheric oxidant concentrations, and their corresponding contribution to the overall chemical loss of isoprene. These values serve as a guide as to the relative importance of each oxidant, but the oxidant concentrations can vary by orders of magnitude. The rest of this section describes the factors controlling the concentrations of each oxidant and the initial steps of their reactions with isoprene.

Table 1.1. Typical lifetimes and loss rates of isoprene due to reaction with OH, O_3, and NO_3. The values will vary depending on oxidant concentrations. Reaction rate constants are taken from the Master Chemical Mechanism (MCM v3.3.1) [28] and typical oxidant concentrations are used of: day-time OH = 1.5×10^6 molecules cm^{-3}; night-time OH = 2×10^5 molecules cm^{-3}; day-time and night-time O_3 = 20 ppb; day-time NO_3 = 0.1 ppt; and night-time NO_3 = 1 ppt.[29-31]

Oxidant	Day-time		Night-time	
	Lifetime (hours)	Fractional Loss Rate (%)	Lifetime (hours)	Fractional Loss Rate (%)
OH	1.85	94.9	13.9	46.1
O_3	44.3	3.97	44.3	14.4
NO_3	162	1.08	16.28	39.3
Total	1.76		6.41	

1.2.1 The OH Radical

Globally, the main source of OH in the atmosphere comes from the photolysis of O_3, producing an excited oxygen atom, $O(^1D)$. $O(^1D)$ can then react with water vapour present in the air to produce two OH radicals.[32] The photolysis of nitrous acid (HONO), formed in polluted environments from NO_2, can also represent a major source of OH.[33] For example, a modelling study of a location in rural China, influenced by nearby cities, showed that an average of 92% of OH was formed from HONO photolysis.[34] The oxidation of alkenes by O_3, which is discussed further in Section 1.2.3, can also act as a source of OH via the decomposition of Criegee intermediates.[35]

HO_x recycling reactions are also central to understanding OH concentrations in many regions. These are reactions initiated by the oxidation of a VOC by OH, where the downstream reactions result in the emission of OH or HO_2, thus regenerating the OH that first initiated the reaction cascade (Figure 1.2).[36-38] One well understood HO_x recycling pathway is the reaction of RO_2 with NO.[39] The key reaction in this process for the generation of HO_2 is the formation of an alkoxy radical (RO). RO can then decompose, assisted by H-abstraction by an oxygen molecule, to form HO_2. This is described further in Section 1.4, along with alternative fates of RO.
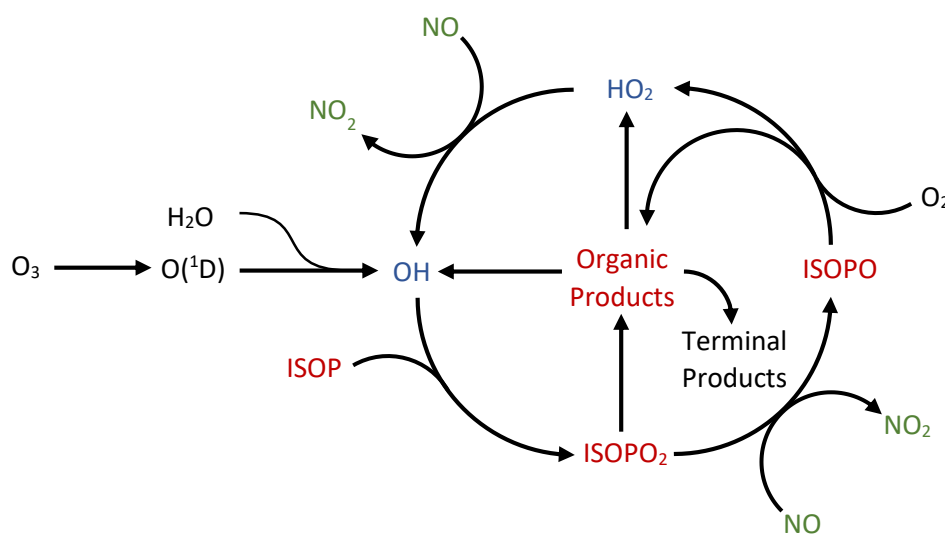
Figure 1.2. HO_x recyclying in the OH-intiated oxidation of isoprene. Additional products and reaction pathways have been omitted for clarity. Isoprene, isoprene peroxy radicals, and isoprene alkoxy radicals are denoted with ISOP, $ISOPO_2$, and ISOPO, respectively.

In less polluted environments, HO_x recycling reactions are less well understood and comprise of many different pathways. Peeters *et al.* first identified the formation of unsaturated hydroperoxy aldehydes (HPALDs) as an important pathway to reforming HO_2 from isoprene RO_2 in low-NO_x environments (Figure 1.3).[28,37,40] HPALDs can also photolyse to generate further HO_x. Recent work by Novelli *et al.* and Medieros *et al.* have identified additional isomerisation pathways of isoprene RO_2 that can reform HO_x.[38,41]
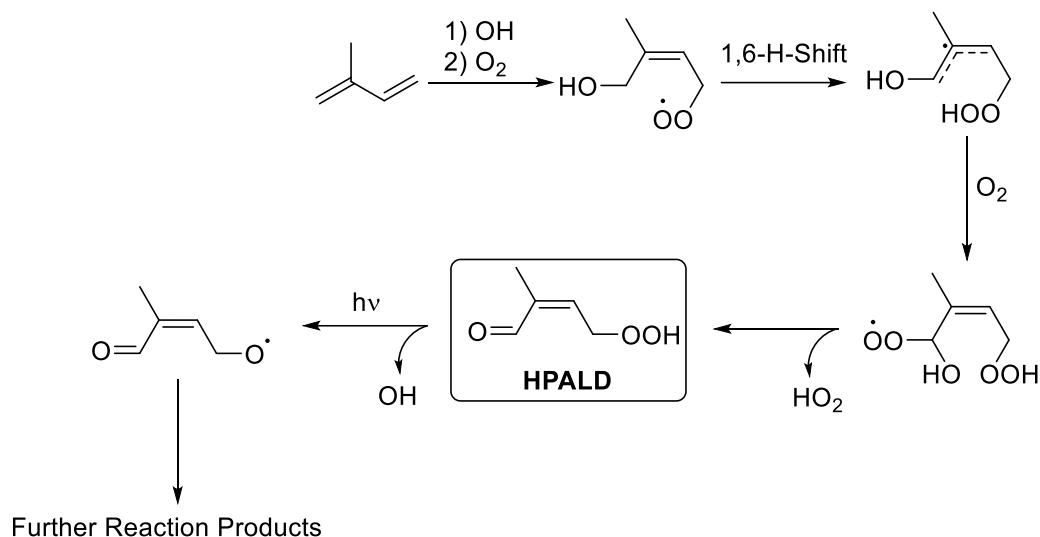
Figure 1.3. The formation of HPALDs from the OH oxidation of isoprene, an important HO$_x$ recycling pathway in low-NO environments. Additional products (including positional isomers) and reaction pathways have been omitted for clarity.
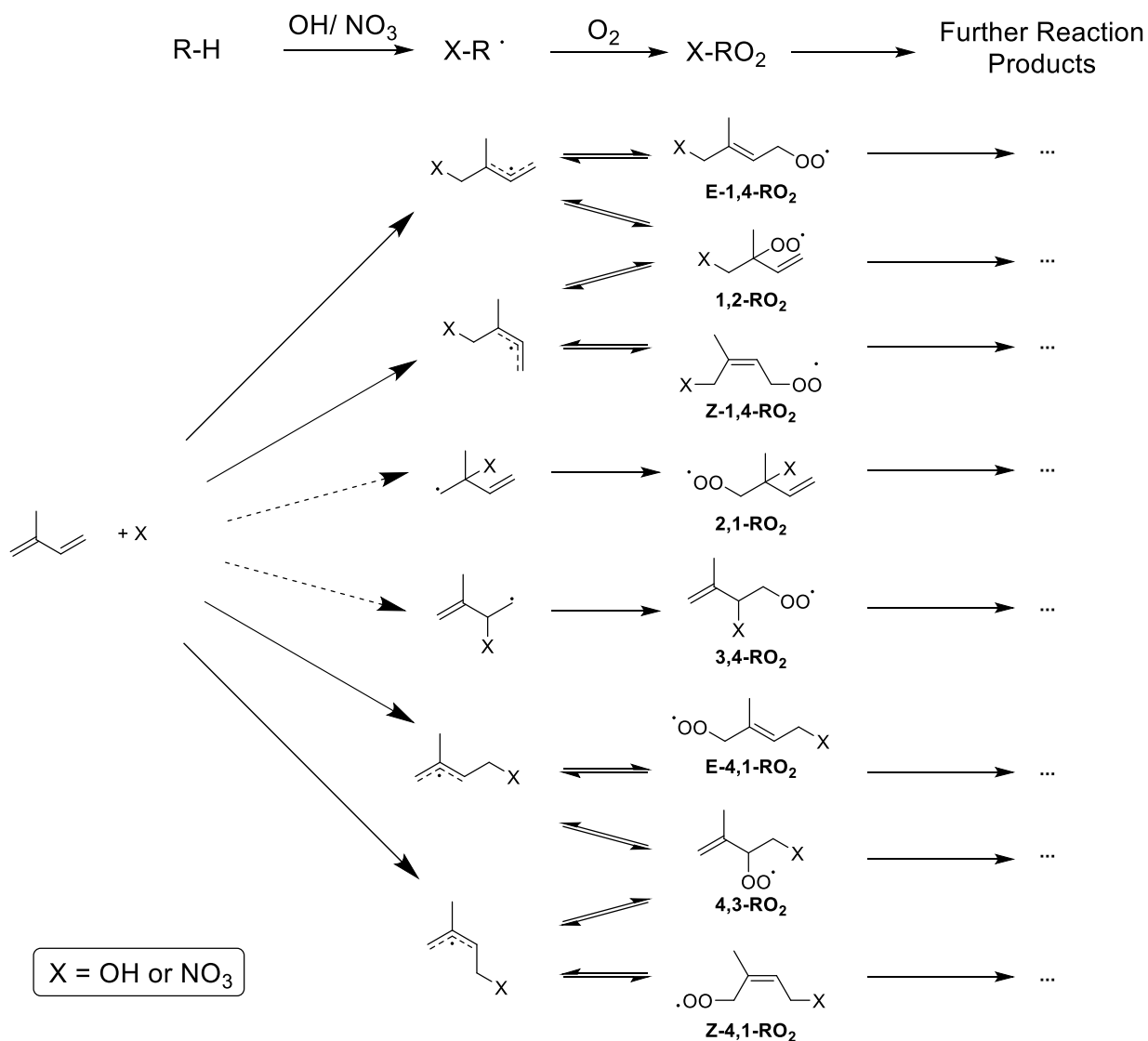
Figure 1.4. The initial stages of the addition of OH or NO$_3$ to isoprene, including all of the possible isomers formed. Reaction pathways with dashed arrows are considered to be minor.

Reaction with OH is usually the major loss route of isoprene in the atmosphere, due to the rapid reaction between the two species and the highest concentrations of OH and isoprene both occurring during the day-time. The reaction between isoprene and OH proceeds via the addition of OH to one of the two carbon-carbon double bonds present in isoprene. This forms an alkyl radical which will rapidly react with O_2 present in the atmosphere to form a peroxy radical (Figure 1.4).[42,43] The fate of this peroxy radical is then determined by the concentrations of other atmospheric species, as outlined in Section 1.3. The OH reaction could proceed via the abstraction of methyl hydrogens from isoprene, but this has been estimated to comprise less than 1% of total OH reactivity.[42,44]

1.2.2 The NO$_3$ Radical

The nitrate radical (NO_3) is generally considered to be a night-time oxidant due to its photolysis during the day-time and its rapid reaction with NO, which is produced by the photolysis of NO_2.[45] NO_3 is predominantly formed in the atmosphere by reaction of NO_2 and O_3, as shown in Figure 1.5. Figure 1.5 also shows the main loss routes of NO_3, which are reaction with NO, photolysis, and reaction with organics such as isoprene. Furthermore, NO_3 exists in rapid thermal equilibrium with N_2O_5 at typical tropospheric temperatures.[45]
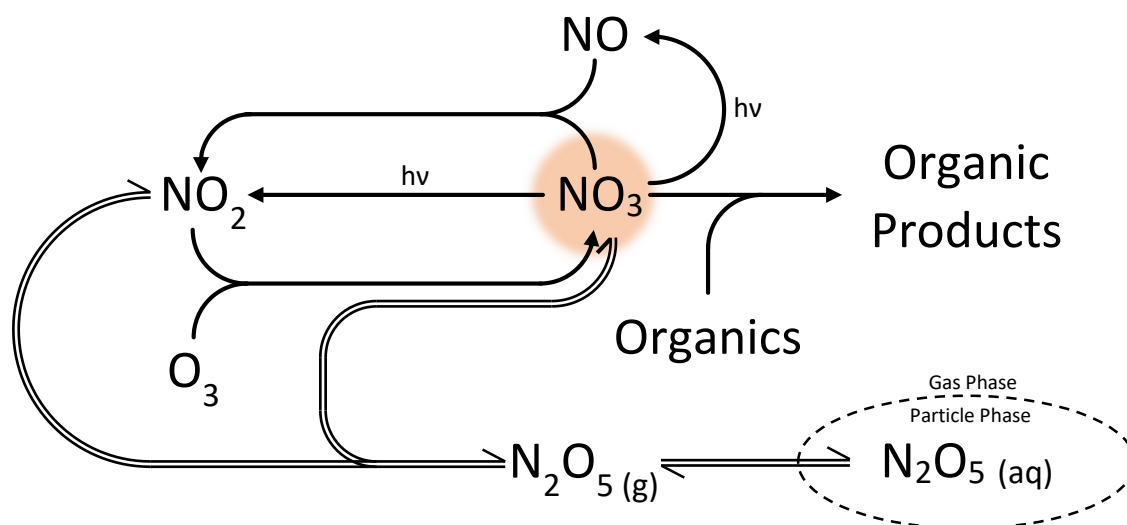
Figure 1.5. Formation and loss processes of the nitrate radical (NO_3).

Although typically considered to be negligible during the day-time, there is growing evidence that NO_3 can reach significant concentrations during the day-time under polluted conditions. This was first identified by Geyer *et al.* in 2003 who identified day-time NO_3 mixing ratios reaching 2-5ppt during the afternoon of a haze period in La Porte, Texas, and NO_3 oxidation was shown to be an important oxidant for VOCs such as terpenes.[46] When O_3 concentrations are high, as was observed by Geyer *et al.*, NO reacts with O_3, leading to reduced NO concentrations. High O_3 also promotes the formation of NO_3 through the $NO_2 + O_3$ pathway. This combination of reduced NO_3 loss and

increased NO_3 production is the cause of the elevated NO_3 concentrations. This phenomenon has also been observed and modelled in several locations in China.[47,48] Lower concentrations of day-time NO_3 and N_2O_5 have been measured and predicted in New England and London.[29,49-51] The role of this day-time NO_3 chemistry in the formation of organonitrates and atmospheric aerosol has become clearer in recent years.[51-53] Organonitrates are discussed further in Section 1.5 and their formation from day-time NO_3 chemistry is explored further in Chapter 3 and Chapter 4.

While high O_3 concentrations can supress the NO loss route of NO_3, other studies have revealed the importance of day-time NO_3 chemistry under forest canopies, where the photolytic loss of NO_3 is supressed.[54,55] An extreme case of this was found in measurements in France in 2017 where day-time NO_3 concentrations were calculated to be higher than at night-time.[56] This unusual finding was justified by reduced NO_3 photolysis during the day under the canopy, high monoterpene concentrations during the night increasing the NO_3 loss rate, and low night-time O_3 concentrations resulting in low NO_3 production rates.

Isoprene is reactive with respect to NO_3 with an IUPAC recommended rate constant of $k=6.5\times10^{-13}$ cm^3 molecule^{-1} s^{-1} at 298 K, giving a lifetime of ≈1.75hrs at 10ppt of NO_3.[57] The reaction of NO_3 with isoprene is analogous to OH oxidation, with the initial oxidation step involving the addition of NO_3 to one of isoprene's double bonds. The resultant allylic radical will rapidly react with O_2 in the air to form a peroxy radical (Figure 1.4).[42]

1.2.3 O_3

The two double bonds in isoprene are also susceptible to ozonolysis. The reaction of alkenes with ozone proceeds by the formation of Criegee Intermediates, which have been the focus of lots of study since their initial detection.[58-61] These intermediates form by the addition of O_3 across the double bond to form a primary ozonide which then dissociates to form a carbonyl and an excited-state zwitterionic Criegee intermediate (Figure 1.6). The excited-state intermediate can then undergo further unimolecular loss or collisional stabilisation to form a stabilised Criegee intermediate (sCI). This sCI has a sufficient lifetime to undergo bimolecular reactions with other atmospheric species such as NO_2, SO_2, and H_2O.

The products of isoprene ozonolysis often include compounds such as formaldehyde, methyl vinyl ketone (MVK), and methacrolein (MACR).[62] Isoprene ozonolysis has also been shown to contribute to secondary organic aerosol,[63,64] which is discussed further in Section 1.6.
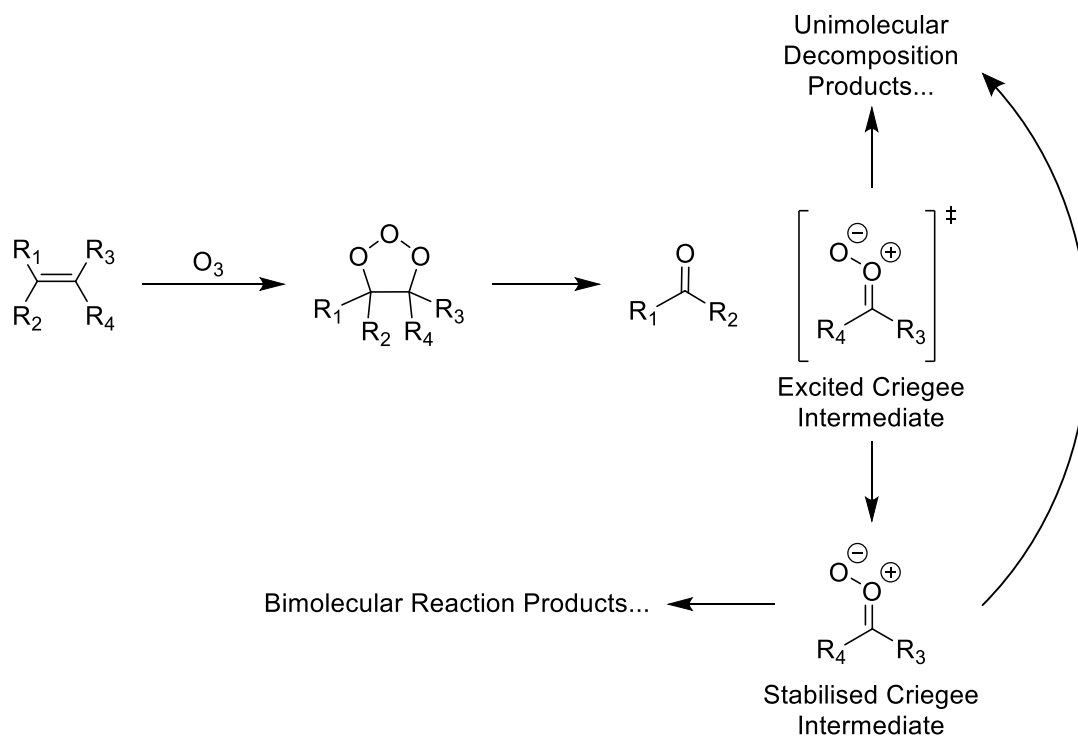
Figure 1.6. Formation and loss routes of Criegee Intermediates from the ozonolysis of an alkene.

1.3 The Fate of Isoprene Peroxy Radicals

Once formed, there are many different potential loss pathways for RO_2 (Figure 1.7). The rate of each of these loss reactions will determine the RO_2 fate, the fractional loss of RO_2 to each pathway. The RO_2 fate in an environment or set of chamber experiments can have large implications for the formation of pollutants such as SOA.[65,66]
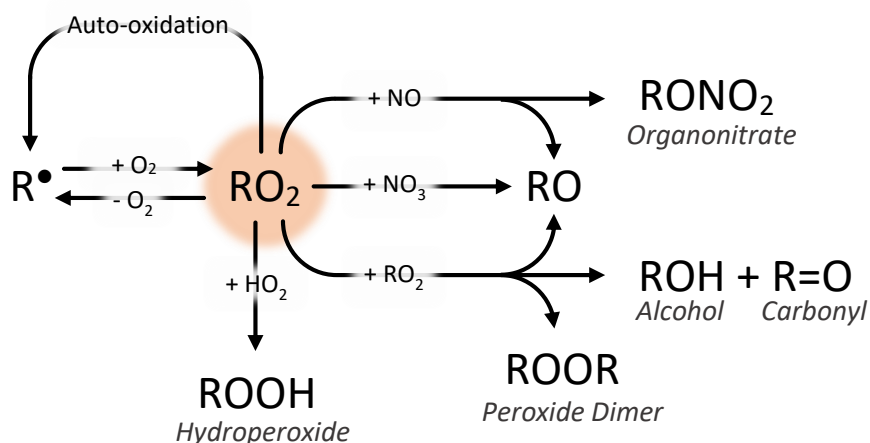
Figure 1.7. The loss pathways of a generic peroxy radical (RO_2).

1.3.1 Reversible O_2 Abstraction/Addition

One of the key considerations for RO_2 chemistry is the reversibility of O_2 addition to the isoprene allylic radical that forms the RO_2.[40,67] The ability to reform the allylic radical allows for the

interconversion between E and Z isomers of the 1,4- and 4,1- substituted RO_2, as well as the 3,4- or 1,2- substituted RO_2 (Figure 1.4). This is true for the oxidation of isoprene by both OH and NO_3.[42,68]

1.3.2 Reaction with NO

Under urban conditions, reaction with NO is often the predominant sink of RO_2, due to high NO_x concentrations resulting from anthropogenic emissions.[69] The reaction between RO_2 and NO can proceed via two pathways. The first is the formation of RO and NO_2 by the abstraction of an oxygen atom from RO_2, and the second is the formation of organonitrates ($RONO_2$) (Figure 1.7).[70]

While the structure of the RO_2 will influence the branching ratio between each of the possible NO reaction pathways, the formation of RO is usually the major route.[71-73] The fate of RO is discussed further in Section 1.4. Despite being a minor product in the RO_2+NO reaction, isoprene nitrates are the focus of a lot of research, including much of the work presented throughout this thesis, due to their potential to contribute to SOA (Section 1.6.1) as well as their potential to act as a sink or reservoir of NO_x (Section 1.5).

1.3.3 Reaction with HO_2

The reaction between RO_2 and HO_2 is often assumed to proceed via the formation of a hydroperoxide in a radical termination reaction (Figure 1.7). This has been shown to be true for alkyl RO_2, though other pathways become more important for substituted RO_2 such as acylperoxy radicals. [70,74] This includes the formation of alcohols and alkoxy radicals.

In the case of isoprene, hydroperoxides are of great interest as they are a major oxidation product in remote environments where NO concentrations are lower and the RO_2+NO reaction is less competitive.[75,76] Since forests are often remote, unpolluted environments and also large sources of isoprene, much of the global isoprene RO_2 will be processed through reaction with HO_2. Hydroperoxides often have low volatilities, making them important species in the understanding of SOA formation.[77] Furthermore, hydroperoxides represent the first identified precursor to forming isoprene epoxydiols (IEPOX), which are discussed in Section 1.6.2 as important SOA precursors.
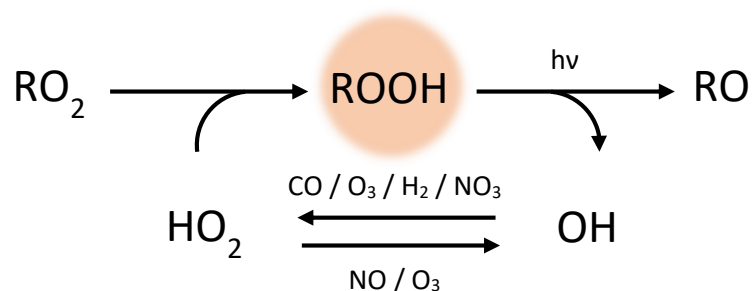
Figure 1.8. The role of hydroperoxides (ROOH) in HO_x cycles.

Hydroperoxides are also of interest due to their impacts on HO_x. The $RO_2 + HO_2$ reaction acts as a sink for HO_x, but the degradation reactions of hydroperoxides often release OH (Figure 1.8).[78,79] This means that transport of the relatively long-lived hydroperoxides can change the HO_x concentrations between regions.[80]

1.3.4 Reaction with NO_3

The reaction between RO_2 and NO_3 proceeds via the abstraction of an oxygen atom from RO_2 to form RO, NO_2, and O_2 (Figure 1.7).[70,81] The fates of the resulting RO is discussed in Section 1.4.

Since NO_3 concentrations are generally higher during the night, this pathway is an important source of night-time HO_x as the RO produced can, in some cases, react with O_2 to form HO_2.[81]

1.3.5 Reaction with RO_2

$RO_2 + RO_2$ reactions, in which an RO_2 reacts with another identical RO_2 (self-reactions) or a different RO_2 (cross-reactions), are often termed permutation reactions. These reactions can proceed via two major pathways as well as a dimerization route (Figure 1.7).[70,82-84]

The first major RO_2 permutation reaction for smaller compounds is the formation of an RO radical from each of the RO_2. The chemistry of RO is described further in Section 1.4. The second pathway involves the formation of an alcohol and carbonyl from each of the RO_2 molecules. In the case of cross-reactions, this could form two different combinations of alcohols and carbonyls. The chemistry of carbonyls is described further in Section 1.4.1. Alcohols are susceptible to removal from the atmosphere via wet and dry deposition, as well as uptake to atmospheric aerosol, as the oxygenation of VOCs generally reduces their volatility provided no fragmentation occurs.[85]

The final pathway for $RO_2 + RO_2$ reactions is the formation of peroxide dimers via peroxy radical (RO_2) cross-reactions. This route is being revealed as increasingly important, particularly for larger compounds.[82-84] Recent work has also indicated that this RO_2 dimerisation reaction may also be an important pathway for small RO_2 by showing a branching ratio for the RO_2 dimerisation reaction of 23% for ethene-derived RO_2.[86] These cross reactions could be an important pathway for the formation of SOA due to the ability to rapidly form large, low-volatility compounds.

1.3.6 Unimolecular Reactions

Recent years have seen increasing evidence of the importance of the unimolecular reactions of RO_2, also known as auto-oxidation reactions (Figure 1.7). These may involve ring closure reactions where the RO_2 reacts with an unsaturated position in the same molecule, or H-shift reactions which involve the abstraction of a hydrogen atom from elsewhere in the molecule to form a hydroperoxide group.

H-shift reactions have been shown to be important in the chemistry of isoprene. One case of this is in the formation of HPALDs discussed in Section 1.2.1. Another example that has recently received

a lot of attention as an important route to SOA formation is the production of highly oxygenated molecules (HOMs).[87,88] HOMs form from the successive addition of O_2 to compounds facilitated by intermediate RO_2 H-shifts to form an alkyl hydroperoxide which can react with O_2 to form a new RO_2 (Figure 1.9).[89] This allows the rapid formation of low volatility compounds which can partition into the particle phase and contribute to SOA.[88] The vast array of potential H-shift reactions, including the possible isomers of each species, makes the mechanistic analysis of HOMs, and their inclusion in chemical models, difficult.

HOM formation from isoprene has been observed in chamber experiments involving both OH- and NO_3-initiated oxidation.[90,91] Measurements of HOMs in Beijing identified many 5- and 10-carbon species that were attributed to isoprene oxidation, as well as other terpenoids.[92] Further measurements of HOMs have been made in the South-eastern United States, which is heavily impacted by BVOCs.[93]

Figure 1.9 also shows one potential RO_2 cyclisation reaction in the isoprene oxidation scheme. A similar cyclisation pathway has been predicted based on quantum chemical calculations investigating the fate of allylic radicals from isoprene.[94]
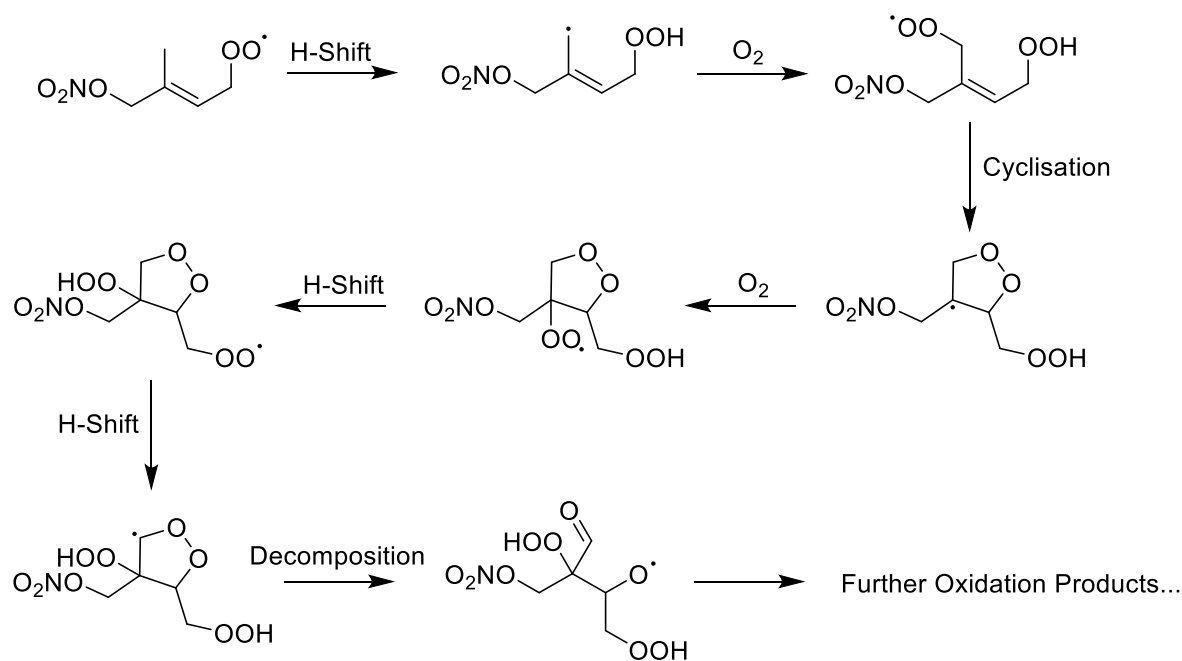
Figure 1.9. An example of a set of unimolecular reactions of organic radicals from isoprene that can form highly oxidised molecules (HOMs). This figure is adapted from chemistry proposed by Zhao et al. 2021.[90]

1.4 The Fate of Alkoxy Radicals

1.4.1 Carbonyl Formation

On formation of RO, O_2 can abstract a hydrogen atom from the carbon atom bound to the radical oxygen. This produces HO_2 and the alkoxy group is converted to a carbonyl, either a ketone or an aldehyde depending on the position of the carbon atom within the molecule (Figure 1.10). The rate

of this H-abstraction reaction is only weakly dependent of the structure of RO, at around $3\text{-}8\times10^4$ s^{-1} for all RO.[95]

As with alcohols (Section 1.3.5), the carbonyls produced from oxidation of hydrocarbons such as isoprene may have lower volatilities than the parent hydrocarbon. For example, MVK and MACR both have lower vapour pressures than isoprene, which is important for the atmospheric fate of these VOCs.[96] Furthermore, aldehydes and ketones can undergo photolysis in the troposphere to form radical species that contribute to further atmospheric chemistry.[97,98]
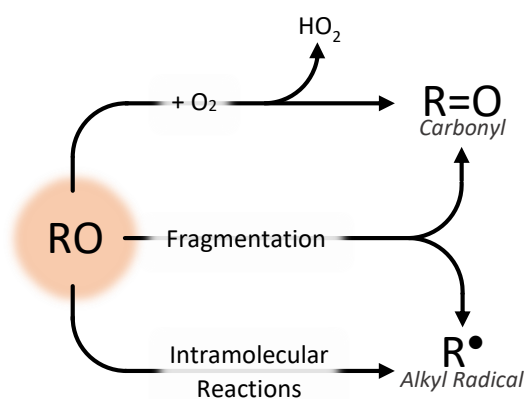
Figure 1.10. The loss pathways of a generic alkoxy radical (RO).

1.4.2 Fragmentation

Unimolecular decomposition is also a common loss pathway for RO (Figure 1.10). Here, a bond adjacent to the alkoxy radical C-O is broken to form one closed-shell species and another radical. The bond cleavage usually occurs across a C-C bond, meaning the products formed are a carbonyl (Section 1.4.1) and an alkyl radical.[95] As with the formation of alkyl radicals from the initial oxidation of isoprene (Section 1.2), the resultant alkyl radical will rapidly react with O_2 in the air to form RO_2.

In the case of substituted RO, with an alcohol or nitrate functionality on the α-carbon, the alkyl radical resulting from C-C bond cleavage will further fragment to form a second carbonyl species (Figure 1.11).[68] For hydroxy-substituted alkoxy radicals, O_2 can abstract the H from the OH group to form HO_2 and allow the formation of the carbonyl (Figure 1.11a). For nitrooxyalkoxy radicals, the breaking of the C-C bond can be accompanied by a breaking of the O-N bond in the nitrate group to form an NO_2 molecule alongside the second carbonyl (Figure 1.11b). These fragmentation pathways have implications for NO_x and HO_x budgets, as they provide mechanisms for reforming NO_x and HO_x that was originally consumed to form the organonitrate or alcohol functionalities.

(a)

(b)
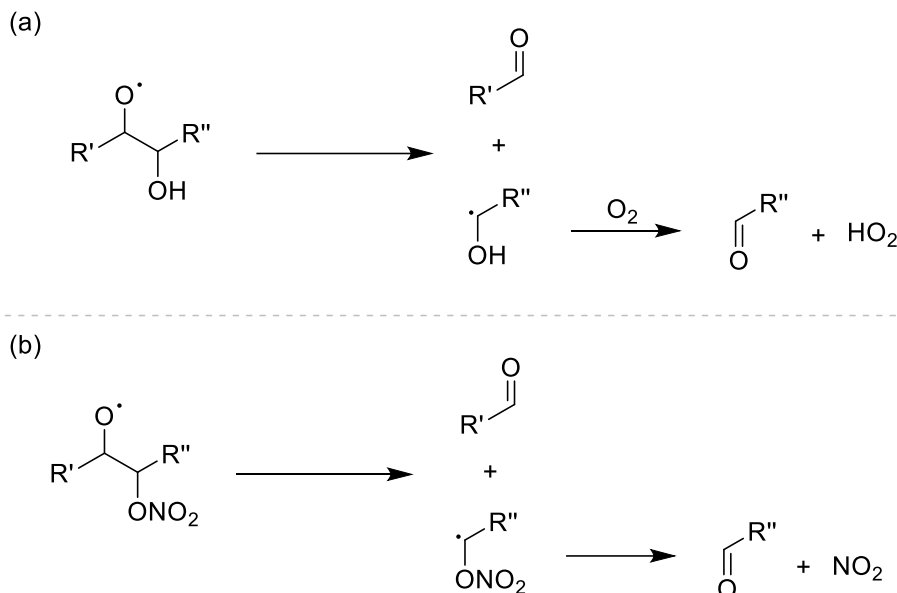
Figure 1.11. Fragmentation of α-substituted alkoxy radicals. (a) shows the decomposition of an α-hydroxy substituted alkoxy radical, (b) shows the decomposition of an α-nitrooxy substituted alkoxy radical.

1.4.3 Unimolecular Reactions

Isomerisation of RO can be another pathway which involves propagation of the radical reaction.[99,100] As with RO_2 (Section 1.3.6), H-shift reactions are a common isomerisation reaction for RO, with the resultant compound being a hydroxy alkyl radical (Figure 1.10).[91]

Cyclisation is also possible for some RO species, including those from isoprene. Importantly, the formation of epoxides from unsaturated alkoxy radicals has been demonstrated in a range of systems, including radicals produced from the oxidation of isoprene.[68,101] This epoxidation is a major finding from the work of Vereecken *et al.* 2021, where the NO_3-initiated oxidation of isoprene is predicted to produce a range of nitrated epoxide species.[68] This is discussed further in Section 1.6.3, and in each of the subsequent chapters.

1.5 Organonitrates

As discussed in the previous sections, there are two possible formation routes to organonitrates. The first is the addition of NO_3 to unsaturated hydrocarbons, and the second is via the RO_2 + NO reaction. In the case of isoprene, this results in the formation of four widely studied primary nitrates: isoprene hydroxy nitrate (IHN); isoprene carbonyl nitrate (ICN); isoprene hydroperoxy nitrate (IPN); and isoprene dinitrate (IDN). The formation routes to these primary nitrates are summarised in Figure 1.12.
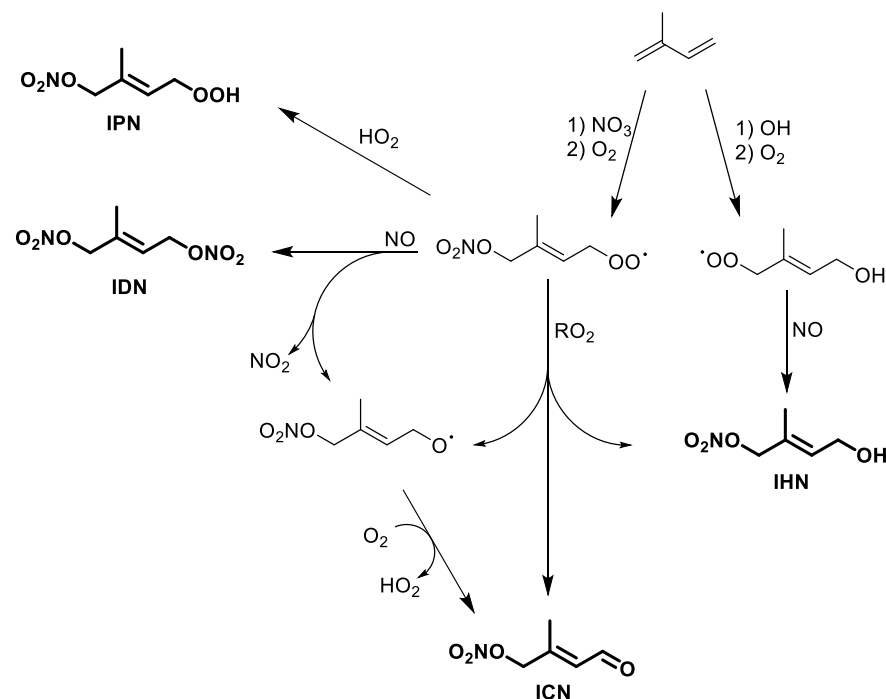
Figure 1.12. Formation pathways to the major primary isoprene nitrates, isoprene hydroperoxynitrate (IPN), isoprene dinitrate (IDN), isoprene carbonyl nitrate (ICN), and isoprene hydroxynitrate (IHN). Additional reaction pathways and products, including positional isomers, have been omitted for clarity.

The chemistry of organonitrates is important, in part, due to the potential impact on NO_x cycles. The formation of nitrates, either by NO_3 or NO, acts as a sink for NO_x. If these organonitrates are subsequently removed from the atmosphere via deposition processes, then NO_x concentrations will be decreased. Alternatively, many of the loss reactions of nitrates, such as photolysis, involve the liberation of NO_2.[27] This means that organonitrates can act as a reservoir species for NO_x, and their transport can change NO_x concentrations in locations far from the original site of formation.[102]

1.6 Secondary Organic Aerosol (SOA) Formation from Isoprene

Particulate matter (PM) in the atmosphere, also known as atmospheric aerosol, has implications for both human health and global climate. Exposure to PM has been linked to an increased risk of cardiovascular disease, decreased lung function, and premature death.[103] PM also impacts on climate through both direct and indirect effects.[104] PM is classed as either primary or secondary, depending on whether the aerosol is directly emitted into the atmosphere, or if it forms from the chemical reactions of precursor VOCs.[105]

Observational studies have established that organic aerosols (OA) comprise 20-90% of the submicron aerosol mass, with the majority of this organic fraction being comprised of secondary organic aerosol (SOA).[105-109] There are many varied SOA formation pathways, making this an important area of research for understanding PM formation in a range of environments. Furthermore, isoprene-derived compounds have been detected in diverse sets of ambient aerosol

measurements. This includes measurements collected in pristine forested environments such as the Amazon,[110-112] as well as in urban areas impacted by high isoprene concentrations.[113,114]

The main formation routes to SOA are gas-particle partitioning or the reactive uptake of gas phase species. Gas-particle partitioning involves the volatility-driven partitioning of compounds from the gas phase into existing particles.[115] The volatility of a compound is driven by the mass of the molecule as well as the functionalities present within the chemical structure. Reactive uptake involves the chemical reaction between gas-phase and particle-phase species, the products of which will contribute to the growth of the particle due to their lower volatility.[115]

1.6.1 Isoprene Nitrates

As discussed in Section 1.5, isoprene nitrates are important species for understanding NO_x budgets around the globe. However, isoprene nitrates are also of interest for particle-phase processes in urban environments due to their potential low volatility, and the potential low volatility of their oxidation products. For example, many organonitrate species, including some isoprene organonitrates, were detected in aerosol samples collected downwind of the Taichung metropolis, Taiwan.[116] Similarly, Xu *et al.* reported that nitrated compounds comprised 72% and 88% of isoprene-derived oxidised organic compounds measured in Shanghai and Nanjing, China, respectively.[113]

In a series of chamber experiments investigating the oxidation of isoprene in the presence of NO_x, Wu *et al.* showed that including seed-aerosol in their experiments resulted in a decrease in gas-phase concentrations of most of the isoprene organonitrates studied, demonstrating their ability to undergo uptake to the particle phase.[117] They also estimated the volatility of various isoprene organonitrates, which confirmed the general trend of decreasing volatilities with increasing molecular mass and functionalisation.

1.6.2 Isoprene Epoxydiols (IEPOX) SOA

IEPOX are an important group of compounds for the formation of SOA from isoprene. IEPOX was first identified as an intermediate in isoprene SOA formation through chamber experiments investigating the OH-initiated oxidation of isoprene which demonstrated the formation of IEPOX from ISOPOOH (Figure 1.13).[118] Later work identified the mechanism for reactive uptake of these epoxides to the particle phase as taking place via acid-catalysed ring-opening of the epoxide ring, followed by a nucleophilic addition reaction (Figure 1.13).[119] However, the tetrol products of this reactive uptake were identified in ambient aerosol samples collected in the Amazon before their formation mechanism was known.[120]

Since the discovery of IEPOX as a precursor to isoprene SOA, measurements of IEPOX and the expected products of reactive uptake have been made in a wide range of environments.[121] For

example, He *et al.* used measurements of IEPOX-uptake products compared to the uptake of another isoprene epoxide, hydroxymethyl-methyl-α-lactone (HMML), to investigate isoprene oxidation involving and excluding NO_x.[122]

1.6.3 Nitrated Epoxides

The role of IEPOX in isoprene SOA formation raises the potential for other epoxides resulting from isoprene oxidation to undergo reactive uptake. Isoprene nitrooxy hydroxyepoxide (INHE) was first identified as a product of the reaction between IPN and OH, and was shown to undergo reactive uptake in a similar fashion to IEPOX (Figure 1.13).[123] The dinitrated analogue, isoprene dinitrooxyepoxide (IDNE), has also been proposed to form from the oxidation of IPN by NO_3 (Figure 1.13).[51]
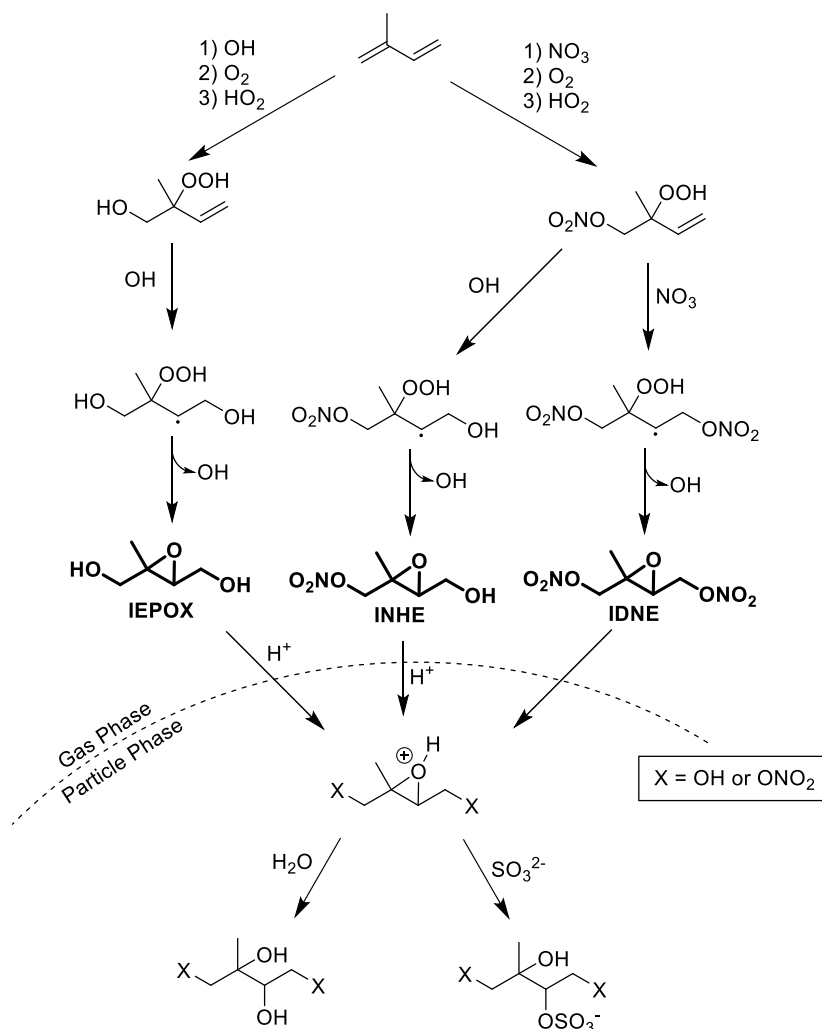
Figure 1.13. Formation routes of the epoxide species IEPOX, INHE, and IDNE and the reactive uptake of each to acidified particles. Additional reaction pathways and products, including positional isomers, have been omitted for clarity.

Recent theoretical calculations have identified unimolecular epoxidation reactions of nitrated alkoxy radicals to play a role in the NO_3-initiated oxidation of isoprene, as mentioned in Section

1.4.3.[68] This alkoxy-epoxidation pathway provides novel formation routes to a range of nitrated epoxides, including INCE, INPE, INHE and IDNE (Figure 1.14), and is described in more detail in Chapter 3. The additional epoxides have since been measured in one set of chamber experiments and in the chamber experiments outlined in Chapter 4.[124]
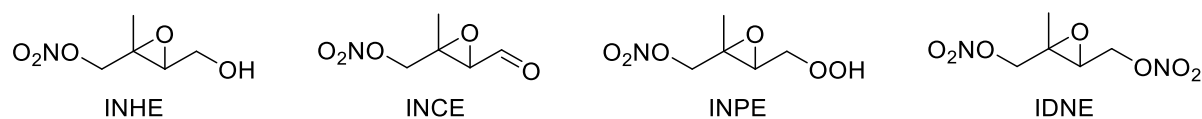
Figure 1.14. Four nitrated epoxides produced via the alkoxy-epoxidation reaction pathway.

1.7 Thesis Outline

Isoprene has been the focus of lots of research over the past decades, however its atmospheric importance and chemical complexity mean that there are still many aspects of isoprene chemistry that require further analysis. Recent years have shown a growing interest in the oxidation of isoprene by NO_3. While generally considered a minor reaction pathway, the potential impacts on SOA formation and NO_x budgets underscore its importance. Coupling this to the potential role of daytime NO_3 chemistry in the oxidation of isoprene presents a potential understudied route to form organonitrates from isoprene. Furthermore, research into the impact of isoprene organonitrates on SOA formation will help to elucidate the effect of isoprene on air quality in urban areas, which impacts the health of large populations.

This thesis presents investigations into our current understanding of the chemistry of isoprene under polluted urban conditions, and investigates the role of anthropogenic-biogenic interactions in the formation of atmospheric pollutants. Much of the analysis makes use of results from the 2017 Atmospheric Pollution and Human Health in a Chinese Megacity (APHH) summer campaign in Beijing,[125] as a case study of a polluted megacity, as well as making use of observations from a range of other measurement campaigns and data from a series of novel chamber experiments. While many of the results presented are applied to the conditions present in Beijing, similar chemistry is expected to be occurring in other polluted urban areas around the world.

Chapter 2 presents a comparison of three existing isoprene oxidation mechanisms in box-model simulations of the Beijing 2017 campaign. While there is widespread agreement between the models using different mechanisms for some organonitrate species, other species show large discrepancies. The impact of calibrations of mass spectrometers is also shown to be an important factor when analysing isoprene nitrates.

Chapter 3 describes a steady-state modelling approach to investigating the response of concentrations of various groups of isoprene organonitrates to changes in NO_x and O_3. This work demonstrates the importance of day-time NO_3 chemistry for the formation of several isoprene

nitrates in high-O_3 environments, as well as highlighting the difference in response to changes in NO_x and O_3 by different groups of isoprene organonitrates depending on their possible formation pathways.

Chapter 4 presents the results from a series of atmospheric simulation chamber experiments performed in the summer of 2021. These experiments aimed to reproduce many aspects of the chemistry discussed in previous chapters, and provides experimental evidence for many of their conclusions. The experiments had a strong focus on particle-phase processes and the analysis of several particle-phase isoprene tracers is presented.

Chapter 5 summarises the work from the previous three chapters, links the findings to make conclusions about the role of night-time chemistry in urban environments, and provides a discussion of the future topics of research in the field of isoprene atmospheric chemistry.

Chapter 2

Evaluation of Isoprene Nitrate Chemistry in Detailed Chemical Mechanisms

This work has been published in *Atmospheric Chemistry and Physics*.[126] My contribution to the work comprised of setting up and running the models, analysing the subsequent data, and writing the paper. Additional authors undertook the data collection during the APHH campaign, and/or provided supervision and guidance on the modelling approach and/or interpretation of the measured data.

2.1 Introduction
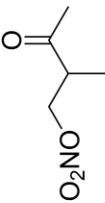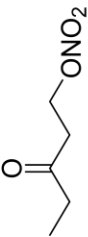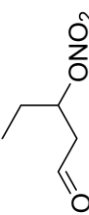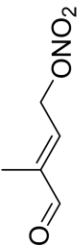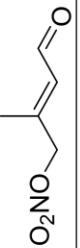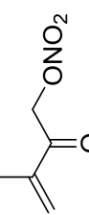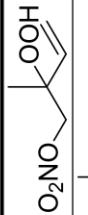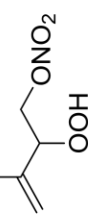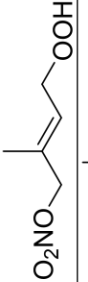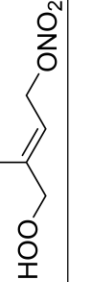
Isoprene (2-methyl-1,3-butadiene) is the most emitted non-methane volatile organic compound (NMVOC) globally, and accounts for around 70% of global biogenic volatile organic compound (BVOC) emissions.[2-5] Isoprene is a dialkene, and so is susceptible to oxidation in the atmosphere, initiated by the breaking of one, or both, of the double bonds.[42] Some of the products of these reactions are organonitrates which are formed either by the reaction of isoprene with hydroxyl radicals (OH) and subsequent reactions with O_2 and NO, or by the addition of the nitrate radical (NO_3) to one of isoprene's double bonds. The resulting nitrates are important for their influence on the NO_x, HO_x, and O_3 budgets, as well as the potential for the formation of secondary organic aerosol (SOA) by condensation or via further reactions.[127-132]
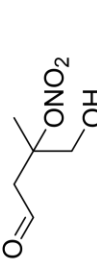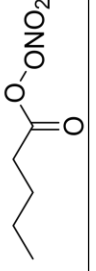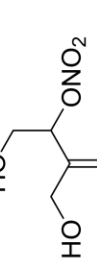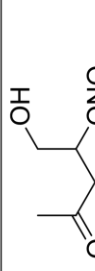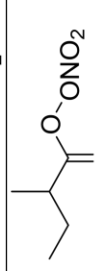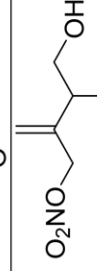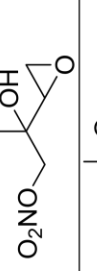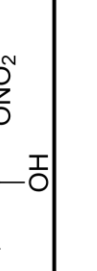
This work focusses on three types of primary nitrates resulting from isoprene oxidation, and one group of secondary nitrates. The primary C_5 nitrates are the isoprene hydroxynitrates (IHN, Figure 2.1), isoprene carbonyl nitrates (ICN, Figure 2.2), and isoprene hydroperoxynitrates (IPN, Figure 2.3). The molecular formulae of IHN, ICN, and IPN are $C_5H_9NO_4$, $C_5H_7NO_4$, and $C_5H_9NO_5$, respectively. Throughout this work an upper-case sigma is used to denote the group of nitrates as well as any other species present in a chemical mechanism with the same molecular formula. For example, ΣIHN will refer to all isoprene hydroxynitrates as well as any other $C_5H_9NO_4$ species present in each chemical mechanism. A glossary of the terms used to refer to different nitrated species is given in Table 2.1.
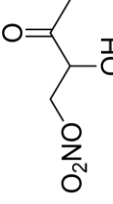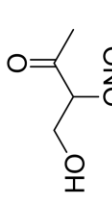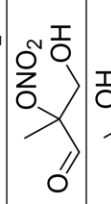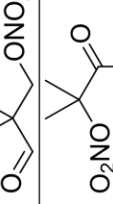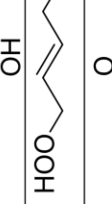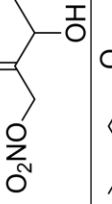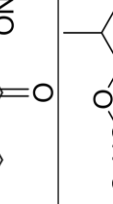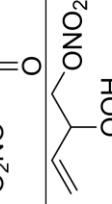
IHN may be formed by OH-initiated oxidation followed by a peroxy radical (RO_2) + NO reaction, or by NO_3-initiated oxidation followed by RO_2 cross-reactions to form the alcohol group (Figure 2.1). ICN is formed by NO_3-initiated oxidation followed by RO_2 cross-reactions, hydrogen abstraction from alkoxy radicals (RO) by oxygen (RO + O_2 → ICN + HO_2), or the reaction of IPN or isoprene dinitrates (IDN) with OH (Figure 2.2). IPN is formed by NO_3-initiated oxidation followed by RO_2 + HO_2 reactions (Figure 2.3).[28,42,68,133]

Table 2.1 Glossary of nitrate species and their names.

Species Group		Structure	Wennberg et al. 2018 Nomenclature	MCM Name	Caltech Mechanism Name	FZJ Mechanism Name
ΣIHN	IHN	O_2NO / OH (structure)	2,1-IHN	-	ISOP1N2OH	ISOP1N2OH
		HO / ONO_2 (structure)	1,2-IHN	ISOPBNO3	ISOP1OH2N	ISOP1OH2N
		OH / ONO_2 (structure)	3,4-IHN	ISOPDNO3	ISOP3N4OH	ISOP3N4OH
		ONO_2 / OH (structure)	4,3-IHN	ISOP34NO3	ISOP3OH4N	ISOP3OH4N
		O_2NO / OH (structure)	E-4,1-IHN	ISOPCNO3	ISOP1N4OHt	EISOP1N4OH
		HO / ONO_2 (structure)	E-1,4-IHN	ISOPANO3	ISOP1OH4Nt	EISOP1OH4N
		O_2NO / OH (structure)	Z-4,1-IHN	-	ISOP1N4OHc	ZISOP1N4OH
		HO / ONO_2 (structure)	Z-1,4-IHN	-	ISOP1OH4Nc	ZISOP1OH4N
		O / ONO_2 (structure)	-	MPRKNO3	MPRKNO3	MPRKNO3

Species Group	Structure	Wennberg et al. 2018 Nomenclature	MCM Name	Caltech Mechanism Name	FZJ Mechanism Name
		-	MIPKBNO3	MIPKBNO3	MIPKBNO3
		-	DIEKBNO3	DIEKBNO3	DIEKBNO3
		-	C4CHOBNO3	C4CHOBNO3	C4CHOBNO3
ΣICN		1,4-ICN	NC4CHO	ISOP1CO4N	ISOP1CO4N
		4,1-ICN	-	ISOP1N4CO	ISOP1N4CO
		3,4-ICN	-	ISOP3CO4N	ISOP3CO4N
ΣIPN / IPN		2,1-IPN	-	ISOP1N2OOH	ISOP1N2OOH
		3,4-IPN	-	ISOP3OOH4N	ISOP3OOH4N
		4,1-IPN	NISOPOOH	ISOP1N4OOH	ISOP1N4OOH
		1,4-IPN	-	ISOP1OOH4N	ISOP1OOH4N

Species Group	Structure	Wennberg et al. 2018 Nomenclature	MCM Name	Caltech Mechanism Name	FZJ Mechanism Name
		-	C530NO3	-	C530NO3
		-	PPEN	PPEN	PPEN
		-	C524NO3	-	C524NO3
		-	C51NO3	C51NO3	C51NO3
		-	C5PAN4	C5PAN4	C5PAN4
		-	-	ISOP1N25O3OH4OH	-
		-	-	ISOP1N23O4OH	ISOP1N23O4OH
		-	-	ISOP1N2OH34O	ISOP1N2OH34O
		-	-	ISOP1OH23O4N	ISOP1OH23O4N
		-	-	ISOP12O3OH4N	ISOP12O3OH4N

Species Group		Structure	Wennberg et al. 2018 Nomenclature	MCM Name	Caltech Mechanism Name	FZJ Mechanism Name
$\Sigma C_4H_7NO_5$	$C_4H_7NO_5$		-	HMVKANO3	MVK3OH4N	HMVKANO3
			-	MVKNO3	MVK3N4OH	MVKNO3
			-	MACRNO3	MACR2N3OH	MACRNO3
			-	MACRNB	MACR2OH3N	MACRNB
			-	MPRNO3CO2H	MPRNO3CO2H	MPRNO3CO2H
			-	NBUTDBOOH	NBUTDBOOH	NBUTDBOOH
			-	CO3C4NO3OH	CO3C4NO3OH	CO3C4NO3OH
			-	PBN	PBN	PBN
			-	PIPN	PIPN	PIPN
			-	NBUTDAOOH	NBUTDAOOH	NBUTDAOOH
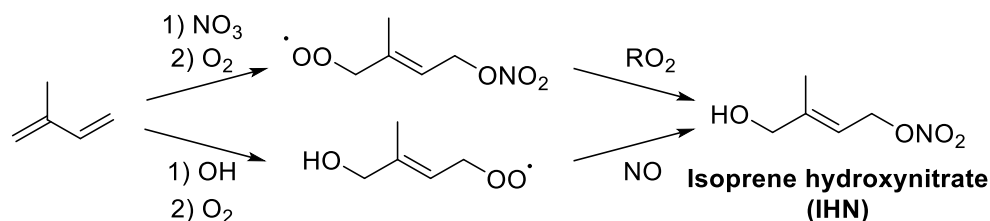
Figure 2.1. OH-initiated and NO₃-initiated formation of IHN. The formation of 1,4-IHN is shown here, other IHN isomers, as well as additional reaction products, will also be formed.
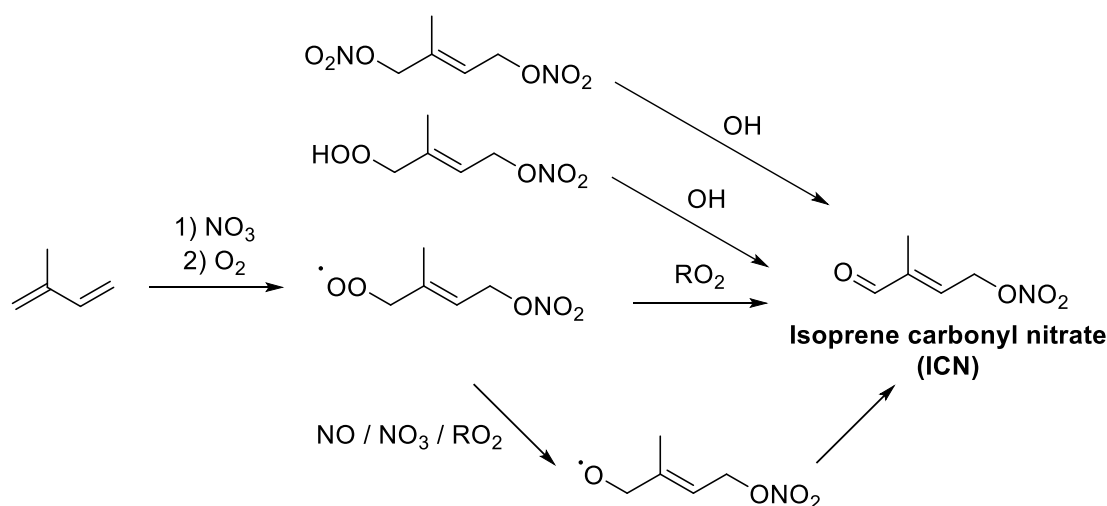
Figure 2.2. NO₃-initiated formation of ICN. The formation of 1,4-ICN is shown here, other ICN isomers, as well as additional reaction products, will also be formed.
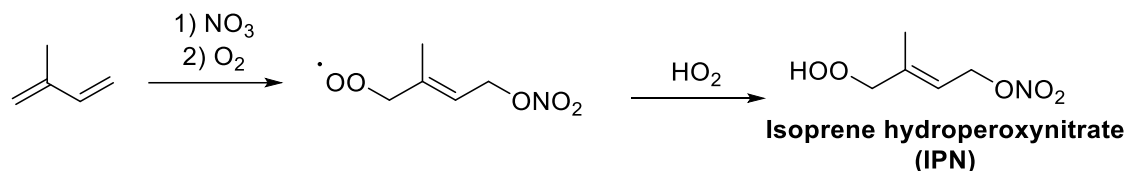
Figure 2.3. NO₃-initiated formation of IPN. The formation of 1,4-IPN is shown here, other IPN isomers, as well as additional reaction products, will also be formed.

The final group of nitrates are secondary nitrates with the formula $C_4H_7NO_5$, corresponding to the hydroxycarbonyl nitrate structures shown in Figure 2.4, which have been shown to be a major contributor to isoprene nitrates as measured by iodide chemical ionisation mass spectrometry (I⁻-CIMS).[134] $\Sigma C_4H_7NO_5$ refers to the isoprene-derived nitrates as well as isomeric species present in the Master Chemical Mechanism (MCM) from other VOC sources.[28] There are several identified formation routes of $C_4H_7NO_5$ including the OH-initiated oxidation of methyl vinyl ketone (MVK) and methacrolein (MACR); NO₃-initiated oxidation of MVK and MACR; OH-initiated oxidation of IHN, IPN, and ICN; the ozonolysis of IHN; and the NO₃-initiated oxidation of hydroxycarbonyls (Figure 2.5).[28,42,123,134,135] Analysis of these multifunctional compounds is further complicated due to their secondary nature, as well as their potentially long atmospheric lifetime.[136]
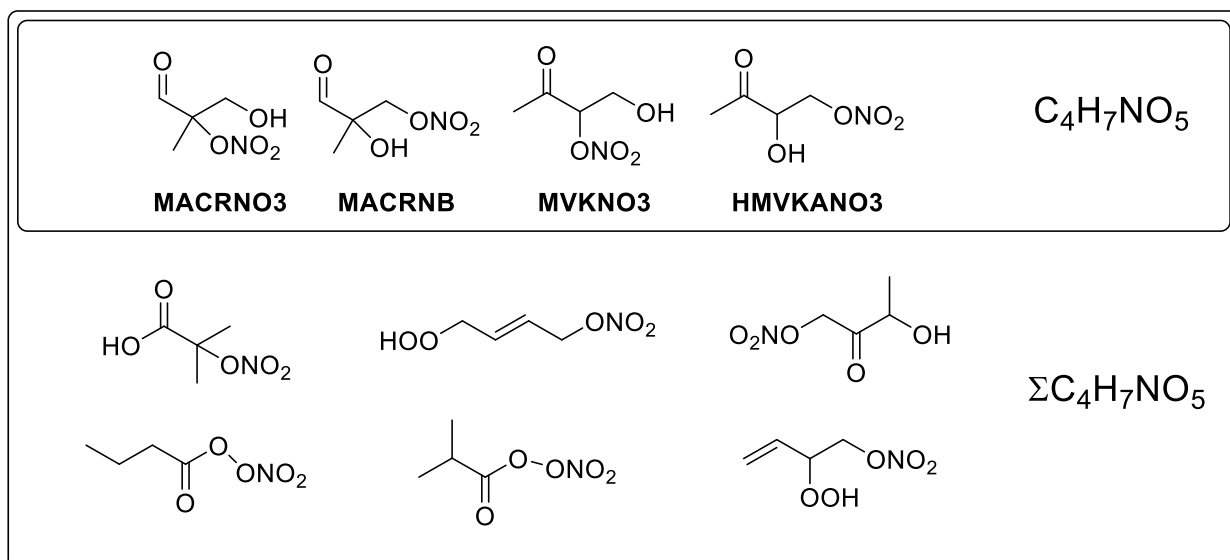
Figure 2.4. The four C₄H₇NO₅ species resulting from isoprene oxidation present in the MCM along with the additional isomeric compounds which complete the set of ΣC₄H₇NO₅
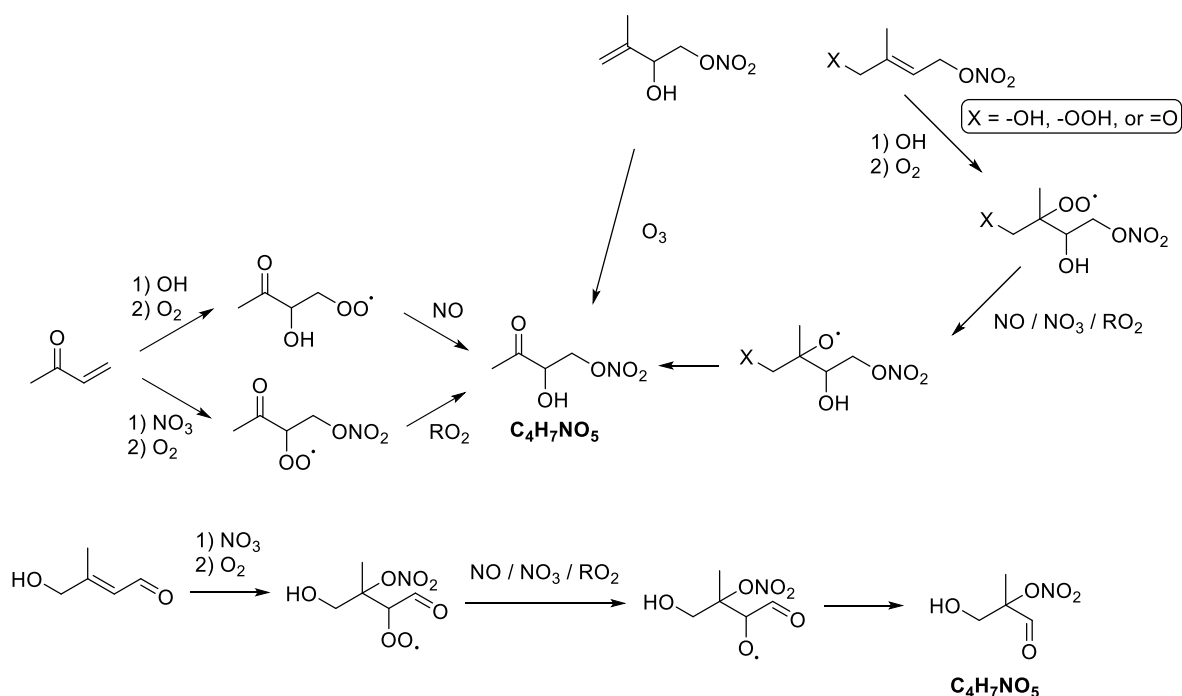
Figure 2.5. Formation of C₄H₇NO₅ compounds. Only two isomers are shown here, other formation routes for these and other isomers are also present. Additional reaction products will also be formed.

Isoprene nitrates are often identified as major products of isoprene oxidation. For example, studies performed in the Forschungszentrum Jülich SAPHIR chamber identified a large range of organonitrates resulting from the NO_3-initiated oxidation of isoprene, including the primary products mentioned here.[117,137] Chamber experiments performed at the California Institute of Technology have also highlighted the role of nitrates in the OH-initiated oxidation of isoprene.[129,131] Such nitrates have also been identified in a range of ambient environments, from rural environments such as those in the south eastern United States, to polluted urban environments such as the San Francisco Bay area.[138,139] Previous modelling studies that investigate isoprene nitrates under ambient conditions, and their impacts on atmospheric chemistry, are also

widespread across polluted and less polluted environments, examining both speciated nitrates and the sum of total organic nitrates.[130,140-144]

Isoprene nitrates have also been identified as significant species during the 2017 Atmospheric Pollution and Human Health in a Chinese Megacity (APHH) summer campaign in Beijing.[51,66] There have been two previous box-modelling investigations focussed on the data collected during the APHH-Beijing intensive field observations.[145,146] Whalley *et al.* focussed on radical chemistry and ozone formation, highlighting several inconsistencies between modelled radical species and relevant measurements. Reeves *et al.* investigated IHN and ICN speciation and demonstrated the value of speciated measurements of isoprene nitrates by identifying several instances where the modelled IHN isomer distribution was not consistent with their measured distribution. They also discussed issues around the simplified representations of ICN isomers with regards to the initial site of attack of NO_3 and the E/Z stereochemistry of 1,4-ICN and 4,1-ICN. This paper uses similar box-modelling approaches as the previously discussed studies to assess the capabilities of three detailed atmospheric oxidation mechanisms for investigating the formation and losses of isoprene derived nitrates in this anthropogenically and biogenically impacted environment. Key statistics for each mechanism are given in Table 2.2.

Table 2.2. Summary of the properties of each mechanism used in this work. Note that the statistics for the "Caltech Mechanism" and "FZJ Mechanism" apply to the mechanisms in the form used in this work, i.e. with the incorporated MCM subset for non-isoprene VOCs and with RO_2 reactions lumped as described in the main text for the Caltech Mechanism.

Property	MCM	Caltech Mechanism	FZJ Mechanism
Number of Reactions	10371	10435	11046
Number of Species	3443	3589	3730
Number of INO_2 Isomers	1	4	8
Number of IPN Isomers	1	4	4
Number of ΣIPN Isomers	6	11	13
Number of IHN Isomers	5	8	8
Number of ΣIHN Isomers	9	12	12
Number of ICN Isomers	1	3	3
Number of ΣICN Isomers	1	3	3
Number of $C_4H_7NO_5$ Isomers	4	4	4
Number of $ΣC_4H_7NO_5$ Isomers	10	10	10

The first mechanism used here is the Master Chemical Mechanism v3.3.1 (MCM).[28] The MCM is a benchmark near-explicit chemical mechanism extensively used by the atmospheric science community in a wide variety of science and policy applications where chemical detail is required. Subsets of the MCM can be directly extracted for a wide variety of VOCs (mcm.york.ac.uk). However, due to the breadth of the MCM, some simplifications have been made when constructing the mechanism. The first major simplification is the use of lumped RO_2 reactions. This means that RO_2-RO_2 cross-reactions are not treated explicitly, and it is assumed that each RO_2 will react with any other RO_2 at the same rate, which helps to greatly reduce the complexity of mechanisms.[97] In

the case of isoprene, further assumptions are made. For example, NO_3-initiated oxidation of isoprene in the MCM is represented by only one isomer (NISOPO2).

Secondly, the full v5 isoprene oxidation mechanism taken from the Wennberg *et al.* 2018 review of gas-phase isoprene oxidation (henceforth, the Caltech Mechanism) was used.[42] This mechanism treats isoprene RO_2 cross-reactions explicitly, unlike the lumped-RO_2 approach of the MCM. This leads to issues when integrating the Caltech Mechanism with the MCM subset for additional measured VOCs, as explained further in the methodology section. The Caltech Mechanism aims to provide a more up-to-date representation of reaction rates and products. For example, the Caltech Mechanism provides four different nitrated RO_2 radicals resulting from NO_3 oxidation. The Caltech Mechanism also introduces some reactions that are not found in the MCM, such as intramolecular RO_2 reactions.

Finally, the mechanism developed by Vereecken *et al.* and further expanded in Tsiligiannis *et al.* was used and is referred to as the FZJ Mechanism.[68,134] This mechanism aims to expand on the Caltech Mechanism, by providing more comprehensive NO_3 chemistry, including the proposed formation of epoxide species from some alkoxy radical species, and additional chemistry relevant to $C_4H_7NO_5$ outlined in Tsiligiannis *et al.*[134]

2.2 Methodology

2.2.1 Ambient Measurements

The Beijing measurements used in this work were collected at ground level at the Tower Section of the Institute of Atmospheric Physics (IAP) in Beijing, China, between 2017-06-01 and 2017-06-18.[125] The nitrates were measured using a Filter Inlet for Gases and Aerosols (FIGAERO) coupled to a time-of-flight iodide chemical ionisation mass spectrometer (I^--CIMS) which allows for the measurement of particle and gas-phase species, although only the gas-phase data are used here as the particle-phase data were unavailable.[147] Each nitrate was calibrated assuming the same sensitivity as trans-beta-IEPOX, though the potential role of calibration on the measured nitrate concentrations is discussed throughout this work.[51] Other organic compounds were measured by proton transfer mass spectrometry (PTR-MS), selected ion flow tube mass spectrometry (SIFT-MS), and dual-channel gas chromatography with flame ionization detection (DC-GC-FID).[125,145,148,149] The sum of monoterpenes measured by PTR-MS and SIFT-MS was used to constrain alpha-pinene and limonene in the models, assuming each compound comprised 50% of the total monoterpenes. Instruments used to measure organic species are summarised in Table 2.3 and the details of the instruments used to measure additional compounds can be found elsewhere.[51,125,146,150-152] Where species constraints were required in the modelling, and multiple measurements were taken, the mean of all of the measurements was used. The scanning mobility particle sizer (SMPS) instruments used to calculate particle surface area as outlined in Section 2.3.1 are described below.

Two scanning mobility particle sizer (SMPS) instruments measured particle size distributions at 15 min time resolution, with one long SMPS with an inlet flowrate of 0.3 L min-1 (TSI 3080 EC, 3082 long DMA, 3775 CPC, TSI, USA) and one nano SMPS with an inlet flowrate of 1.5 L min-1 (3082 EC, 3082 nano DMA, 3776 CPC, TSI, USA) measuring the ranges 14–615 and 4–65 nm respectively. A particle size magnifier (A10, Airmodus, FN) linked to a CPC (3775, TSI, USA) measured the sub-3 nm size fraction with an inlet flowrate of 2.5 L min-1. The PSM was run in stepping mode, operating at four different saturator flows to vary the lowest size cut-off of particles that it will grow (this cut-off is technically a point of 50 % detection efficiency) of < 1.30, 1.36, 1.67, and 2.01 nm. The instrument switched between saturator flows per 2.5 min, giving a sub2.01 nm size distribution every 10 min. The data were treated with a moving-average filter to account for jumps in total particle count, and due to the similar behaviour of the two upper and two lower size cuts, these have been averaged to two size cuts at 1.30 and 1.84 nm. No drying was performed on the inlet air.

Table 2.3. List of VOCs (and their names in the MCM) constrained to measured concentrations in the models. The "Measurement(s) Used" column indicates which instrument's measurements were used to constrain each species in model runs: proton transfer mass spectrometry (PTR), selected ion flow tube mass spectrometry (SIFT), and dual-channel gas chromatography with flame ionization detection (DC-GC).

Compound	MCM Name	Measurement(s) Used	Compound	MCM Name	Measurement(s) Used
isoprene	C5H8	DC-GC, SIFT, PTR	ethane	C2H6	DC-GC
monoterpenes	APINENE, LIMONENE	SIFT, PTR	propane	C3H8	DC-GC, SIFT
ethene	C2H4	DC-GC, SIFT	n-butane	NC4H10	DC-GC
propene	C3H6	DC-GC, SIFT,	i-butane	IC4H10	DC-GC
trans-2-butene	TBUT2ENE	DC-GC	n-pentane	NC5H12	DC-GC
1-butene	BUT1ENE	DC-GC	i-pentane	IC5H12	DC-GC
i-butene	MEPROPENE	DC-GC	n-hexane	NC6H14	DC-GC
cis-2-butene	CBUT2ENE	DC-GC	n-heptane	NC7H16	DC-GC
trans-2-pentene	TPENT2ENE	DC-GC	n-octane	NC8H18	DC-GC
cis-2-pentene	CPENT2ENE	DC-GC	benzene	BENZENE	DC-GC, SIFT, PTR
1,3-butadiene	C4H6	DC-GC, SIFT	ethylbenzene	EBENZ	DC-GC, SIFT, PTR
acetylene	C2H2	DC-GC, SIFT	propylbenzene	PBENZ	SIFT, PTR
methanol	CH3OH	DC-GC, SIFT	toluene	TOLUENE	DC-GC, SIFT, PTR
ethanol	C2H5OH	DC-GC, SIFT	o-xylene	OXYL	DC-GC
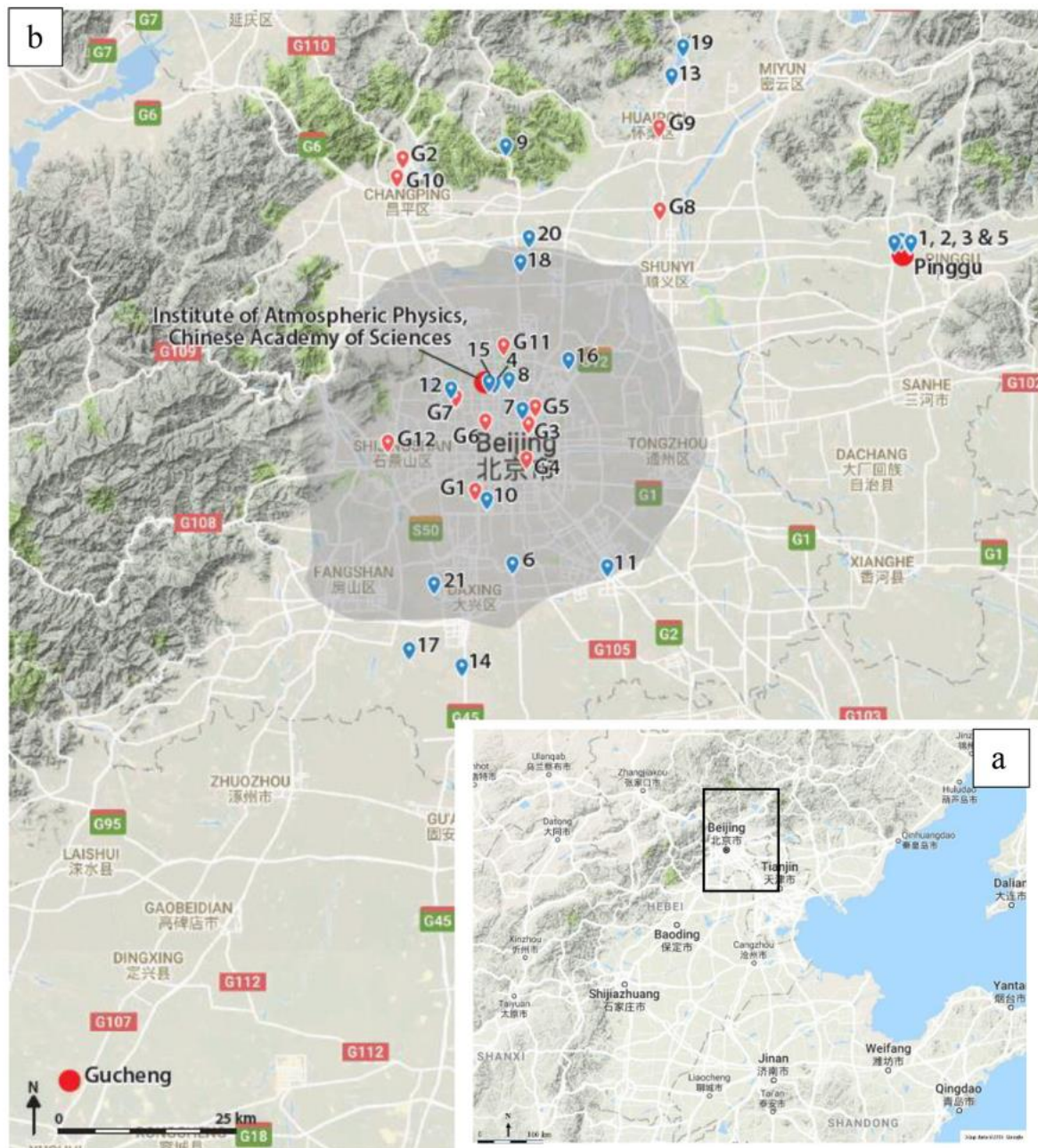
Figure 2.6. Map showing the location of Beijing within China (a) and the location of the Institute of Atmospheric Physics within Beijing (b). Red and blue markers show the location of other measurement sites used during the APHH Beijing campaign. This figure is taken from Shi et al. 2019.[125]

2.2.2 Mechanisms

This investigation involved a comparison of three different isoprene oxidation mechanisms. The MCM subset for isoprene and the additional VOCs which were measured throughout the campaign and were available in the MCM (Table 2.3) was extracted directly from the MCM website (mcm.york.ac.uk).[28] The MCM inorganic chemistry scheme was used for all three mechanisms.

The Caltech Mechanism was integrated with the MCM subset for the additional VOCs by producing lumped RO_2 cross-reactions using the approach outlined in Jenkin *et al*.[97] For each RO_2 species where explicit reactions are given, the geometric mean of the self-reaction rate and the CH_3O_2 self-

reaction rate was used. If a self-reaction was not specified, then the CH_3O_2 self-reaction rate was used. Branching ratios were then applied to the alcohol-forming, carbonyl-forming, and alkoxy-forming reactions according to Jenkin *et al.*

The FZJ Mechanism was produced by adding the reactions outlined in Tsiligiannis *et al.* to the mechanism provided in Vereecken *et al.* and combining it with the MCM subset for measured non-isoprene species.[68,134]

Each of the mechanisms used in this work have been made available online (doi.org/10.15124/500474f7-6e69-47db-baf7-36310451fd15).

2.2.3 Modelling Approach

AtChem2, an open-source zero-dimensional box-model tool, was used in this work.[153] A separate model was run for each day to avoid compounding errors carrying across multiple days of the model, for example the uncertainty that may result from imperfect accounting for physical processes. NO_2, O_3, CO, SO_2, HONO, and formaldehyde, along with 29 primary VOCs for which data were available (Table 2.3), were all constrained to the 30-minute averaged measured values throughout the campaign. Figure 2.7 shows the average diurnal concentration of a selection of constrained chemical species, and Figure 2.8 shows the diurnal profile of constrained physical properties. NO was left unconstrained due to the potential for local NO emissions to result in mixing ratios unrepresentative of the larger area that is important for the formation of long-lived organic products such as organonitrates. Constraining to NO would result in unrealistically low NO_3 concentrations by increasing the rate of the NO_3 + NO reaction based on elevated NO concentrations. Temperature, boundary-layer height, and relative humidity were also constrained to measured values. Pressure was held constant at 1013 mbar. Photolysis values in the models were constrained to measured values where available (J_{O1D}, J_{NO2}, J_{HONO}, J_{HCHOr}, J_{HCHOnr}, $J_{NO3toNO}$, $J_{NO3toNO2}$, J_{CH3CHO}, $J_{CH3OCH3}$), and remaining photolysis rates were calculated according to the parameterization used in the MCM and scaled based on the ratio of the calculated and measured J_{NO2}. The models consisted of a 24-hour spin-up period followed by a further 24-hour period. Constraints were made by duplicating the measured values for each day to provide a 48-hour constraint of two repeated 24-hour periods. The model output was then considered to be the model output in the second 24-hour period of the model run. The model outputs were then concatenated to produce a time series across the whole period of interest.
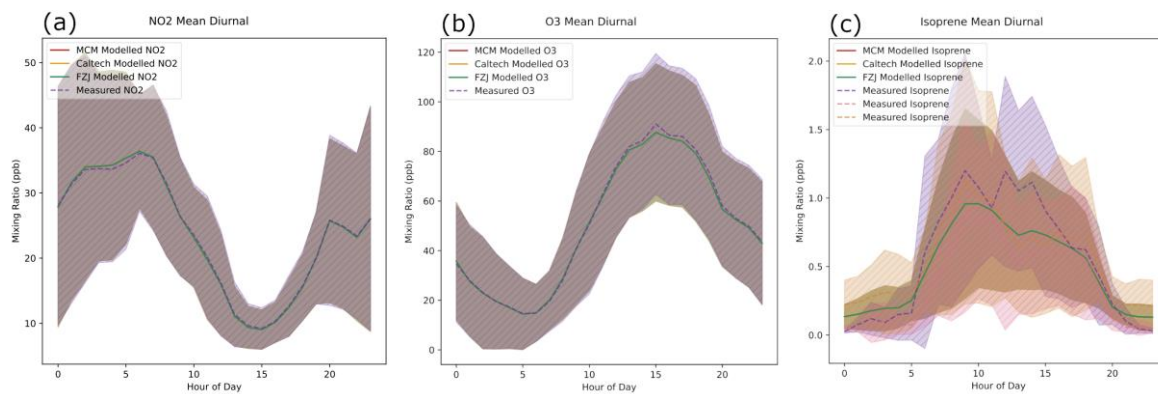
Figure 2.7. Measured and modelled concentrations for (a) NO$_2$, (b) O$_3$, and (c) isoprene, which are all constrained in each model to match the measured concentrations. Each line shows the mean value for each dataset, with the shaded area indicating one standard deviation above and below the mean. The model values all overlap due to the same constraint being applied to each model.
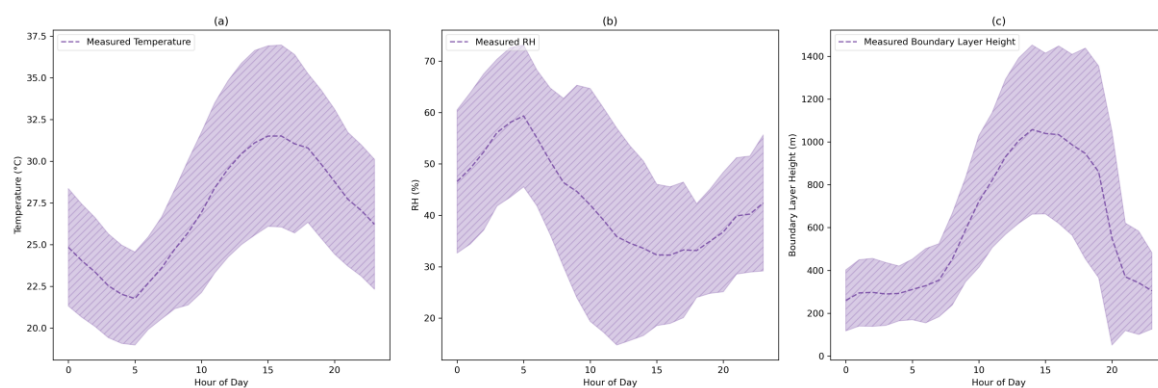
Figure 2.8. Measured values of (a) temperature, (b) RH, and (c) boundary layer height, which are all constrained in each model to match these measured concentrations. Each line shows the mean value for each dataset, with the shaded area indicating one standard deviation above and below the mean.

To account for the deposition of species to surfaces, deposition reactions were added for all species. Each species was assigned a deposition velocity based on the functionality of that compound. Deposition velocities for H$_2$O$_2$, HNO$_3$, and O$_3$ were applied directly to each compound. Separate deposition velocities for organic hydroperoxides and organic nitrates were applied to compounds containing the hydroperoxide and nitrate functional groups. Organic acid species were assigned the formic acid deposition velocity, and a general oxidised VOC deposition was assigned to carbonyl and alcohol containing compounds. The rate of deposition was determined by dividing the assigned deposition velocity by the measured boundary layer height. All deposition velocities were taken from Nguyen *et al.* 2015 and are summarised in Table 2.4.[154] For multifunctional compounds, the largest deposition velocity of each of the functional groups present in the compound was selected from Table 2.4.

Additionally, a loss term was included for all species to account for mixing and ventilation. A diurnally varying ventilation rate was applied, where the rate was scaled such that the modelled glyoxal concentrations matched measurements, in a similar fashion to previous work.[145,146] The sensitivity of the model results to this term is assessed in the Model Validation section.

Table 2.4. Deposition rates used in the models depending on functionality. All values are taken from Nguyen et al. 2015.

Functionality	Deposition Velocity (cm s^{-1})
H2O2	5.2
HNO3	3.8
O3	0.1
Organic Hydroperoxide (R-OOH)	1.8
Organic Nitrate (R-ONO2)	2.0
Formic Acid and All Carboxylic Acids (R-COOH)	1.0
Oxidised Volatile Organic Compound (OVOC)	1.2

2.2.3.1 Particle Phase Processes

In the cases of ΣIHN and ΣIPN, an analysis of the impact of the particle-phase hydrolysis of 1,2-IHN and the reactive uptake of INHE is performed. For both of these cases, the rates of loss (k_{IHN} and k_{IHNE} for IHN hydrolysis and INHE uptake respectively) are calculated using Equation 1. S_a is the aerosol surface area, as calculated for each model time-step from scanning mobility particle sizer (SMPS) measurements, r_p is the effective particle radius calculated as a weighted median of the SMPS number measurements at each model time-step, D_g is the gas-phase diffusion coefficient, v is the mean molecular speed of IHN or INHE molecules in the gas phase, and γ is the reactive uptake coefficient. v was calculated using Equation 2 where R is the ideal gas constant (8.314 J K^{-1} mol^{-1}), T is the measured temperature at each time-step, and M_r is the molecular mass of the compound of interest (0.147 kg mol^{-1} for IHN and 0.163 kg mol^{-1} for INHE). A value of 1×10^{-5} m^2 s^{-1} was used for D_g, as is assumed in Gaston *et al.* for IEPOX.[155] This method has been extensively used to calculate the rate of reactive uptake of IEPOX.[155-157]

$$k_{IHN} = \frac{S_a}{\dfrac{r_p}{D_g} + \dfrac{4}{v\,\gamma_{IHN}}} \qquad \text{Equation 1}$$

$$v = \sqrt{\frac{3\,R\,T}{M_r}} \qquad \text{Equation 2}$$

An estimation of γ is complicated by the dependence on particle properties. In each case, results are shown for models where a range of γ values are assumed, between the limits of 0 and 1.

2.3 Model Validation

When comparing the measured and modelled NO mixing ratios, there is good agreement during the day-time, with the models deviating from the measurement by a maximum of around 2 times (Figure 2.10a). The models do not reproduce the elevated night-time NO concentrations observed in Beijing, however this night-time NO is likely the result of local emissions and so will have little impact on the chemistry that is the focus of this study. Figure 2.9 shows the good match between modelled NO and NO measured at an altitude of 100m showing the ability of the model to predict NO away from local sources. This is further confirmed by NO$_3$ predictions provided by the models

being, at most, 2.5 times over-predicted (Figure 2.10b). There is also a slight under-prediction of NO_3 by a factor of around 0.4 during the afternoon.
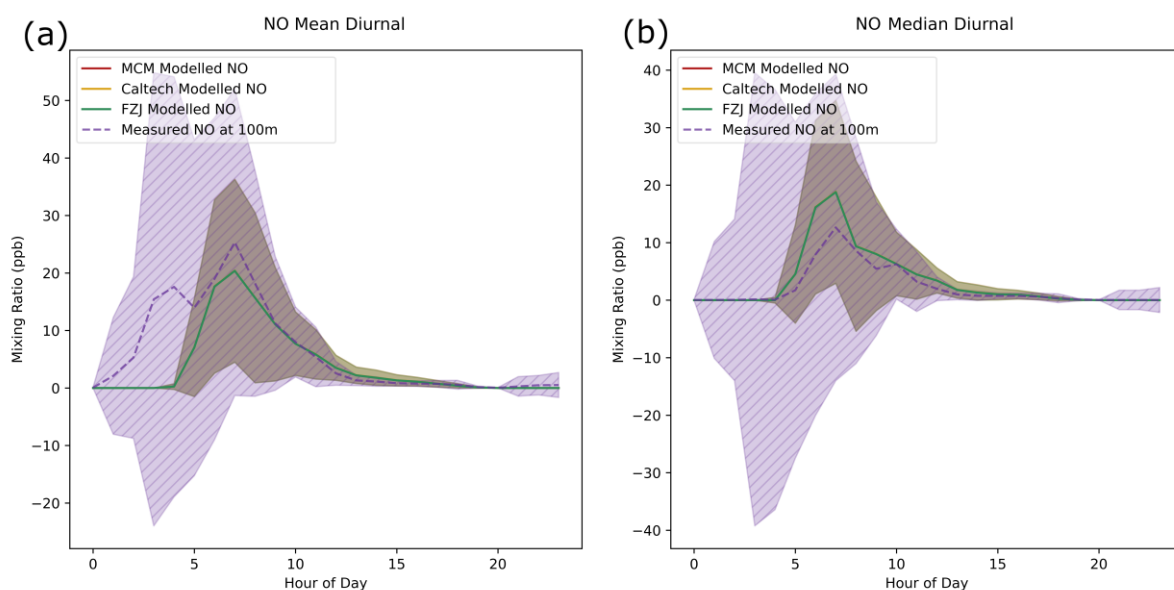
Figure 2.9. Measured NO at 100m and modelled NO in each model. The mean values (a) show a peak before sunrise due to large spikes in the measurements in the morning on some days, so the median diurnal (b) is also shown.

HO_x predictions from the models are generally good. There is close agreement to the measured OH concentrations, although the modelled concentrations are around 0.5 times the measured values during the morning period (Figure 2.10c). Day-time HO_2 concentrations are around 2 times higher than the measurement during the evening in all models (Figure 2.10d), which is consistent with findings from Whalley *et al.* 2021 where a similar box-model run using the MCM over-predicted HO_2, particularly during low-NO periods. Whalley *et al.* hypothesises that the HO_2 over-prediction may be caused by unaccounted for RO isomerisation reactions that result in RO_2 radical formation without concurrent HO_2 formation.[146] While the Caltech Mechanism and FZJ Mechanism both include additional RO isomerisation reactions for isoprene, they inherit the MCM RO chemistry for other VOCs, including longer-chain VOCs that may be more susceptible to RO isomerisations, and so this could still be a reasonable hypothesis. The major contributors to RO composition in the models are aromatic species owing to their relatively long lifetimes.
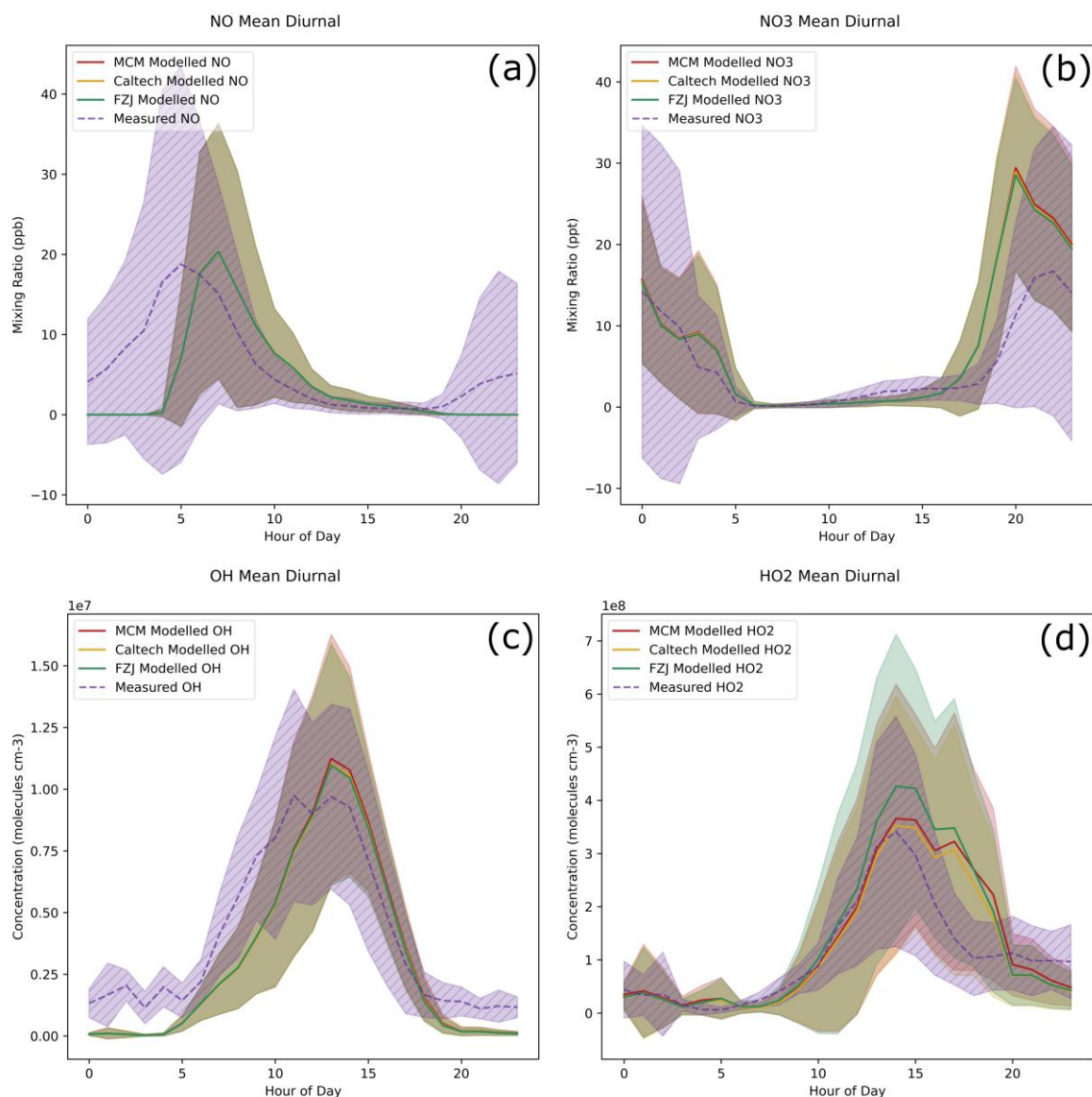
Figure 2.10. A selection of measured values and model predictions of inorganic species left unconstrained in the models. Each line shows the mean value for each dataset, with the shaded area indicating one standard deviation above and below the mean. The values of NO from each model are all overlapping in (a).

When comparing the modelled and measured MVK and MACR mixing ratios, while day-time concentrations are at-most half of the measured values, the night-time concentrations fall far below the measurements (Figure 2.11). This may be the result of the long lifetime of MVK and MACR, meaning there is a high background concentration not captured by the models. Alternatively, it may be due to imperfect accounting for physical processes such as mixing and ventilation within the models or a poor understanding of MVK+MACR chemistry in this environment. There may also be some role played by the conversion of isoprene hydroxyhydoperoxides to MVK+MACR on the metal inlets of the mass spectrometers resulting in an artificially increased measurement.[66,158] It is also important to consider the effect of upwind isoprene concentrations for all of the isoprene oxidation products discussed in this work. While our modelling makes use of isoprene concentrations measured at the same site as the product

measurements, the upwind isoprene concentrations would be more useful for predicting the concentrations of isoprene oxidation products.

Figure 2.11. Measured and modelled MVK+MACR mixing ratios. Each line shows the mean value for each dataset, with the shaded area indicating one standard deviation above and below the mean.

While a ventilation term is included in the models, and is scaled to glyoxal concentrations, there is uncertainty as to its true rate and diurnal variability. As a test of the models' sensitivity to the ventilation rate, the rate was halved and doubled in two separate tests (Figure 2.12). The halving of the ventilation rates resulted in an average change in concentration across the models run with each mechanism of 3.1, 1.5, 1.8, and 1.8 times for $\Sigma C_4H_7NO_5$, ΣIHN, ΣICN, and ΣIPN respectively. The average changes for doubling the ventilation rate were 0.32, 0.62, 0.60, and 0.56 for $\Sigma C_4H_7NO_5$, ΣIHN, ΣICN, and ΣIPN respectively. Xiong *et al.* aimed to reduce the impact of ventilation by analysing nitrates as ratios with the sum of MVK and MACR.[141] However, due to the differences in MVK+MACR predicted using each mechanism, using the MVK+MACR ratio as a proxy for the absolute concentration of the nitrates complicates the comparison of different mechanisms. As such, the analysis here involves the use of mixing ratios as opposed to the ratios relative to MVK+MACR. In order to analyse the average trends over a day within the modelled period, average diurnal plots are used to examine the modelled and measured data. The mean diurnals are used here, though use of the median had little impact on the diurnal values.

Comparison of the MVK+MACR predicted using each mechanism is consistent with the work presented in Vereecken *et al.*[68] Figure 2.11 shows that the Caltech Mechanism produces the highest night-time MVK+MACR concentrations with the MCM and FZJ Mechanism producing the lowest night-time concentrations. The MCM does not include MVK+MACR formation from isoprene+NO₃

chemistry, while the Caltech Mechanism does. The FZJ Mechanism does include some MVK+MACR formation from isoprene NO_3 chemistry, but also reduces the yield from ozonolysis reactions resulting in similar MVK+MACR yields between the MCM and FZJ Mechanism in Vereecken *et al.* and in the night-time period of the models presented here. During the day-time, the FZJ models produce the lowest MVK+MACR concentrations as this adjusted ozonolysis chemistry becomes more significant.

Isoprene epoxydiols (IEPOX) are a significant contributor to isoprene-derived SOA and are significant isoprene oxidation products along with the isobaric isoprene hydroxyhydoperoxides (ISOPOOH).[118,119,159] Figure 2.13 shows the modelled and measured ΣIEPOX+ISOPOOH. All three mechanisms resulted in a large under-prediction of ΣIEPOX+ISOPOOH. As with MVK+MACR, this under-prediction may result from ventilation from the model being too rapid. As discussed throughout the manuscript, there may also be an issue of calibration for the I⁻-CIMS data. Although the I⁻-CIMS data is calibrated using IEPOX, all three models predict around half of the ΣIEPOX+ISOPOOH to be comprised of ISOPOOH. Accounting for particle-uptake of IEPOX would only increase this fraction of ISOPOOH. Additionally, there are multiple IEPOX isomers whereas this data is calibrated to only one isomer. More discussion of calibration issues is given in Section 3.2.1.

The volatility of the nitrate species was assessed in order to determine the potential impact of condensation to the particle phase. An equilibrium partitioning approach was taken, as described in Mohr *et al.* 2019.[160] This resulted in common logarithm of saturation concentrations in units of molecules cm⁻³ (log(C_{sat})) of between 4.0 and 5.3, revealing the high volatility of these compounds. As such, the condensation of these nitrates to the particle phase is assumed to be negligible, though this approach does not account for reactive uptake to particles.
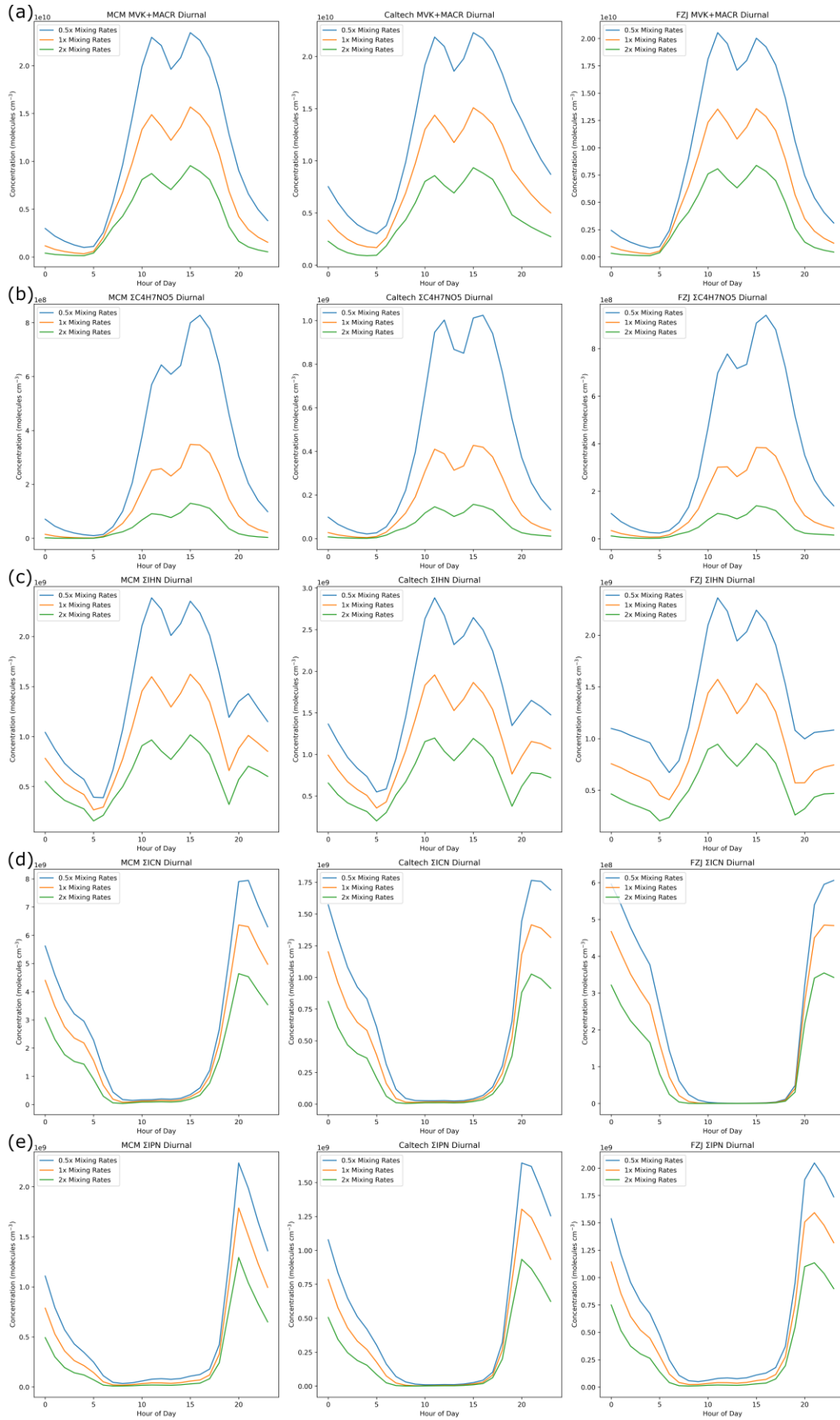
Figure 2.12. Impact on MVK+MACR (a), ΣC₄H₇NO₅ (b), ΣIHN (c), ΣICN (d), and ΣIPN (e) of varying the ventilation rate used in each model by 0.5 times and 2 times from the base mixing lifetime.

Figure 2.13. Measured and modelled ΣIEPOX+ISOPOOH mixing ratios. Each line shows the mean value for each dataset, with the shaded area indicating one standard deviation above and below the mean.

2.4 ΣIHN ($C_5H_9NO_4$)

Throughout the day, the three mechanisms produce similar ΣIHN mixing ratios, at approximately half of the measured value (Figure 2.14). Despite the absolute differences, the profile of modelled ΣIHN matches the measurement, with decreasing mixing ratios in the afternoon reflecting the titration of NO by increasing O_3.[66] Reeves *et al.* shows reasonable predictions of the major IHN isomer (1,2-IHN) made by their MCM-based model, whereas the modelled 4,3-IHN showed an over-prediction of around two times at mid-day.[145] This discrepancy is likely the result of different representations of physical processes in the models. The time series for modelled and measured ΣIHN is shown in Figure 2.15.

Figure 2.16 shows the clear split between the day-time and night-time IHN speciation in all of the models. Figure 2.16 also demonstrates that the contribution of non-IHN species to ΣIHN in the models is very small, meaning a measured ΣIHN ($C_5H_9NO_4$) signal is likely to be a reasonable measurement of IHN. Both OH and NO_3 addition to isoprene favours the terminal carbon atoms, so OH oxidation followed by reaction with NO results in the nitrate group being formed either on one of the central positions or the remaining terminal carbon. This means OH-initiated oxidation predominantly forms 1,2-IHN, 4,3-IHN, E/Z-1,4-IHN, and E/Z-4,1-IHN. NO_3 addition results in the nitrate group being present on the terminal carbons, at the initial site of attack.[42] This means NO_3-initiated oxidation predominantly forms 2,1-IHN, 3,4-IHN, E/Z-1,4-IHN, and E/Z-4,1-IHN.

Figure 2.14. Measured and modelled ΣIHN. Each line shows the mean value for each dataset, with the shaded area indicating one standard deviation above and below the mean.

Figure 2.15. Time series for measured and modelled ΣIHN.
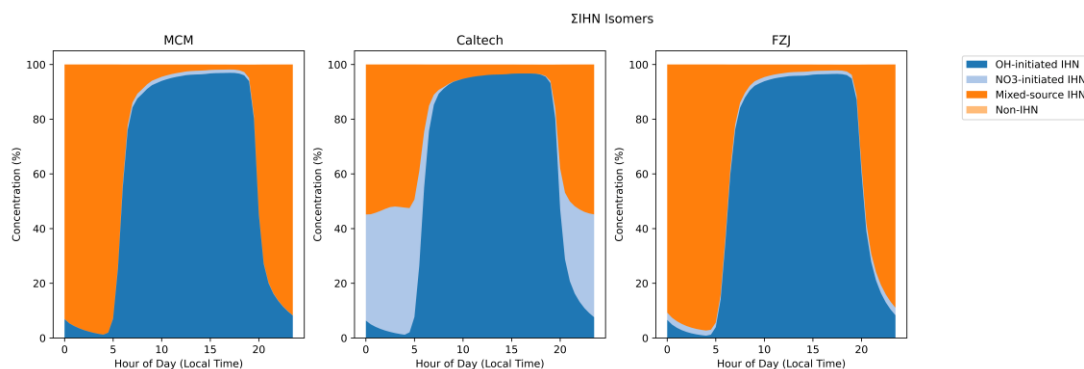
Figure 2.16. Isomer composition of the modelled ΣIHN. OH-initiated IHN are those primarily formed by OH chemistry, the 1,2-IHN and 4,3-IHN. NO3-initiated IHN are those primarily formed by NO3 chemistry, the 2,1-IHN and 3,4-IHN. Mixed-source IHN is formed in large amounts by both routes, the E/Z-1,4-IHN and E/Z-4,1-IHN.

The night-time shows an enhancement in IHN species produced by NO_3 chemistry. This is most obvious in the MCM model, where all isoprene + NO_3 chemistry is channelled through just one isomer, ISOPCNO3. As such, ISOPCNO3 makes up very little of the day-time IHN, but up to 80% of night-time IHN just before sunrise. Similarly, the ΣIHN modelled using the Caltech Mechanism and FZJ Mechanism are almost exclusively comprised of ISOP1OH2N and ISOP3N4OH during the day, but there is a more even distribution at night with major contributions from ISOP1N2OH, ISOP1N4OHt, and ISOP1N4OHc. The FZJ Mechanism contains a reduced rate of ISOP1N2OH formation from ISOP1N2OO cross-reactions compared to the Caltech Mechanism, hence the lower contribution of 'NO_3-initiated IHN' to ΣIHN in the FZJ Mechanism model.

Previous work has shown that the hydrolysis of 1,2-IHN occurs rapidly in the atmosphere.[131,161] To test the sensitivity of our results to 1,2-IHN hydrolysis, loss reactions of 1,2-IHN were added to each of the mechanisms with a rate calculated as described in Section 2.3.1. Figure 2.17 shows the modelled ΣIHN using each of the mechanisms with 1,2-hydrolysis reactions included. Since the majority of daytime ΣIHN is comprised of 1,2-IHN, removal of this compound can have a large effect on the modelled ΣIHN. A γ_{IHN} value of 1 removes most, but not all, of the 1,2-IHN and a value of 0.1 brings modelled ΣIHN concentrations close to when the value is 1. Conversely, γ_{IHN} values below 0.01 only result in small changes to modelled ΣIHN compared to the base model where no IHN hydrolysis is included.

2.4.1 ΣIHN Calibration

As previously noted, the I⁻-CIMS data presented here is calibrated relative to IEPOX, which results in two potential issues. Firstly, the sensitivity of I⁻-CIMS to the compounds of interest may be significantly different from the sensitivity to IEPOX, leading to a bias in the measurement. Secondly, if I⁻-CIMS has different sensitivities to the different isomers of a particular formula, the changing isomer distribution over time will result in a varying sensitivity to the entire m/z signal as each isomer contributes more or less. For example, it has been previously shown that I⁻-CIMS is more sensitive to IHN isomers in which the NO3 group is located close to the OH group, such as 4,3-IHN
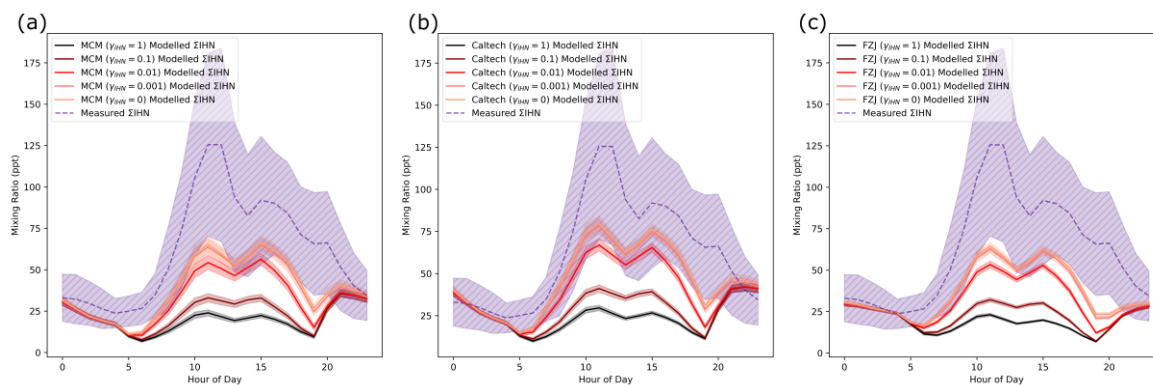
Figure 2.17. Measured and modelled ΣIHN mixing ratios for models using a range of γ_{IHN} values to account for the hydrolysis of 1,2-IHN. The mechanisms used in each model are as follows: (a) MCM, (b) Caltech Mechanism, (c) FZJ Mechanism. Each line shows the mean value for each dataset, with the shaded area indicating one standard deviation above and below the mean.

and Z-1,4-IHN. Isomers where the NO3 and OH groups are not in close proximity, such as E-1,4-IHN, show much lower responses to iodide-adduct ionisation. (Lee et al., 2014) The "Mixed-source IHN" in Figure 2.16 includes both E and Z isomers of 1,4-IHN and 4,1-IHN. Since there is a higher proportion of mixed-source IHN during the night in all models, the sensitivity of ΣIHN can be expected to be lower at night than during the day due to a higher proportion of E-1,4-IHN and E-4,1-IHN.

Lee *et al.* report sensitivity values for IEPOX alongside the sensitivity values for three IHN isomers (4,3-IHN, Z-1,4-IHN, and E-1,4-IHN).[162] Dividing the sensitivities of each of these isomers by the IEPOX sensitivity allows a relative sensitivity to be obtained for each. These relative sensitivities are 15.64, 14.62, and 0.9487 for 4,3-IHN, Z-1,4-IHN, and E-1,4-IHN respectively. Relative sensitivities for the remaining IHN isomers can be assigned based on the orientation of the OH and NO_3 groups.[141] A total ΣIHN sensitivity can then be estimated using the modelled isomer distribution from each set of models. Figure 2.18a shows the diurnally varying relative sensitivity for each of the models. The largest discrepancy between the models can be seen at night, resulting from the differing NO_3 chemistry in each mechanism. Taken together, the models indicate that I⁻-CIMS may be between 2.5 to 1.4 times less sensitive to ΣIHN during the night than during the day.

Applying this relative ΣIHN sensitivity to the IEPOX calibrated data dramatically reduces the measured concentrations of ΣIHN, due to the high sensitivities of the majority of IHN isomers (Figure 2.18b). It is interesting to note differing ΣIHN concentrations predicted using the isomer distribution from each mechanism. At midnight, the FZJ-adjusted ΣIHN data is around twice that of the Caltech-adjusted data. According to this adjusted ΣIHN data, all of the models would be over-predicting ΣIHN by around an order of magnitude. Even when comparing to the most extreme 1,2-IHN hydrolysis case previously presented, ΣIHN concentrations are over-predicted by 1.5 to 3 times compared to the adjusted I⁻-CIMS data. Additionally, the adjusted calibration factors change the shape of the ΣIHN diurnal, resulting in a second peak in mixing ratios at around 20:00. Using the

isomer distribution predicted by the FZJ mechanism suggests that this second night-time peak could be as large as the mid-day peak.
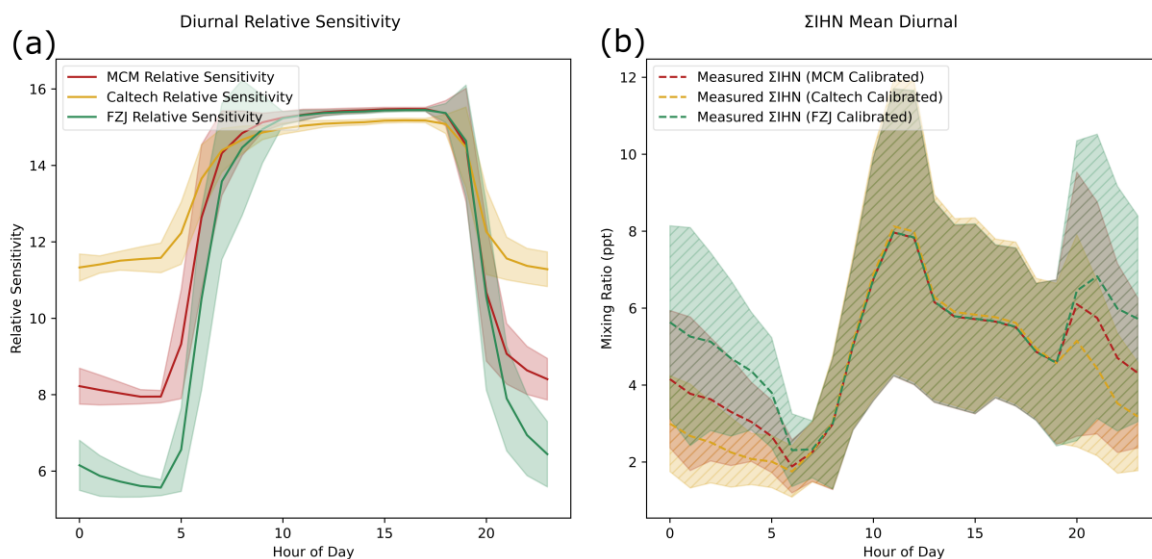
Figure 2.18. (a) Diurnal variation in the sensitivity of I⁻-CIMS to ΣIHN relative to IEPOX according to the isomer distribution predicted by each model. (b) The measured ΣIHN data adjusted using the relative sensitivity values from each mechanism.

The use of relative responses here aims to eliminate some issues associated with the direct comparison of data from different instruments, but may not eliminate all of the unknown differences. Nevertheless, adjusting the measured ΣIHN in this way suggests that the perceived under-prediction in ΣIHN by all of the models may instead be a closer representation to the true ΣIHN concentrations, if not an over-prediction. IHN is the most widely studied of the nitrates presented here and so the calibration correction can be applied quantitatively, however the impact of calibration on the measured organonitrate concentrations must be considered throughout this work.

2.5 ΣIPN ($C_5H_9NO_5$)

The measured ΣIPN shows little diurnal variation (Figure 2.19). Contrary to observations, all models produced strong diurnal profiles of ΣIPN. This is because the majority of IPN is formed through NO_3 oxidation of isoprene at night when there are few losses. The only losses of IPN in all mechanisms, besides the added deposition reactions, are photolysis reactions and the reaction with OH. The strong diurnal profile results in night-time mixing ratios being over-predicted by around 1.5 times and day-time mixing ratios being close to 0. Both the MCM and FZJ Mechanism result in ΣIPN reaching a minimum at sunrise, slightly increasing throughout the day, before a rapid night-time increase. The daytime under-prediction of ΣIPN may be indicative of mixing in the models being overestimated. The time series for modelled and measured ΣIPN is shown in Figure 2.20. The data presented in Figure 2.20 show that there is substantial noise in the ΣIPN data, which may also mask
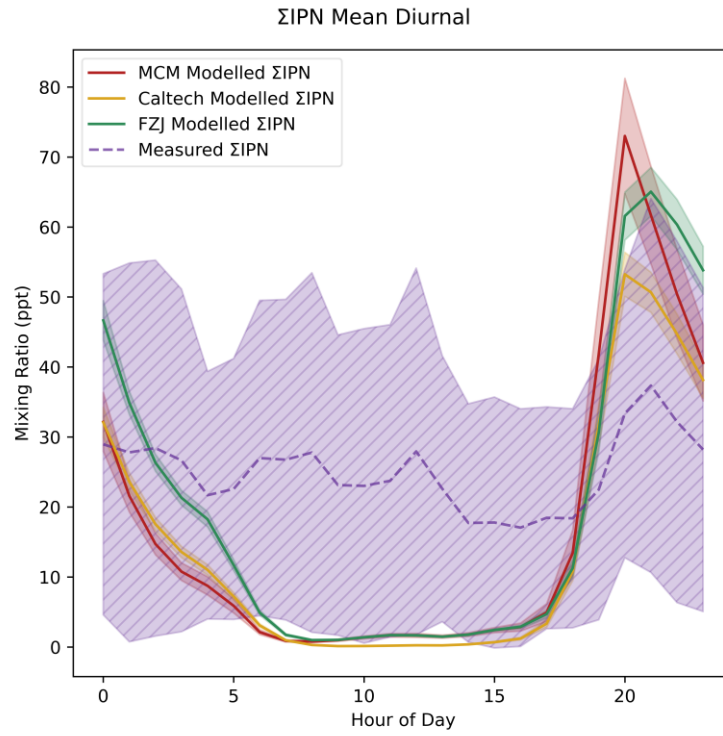
Figure 2.19. Measured and modelled ΣIPN (a). Each line shows the mean value for each dataset, with the shaded area indicating one standard deviation above and below the mean.
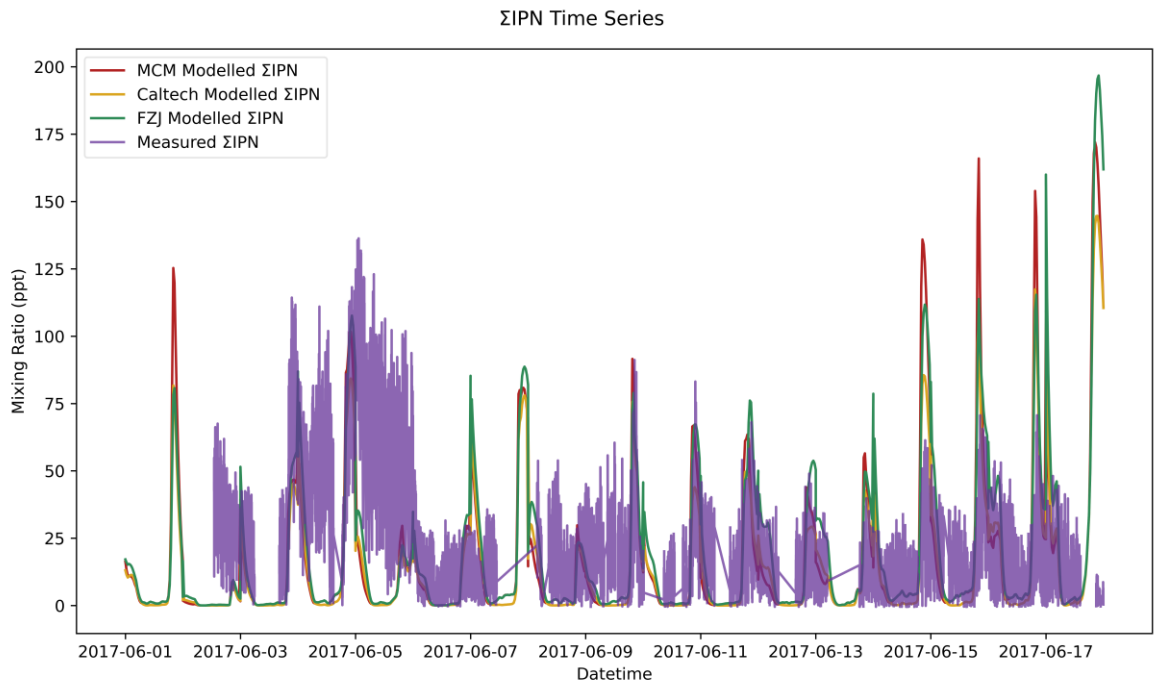
Figure 2.20. Time series for measured and modelled ΣIPN.

diurnal trends and indicates that the ΣIPN concentrations are close to the instrument's detection limit for these compounds.

While none of the mechanisms include NO_3 or O_3 oxidation of IPN, the Wennberg *et al.* 2018 review of isoprene chemistry does list estimated reaction rates of IPN, ICN, and IHN with NO_3, O_3, and OH.[42] Figure 2.21 shows the average proportional night-time chemical loss for IHN, IPN, and ICN calculated using the rates given in Wennberg *et al.* and the measured OH, O_3, and NO_3 concentrations between 20:00 and 05:00. For the IPN isomers, OH oxidation accounts for the majority of the chemical loss of IPN at night, with around 10-15% being lost to reaction with NO_3. Reaction with O_3 also makes up a substantial fraction of the chemical loss in the 1,4-IPN and 4,1-IPN isomers, though OH is still the major sink. Since OH oxidation is included in the mechanisms, then the majority of the chemical losses should be captured by the models. Physical processes also dominate the losses of ΣIPN at night, so the addition of more chemical losses would not have a large impact on ΣIPN concentrations.
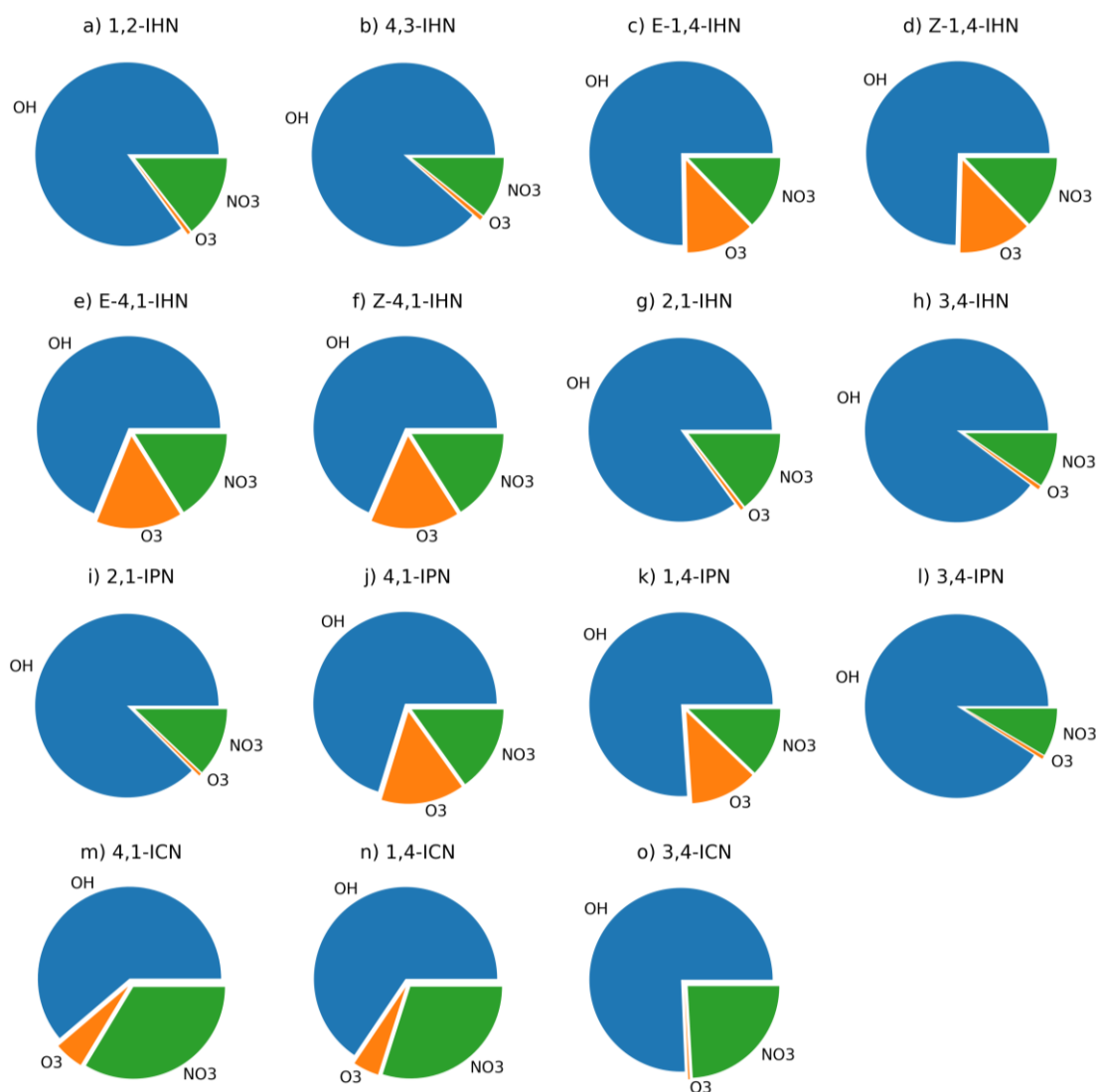
Figure 2.21. Proportional contribution of OH, O_3, and NO_3 to the night-time chemical loss (between 20:00 and 05:00) of IHN (a-h), IPN (i-l), and ICN (m-o) isomers. The loss rates are calculated using measured OH, O_3, and NO_3 concentrations and the rate constants listed in Wennberg et al. 2018.

To understand the trends in ΣIPN, it is important to consider the multiple isomeric (non-IPN) species present in each of the mechanisms which can make up a large proportion of the modelled ΣIPN (i.e. species with the formula $C_5H_9NO_5$). The most significant isomers of IPN are C51NO3, originally from the MCM and present in all mechanisms, C524NO3, originally from the MCM and also present in the FZJ mechanism, ISOP1N23O4OH, present in the Caltech Mechanism and FZJ Mechanism, and ISOP1N253OH4OH, present in the Caltech Mechanism (Figure 2.22).

C51NO3 is a nitrated hydroxy carbonyl compound in the MCM with formation routes from isoprene, as well as from hydrocarbons such as pentane. C524NO3 is an isoprene OH oxidation product from the MCM. In the MCM and FZJ Mechanism models, C51NO3 and C524NO3 make up the majority of modelled ΣIPN composition during the day-time (Figure 2.23). These are the species responsible for the slight increase in ΣIPN throughout the day in the MCM and FZJ Mechanism models. C51NO3 and C524NO3 production from isoprene is not included in the Caltech Mechanism, and the only formation routes to C51NO3 are from non-isoprene species. As such, C51NO3 and C524NO3 only makes a small contribution to total ΣIPN in the Caltech Mechanism model and the day-time increase is not present.
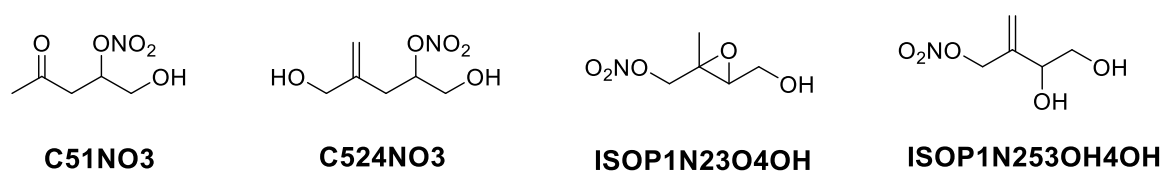
Figure 2.22. Structures of the three isomers of IPN that collectively comprise the majority of ΣIPN ($C_5H_9NO_5$) in the models.
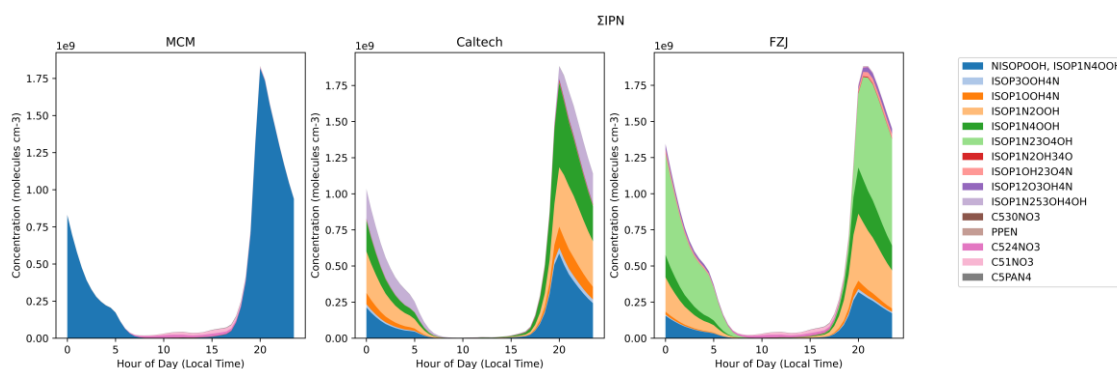
Figure 2.23. Isomer composition of the modelled ΣIPN.

ISOP1N253OH4OH is only present in the Caltech Mechanism and is initially formed from an intramolecular H-shift of the 1,4 isoprene alkoxy nitrate (INO), ISOP1N4O. The Caltech Mechanism does not contain any loss reactions for this species, which may account for its moderate contribution to modelled night-time ΣIPN (Figure 2.23). This INO H-shift pathway is not included in the FZJ Mechanism and so ISOP1N253OH4OH is not present.

ISOP1N23O4OH is a nitrated hydroxyepoxide that was proposed, alongside other positional isomers which are produced by the models in lower amounts, as a product of IPN OH oxidation by

Schwantes *et al*. where it is termed isoprene nitrooxy hydroxyepoxide (INHE).[123] While the formation of INHE from IPN is present in the Caltech Mechanism, epoxidation reactions from alkoxy radicals that are predicted in Vereecken *et al.* result in much more INHE production in the FZJ Mechanism model. The FZJ Mechanism model results predict that at midnight, around half of the total ΣIPN is composed of INHE (Figure 2.24). If such large concentrations of these epoxides are produced, then this could have a significant impact on SOA formation via reactive uptake in a similar fashion to IEPOX.[51,118,119,123]
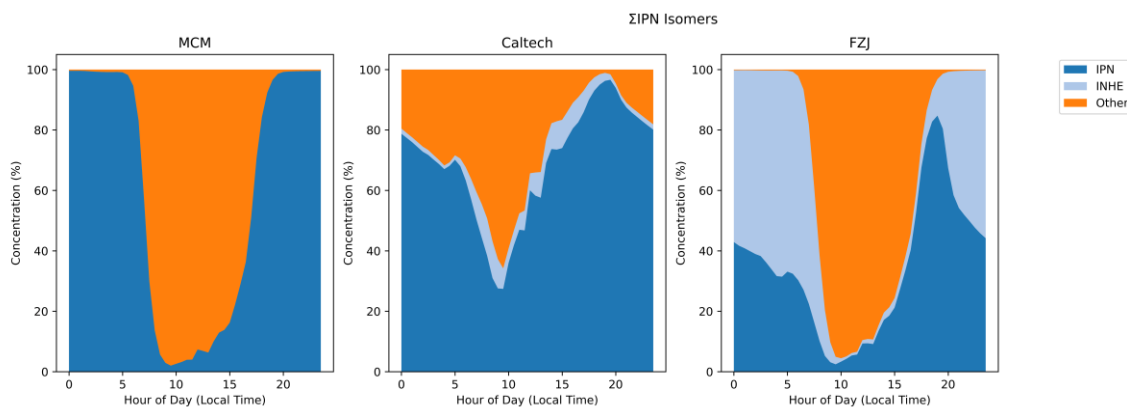
Figure 2.24. Isomer composition of the modelled ΣIPN as a percentage of total ΣIPN. "Other" comprises of ISOP1N253OH4OH, C530NO3, PPEN, C524NO3, C51NO3, and C5PAN4.

In order to assess the potential for reactive uptake of INHE on the modelled ΣIPN, loss reactions for each of the four INHE isomers in the FZJ Mechanism were added to the mechanism and the models rerun. The rate coefficient for the reactive uptake of INHE (k_{INHE}) was calculated as described in Section 2.3.1. Figure 2.25 shows the modelled ΣIPN produced by a set of models for which a range of γ_{INHE} were assumed, between the limits of 0 and 1. When $\gamma_{INHE}=1$ and $\gamma_{INHE}=0.1$, almost all of the INHE is removed from the gas-phase at any time which brings the modelled night-time concentrations of ΣIPN to around two thirds of the measured value. When $\gamma_{INHE} = 0.01$, the modelled night-time ΣIPN is reasonably in line with the measurements between 20:00 and 00:00, after which the modelled concentrations fall with the diurnal profile explained previously. $\gamma_{INHE} = 0.001$ results in modelled concentrations close to the values without any particle uptake. Previous estimations of the reactive uptake coefficient of IEPOX (γ_{IEPOX}) usually range between 7×10^{-2} and 2×10^{-4}, though measurements have been made as low as 9×10^{-7}.[155,157,163]

As with all of the nitrates investigated here, the role of the I⁻-CIMS calibration on the data presented must be considered. As shown previously, all models predict a diurnally varying isomer distribution with night-time ΣIPN being largely comprised of IPN and/or INHE, and daytime ΣIPN being comprised of smaller concentrations of other species. If the daytime isomers were much more sensitively detected than the night-time isomers then this could offset the diurnal concentration profile modelled to produce a constant measured signal throughout the day, as is observed. The daytime ΣIPN concentrations predicted by the MCM and FZJ models is around 0.06 times the

measured values, meaning that the daytime isomers would need to be around 17 times more sensitively detected than IEPOX to reproduce the flat diurnal signal observed, assuming the night-time isomers had the same sensitivity as IEPOX. There has been very little research to quantify the sensitivity of I⁻-CIMS to hydroperoxides, but Lee *et al.* reported the sensitivity of peroxyacetic acid to be 0.04 times that of acetic acid suggesting that the non-hydroperoxide daytime nitrates may be more sensitively detected than the night-time IPN.[162]
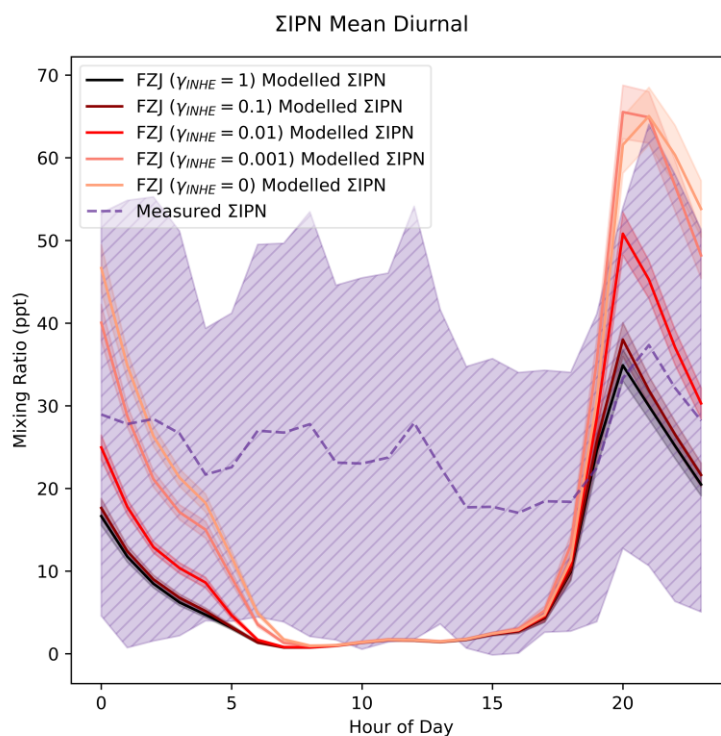
Figure 2.25. Measured and modelled ΣIPN mixing ratios for FZJ models using a range of γ_{INHE} values to account for the reactive uptake of INHE. Each line shows the mean value for each dataset, with the shaded area indicating one standard deviation above and below the mean.

2.6 ΣICN ($C_5H_7NO_4$)

ΣICN shows the largest difference between mechanisms. In line with the measurements, all models show low concentrations of ΣICN during the day (Figure 2.26). ΣICN then increases at sunset, due to NO_3-initiated formation from isoprene, and then reduces in concentration into the early morning as production ceases. There is a large over-prediction of a factor of around 25 times in the night-time mixing ratio modelled using the MCM which is consistent with findings from Reeves *et al.* who also found ICN to be over-predicted in their models using the MCM, however the lack of NO constraint in our models results in slightly higher modelled ICN concentrations due to elevated NO_3 concentrations, hence the discrepancy between the model and measurement is slightly larger in this work.[145] This over-prediction decreases to around 7 times when using the Caltech Mechanism, and decreases further to around 3 times when using the FZJ Mechanism. A plot of ΣICN concentrations normalised to the concentration at midnight is shown in Figure 2.28. The time series for measured and modelled ΣICN is given in Figure 2.27.
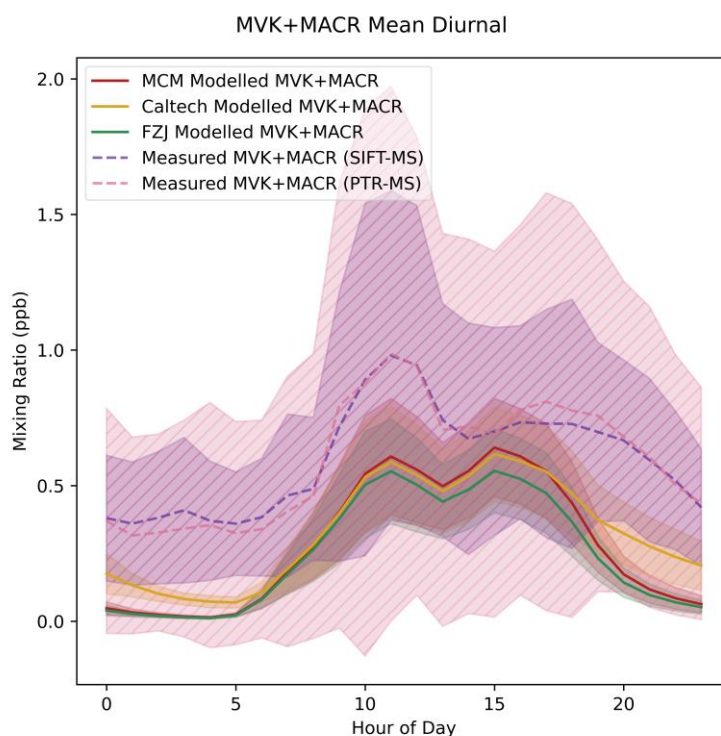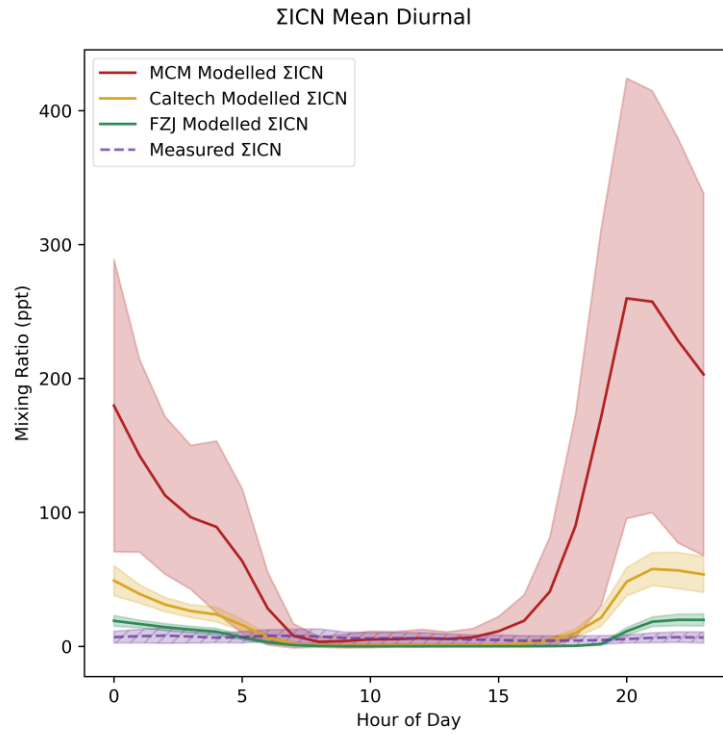
Figure 2.26. Measured and modelled ΣICN. Each line shows the mean value for each dataset, with the shaded area indicating one standard deviation above and below the mean.
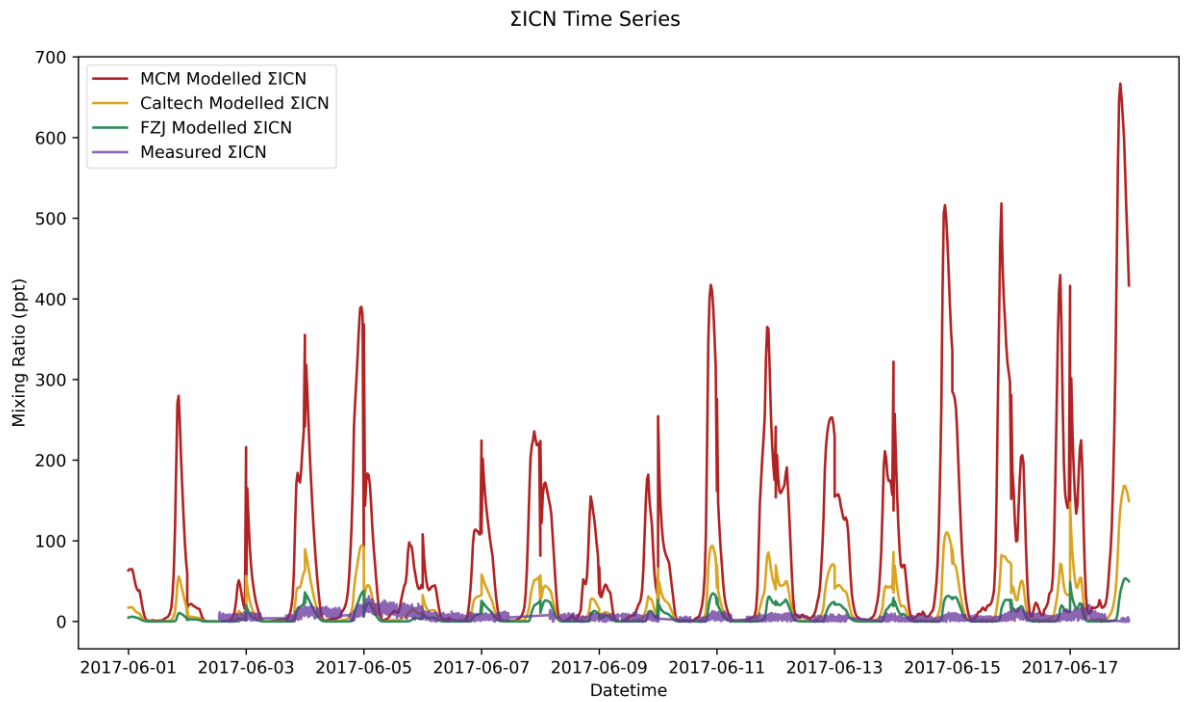
Figure 2.27. Time series for measured and modelled ΣICN.

69
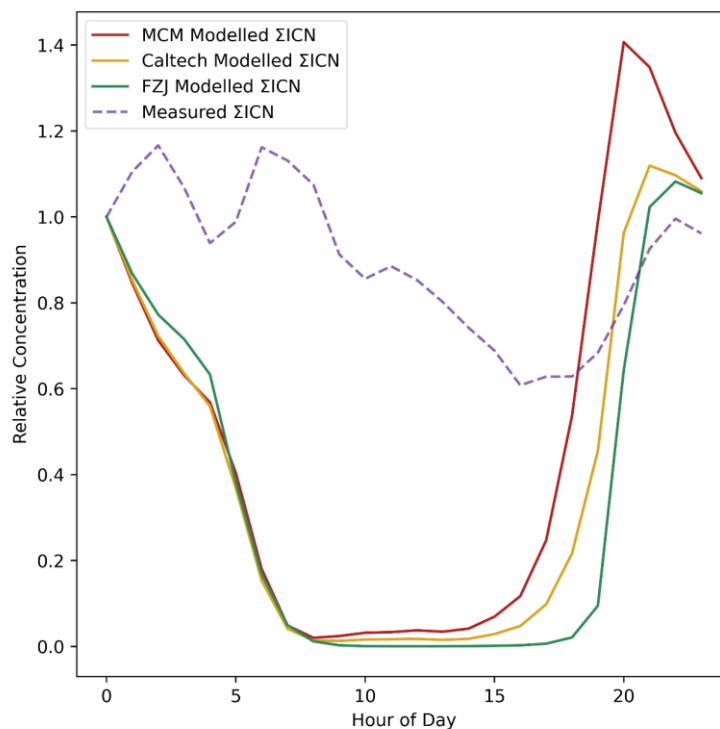
Figure 2.28. Measured and modelled ICN relative to the concentration at 00:00.

The large over-prediction made by the MCM is the result of large production terms from the decomposition of all INO radicals (represented by NISOPO in the MCM) into ICN. In contrast, the Caltech Mechanism provides alternative INO decomposition routes including fragmentation and H-shift autoxidation reactions (Figure 2.29). The FZJ Mechanism includes much of this updated chemistry as well as proposing the previously discussed epoxide formation reactions from some alkoxy radicals, which further reduces the ICN production route (Figure 2.29). The improvement in predictions of ΣICN indicates that the assumption made by the MCM of 100% of INO decomposing to form ICN is unlikely to be valid. The loss of ΣICN is dominated by physical processes in all of the models, particularly at night when ΣICN concentrations are the highest. Additional ICN losses being added to the MCM may improve ΣICN predictions, for example Hamilton *et al.* proposed ICN as a precursor to particle-phase species observed in Beijing via an isoprene nitrooxy hydroxy-α-lactone (INHL) species.[51] However, the MCM already includes reactions with O_3 and NO_3 that are not included in the Caltech or FZJ Mechanisms, suggesting that the issue lies in the MCM's faster formation processes. Further discussion of the uncertainties in ICN losses is given by Reeves *et al.*[145]

While this account of increasingly complex alkoxy radical chemistry gives good reason to question the high ICN formation rates from the MCM, it is also important to consider that previous work has found the lower sensitivity to aldehyde and ketone groups by I⁻-CIMS compared to alcohols, as such it should be expected that the measured ΣICN is most likely to be under-quantified by use of the IEPOX calibrant compared to species such as IHN.[147,162,164] For example, Lee *et al.* 2014 shows that the sensitivity to hydroxyacetone is around 20 times lower than the similarly structured 1,2-butanediol and the sensitivity to 2,5-hexanedione is around 70 times lower than that of

5-hydroxy-2-pentanone. Assuming the relative sensitivity of ICN to IEPOX is lower than that of IHN, i.e. the sensitivity relative to IEPOX is lower than 15.64 (Section 3.2.1), would mean that the over-prediction made by the MCM could not be solely accounted for by the calibration. However, it is more difficult to comment on the accuracy of the FZJ mechanism compared to the Caltech mechanism in this respect as a reasonable calibration correction could bring the measurement in line with either model.
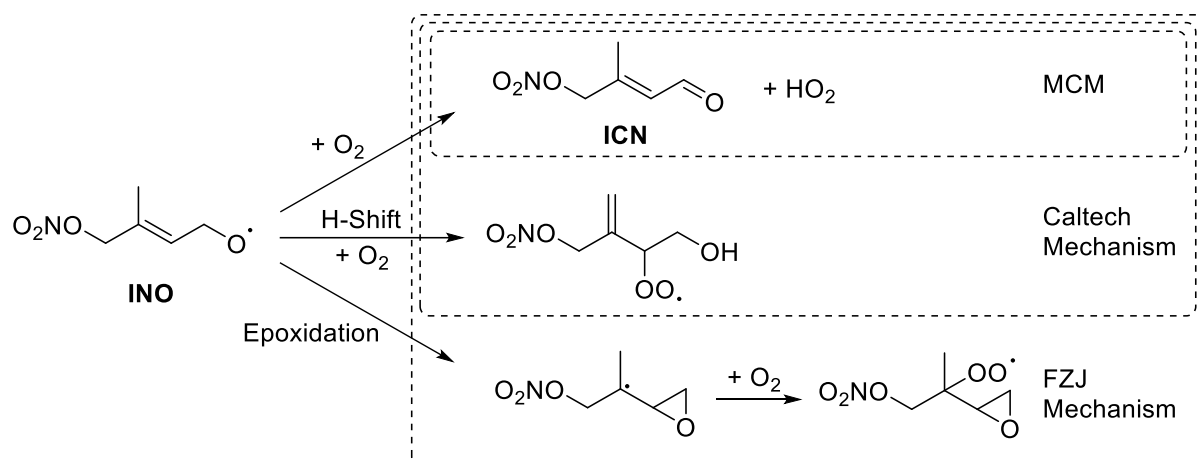
Figure 2.29. Examples of INO loss routes in each of the three mechanisms. Only one isomer is shown here, other isomers are present in the Caltech and FZJ Mechanisms. Additional reaction pathways are also possible in the Caltech and FZJ Mechanisms.

2.7 $\Sigma C_4H_7NO_5$

$\Sigma C_4H_7NO_5$ mixing ratios are under-predicted by around an order of magnitude in all models (Figure 2.30). The modelled $\Sigma C_4H_7NO_5$ diurnals only slightly vary between each model, despite the additional dark formation rates added to the FZJ mechanism, with the Caltech mechanism actually producing the highest concentrations. This is because the formation of $\Sigma C_4H_7NO_5$ is dominated by the OH oxidation of MVK and MACR. The time series for measured and modelled $\Sigma C_4H_7NO_5$ is given in Figure 2.31.

The under-prediction in MVK+MACR and the potentially high ventilation (see Section 3.1) may account for some of this under-prediction, particularly in light of the potentially long lifetime of $C_4H_7NO_5$, however the under-prediction is much stronger than is observed for the MVK+MACR precursors.[136] Without previous work investigating the sensitivity of I⁻-CIMS to $C_4H_7NO_5$ it is difficult to assess the impact of calibration on this measurement. Assuming a similar sensitivity as the most sensitively detected IHN isomer, where the OH and NO_3 groups are in close proximity like in the $C_4H_7NO_5$ isomers, would bring the measurement in line with the models.
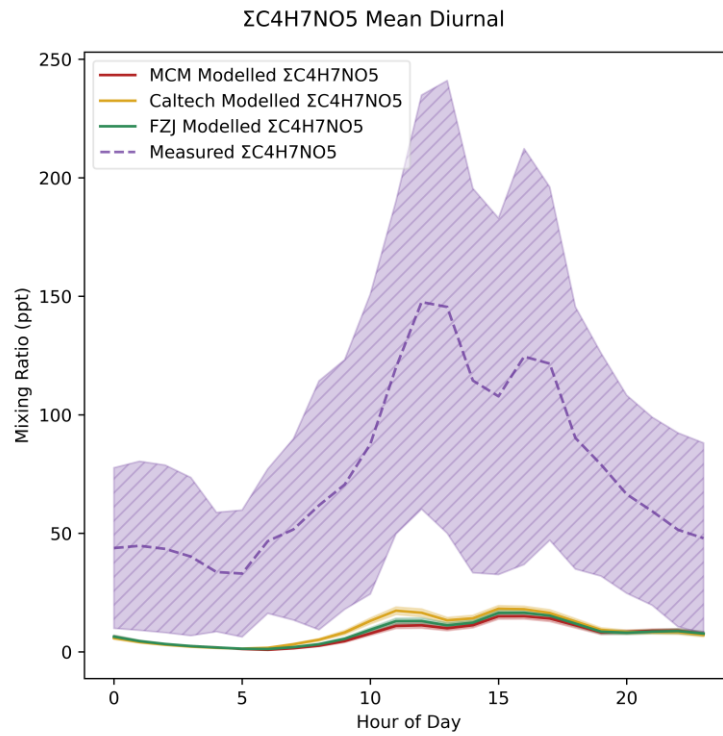
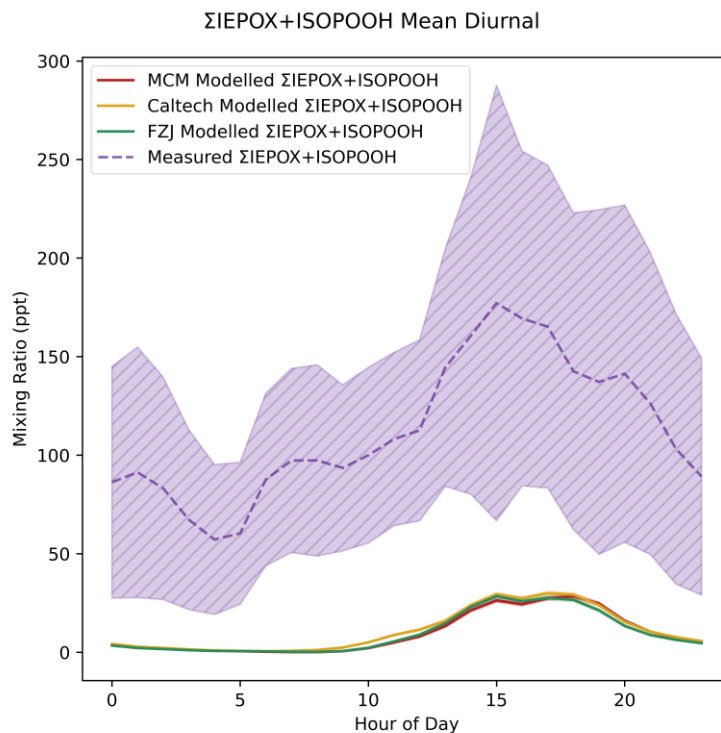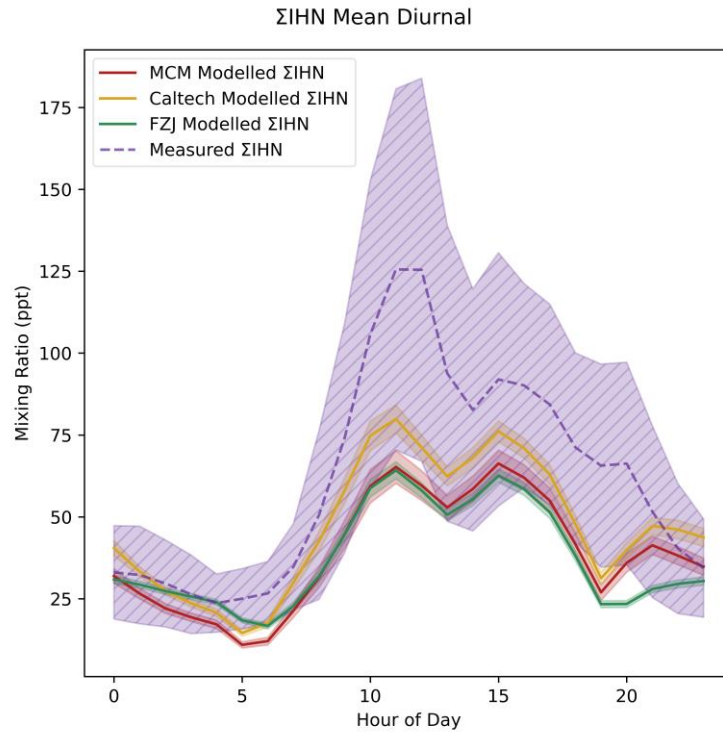*Figure 2.30. Measured and modelled $\Sigma C_4H_7NO_5$. Each line shows the mean value for each dataset, with the shaded area indicating one standard deviation above and below the mean.*
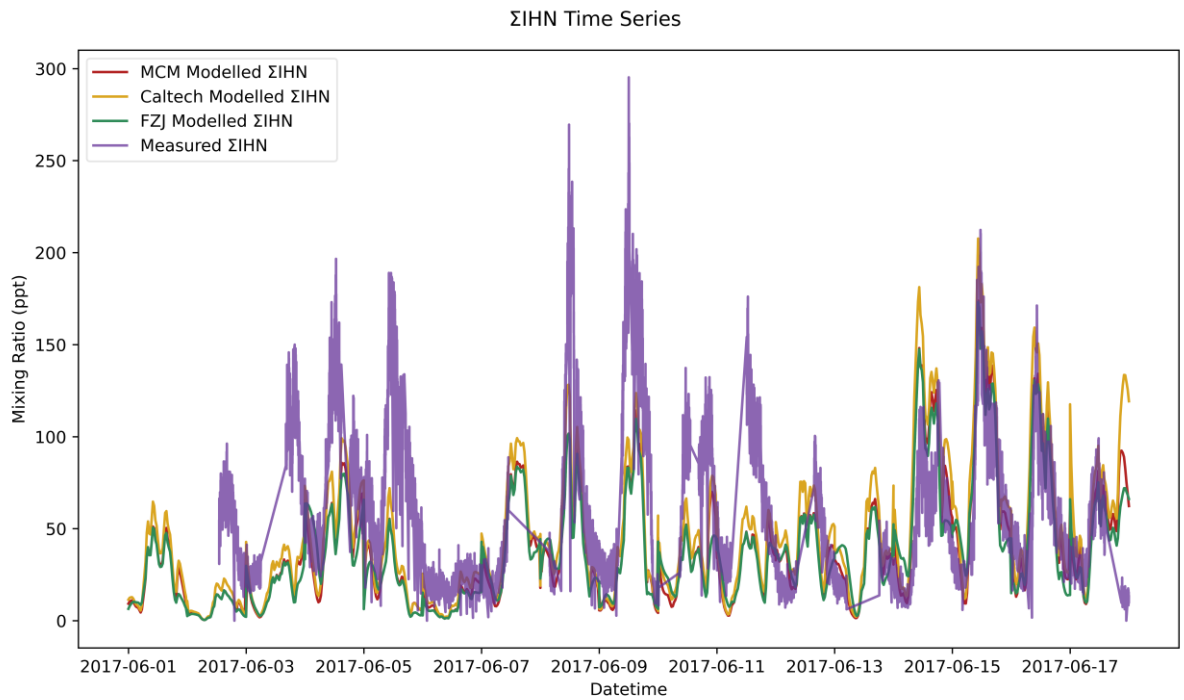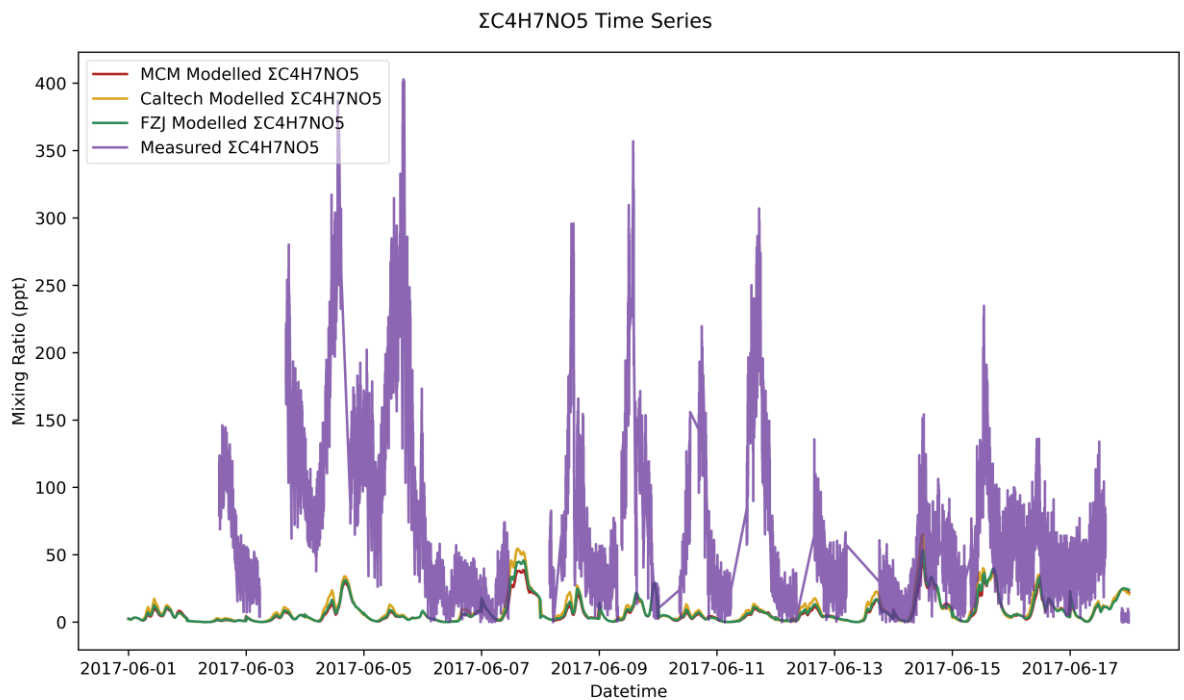

*Figure 2.31. Time series for measured and modelled $\Sigma C_4H_7NO_5$.*

2.8 Conclusions

Model results have been presented making use of three different detailed chemical mechanisms, comparing their predictions of several isoprene organonitrates. While the gas-phase box-modelling approach used here allows for the use of such complex mechanisms, the simplified representation may not fully represent physical processes such as boundary layer mixing in the morning and evening. Additionally, hydrolysis and aerosol uptake processes are not included in the mechanisms, meaning there may be unaccounted losses for species such as INHE. While the impact of I⁻-CIMS sensitivity on measurements of these nitrates has been considered throughout this work, the availability of authentic standards would greatly improve the ability to quantify such organonitrates.

When considering ΣIPN, the model results presented here indicate that large proportions of the measured ΣIPN can be composed of non-IPN species. This is especially true during the day-time, when ΣIPN concentrations are lowest. However, the epoxide-forming reactions proposed by Vereecken *et al.* suggest that around half of the measured night-time ΣIPN could be comprised of INHE.[68] Assuming reactive uptake coefficients similar to those previously measured for IEPOX results in small reductions in predicted ΣIPN, meaning that the FZJ mechanism predicts ΣIPN to be comprised of mostly non-IPN species for the majority of the day. Further studies of isoprene nitrate chemistry should investigate these species with techniques able to distinguish between the isomeric ΣIPN compounds and their reaction products, such as chromatographic techniques, in order to determine the role of INHE in isoprene oxidation. Such large INHE production terms would have implications for the formation and growth of secondary organic aerosol (SOA) by reactive uptake to acidified particles.[51] Generally, the large contribution of non-IPN species to the modelled ΣIPN highlights the caution that should be applied in interpreting measurements of ΣIPN solely as a measurement of IPN.

The changing distribution of ΣIHN isomers over the course of 24-hours has implications for the calibration of ΣIHN measurements. For example, I⁻-CIMS could be 2.5 to 1.4 times less sensitive to ΣIHN overnight where NO_3 chemistry is dominant, due to the increased contribution of E-1,4-IHN and E-4,1-IHN to ΣIHN. This means that the use of a constant calibration factor is likely to under-quantify night-time IHN, even if the calibration factor was accurate during the day. Furthermore, while comparison of the models to IEPOX-calibrated data suggests an under-prediction by the models, adjusting this calibration to account for the sensitivity of IHN isomers suggests a potentially very large over-prediction by the models.

The much improved ΣICN predictions when using the Caltech and FZJ Mechanisms compared to the MCM indicates that the assumptions around alkoxy radical decomposition made by the MCM are likely to be inaccurate, even when calibration uncertainties are accounted for. Future studies

focussed on isoprene nitrates should not overlook the inclusion of more complex INO decomposition routes, beyond the direct decomposition route to ICN present in the MCM.

While the results presented here surrounding $C_4H_7NO_5$ are not conclusive, there is potential for all of the mechanisms to be under-predicting $C_4H_7NO_5$. Additional $C_4H_7NO_5$ from NO_3 chemistry, as is included in the FZJ Mechanism model, does not improve predictions as the majority of the modelled $C_4H_7NO_5$ resulted from OH chemistry. Assuming an I^--CIMS sensitivity of $C_4H_7NO_5$ similar to that of the more sensitively detected IHN isomers would mean that the modelled $C_4H_7NO_5$ is approximately correct.

While physical processes dominated the loss of the organonitrates in all of the models presented here, the chemical losses of these species are not well understood. Estimated rate constants for the reaction of IHN, IPN, and ICN from Wennberg *et al.* indicate that the OH reactions which are included in all of the mechanisms may be the major chemical loss pathways, with NO_3 oxidation comprising a larger loss than reaction with O_3. This has implications for NO_x recycling, indicating that most of the NO_x consumed to form the organonitrates is subsequently lost from the gas-phase or transported away from the site of formation.[128]

Generally, the mechanisms presented here do a reasonable job at reproducing isoprene nitrate chemistry in Beijing, particularly with the inclusion of improved alkoxy radical chemistry, though it is clear that better constraints on the sensitivity of I^--CIMS to nitrated compounds would aid in the analysis of these compounds.

Chapter 3

Daytime Isoprene Nitrates Under Changing NO$_x$ and O$_3$

This work has been submitted to *Atmospheric Chemistry and Physics* and is currently under review.[165] My contribution to the work comprised of setting up and running the models, analysing the subsequent data, and writing the paper. Additional authors provided supervision, guidance on the modelling approach, and interpretation of the model data. At the time of thesis submission, one peer-review comment has been received, but the changes have not yet been implemented here.[166]

3.1 Introduction

Organonitrates are important species in the atmosphere due to their potential to impact on NO_x, HO_x, and O_3 budgets through gas-phase chemistry.[127-131] Their relatively low volatility also results in the potential to form secondary organic aerosol (SOA) via condensation onto existing particles, and some organonitrates can undergo reactive uptake to the particle phase.[105,129,132] Isoprene organonitrates have been widely studied due to the large emissions of isoprene resulting in the relevance of isoprene chemistry to a range of environments around the globe. [3,134,145,167]

Isoprene hydroxynitrate (IHN) is widely studied due to its formation from OH oxidation in the presence of NO resulting in high concentrations during the daytime (Figure 3.1).[42,141] IHN also has formation routes from oxidation with the nitrate radical (NO_3). Other commonly studied isoprene mononitrates include isoprene carbonyl nitrate (ICN) and isoprene hydroperoxy nitrate (IPN). IPN forms through the initial NO_3 oxidation of isoprene to form an isoprene nitrooxyperoxy radical (INO_2). Reaction of INO_2 with HO_2 then forms IPN. ICN has a range of formation pathways initiated by OH and NO_3 oxidation. Isoprene dinitrate (IDN) can also form from INO_2 by its reaction with NO.
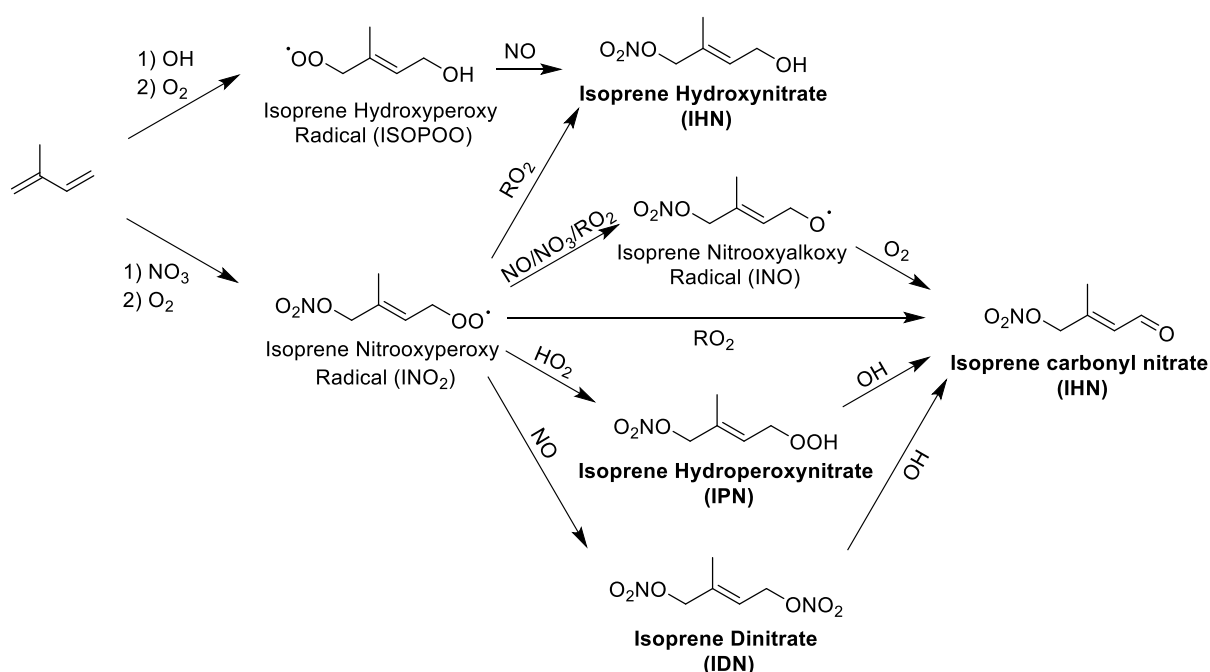
Figure 3.1. Formation routes to form IHN, ICN, IPN, and IDN from the OH- and NO_3-initiated oxidation of isoprene. Additional isomers and reaction pathways have been omitted for clarity.

Isoprene epoxides, such as isoprene epoxydiols (IEPOX), have long been of interest due to their potential to contribute to SOA by reactive uptake to acidified particles. [118,119] Later work outlined the similar SOA-forming properties for the nitrated epoxide, isoprene nitrooxyhydroxy epoxide (INHE), with the first proposed formation route to INHE involving the OH oxidation of IPN (Figure 3.2).[123] Recent work aiming to improve the representation of isoprene NO_3 chemistry in chemical mechanisms highlighted a previously unrepresented reaction pathway to forming nitrated epoxides from alkoxy radicals (RO). [68,124] This alkoxy-epoxidation pathway provides an alternative formation route to INHE that doesn't rely on a stable intermediate or the presence of OH (Figure 3.3). Additionally, three more nitrated epoxides can result from this pathway: isoprene nitrooxycarbonyl epoxide (INCE), isoprene nitrooxyhydroperoxy epoxide (INPE), and isoprene dinitrooxy epoxide (IDNE).
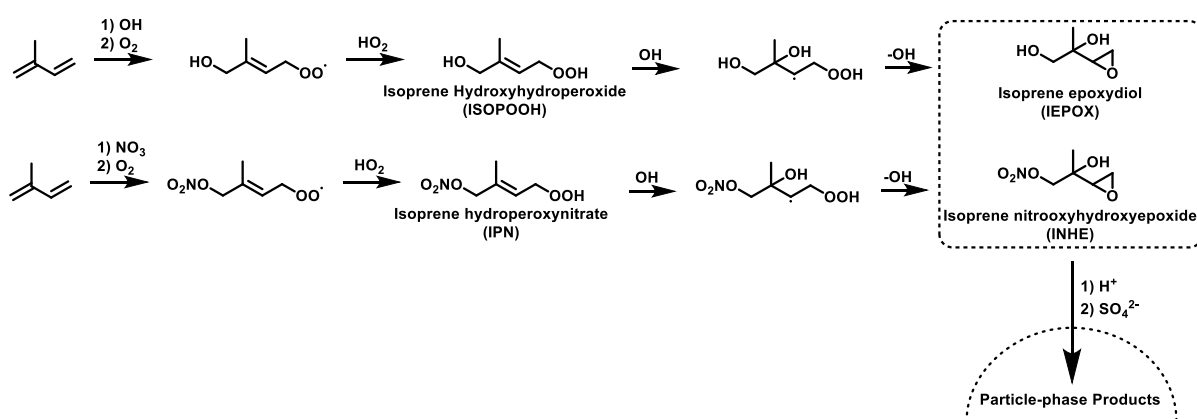
Figure 3.2. Established formation routes to form IEPOX and INHE via the OH oxidation of stable hydroperoxide intermediates. Additional isomers and reaction pathways have been omitted for clarity.
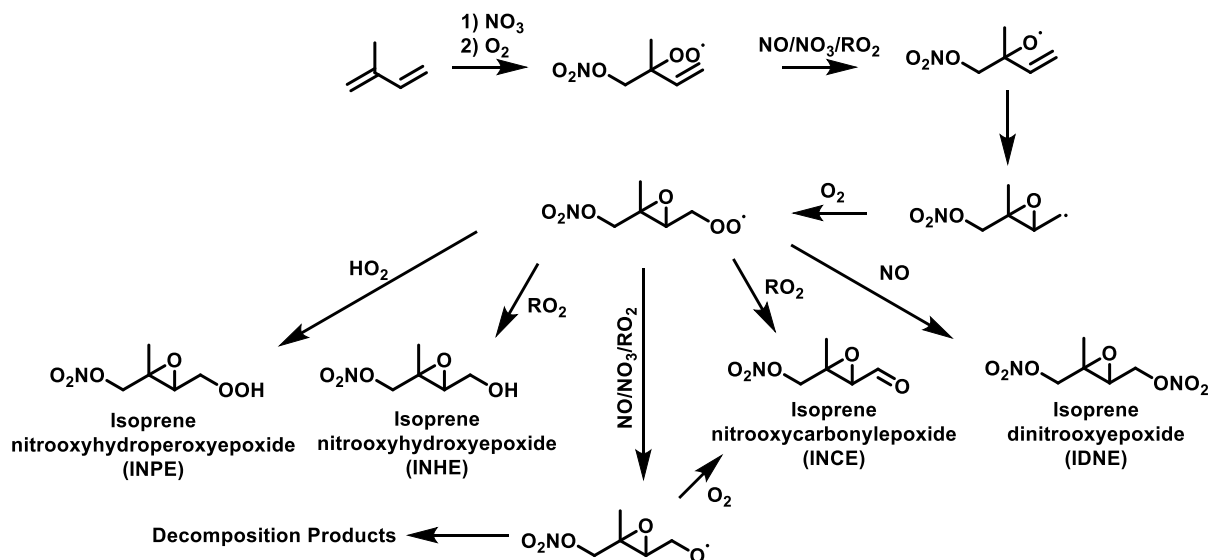
Figure 3.3. The alkoxy-epoxidation pathway to form a range of nitrated epoxides, as proposed by Vereecken et al. 2021. Additional isomers and reaction pathways have been omitted for clarity.

The motivation for the work presented here stems from findings from the 2017 Atmospheric Pollution and Human Health in a Chinese Megacity (APHH) summer campaign in Beijing, showing the role of NO_3 in the formation of isoprene organonitrates and their successive particle-phase

products, including in the afternoon due to the presence of high O_3 concentrations. [51,66] The presence of high O_3 concentrations increased the conversion of NO to NO_2 which subsequently reduced the loss of NO_3 to reaction with NO. Geyer *et al.* first highlighted this in 2003, calculating daytime NO_3 mixing ratios of up to 2-5ppt during the afternoon during a haze period in La Porte, Texas.[46] Since then, daytime NO_3 has been highlighted as a potentially important chemical pathway from a range of field campaigns in various cities around the world. [29,47-50,53] Daytime NO_3 chemistry has also been shown to be potentially significant under forest canopies, where photolytic processes are diminished. [54-56]

The co-occurrence of organonitrate formation from OH and NO_3 chemistry, along with the multi-stage chemistry often required for their formation, results in the potential for complex dependencies on NO_x and O_3 concentrations. This work describes efforts to investigate the dependence of daytime isoprene organonitrate concentrations on changes to NO_x and O_3 through a series of steady-state models. While the data presented here solely focusses on nitrated species resulting from isoprene, similar variations in organonitrate speciation under different NO_x-O_3 regimes are likely to hold for any VOC which can undergo oxidation by both OH and NO_3 radicals.

3.2 Experimental

3.2.1 Model Description

The goal of this work is to investigate the effect of changes in NO_x and O_3 on the chemistry of isoprene nitrates in the afternoon period in Beijing. To do this, the models should demonstrate the favoured reaction pathways under different oxidant concentrations in the absence of other variables. This means that physical and photolytic processes should be held constant, i.e. the models will describe the chemistry occurring at a representative point in the day. Species must also be allowed to reach their steady-state concentrations in order to eliminate the role of the model spin-up period on resultant species concentrations. Comparison of the concentrations of species in these so-called steady-state models then allows for conclusions to be drawn as to the preferred oxidation products under various conditions.

All models described in this work were run using AtChem2, an open-source zero-dimensional box model. [153] All models also made use of the Isoprene mechanism published by Vereecken *at al.* (henceforth the FZJ Mechanism) which aimed to improve the representation of NO_3 chemistry of isoprene by building on chemistry from the Master Chemical Mechanism (MCM) and the review of isoprene chemistry published by Wennberg *et al.* [28,42,68,124] This mechanism was chosen on the basis of results from Chapter 2 which demonstrate that the representation INO decomposition in this mechanism, along with the Caltech mechanism, are important for improving the representation of ICN. Additionally, the representation of nitrated epoxide formation from INO motivated the use of the FZJ mechanism as this chemistry is relatively under-investigated.

The steady-state models are sets of models run at a range of fixed NO_x and O_3 mixing ratios. Models were run for NOx mixing ratios up to 45 ppb and O_3 mixing ratios of 140 ppb, corresponding to the upper limit of measurements made in the Beijing 2017 campaign. In order to provide additional OH reactivity, a constant concentration of methane was added to all of the models to ensure that the modelled OH reactivity matched measured values under Beijing-like conditions, this is discussed further in the Model Validation section. The required mixing ratio corresponded to 82 ppm of methane in all of the models. Methane was chosen to make-up the OH reactivity, as opposed to another reactive gas such as CO or H_2, as it provides an analogue for the complex mixture of VOCs found in real-world ambient air by producing methylperoxy radicals which react similarly to the complex mixture of ambient RO_2. Use of H_2 or CO would result in the increased formation of HO_2 as the H_2 + OH and CO + OH reactions both produce HO_2 without producing an intermediate RO_2. This is particularly important in light of the HO_2 overprediction already made by these models, as described in Section 3.3.

The modelled concentration of species is taken as the final concentration after 5 model days, after all species had been allowed to reach steady-state concentrations. Each model was run at photolysis conditions corresponding to those calculated by AtChem2 for 16:00 local time in Beijing, China. This was around the time of peak daytime NO_3 concentrations in Beijing, before concentrations rapidly increased during sunset. To ensure steady-state was reached in a reasonable time, and to provide loss routes for species without losses, species were removed from the model at a dilution rate of 2.31×10^{-5} s^{-1}, corresponding to a dilution lifetime of 12 hours.

All models were run at a temperature of 298.15 K, a pressure of 1013 mbar, and a relative humidity of 50%. The latitude, longitude, and date used for photolysis calculations were 39.909°, 116.398°, and 2022-06-01. NO_x was constrained by adjusting the NO and NO_2 concentrations at the beginning of each time step such that the total NO_x matched the desired concentration but the ratio of NO and NO_2 remained constant.

Models were also run to simulate conditions in the Amazon region, with VOC concentrations adjusted to match observations of isoprene concentrations and OH reactivity in this region. These models were run at a higher isoprene concentration of 5 ppb, and methane concentrations of 100 ppm. [11,168,169] The latitude and longitude values used corresponded to the city of Manaus and were -3.132° and -60.01° respectively. The time of day was kept at 16:00 local time.

These models are designed for comparison between one another to gain insight into the impact of changes in NO_x and O_3 on organonitrate concentration. The models show the concentrations at steady-state for the provided photolysis conditions, chemistry, and dilution rate, which is in contrast to the constantly changing photolysis and dilution encountered under ambient conditions. However, Section 3.3 illustrates that the conclusions made in this paper are applicable to the Beijing

afternoon conditions being investigated and that the conclusions are robust to changes in the modelling approach.

3.2.2 Model Isopleths

Throughout this paper, the model results are investigated through the use of isopleth plots. These plots consist of the steady-state concentration of a species (or another model output such as OH reactivity) in each of the models plotted as a coloured circle at the corresponding position on a set of NO_x-O_3 axes. The colour scale is indicated by a colour bar placed alongside each set of axes and will be a different scale for each plot. A continuous colour gradient is then overlaid on the axes by interpolation over a triangular grid of the model points. 10 contour lines are also drawn over the top of each plot to highlight the contour shape. These lines are equally spaced in the coloured dimension (e.g. species concentration), meaning close vertical lines would correspond to a strong sensitivity to changes in O_3 and close horizontal lines would correspond to a strong sensitivity to changes in NO_x.

3.2.3 Volatility Calculations

Section 3.9 makes use of the vapour pressure (often expressed as a log value to the base of 10) to investigate the potential contributions to SOA. The UManSysProp facility was used to do this.[170] UManSysProp can estimate the vapour pressure of compounds represented as SMILES strings via a range of different group contribution methods. [171,172] This work used predictions at 298 K throughout and used the 'evaporation' technique, though sensitivity to all of the available prediction methods is described in Section 3.9.

3.3 Model Validation

As a test of the ability of the steady-state models to represent conditions present under ambient scenarios, the model results were compared to measurements collected in the summer of 2017 in Beijing. [51,66,125,126,145,146] The NO_x mixing ratios measured in the afternoon periods in Beijing ranged between 5 ppb and 20 ppb, and O_3 mixing ratios ranged from around 60 ppb to 140 ppb. Isoprene mixing ratios ranged up to around 2 ppb in the afternoon period, hence a typical value of 1 ppb was chosen for the steady state models. The concentration isopleths for inorganic species zoomed in to this representative range of O_3 and NO_x mixing ratios are provided in Figure 3.7 and Figure 3.9.

Measurements of OH reactivity (k_{OH}) during the afternoon period were between around 10 s^{-1} and 30 s^{-1} [146], which the models reproduced at the appropriate NO_x and O_3 mixing ratios by design due to the additional methane included in the model run for this purpose (Figure 3.4a). The modelled NO_3 reactivity (k_{NO3}) is around 0.4-1.9 s^{-1} compared to the estimated value of around 0.5 s^{-1} presented in Hamilton *et al.* (Figure 3.4b). [51]. k_{OH} and k_{NO3} values at a wider range of NO_x and O_3 mixing ratios is provided in Figure 3.5.

In the NO$_x$-O$_3$ space corresponding to typical Beijing afternoon conditions, the models show NO mixing ratios of around 0.3-2.8 ppb (Figure 3.6a, Figure 3.7a), consistent with the low-NO observations in the afternoon period in Beijing with observed mixing ratios of around 0.25 ppb and 3 ppb. [66] The models show NO$_3$ mixing ratios of 0.4 to 2 ppt (Figure 3.8a, Figure 3.9a), which is slightly below the measured NO$_3$ mixing ratio in the afternoon of around 2 ppt. [51] The modelled OH concentrations are between 2.5×10^6 and 6.5×10^6 molecules cm^{-3} (Figure 3.8b, Figure 3.9b), which is slightly below the measured concentrations of around 7.5×10^6 molecules cm^{-3}. HO$_2$ is also reasonably predicted with a range between 4.2×10^8 and 9.1×10^8 molecules cm^{-3}, compared to measurements of around 2.5×10^8 molecules cm^{-3} (Figure 3.8c, Figure 3.9c). [146]
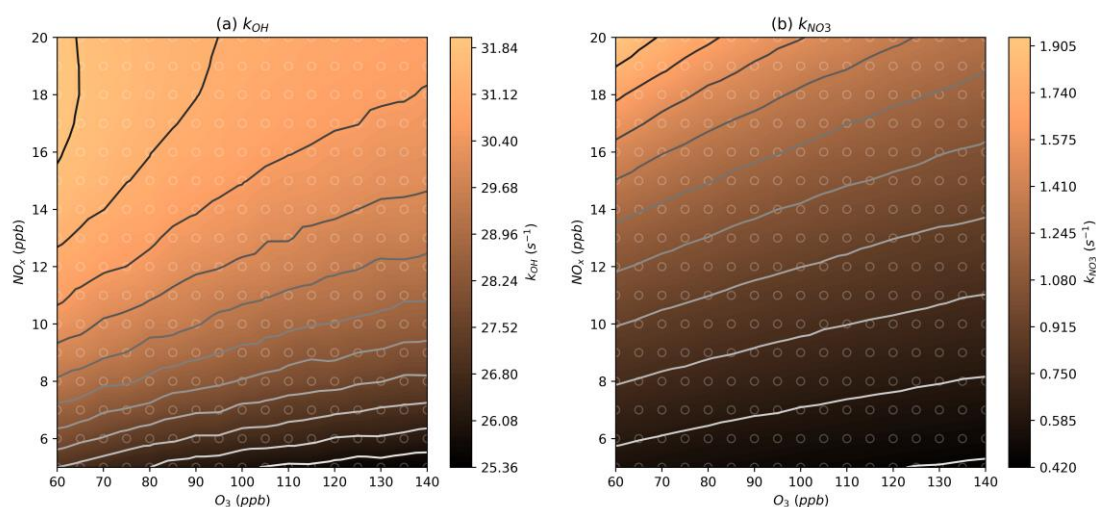
Figure 3.4. Modelled steady-state kOH and kNO$_3$ values at different NO$_x$ and O$_3$ mixing ratios. Further details on interpreting these plots is given in Section 3.2.2.
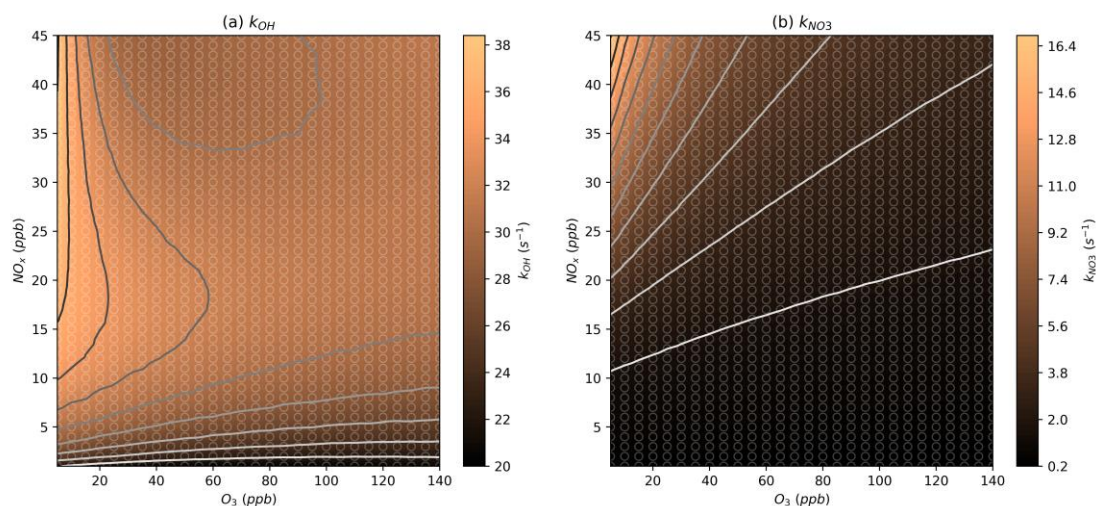
Figure 3.5. Modelled steady-state k$_{OH}$ and k$_{NO3}$ values at a wider range of NO$_x$ and O$_3$ mixing ratios.
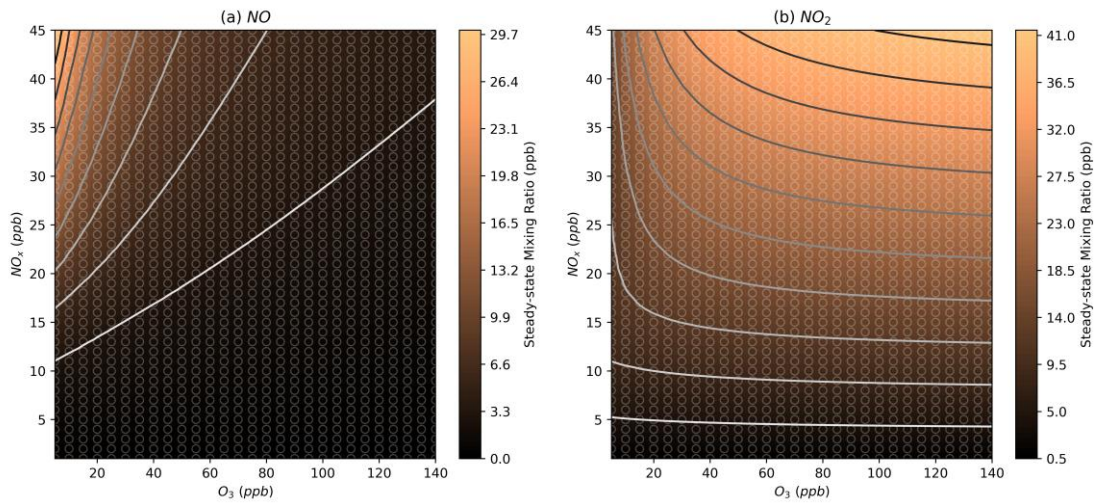
Figure 3.6. Modelled steady-state mixing ratios of NO and NO₂ at different NOₓ and O₃ mixing ratios. Further details on interpreting these plots is given in Section 3.2.2.
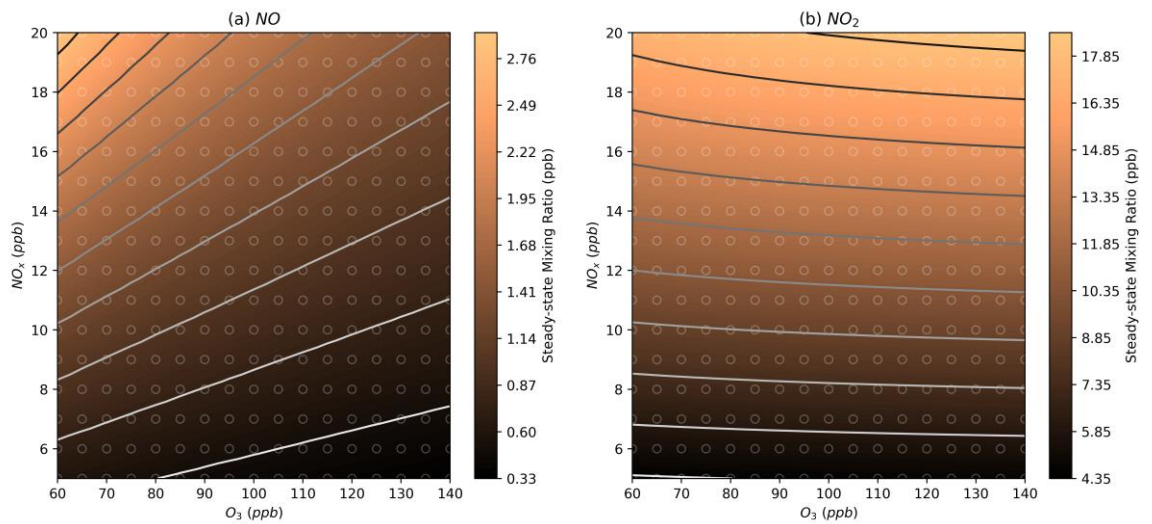
Figure 3.7. Modelled steady-state mixing ratios of NO and NO₂ at NOₓ and O₃ mixing ratios representative of those observed during the Beijing 2017 campaign.
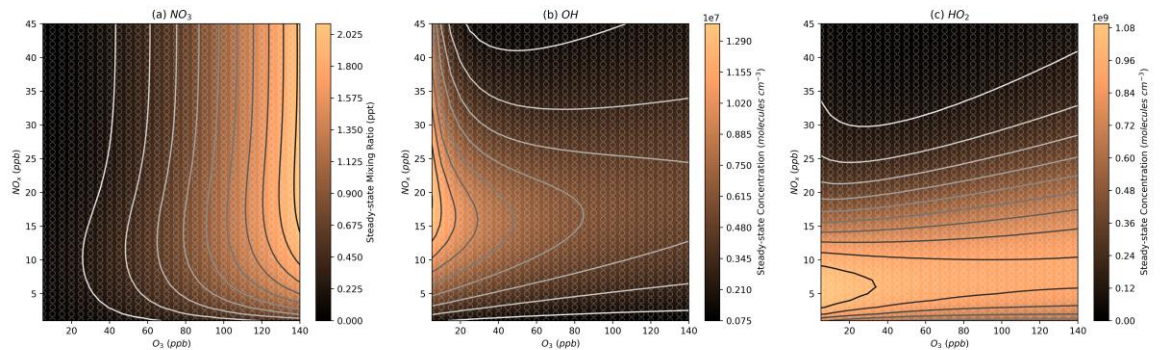
Figure 3.8. Modelled steady-state concentrations of NO₃, OH, and HO₂ at different NOₓ and O₃ mixing ratios. Further details on interpreting these plots is given in Section 3.2.2.
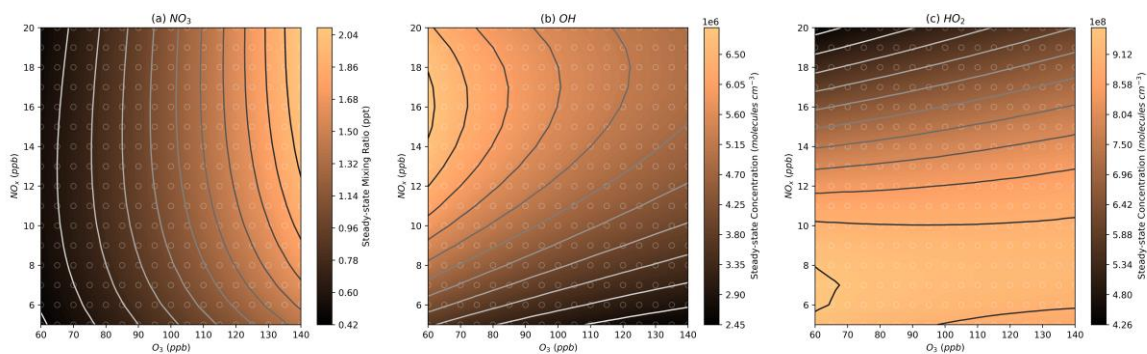
Figure 3.9. Modelled steady-state concentrations of NO₃, OH, and HO₂ at NOₓ and O₃ mixing ratios representative of those observed during the Beijing 2017 campaign.
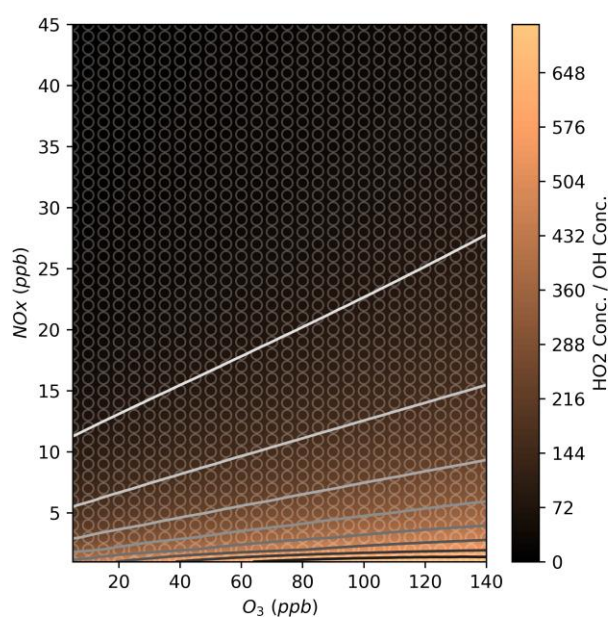
Figure 3.10. Modelled steady-state HO2 concentrations divided by OH concentrations at NOₓ and O₃ mixing ratios representative of those observed during the Beijing 2017 campaign.

A series of sensitivity tests were carried out in order to assess the sensitivity of our conclusions to changes in model parameters. Four different parameters were adjusted: the concentration of isoprene, the concentration of methane, the dilution rate, and the time of day. These sensitivity tests were found to have little impact on the conclusions drawn in this work, and any potential impacts are discussed where required. Further details on tests is provided in Section 3.4.

3.4 Sensitivity Tests

Figure 3.11 and Figure 3.12 show the isopleths for each organonitrate group investigated in this work under a lower isoprene mixing ratio of 0.5 ppb and a higher isoprene mixing ratio of 3 ppb. Increasing the isoprene mixing ratio has three effects: the absolute concentration of isoprene oxidation products increases for a given model run; the peak concentrations of IHN and other OH-

initiated products occurs under higher NO$_x$ conditions; the transition from NO$_x$-sensitive to O$_3$-sensitive regions in NO$_3$-initiated species occurs more gradually over a broader range of NO$_x$ mixing ratios. These effects are explained later in this section. The shape of the isopleths, and hence the conclusions drawn regarding changes in O$_3$ and NO$_x$ concentrations, are consistent despite changing isoprene concentrations, and a discussion of the impact of changing isoprene concentrations on organonitrate concentrations will be included where necessary throughout the paper.
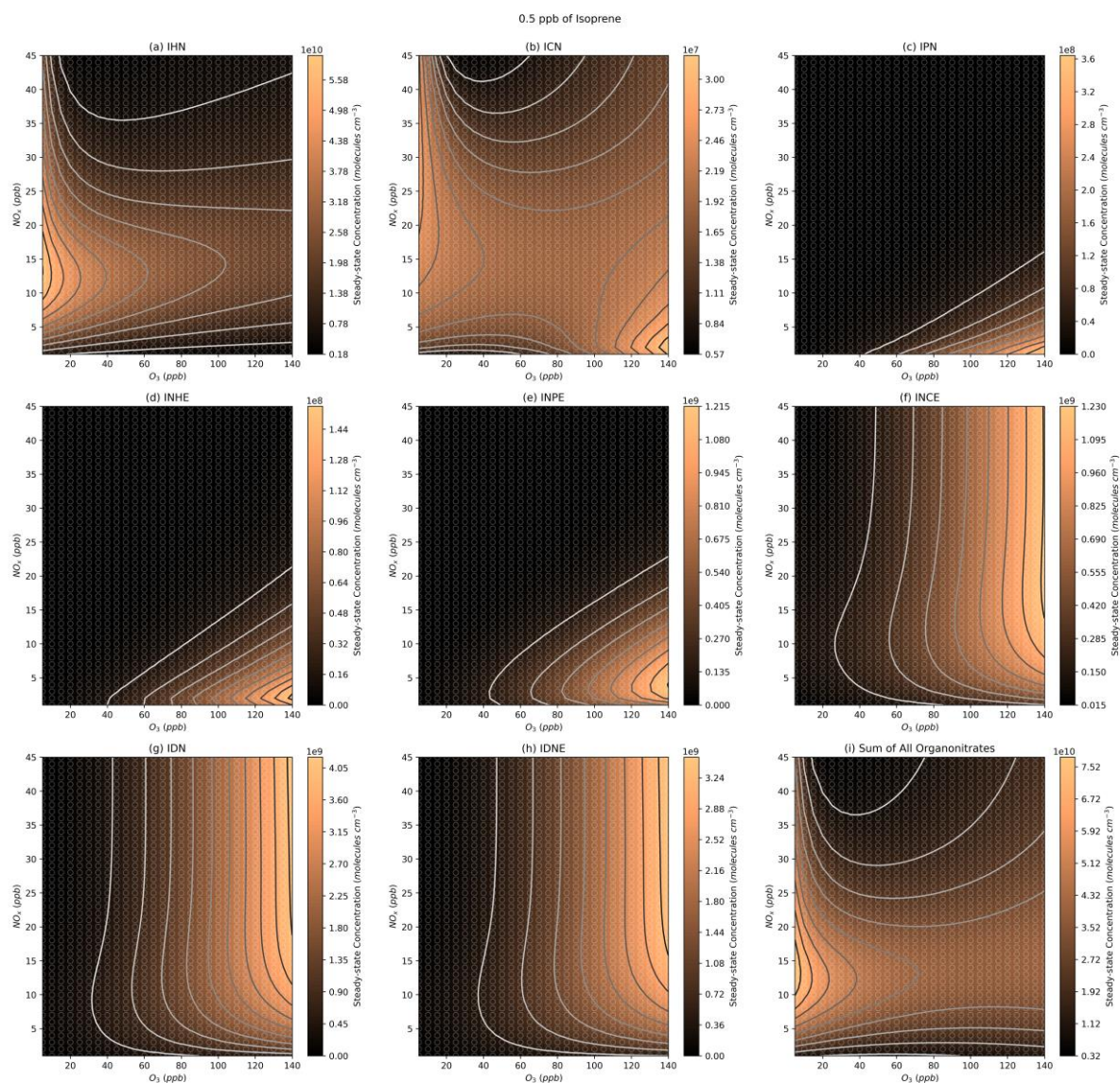
Figure 3.11. Modelled steady state organonitrate concentrations at the lower isoprene mixing ratio of 0.5 ppb.
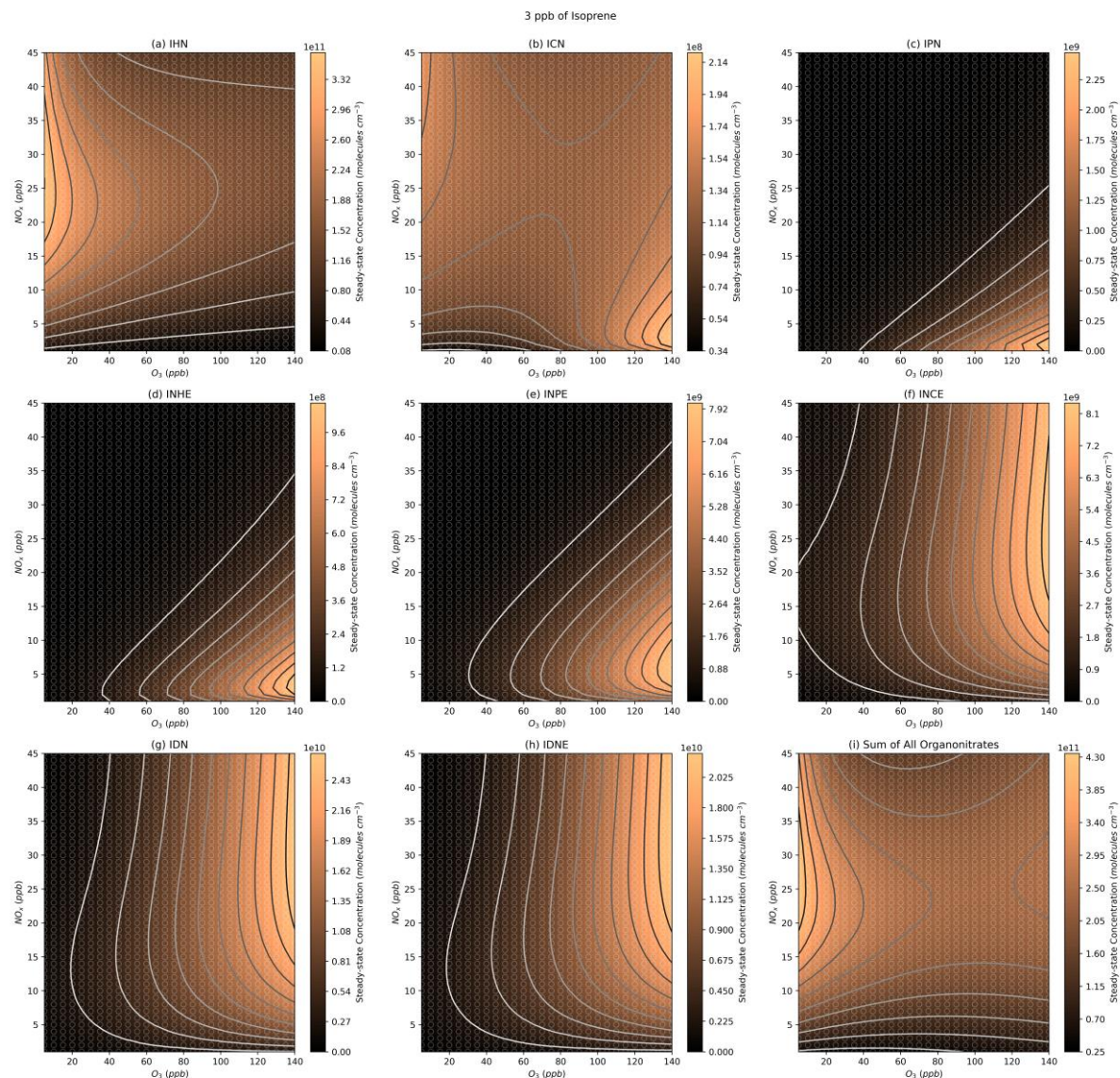
Figure 3.12. Modelled steady state organonitrate concentrations at the higher isoprene mixing ratio of 3 ppb.

Methane was added to the model in order to account for additional reactivity which would be provided by other VOCs under ambient conditions. The mixing ratio of methane in the models was halved and doubled in two tests (41 ppm and 164 ppm respectively), and the results are shown in Figure 3.13 and Figure 3.14. The effect of increasing methane in the models on the shape of the concentration profiles is similar to the effect of increasing isoprene concentrations, though the absolute peak concentrations of the isoprene oxidation products does not change significantly. Higher methane concentrations result in the peak concentrations of OH-initiated products occurring at higher NO$_x$ mixing ratios and also the broadening of the transition between NO$_x$-sensitive and O$_3$-sensitive regions in NO$_3$-initiated products.
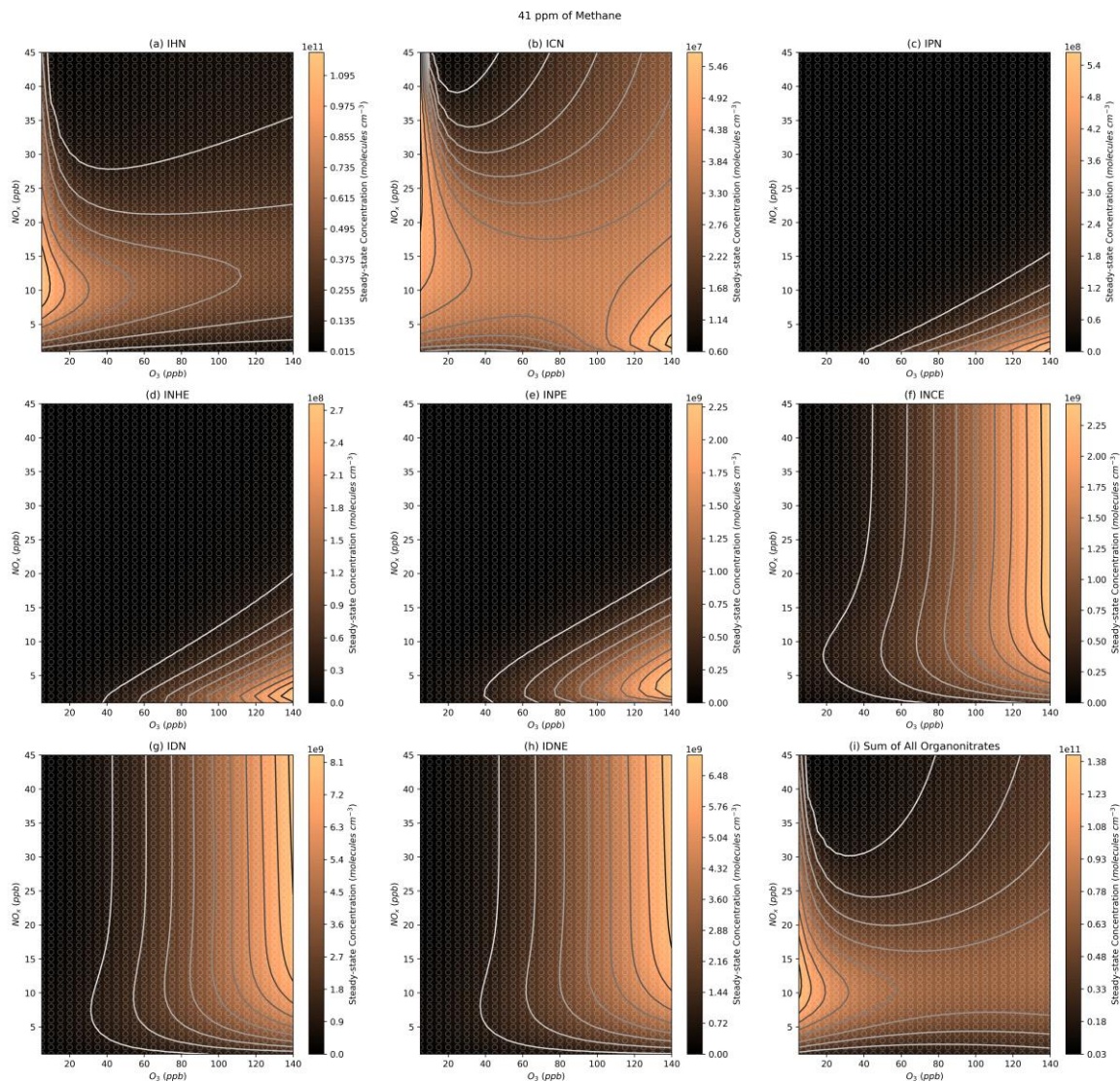
Figure 3.13. Modelled steady state organonitrate concentrations at the lower methane mixing ratio of 41 ppm.

For OH, the higher VOC concentrations mean that more NO_x is required to produce the same amount of OH at a given O_3 to compensate for the increased conversion of OH to HO_2 (Figure 3.15).

Similarly, for a given pair of O_3 and NO_x concentrations, the NO_3 concentrations will be higher at a higher NO_2/NO ratio due to higher formation from the NO_2+O_3 reaction as well as lower loss from the NO_3+NO reaction. In these models, the NO_2/NO ratio is largely dictated by HO_2 and O_3 concentrations. Since O_3 is held constant and HO_2 concentrations are low at high NO_x concentrations (Figure 3.8c), the NO_2/NO ratio is constant for a given O_3 concentration at high NO_x (Figure 3.16). There is an increase in NO_2 at low-NO_x where HO_2 concentrations are important for converting NO to NO_2. The NO_3 profile corresponds to this NO_2/NO ratio profile, with the added decrease in NO_3 concentrations at low NO_x due to the availability of NO_2 for NO_3 formation (Figure 3.8a). Therefore, when HO_2 concentrations increase due to higher VOC concentrations, the NO_2/NO ratio will increase allowing greater concentrations of NO_3.
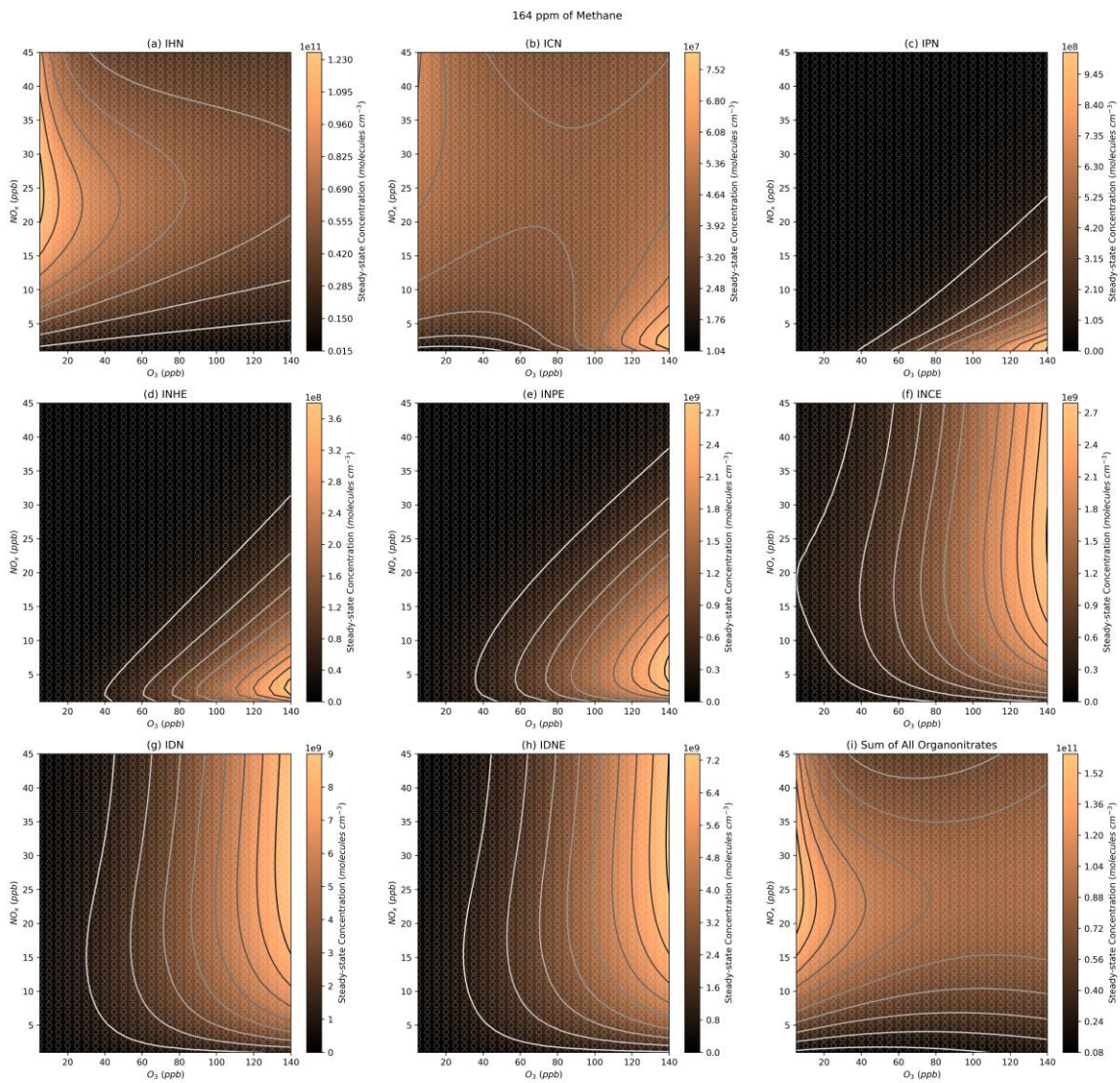
Figure 3.14. Modelled steady state organonitrate concentrations at the higher methane mixing ratio of 164 ppm.
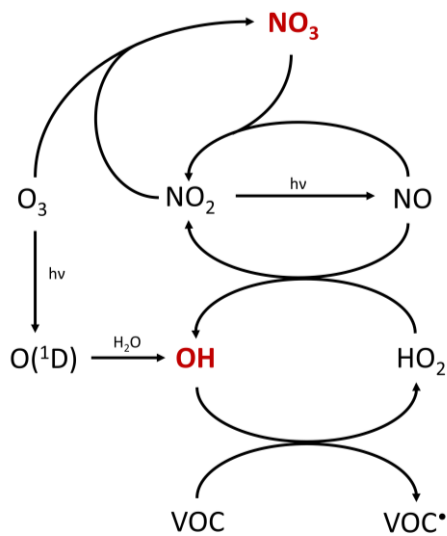
Figure 3.15. The chemical cycles controlling NO$_3$ and OH. Some reaction pathways have been omitted for clarity.
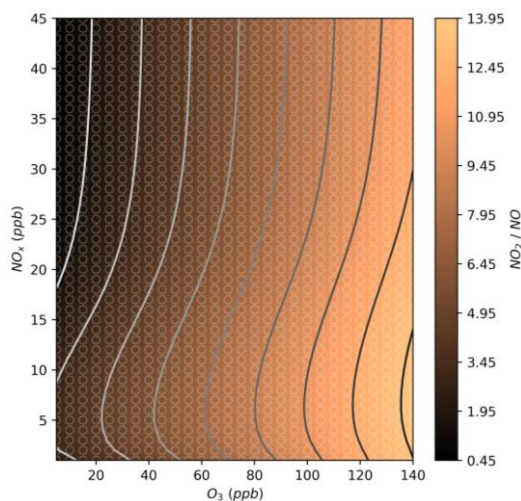
Figure 3.16. Modelled steady-state NO₂/NO ratios at a range of NOₓ and O₃ mixing ratios.

The dilution rate included in the models of 2.31×10^{-5} s^{-1} was chosen to give a lifetime with respect to dilution of 12 hours. To test the sensitivity of the results to this decision, additional models were run with dilution lifetimes of 1 hour, 6 hours, and 24 hours. When halving the dilution rate such that the lifetime with respect to dilution is 24 hours (Figure 3.17), the absolute concentrations of the organonitrates increase due to the reduction in losses. However, the profile of the isopleths does not change. Similarly, doubling the dilution rate decreases species concentrations but does not alter the isopleth profiles (Figure 3.18). Increasing the dilution rate further, resulting in a dilution lifetime of 1 hour, does skew the isopleth profiles compared to the longer lifetime models, particularly impacting OH and OH-initiated products like IHN (Figure 3.19). Despite the difference made by this extreme change, many of the conclusions made in this work would hold true with regards to the NO_x-O_3 regimes favoured by different organonitrate groups.

Although these models focus on the afternoon-period in Beijing, two separate sets of models were run under differing photolysis conditions corresponding to different times in the afternoon in Beijing, 2 hours before and after the chosen time of 16:00 local time (Figure 3.20 and Figure 3.21). The earlier time of 14:00 results in higher absolute concentrations of OH-initiated species such as IHN and slightly lower absolute concentrations of NO_3 initiated species as a result of increased NO_3 photolysis and higher NO concentrations. Despite the absolute differences in concentration, the profile of the NO_x-O_3 isopleth for each organonitrate group does not change significantly, though the impact of the NO_3-initiated organonitrates at high O_3 mixing ratios in the total organonitrate isopleth is lessened. The later time of 18:00 is entering dusk in the summer of Beijing, so the role of NO_3 chemistry is amplified and the OH chemistry is reduced. This is clear from the IHN profile which shows that the peak concentration occurs at high O_3 and NO_x, since the NO_3-initiated pathway becomes the dominant formation route. This change means that the total organonitrate isopleth shape is very different in the 18:00 model, with the highest concentrations occurring under high-O_3-high-NO_x conditions, where NO_3 is the highest. These time-of-day sensitivity tests illustrate that the conclusions made in this work are applicable during daytime photolysis conditions.
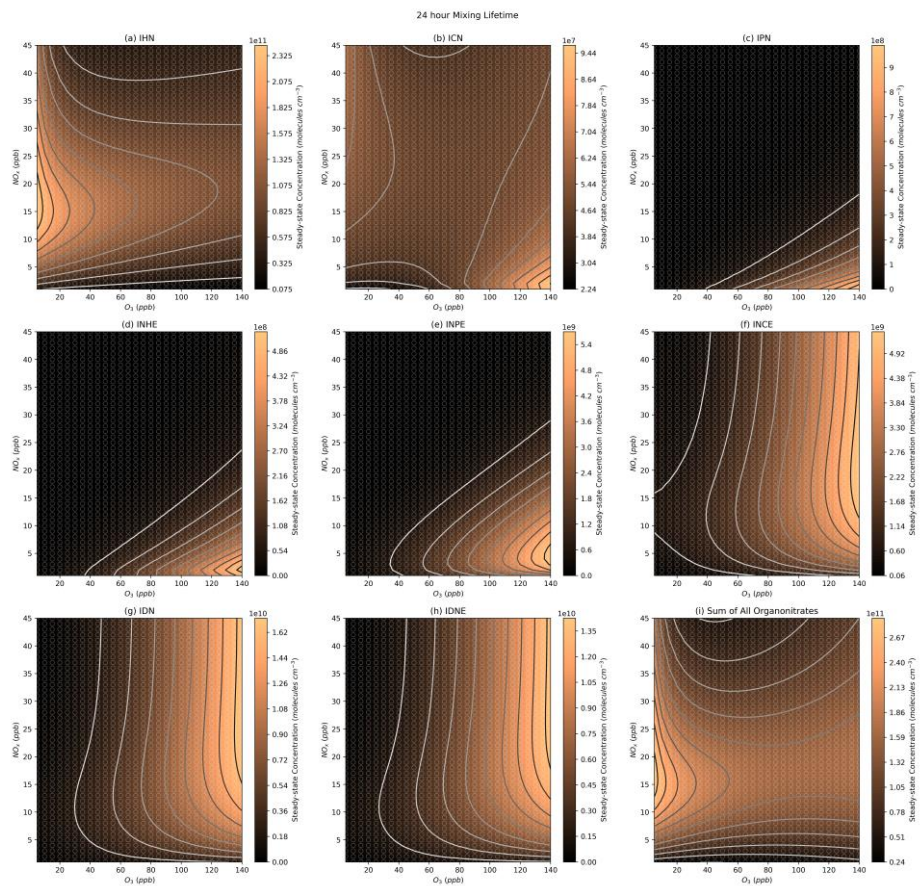
Figure 3.17. Modelled steady state organonitrate concentrations at the longer dilution lifetime of 24 hours.
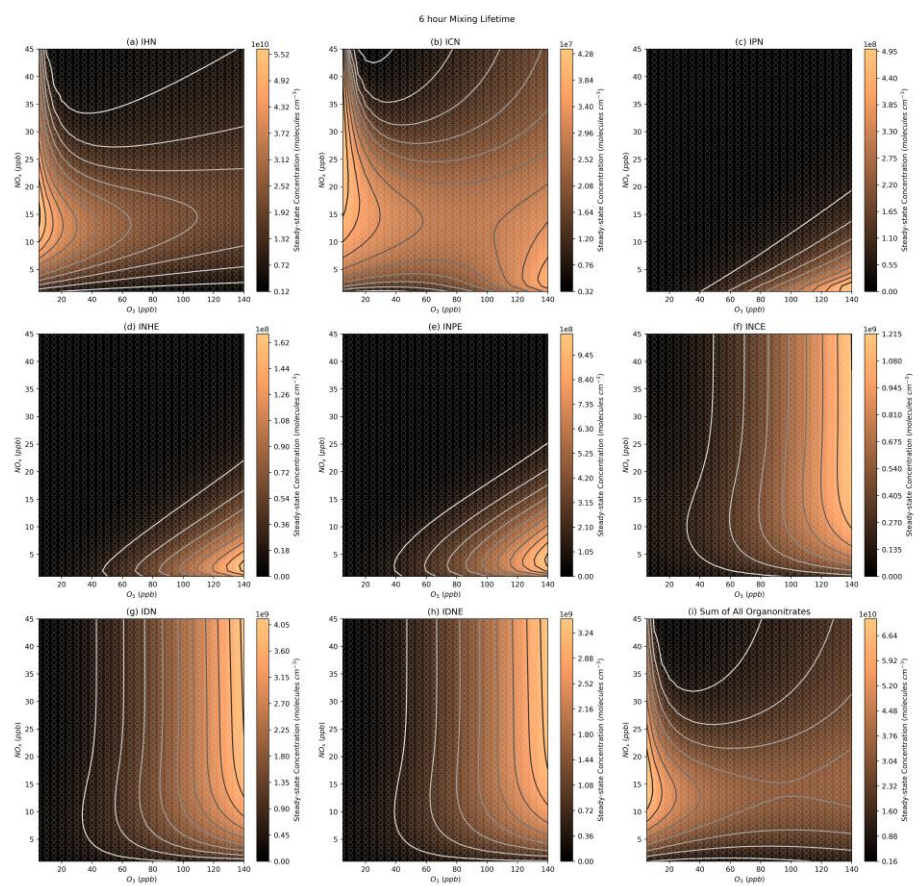
Figure 3.18. Modelled steady state organonitrate concentrations at the shorter dilution lifetime of 6 hours.
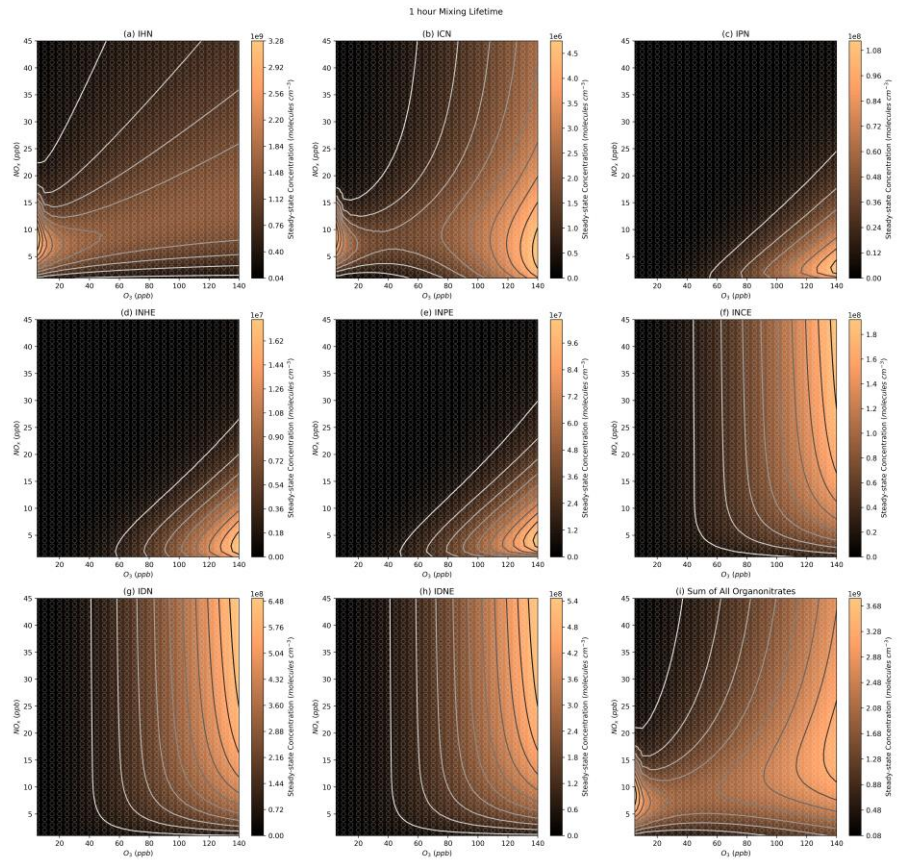
Figure 3.19. Modelled steady state organonitrate concentrations at the shorter dilution lifetime of 1 hour.
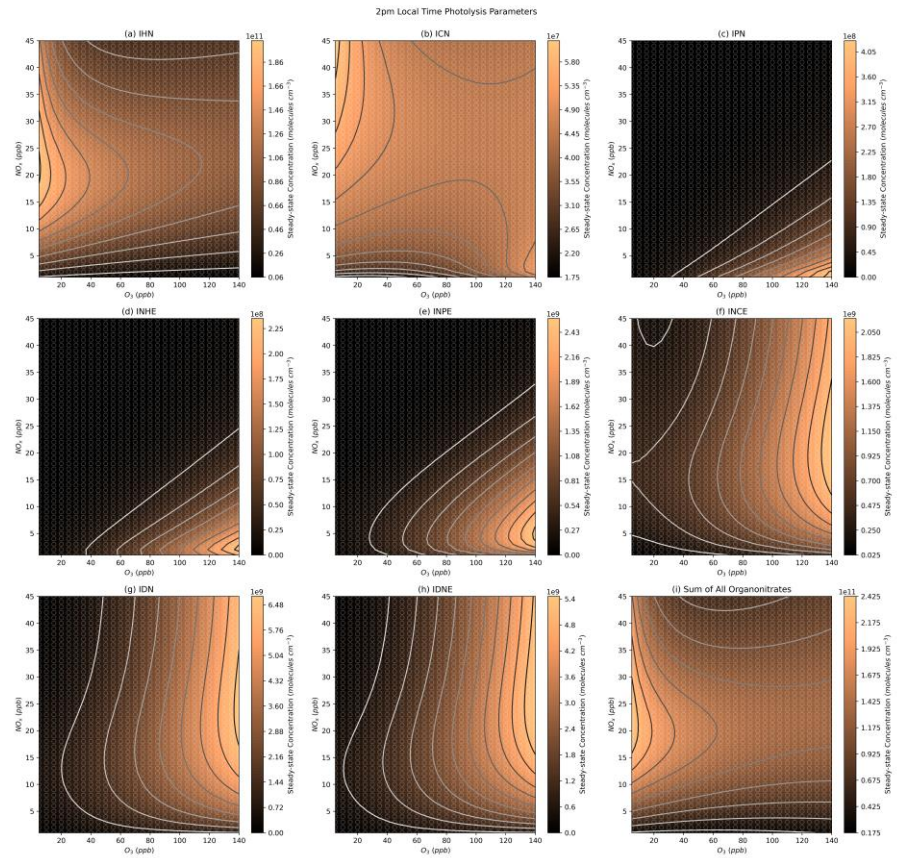
Figure 3.20. Modelled steady state organonitrate concentrations with photolysis conditions corresponding to the earlier model time of 14:00 local time.

90
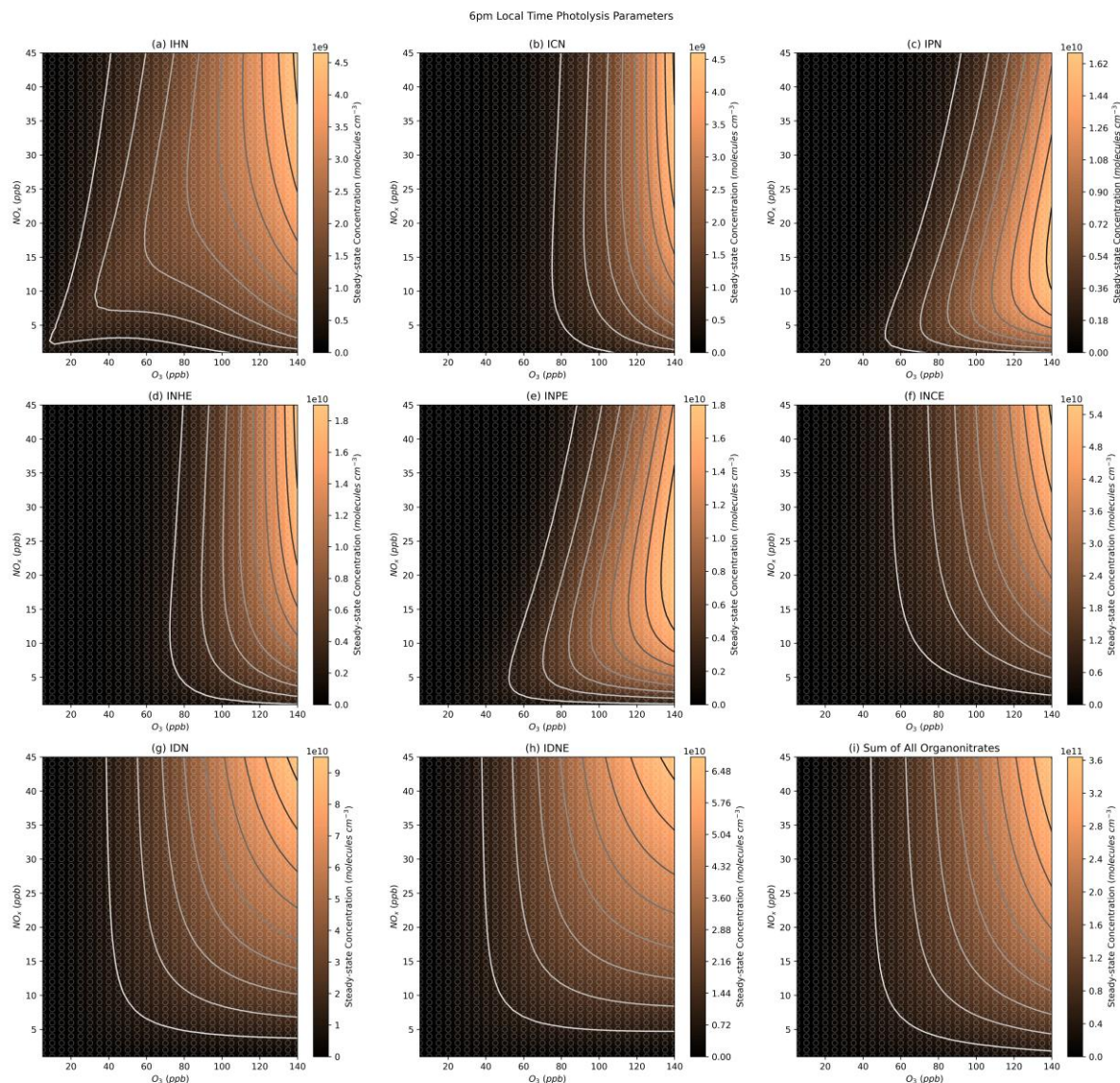
Figure 3.21. Modelled steady state organonitrate concentrations with photolysis conditions corresponding to the later model time of 18:00 local time.

3.5 Mononitrates

The IHN concentration isopleth (Figure 3.22a) shows a strong similarity to the OH isopleth (Figure 3.8b), highlighting its rapid formation from the OH oxidation of isoprene and subsequent RO_2 + NO reaction to form the nitrate group (Figure 3.1). This means that at high O_3 mixing ratios, IHN shows a strong dependence on NO_x, and the dependence on O_3 becomes more significant at lower O_3 mixing ratios.

IPN shows increasing concentrations with increasing O_3 and decreasing NO_x (Figure 3.22b). This reflects the requirement for low NO concentrations to be present for two reasons. Firstly, high NO_3 concentrations are required to form the INO_2 radical by the reaction of isoprene with NO_3. Secondly, the RO_2+HO_2 reaction is required to form the hydroperoxide group of IPN, and so lower NO concentrations will reduce competition with the rapid RO_2 + NO reaction. Additionally, HO_2

concentrations are highest under low NO_x conditions (Figure 3.8c), further favouring the $RO_2 + HO_2$ reaction.

In contrast to the other nitrated species investigated here, ICN shows two peaks in concentration, one at very low O_3 and the other at very high O_3 (Figure 3.22c). This is because ICN can be formed from many different routes. Firstly, the abstraction of an H atom from IHN which provides a formation route under lower O_3 conditions, when OH and IHN are both high in concentration. Alternatively, under higher O_3 conditions, ICN can form from the reaction of OH and IPN, or the decomposition of nitrated alkoxy radicals (INO). The result of these multiple peaks is that under moderate NO_x and O_3 conditions, the concentration of ICN is relatively insensitive to changes in both NO_x and O_3. It is also important to note that the absolute concentrations of ICN predicted to form in these models are very low (the peaks in concentration corresponding to mixing ratios of just over 1 ppt), due to low production rates, which is consistent with low daytime ICN mixing ratios previously identified in Beijing. [126,145]
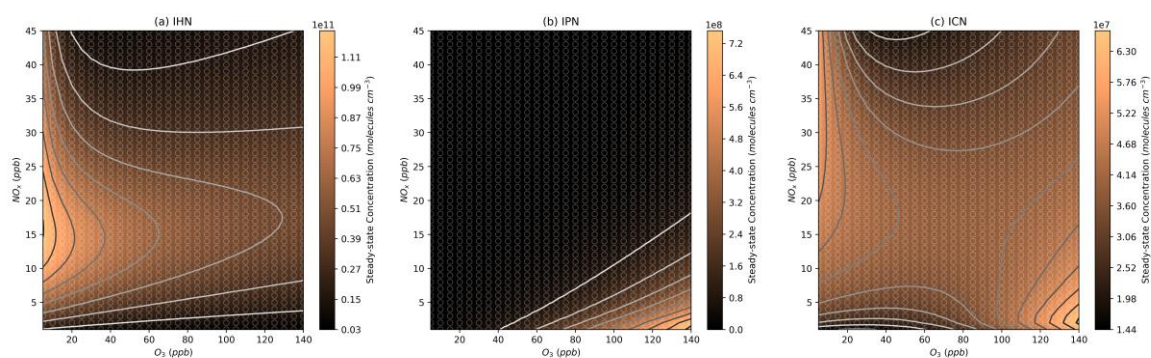
Figure 3.22. Modelled steady-state concentrations of isoprene hydroxynitrate (IHN), isoprene carbonylnitrate (ICN), and isoprene hydroperoxynitrate (IPN) at different NO_x and O_3 mixing ratios. Further details on interpreting these plots is given in Section 3.2.2.

Recent work has highlighted species with the formula $C_4H_7NO_5$ as potentially major oxidation products of isoprene. [134] Consistent with previous modelling studies [126], these models largely form $C_4H_7NO_5$ from OH-initiated oxidation, meaning the concentration isopleth is similar to that of OH and IHN.

3.6 Nitrated Epoxides

Both INHE and INPE show a similar pattern as IPN in the NO_x-O_3 isopleths (Figure 3.23a,b), with the highest concentrations occurring at low NO_x and very high O_3. INPE is reliant on high NO_3 and HO_2 in a similar manner to IPN as the RO_2+HO_2 step is still required to form INPE. While HO_2 is not required to form INHE via the alkoxy-epoxidation pathway, the formation of INHE from IPN is the major formation route under lower NOx conditions. Additionally, the alkoxy-epoxidation pathway to the formation of INHE relies on an RO_2-RO_2 cross-reaction. This cross reaction will be favoured under low-NO_x-high-O_3 conditions, where NO concentrations will be the lowest, meaning that the competition with the rapid RO_2-NO reaction is minimal. This requirement for very high O_3 and low

NO$_x$ means that we should expect very low concentrations of daytime INHE and INPE under typical urban conditions. This is consistent with modelling of Beijing which showed that while INHE may comprise a large fraction of night-time C$_5$H$_9$NO$_5$ compounds, the daytime contribution is very small.[126]
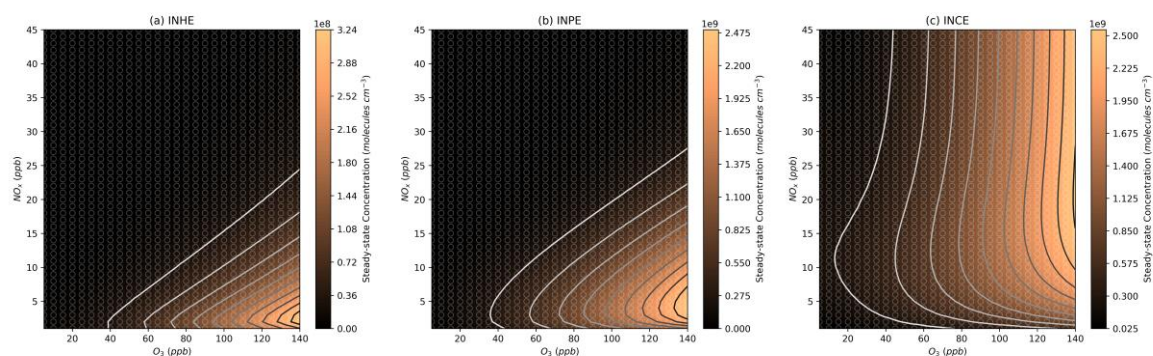
Figure 3.23. Modelled steady-state concentrations of isoprene hydroxynitrooxyepoxide (INHE), isoprene carbonylnitrooxyepoxide (INCE), and isoprene hydroperoxynitrooxyepoxide (INPE) at different NO$_x$ and O$_3$ mixing ratios. Further details on interpreting these plots is given in Section 3.2.2.

In contrast, INCE shows reasonably high concentrations under high-O$_3$ mixing ratios at a range of NO$_x$ mixing ratios. The profile of these concentrations is very similar to the NO$_3$ isopleth (Figure 3.8a), and stems from the main formation route to INCE requiring the NO$_3$ oxidation of isoprene followed by an RO$_2$ + NO reaction step. This formation route shares similarities with the dinitrates discussed in Section 3.7.

3.7 Dinitrates

As previously noted for INCE, Figure 3.24 shows that the steady-state concentrations of isoprene dinitrate (IDN) and isoprene dinitrooxyepoxide (IDNE) are very similar to the NO$_3$ concentration isopleth (Figure 3.8a). This is indicative of the formation route of IDN and IDNE, where an initial NO$_3$ oxidation is followed by the reaction of the resulting RO$_2$ with NO to form the second nitrate group (Figure 3.1 and Figure 3.3). At any daytime concentration of NO$_x$ where sufficient NO$_3$ is present to perform the initial oxidation step, there will also be sufficient NO present to rapidly react with the resulting RO$_2$. Although the high O$_3$ mixing ratios observed in Beijing result in low NO concentrations compared to typical daytime concentrations in a polluted megacity, there is still ample NO present to react with peroxy radicals produced by the initial NO$_3$ oxidation. Figure 3.24 shows that at each O$_3$ there is a critical NO$_x$ concentration, above which the concentration of IDN, IDNE, and INCE is almost exclusively controlled by O$_3$ concentrations. This critical NO$_x$ mixing ratio is reasonably low compared to typical urban NO$_x$ mixing ratios, indicating that the concentration of dinitrates in urban environments may be largely controlled by the O$_3$ mixing ratios present.
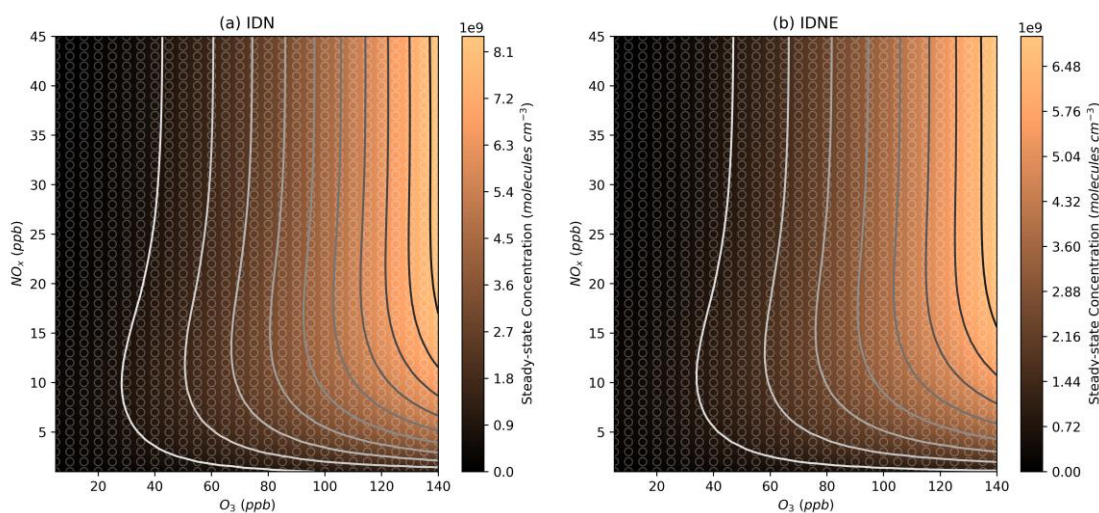
Figure 3.24. Modelled steady-state concentrations of isoprene dinitrate (IDN) and isoprene dinitrooxyepoxide (IDNE) at different NO_x and O_3 mixing ratios. Further details on interpreting these plots is given in Section 3.2.2.
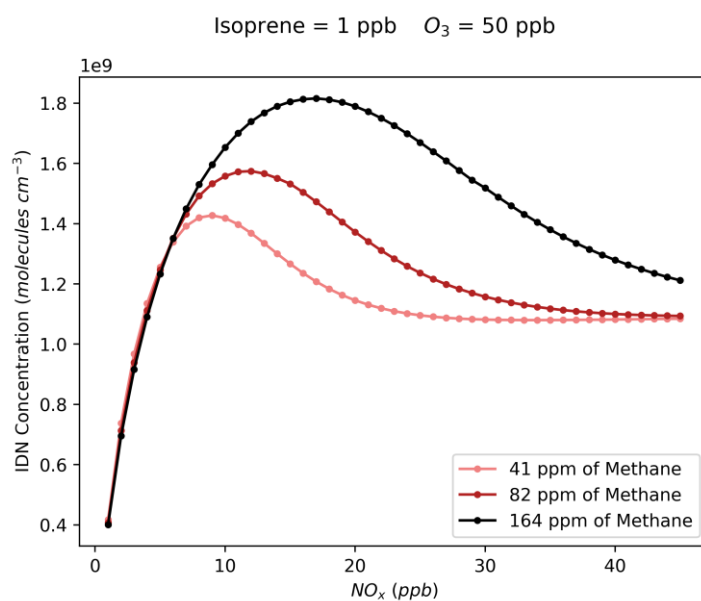
Figure 3.25. Modelled steady-state concentrations of IDN with changing NO_x in models runs with 50 ppb of O_3 and different mixing ratios of NO_x and additional methane.

These dinitrate species do not have any chemical losses in the FZJ mechanism, meaning that their loss is controlled by the dilution reaction which is constant across all NO_x and O_3 concentrations. This means that the steady-state concentrations of IDN and IDNE are controlled by the formation from INO_2 + NO reactions. Since NO concentrations are much higher than INO_2 concentrations across the isopleth, the rate of this reaction will be controlled by the availability of INO_2. Furthermore, since isoprene concentrations are held constant, the formation of INO_2 will be controlled by NO_3. As discussed in Section 3.4, increasing the total VOC in the model results in a broadening in the NO_x axis of the transition between NO_x and O_3 sensitive regimes for NO_3, and so the same applies to IDN, IDNE, and INCE. For a fixed ozone concentration, increasing the NO_x from 0 will increase IDN, IDNE, or INCE concentrations due to the increased NO_3 resulting from the increased availability of NO_2 (Figure 3.25). Then, once the threshold NO_x concentration is reached

94

and NO_3 concentrations are not limited by the availability of NO_x, the concentration becomes controlled by O_3 and HO_2 (Section 3.4) creating the "hump" in concentration which then stabilises as HO_2 concentrations begin to decrease at high NO_x and the NO_2/NO ratio becomes increasingly controlled by the fixed O_3 concentration. This means that with high VOC concentrations, at a given O_3 concentration, reductions in NO_x will result in increased IDN, IDNE, or ICNE concentrations sooner than under lower VOC conditions.

3.8 Total Organonitrates

By summing the model concentrations for all organonitrates present in the mechanism, an isopleth of total organonitrates was obtained (Figure 3.26). This shows a band of high organonitrate concentrations at moderate NO_x. At high O_3, further changes to O_3 have little effect on the total organonitrate concentration. Total organonitrates also become less sensitive to changes in NO_x in this high-O_3 region. This band is the result of organonitrates produced by OH and NO_3 oxidation of isoprene. At low O_3 mixing ratios, the total organonitrates are dominated by OH-initiated species such as IHN (Figure 3.22a). Conversely, at high O_3 mixing ratios, NO_3-initiated species such as IDN comprise a larger fraction of total organonitrates (Figure 3.24a). This is illustrated in the pie charts in Figure 3.26 which show the organonitrate composition under different NO_x-O_3 regimes.
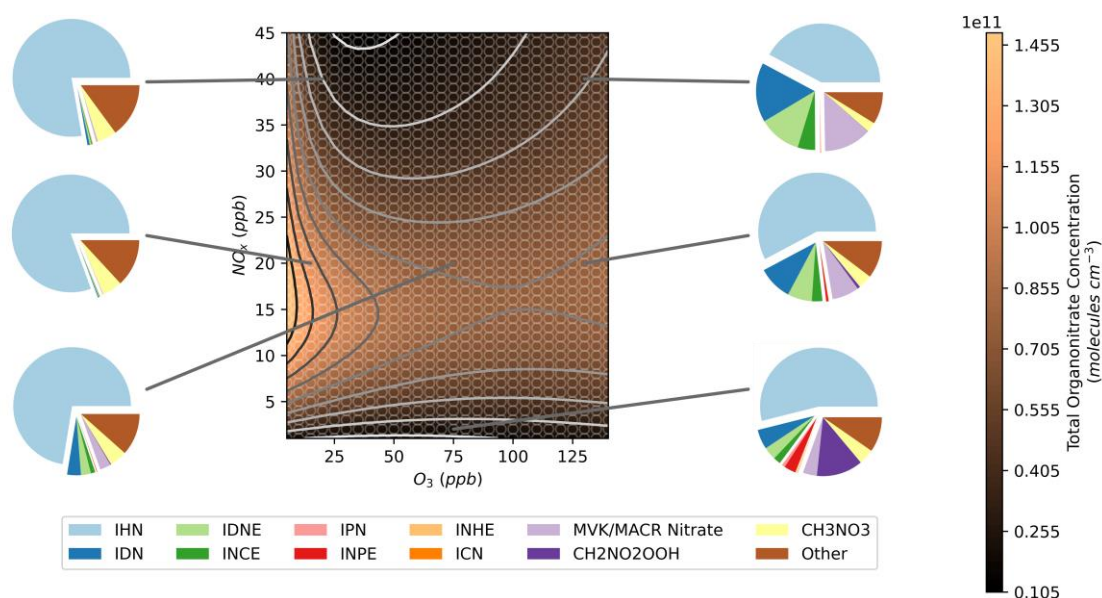
Figure 3.26. Modelled steady-state concentrations of the total organonitrates at different NO_x and O_3 mixing ratios along with the composition of the total organonitrates at selected NO_x and O_3 mixing ratios. Further details on interpreting these plots is given in Section 3.2.2.

The composition breakdown also reveals that total isoprene organonitrates are dominated by IHN under most conditions, but this fraction decreases as ozone mixing ratios increase. At higher O_3, a large fraction of the composition comes from IDN, IDNE, and INCE due to their higher concentrations under high-O_3 conditions (Section 3.6 and Section 3.7). CH3NO3 comprises a substantial fraction of total organonitrates in these models. CH3NO3 can be formed by the OH oxidation of methane via the methylperoxy radical, and so its concentrations in these models are

exaggerated due to the large amounts of methane added to the model. Formation from the OH oxidation of methane comprises the majority of all of the methylperoxy formation in all of the models, excluding formation from the reversible decomposition of methane peroxynitrate (CH3O2NO2) which is balanced by the opposing formation reaction. CH2NO2OOH is also listed in Figure 3.26. CH2NO2OOH is formed from the products of isoprene ozonolysis, explaining the higher concentrations under high-O_3 conditions. There are no chemical losses in the mechanism for CH2NO2OOH, which likely explains the high contribution to total organonitrates. The remaining portion of "other" organonitrates corresponds to a wide range of species, none of which contribute more than 6% to the total organonitrate sum in any models.

As noted in Section 3.4, changing the VOC concentration effects the position in NO_x-O_3 space where the maximum organonitrate concentrations are observed. In the case of total organonitrates, decreasing the total VOC concentration results in the band of high concentrations moving to lower NO_x. Figure 3.13 and Figure 3.14 show that with lower methane concentrations in the model, the peak organonitrate concentrations occur at around 12 ppb of NO_x whereas this increases to around 25 ppb of NO_x in the high methane case. The peak organonitrate concentrations at each of these NO_x concentrations are similar in each of these sets of model runs.

3.9 Volatility Assessment

One of the major motivations for studying isoprene nitrates is their potential to contribute to secondary organic aerosol (SOA) by condensation or reactive uptake to existing particles. While the highest concentration species such as IHN and IDN may be most significant when considering the role of isoprene nitrates as NO_x reservoirs, low concentration species can be much more important for SOA formation if they are of a sufficiently low volatility. As an estimation of the impact of changing NO_x and O_3 on particle-phase processes, the log of the vapour pressure was estimated for each organonitrate in the mechanism based on the species' structure using UManSysProp.[170] As a measure of a compound's volatility, a lower vapour pressure value corresponds to a less volatile compound which will more readily partition into existing particles. This volatility-based approach does not account for potential reactive uptake which is likely to be important for the epoxide species previously discussed.

Figure 3.27 shows the total organonitrate plot normalised to the vapour pressure value for each compound, which gives an estimation of the contribution of organonitrate uptake to SOA at each NO_x and O_3 mixing ratio. Since the predicted vapour pressures range over 10 orders of magnitude, lower volatility species can have a large effect on SOA formation despite their much lower concentration. The lowest vapour pressures predicted here are for the two MCM species NC524NO3 and NC524OOH. These two compounds comprise almost 100% of the normalised concentration in Figure 3.27 under all NO_x and O_3 conditions, and their individual concentration profiles can be seen in Figure 3.29. The concentration isopleths for the 15 lowest volatility

compounds are shown in Figure 3.28. Many of these species show profiles similar to that of NC524OOH, with the highest concentrations occurring at low urban NO_x concentrations.

According to Figure 3.27, reductions in NO_x from typical urban conditions would result in higher normalised concentrations of organonitrates, meaning the contribution of isoprene nitrates to SOA may increase with decreasing NO_x until very low urban NO_x conditions are met. However, it is important to note the difficulty in representing the lowest volatility species in the isoprene oxidation mechanism. Many of these species are the product of multiple oxidation steps with large uncertainties surrounding their rates of formation. Additionally, many of the lowest volatility species do not contain any chemical losses in the mechanism due to a lack of information on their reactions.

The low predicted volatilities of NC524NO3 and NC524OOH are the result of the many functional groups present in the molecules. Similarly oxidised species could be described as highly oxidised molecules (HOMs). [89] The chemistry of HOMs is not currently well represented in many mechanisms due to their varied autooxidation formation pathways. For example, the profile of NC524OOH concentrations in Figure 3.29b results from the requirement of HO_2 to form the hydroperoxide group, hence the profile is similar to that of HO_2. If an RO_2 H-shift formation pathway to NC524OOH, or similar HOMs, were included in the mechanism, then this might alter the profile in Figure 3.27.[173] It should be expected that the formation of HOMs would be sensitive to changes in ozone as the lower NO concentrations at higher ozone will reduce the competition of the RO_2+NO pathway with the RO_2 autooxidation reactions that form HOMs. Inclusion of improved autooxidation chemistry in the mechanisms would also increase the number of low volatility compounds produced from the oxidation of isoprene.
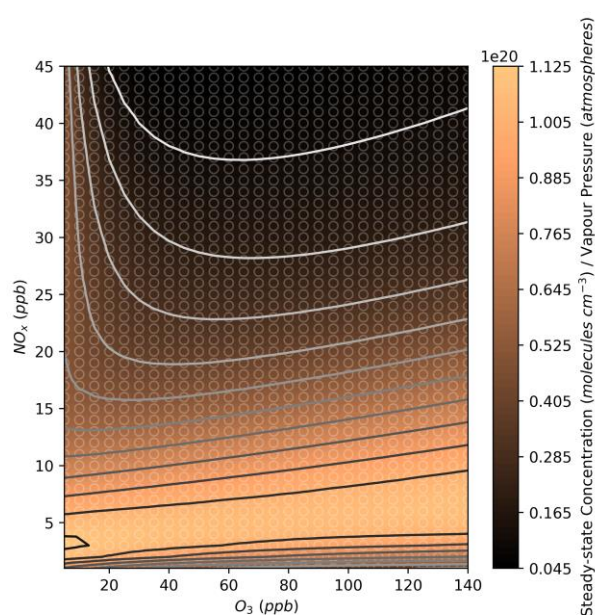
Figure 3.27. Modelled steady-state concentrations of the total organonitrates normalised to each compound's estimated vapour pressure at different NO_x and O_3 mixing ratios. Further details on interpreting these plots is given in Section 3.2.2.
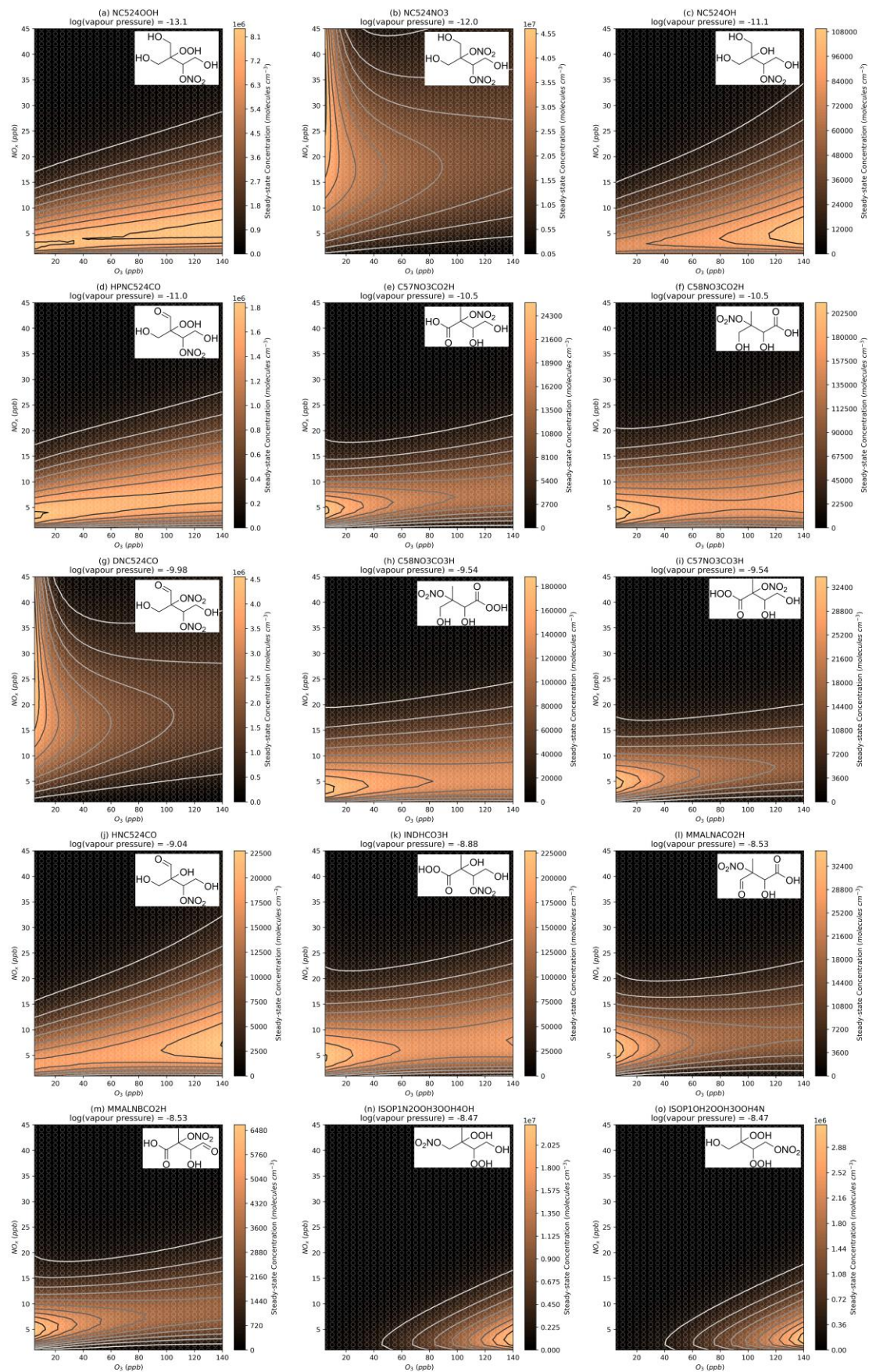
Figure 3.28. Modelled steady state concentrations of the 15 lowest volatility compounds at different NO$_x$ and O$_3$ mixing ratios.
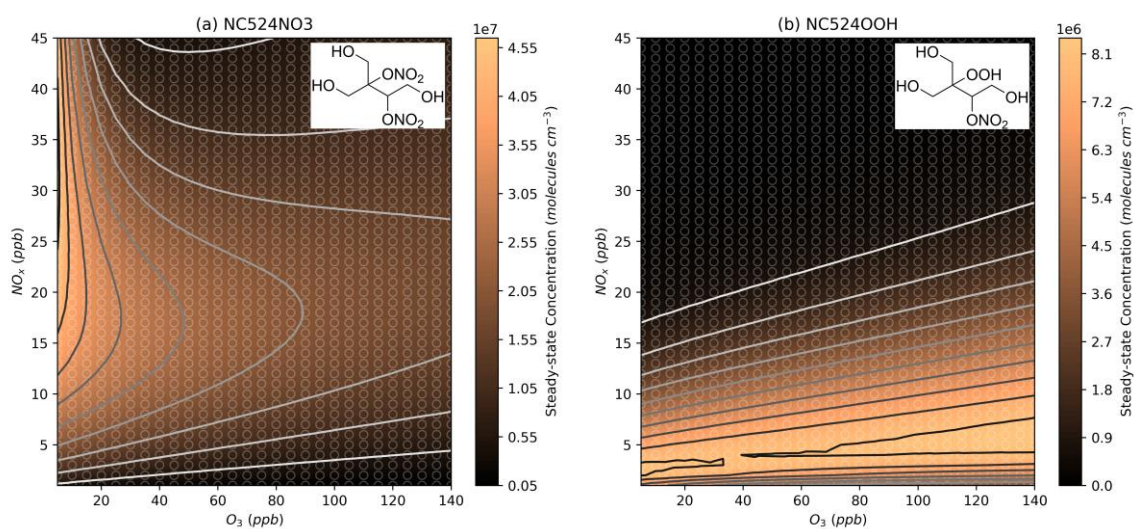
Figure 3.29. Modelled steady-state concentrations of the MCM species NC524NO3 and NC524OOH at different NO_x and O_3 mixing ratios. Further details on interpreting these plots is given in Section 3.2.2.
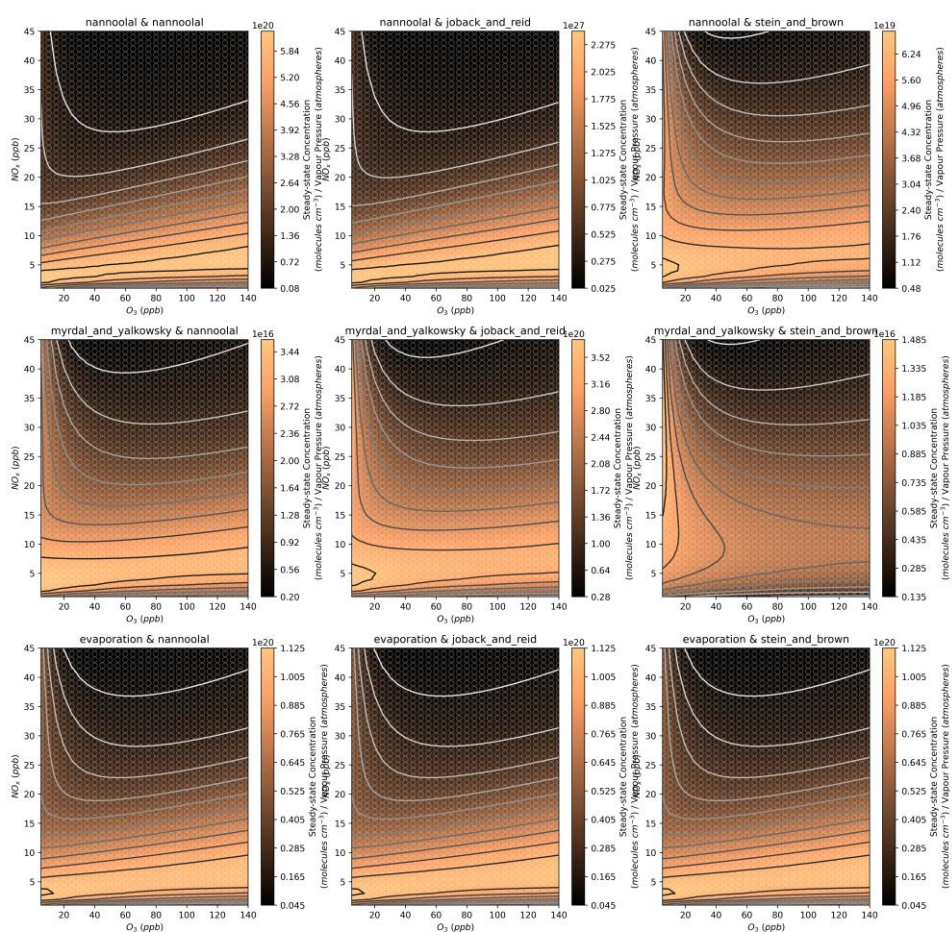
Figure 3.30. Modelled steady-state concentrations of the total organonitrates normalised to each compound's estimated vapour pressure at different NO_x and O_3 mixing ratios using each combination of vapour pressure and boiling point methods available through the UManSysProp API.

99

Figure 3.30 shows that the results presented here are reasonably insensitive to the choice of vapour pressure and boiling point prediction methods selected within UManSysProp. Section 3.9.1 also outlines the results using an alternative volatility estimation method, making use of only the molecular formula of each compound.

3.9.1 Saturation Concentration

As an alternative to the compound vapour pressures used previously, the saturation concentration (expressed as a log value, $\log_{10}(C_{Sat})$)) was estimated in order to assess the impact of changes in NO_x and O_3 on SOA. The method for estimating $\log_{10}(C_{Sat})$ is taken from Mohr *et al.* 2019, and uses Equation 1 to estimate $\log_{10}(C_{Sat})$ based on the molecular formula of each compound. n_C, n_N, and n_O are the number of carbon, nitrogen, and oxygen atoms respectively. b_C, b_O, b_{CO} and b_N are 0.475, 0.2, 0.9, 2.5 respectively. [160,174]

$$\log_{10}(S_{sat}) = (25 - n_C)b_C - (n_O - 3n_N)b_O - 2\frac{(n_O - 3n_N)\,n_C}{n_C + n_O - 3n_N}b_{CO} - n_N b_N \qquad Equation\ 1$$
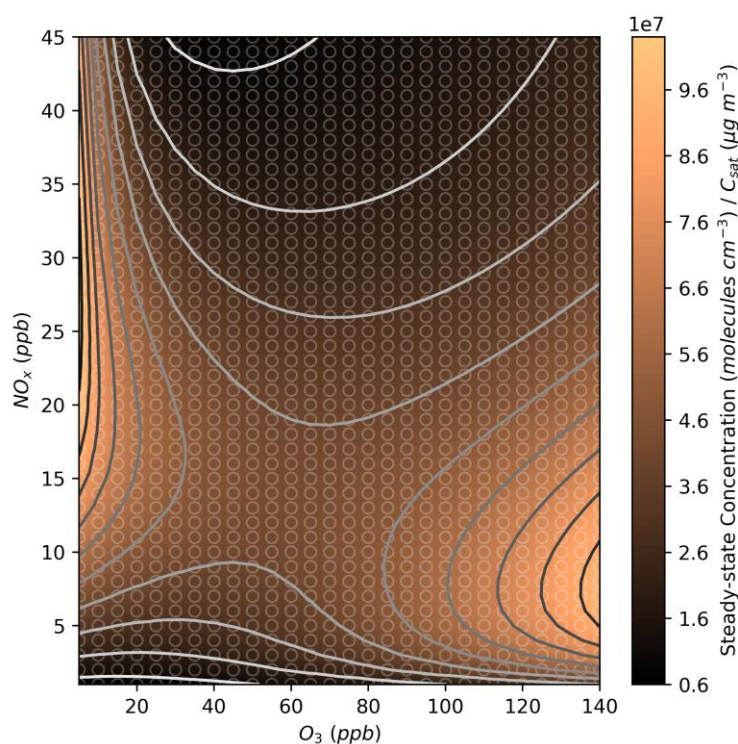
Figure 3.31. Modelled steady-state concentrations of the total organonitrates normalised to each compound's estimated saturation concentration at different NO_x and O_3 mixing ratios.

This method does not account for the structure of each individual compound, hence the use of UManSysProp previously, but is presented here as an alternative method due to the different profile in Figure 3.31 compared to Figure 3.27. Figure 3.31 shows two peaks in normalised concentration, one at low O_3 and one at high O_3, in a similar fashion to the total organonitrate plot in Figure 3.27. However, due to the lower volatilities of the species formed under high O_3, the two

normalised concentration peaks are of a similar magnitude in Figure 3.31. This means that, depending on the initial position in NO_x-O_3 space, reductions in either NO_x or O_3 may result in increases in organonitrate SOA.

3.10 Accounting for Isoprene Flux

The use of constant isoprene concentrations in these models means that as oxidant concentrations change, the amount of isoprene reacting with oxidants to form the products of interest changes. Figure 3.32 shows the loss rate of isoprene to reaction with OH, NO_3, and O_3, as well as the total loss of isoprene, across the range of NO_x and O_3 mixing ratios. This shows that reaction with OH always dominates the loss of isoprene, which is consistent with the oxidation occurring under daylight conditions, when OH concentrations are high. The isopleths for the loss of isoprene to reaction with OH and NO_3 match the concentration isopleths for species controlled by the availability of OH and NO_3, for example, IHN and IDN respectively.
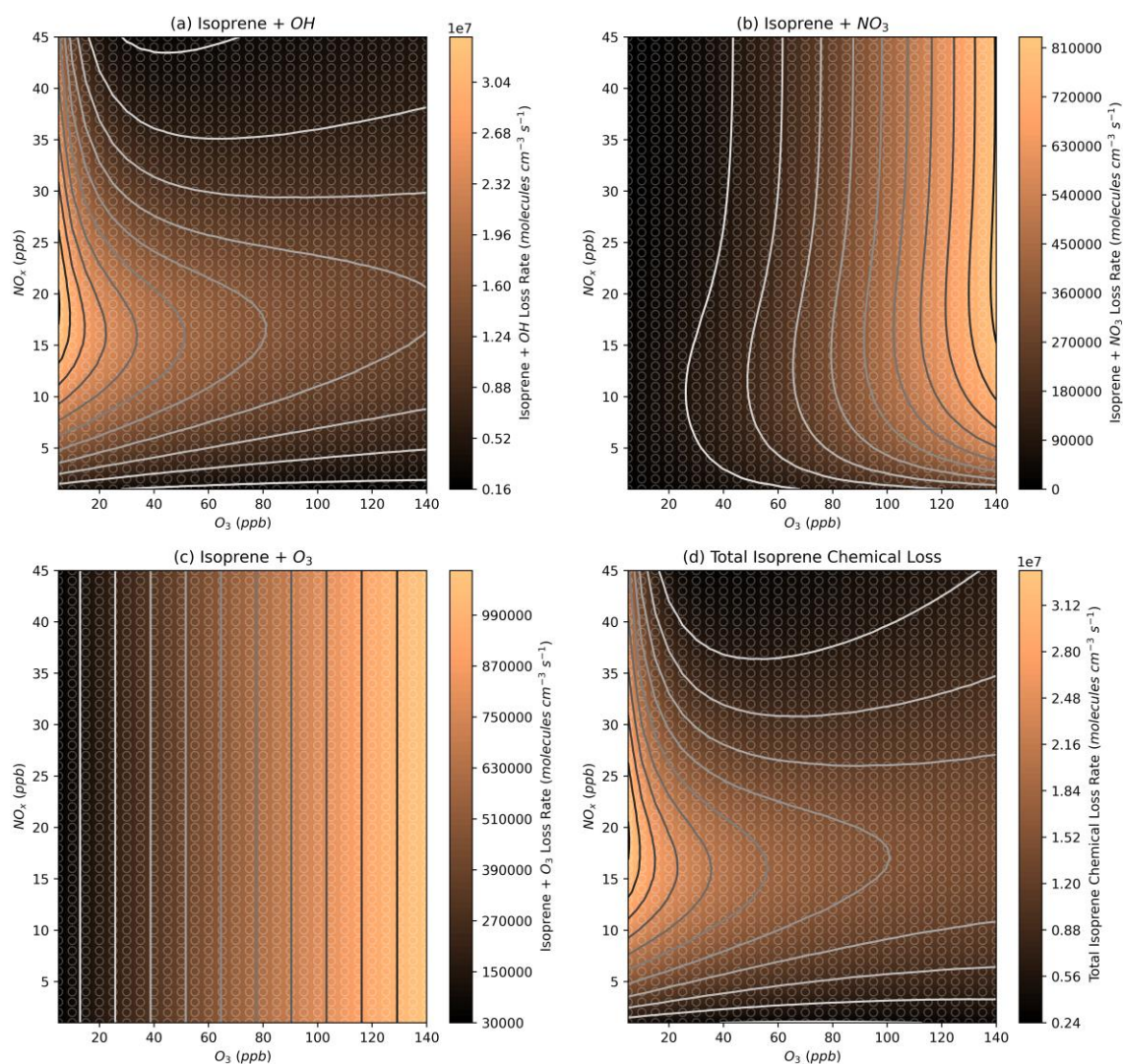
Figure 3.32. Modelled loss rates of isoprene to reaction with (a) OH, (b) NO_3, (c) O_3, and (d) the total chemical loss of isoprene at different NO_x and O_3 mixing ratios.

In order to investigate the impact of this changing isoprene flux on the conclusions presented here, Figure 3.33 shows the steady-state concentration of the organonitrates of interest divided by the total loss rate of isoprene. This shows the steady-state concentration of a compound of interest normalised by the amount of isoprene reacted.

Since IHN is predominantly formed from OH, and OH dominates the loss of isoprene in these models, the normalised IHN concentration isopleth (Figure 3.33f) is much less variable than the steady-state concentration isopleth (Figure 3.22a). Therefore, the changes observed in the concentration isopleth are the result of higher amounts of isoprene reacting in total, rather than a greater proportion of isoprene forming IHN vs other oxidation products.

Species controlled by the availability of NO_3, such as IDN (Figure 3.33a), IDNE (Figure 3.33b), and INCE (Figure 3.33e), still show a strong dependence on O_3 concentrations but the isopleth shape is altered such that values are suppressed in the centre of the isopleth. This is due to the high rate of loss to reaction with OH in this region, meaning that less of the isoprene that is reacted forms these NO_3-derived products.

Species that showed the highest steady-state concentrations under high O_3 and low NO_x (i.e. at the bottom-right of the isopleths), such as IPN (Figure 3.33h), INHE (Figure 3.33c), and INPE (Figure 3.33d), still show a similar profile when normalising for the total amount of isoprene reacted. This is because the concentration isopleths of these species are not dictated by the primary oxidation steps but are instead controlled by the secondary chemistry which remains unchanged when the isoprene loss rate is accounted for. This may not be true if the models were rerun with the isoprene flux actually held constant in each model as this would have knock-on repercussions for secondary chemistry such as OH concentrations.

Finally, the total organonitrate isopleth (Figure 3.33i) shows enhanced values in the high O_3 region, compared to Figure 3.26. This reflects the enhanced formation of organonitrates from the daytime NO_3 chemistry which is favoured under these high-O_3 conditions. Interestingly, the band of higher concentrations at moderate urban NO_x concentrations remains present in this normalised concentration plot, meaning that changes to ozone at around 10 ppb of NO_x have little impact on organonitrate concentrations until high ozone concentrations of around 100 ppb of O_3 are reached.
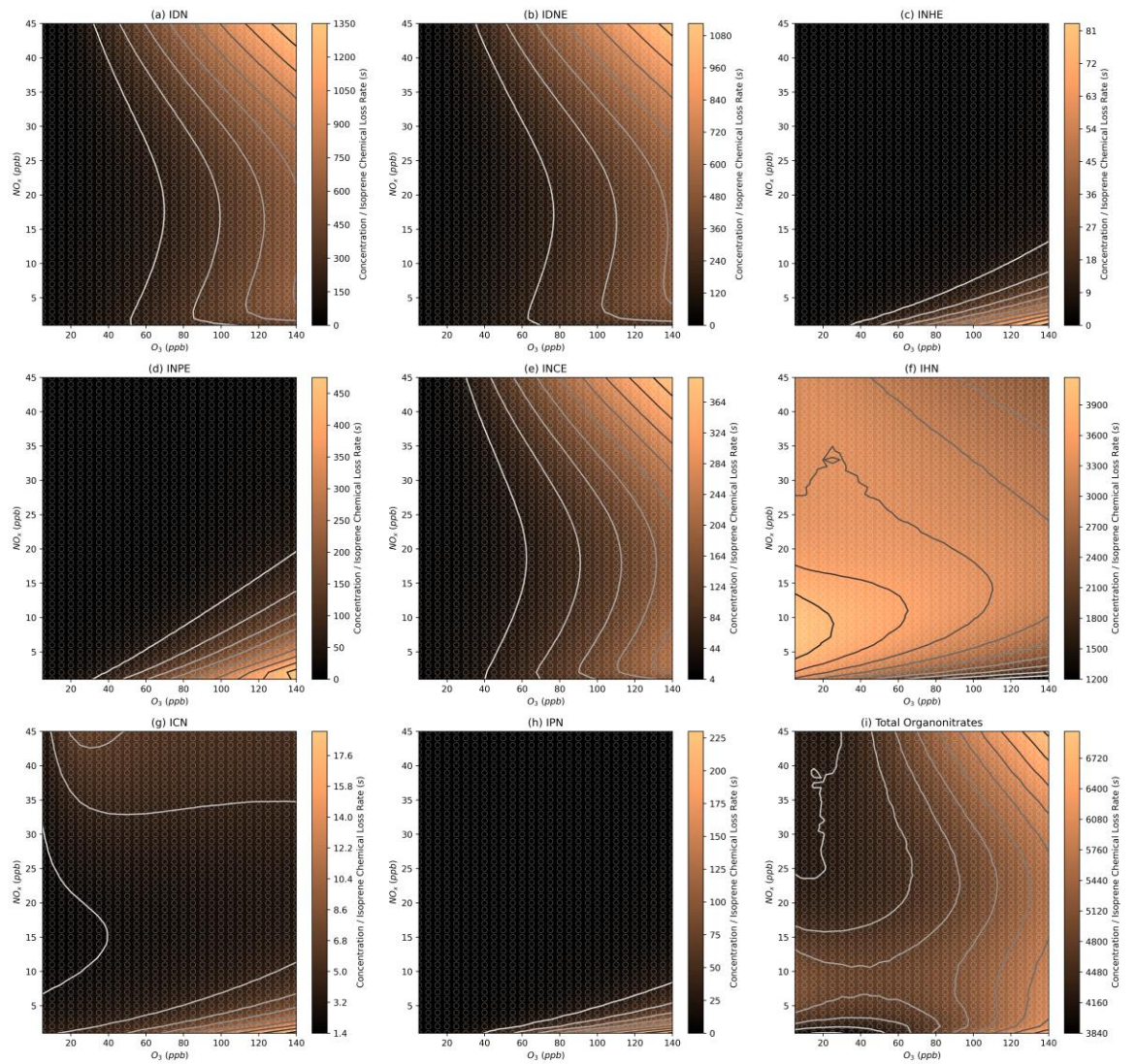
Figure 3.33. Modelled steady-state concentrations of different groups of organonitrates at different NO_x and O_3 concentrations, normalised by the total chemical loss rate of isoprene.
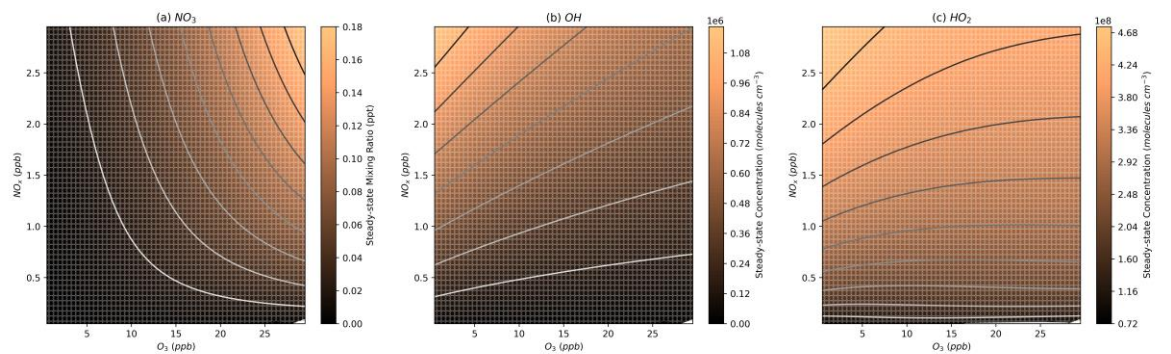
Figure 3.34. Modelled steady-state concentrations of NO_3, OH, and HO_2 in the Amazon models (lower NO_x and O_3 concentrations and higher VOC concentrations than the Beijing models).

3.11 Application to Less Polluted Environments

In order to test the investigation of less polluted environments, a series of models were run at a range of lower NO_x and O_3 mixing ratios. Measurements collected in the amazon rainforest were taken as an example of an unpolluted environment, and the model was adjusted to match typical isoprene mixing ratios and OH reactivity observed in this environment. The results from these models are presented in Figure 3.34 and Figure 3.35.

The reduced NO_x and O_3 mixing ratios used in these models mean that, despite the changes to isoprene and methane concentrations, they correspond well to higher resolution models of the low NO_x and O_3 portions of the Beijing models. Figure 3.35 shows that the total organonitrates in the Amazon models are sensitive to changes in NO_x, with increasing ozone slightly reducing total organonitrates.

As discussed in the introduction, IEPOX is one of the major precursors of isoprene SOA, particularly under low-NO_x conditions where the IEPOX precursor, ISOPOOH, can form from oxidation by OH and further reaction with HO_2. This dependence on HO_2 means that the amazon models predict increasing concentrations of IEPOX as NO_x is increased from close to 0, regardless of the O_3 concentration (Figure 3.36b). This is in agreement with findings from Shrivastava et al. who found increases in isoprene SOA resulting from increases in NO_x and O_3 from an urban plume.[175] The increased SOA could be further explained by the increases in nitrated epoxides and dinitrated species predicted on increasing both NO_x and O_3 (Figure 3.35).

Methyl vinyl ketone (MVK) and methacrolein (MACR) are also often of interest in isoprene oxidation, particularly in pristine environments such as the Amazon where the production of MVK and MACR relies on the presence of NO.[169] This is illustrated in Figure 3.36d, whereas Figure 3.36c illustrates that the abundance of NO under typical urban conditions means that the MVK+MACR concentrations in the Beijing models are dependent on OH concentrations.
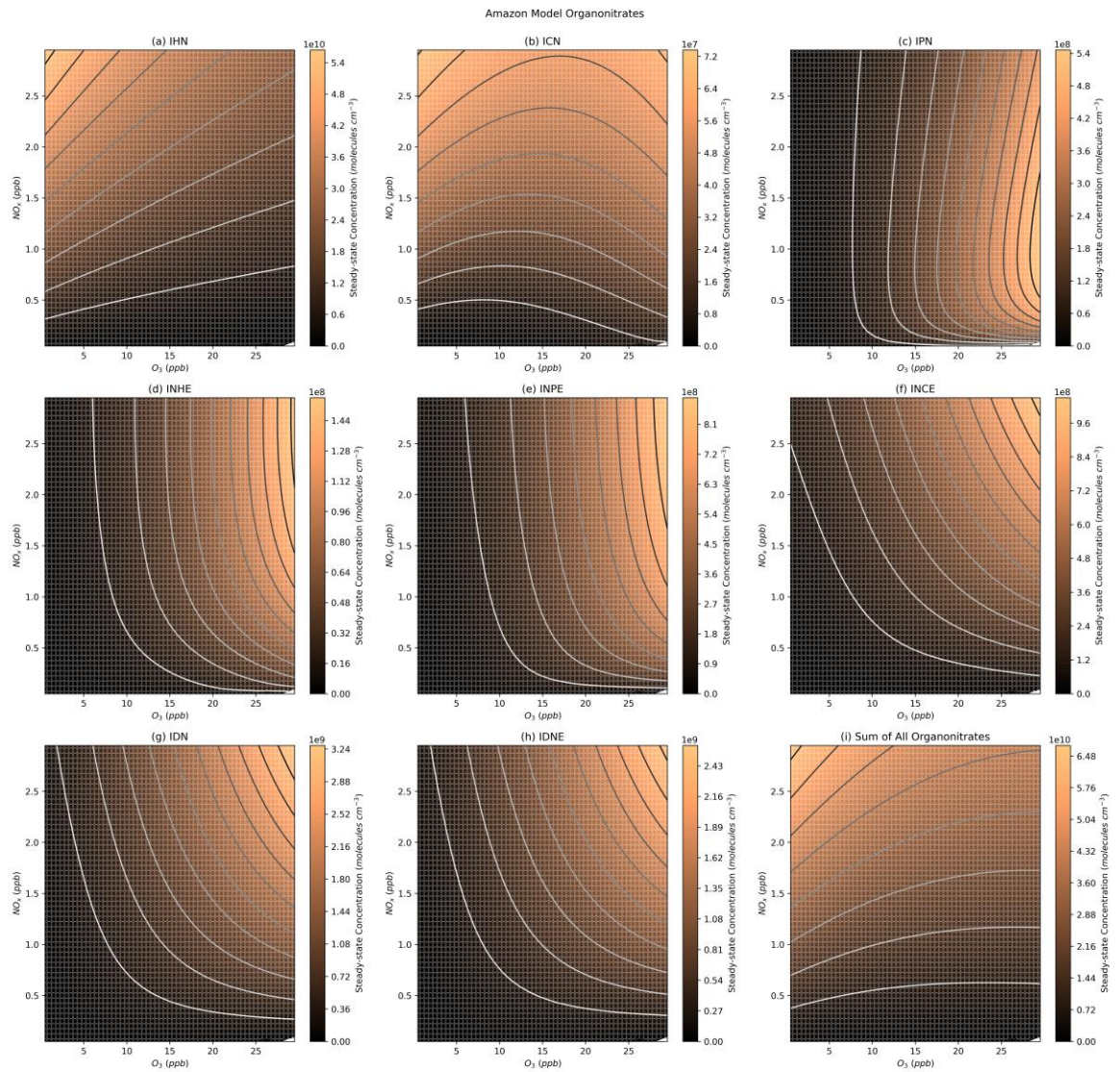
Figure 3.35. Modelled steady state organonitrate concentrations for the Amazon models (lower NO$_x$ and O$_3$ concentrations and higher VOC concentrations than the Beijing models).
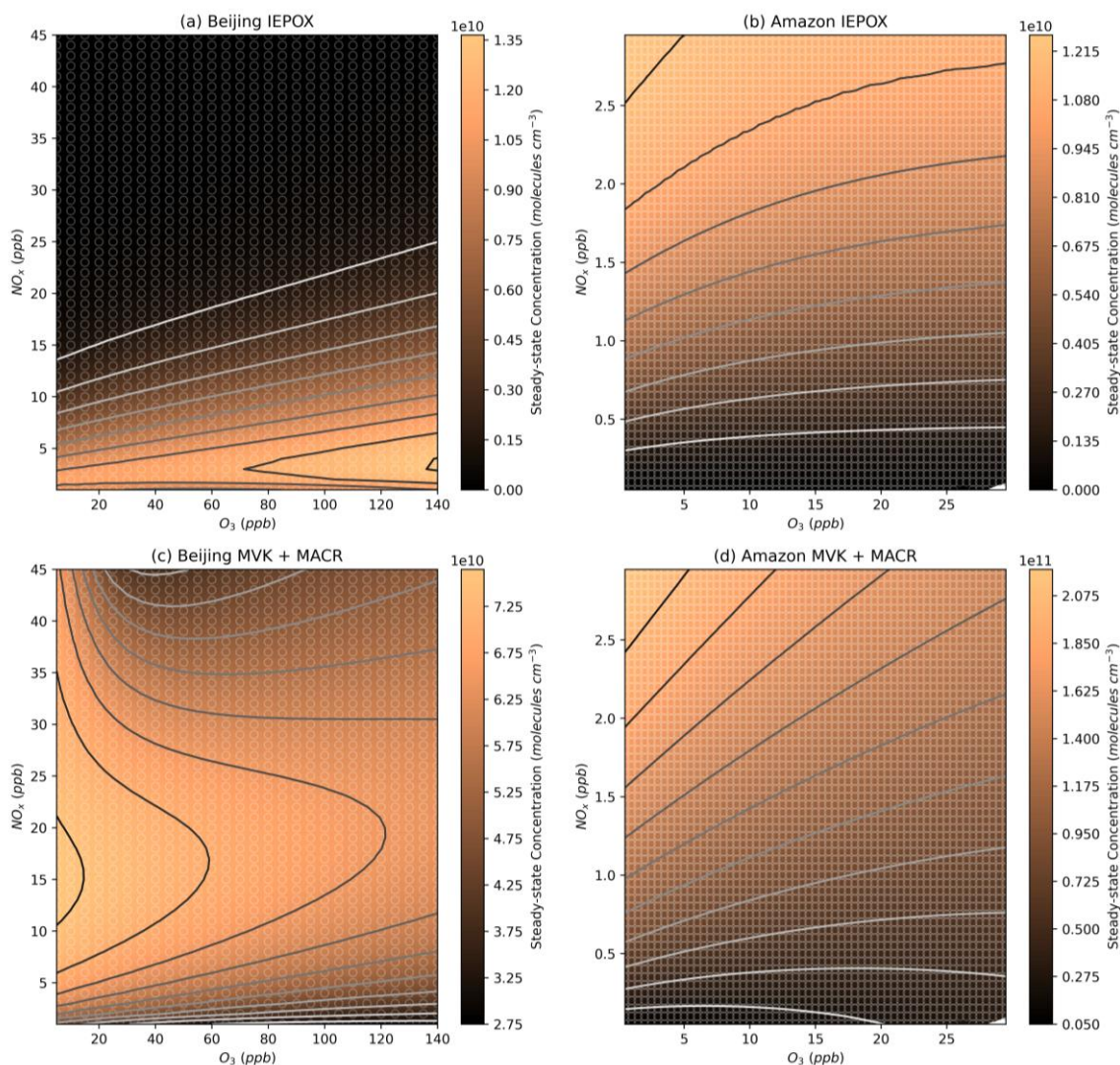
Figure 3.36. Modelled steady state IEPOX and MVK + MACR concentrations for the Beijing (a,c) and Amazon (b,d) models.

3.12 Conclusions

The work presented here illustrates that each isoprene nitrate species will have a different NO_x-O_3 regime in which maximum concentrations will be produced. For example, the facile formation of IHN from OH oxidation means that daytime concentrations are largely dictated by the concentration of OH. Alternatively, the concentrations of species such as IDN, IDNE, and ICN are largely dictated by the available daytime NO_3 as the reaction of RO_2 with NO is very rapid, even under low urban NO_x conditions. Finally, IPN, INHE, and INPE only show the highest concentrations under low-NO_x-high-O_3 conditions due to their increased formation under high NO_3 concentrations and their requirement for low-NO_x to avoid competition with the RO_2+NO reaction pathway.

The fact that the concentrations of different organonitrates will respond differently to changes in NO_x and O_3 will have implications for those considering pathways to reducing the concentrations of organonitrates in the atmosphere. The work presented here indicates that reductions in NO_x may not reduce total organonitrate concentrations until low urban NO_x conditions are met and that, for many of the species resulting from the daytime NO_3 oxidation of isoprene, organonitrate

concentrations may be much more sensitive to changes in O_3 than in NO_x. Additionally, accounting for the volatility of the organonitrates can have very large impacts, and the models presented here are dominated by a small number of low volatility compounds. An improved representation of late-stage oxidation and autooxidation is likely to improve the ability to predict the effect of changing O_3 and NO_x on SOA formation.

As efforts are made to reduce NO_x, VOC, and O_3 concentrations around the world, care should be taken to ensure that the non-linearity of responses to changes does not result in unintended increases in important SOA precursors. For example, previous work has indicated that Beijing occupies a VOC-limited regime with respect to O_3 formation and that decreasing NO_x concentrations without a concurrent decrease in VOC concentrations would result in increased O_3.[176,177] Mapping this trajectory of decreasing NO_x and increasing O_3 onto Figure 3.27 would suggest that SOA from isoprene organonitrates may increase in concentration due to the gradient with changing NO_x. However, the effect could be worsened when considering the reactive uptake of INHE, IDNE, INPE, and INCE which all favour formation under high-O_3 conditions. This may be further compounded or mitigated with changing VOC concentrations due to the impact on the organonitrate isopleths as well as the non-linear behaviour of O_3 with changing NO_x and VOC.

Chapter 4

Investigations into Isoprene Chemistry Using an Atmospheric Simulation Chamber

4.1 Introduction

4.1.1 Chamber Experiments

The complex nature of ambient air often necessitates a comparatively simple system by which atmospheric chemistry can be investigated. Chamber experiments offer this control and simplicity. An atmospheric simulation chamber consists of a container into which compounds are injected and allowed to react while the composition of air in the chamber is monitored over time.[178,179]

A major consideration in the use of chambers is that of wall interactions. Particles can be lost to the walls through deposition, and compounds can diffuse into the wall surface.[179-181] Heterogeneous reactions can also take place on the chamber walls, for example the reaction of NO_2 to form HONO.[182] These affects will impact the rate of loss of species in the chamber and must be considered when analysing data from chamber experiments.[183] The concentration of precursor species used in chamber experiments can also influence the composition of products such as SOA,[184] so further care must be taken when applying the findings of chamber experiments to ambient analyses. Wall effects are minimised in large chambers, as the wall surface area to volume ratio is reduced.

Chamber experiments have been integral to the development of isoprene mechanisms such as the MCM, Caltech, and FZJ mechanisms discussed in previous chapters.[28,42,68] For example, the inclusion of the reversibility of the addition of O_2 to form isoprene hydroxyperoxy radicals was included in the MCM on the basis of theoretical calculations, but chamber experiments demonstrated that the rate of the O_2 addition and peroxy radical decomposition reactions occurred much faster than predicted.[40,185] As such, these experimental rates are used in the MCM. Similarly, the theoretical findings from Vereecken *et al.* regarding the NO_3-initiated oxidation of isoprene were validated against chamber experiments that investigated the dark oxidation of isoprene, before incorporation into the FZJ mechanism.[68,124]

The work presented in this chapter outlines the findings from a series of chamber experiments performed at the EUropean PHotoREactor (EUPHORE) in Valencia, Spain, in the summer of 2021. These experiments were designed to investigate the oxidation of isoprene, including the impact of particle-phase processes, in conditions similar to those from the 2017 Atmospheric Pollution and Human Health in a Chinese Megacity (APHH) summer campaign in Beijing.[51] Chen *et al.* recently performed a series of chamber experiments under similar conditions.[186] While this work focussed only on dark oxidation, it showed the importance of the contribution of low-volatility HOMs to SOA.

4.2 Methodology

4.2.1 Chamber Description

The EUPHORE experiments were conducted between the dates of 2021-05-31 and 2021-07-08. The EUPHORE chamber used in this work consists of a 200 m^3 fluoropolymeric bag contained within a housing, with a roof that can be retracted to allow the irradiation of the bag contents by sunlight. Large fans are present within the chamber to allow for rapid mixing of the air. Further details of the chambers' operation can be found elsewhere. [187,188]

A dew point hygrometer (TS-2, Walz, Effeltrich, Germany) was used to measure humidity and temperature. J_{NO2} was measured using filter radiometers (Schmitt, Glashütten).[189] A TAPI NOx monitor (T200UP, Teledyne, San Diego, USA) was used to measure NO, NO2, and NOx. Ozone was measured with a Serius 10 ozone analyser (Echotech, Knoxfield, Victoria, Australia). Also, a proton transfer reaction mass spectrometer (PTR-MS) instrument was used for monitoring organic compounds in the gas phase, such as isoprene. OH and HO$_2$ were measured via laser induced fluorescence (LIF) and particle concentration measurements were made with a scanning mobility particle sizer (SMPS).[190,191]

SF$_6$ was added to the chamber in order to monitor the dilution of the chamber air due to the replacement of air removed for analysis. The concentration of SF$_6$ was monitored over time by fourier-transform infra-red (FTIR) spectroscopy. SF$_6$ is chemically inert, so the loss rate of SF$_6$ over time is assumed to be equal to the dilution rate of the chamber.

A chemical ionisation mass spectrometer, using an iodide ionisation source (I$^-$-CIMS) was used to monitor the gas-phase organonitrates. Since no standards could be obtained for the nitrates of interest, and the sensitivity of the instrument to different species is highly uncertain,[192] the I$^-$-CIMS data presented here is uncalibrated. The uncalibrated signal is normalised to the sum of the iodide (I$^-$) and iodide-water cluster (H$_2$OI$^-$) signal, hence the I$^-$-CIMS data is presented in units of normalised counts per second (ncps).

4.2.2 Experimental Description

The central motivation for conducting the experiments at EUPHORE was to investigate the daytime NO$_3$ chemistry observed in the 2017 Beijing campaign, as discussed in Chapter 1 and Chapter 3.[51] In order to reproduce these conditions, the experiments were conducted in the presence of high ozone concentrations, as was observed during the Beijing campaign. Experiments were performed at O$_3$ mixing ratios of around 400 ppb, as well as at the more representative mixing ratios of around 100 ppb, in an effort to exaggerate the daytime NO$_3$ chemistry. NO$_x$ concentrations were also kept low to ensure low NO concentrations were present, though enough NO$_x$ had to be available to allow the production of NO$_3$.

In an effort to probe particle-phase processes, each of the experiments was repeated in the presence and absence of acidified ammonium sulfate seed. The aim was that by observing the differences in gas-phase species, then those involved in particle-phase chemistry could be identified. This is discussed further in Section 4.3.

As well as adjusting O_3 and NO_x concentrations, the isoprene concentration was also varied across experiments. Some experiments were performed at atmospherically representative isoprene concentrations of less than 10 ppb, whereas other experiments were performed using tens of ppb of isoprene. These higher isoprene experiments were designed to allow more minor products in the gas and particle phases to be detected, since the overall organic mass will be higher. However, increasing the isoprene concentrations will also skew the RO_2 fate by increasing the rate of RO_2 cross reactions and changing the concentration of inorganic species such as OH.

The final variable adjusted in these experiments was the photolysis conditions. The retractable roof of the EUPHORE chamber allowed for sunlight to be blocked from the reaction chamber for portions of the experiments. Most of the experiments involved an initial light portion, while isoprene was added to the chamber, then the roof was closed to simulate the day-to-night transition.

A summary of each of the experiments performed in the campaign is provided in Table 4.1. Several different named groups of experiments are used throughout this chapter. Each experiment involved multiple injections of NO_x, O_3, and isoprene. The median values are presented in Table 4.1, as well as the total amount of isoprene consumed across the multiple additions, to give a comparative guide for the mixing ratios of each species in each experiment. Time series for NO_x, O_3, and isoprene mixing ratios in several representative experiments are presented in Figure 4.1. "Seeded" and "unseeded" experiments refer to those in which acidified ammonium sulfate seed aerosol was and wasn't initially added to the chamber, respectively. "Beijing reproduction experiments" refers to the sequence of experiments aiming to reproduce the daytime NO_3 chemistry by varying the concentration of ozone. Each of these experiments consisted of an initial period with the chamber roof open, where isoprene was added to the chamber. The roof was then closed at 15:00 local time and nothing else was introduced into the chamber, with the air being monitored over the course of 2 to 3 hours. "Dark", "light-to-dark", and "dark-to-light" experiments refer to those where the chamber roof is closed throughout the experiment, is initially open but is closed mid-experiment, and is initially closed but is opened mid-experiment. The light-to-dark experiments differ from the Beijing reproduction experiments as the roof is closed at 13:00 local time, allowing for more dark oxidation. "Non-dark" is used to refer to the group of light-to-dark, dark-to-light, and Beijing-reproduction experiments. "Empty-chamber" experiments are those where no isoprene, NO_x, or O_3 are added to the chamber, however they may be seeded or unseeded.

Table 4.1. Information on each experiment performed in the 2021 EUPHORE campaign. Each experiment involved multiple injections of isoprene, O_3, and NO_x.

Date	Category	Median O_3 (ppb)	Median NO_x (ppb)	Median Isoprene (ppb)	Total Isoprene Consumed (ppb)	Seeded
2021-05-31	Test Day	N/a	N/a	N/a	N/a	Yes
2021-06-01	Test Day	N/a	N/a	N/a	N/a	No
2021-06-02	Empty Chamber	N/a	N/a	N/a	N/a	Yes
2021-06-03[a]	Dark-to-light	82.9	66.1	24.0	-	No
2021-06-04	Dark-to-light	69.4	79.5	16.9	55.9	Yes
2021-06-07	Empty Chamber	N/a	N/a	N/a	N/a	No
2021-06-08	Beijing Reproduction	375.8	10.3	4.4	54.6	No
2021-06-09	Beijing Reproduction	346.7	10.5	3.5	50.1	Yes
2021-06-10	Beijing Reproduction	372.6	13.4	20.2	264.8	No
2021-06-11	Light-to-dark	118.6	12.6	21.2	116.3	Yes
2021-06-14	Beijing Reproduction	355.1	12.1	17.0	232.5	Yes
2021-06-15 [b]	Beijing Reproduction	120.4	15.9	3.5	47.2	No
2021-06-16 [c]	Beijing Reproduction	63.1	31.9	4.37	18.6	Yes
2021-06-17	Dark	61.8	69.2	24.1	85.3	Yes
2021-06-18	Light-to-dark	122.5	12.6	23.2	89.8	No
2021-06-21	Dark	60.7	82.0	14.4	78.9	No
2021-06-22	Beijing Reproduction	98.0	13.1	2.1	29.2	Yes
2021-06-23	Dark	98.5	23.5	1.2	8.7	Yes
2021-06-25 [d]	Dark	98.4	-	1.0	10.8	No
2021-06-28 [e]	Beijing Reproduction	92.3	6.5	4.0	42.2	Yes
2021-06-29	Beijing Reproduction	108.6	6.2	3.6	35.6	No
2021-06-30 [f]	Dark	103.2	33.5	4.5	35.0	No
2021-07-01	Beijing Reproduction	168.8	15.1	13.9	141.6	Yes
2021-07-02	Empty Chamber	N/a	N/a	N/a	N/a	Yes
2021-07-05	Beijing Reproduction	191.4	13.7	8.1	87.6	No
2021-07-07	Dark	65.0	36.8	29.7	59.2	Yes
2021-07-08	Beijing Reproduction	137.0	13.3	2.5	33.7	No

[a] PTR data incomplete, so total isoprene consumed cannot be calculated.
[b] NOx addition was accidentally continued after roof closure.
[c] Rain forced early roof closure.
[d] No NO_x measurements for this experiment.
[e] Two filters collected. One just before roof closure, and one at the end of the experiment.
[f] 0% RH used.
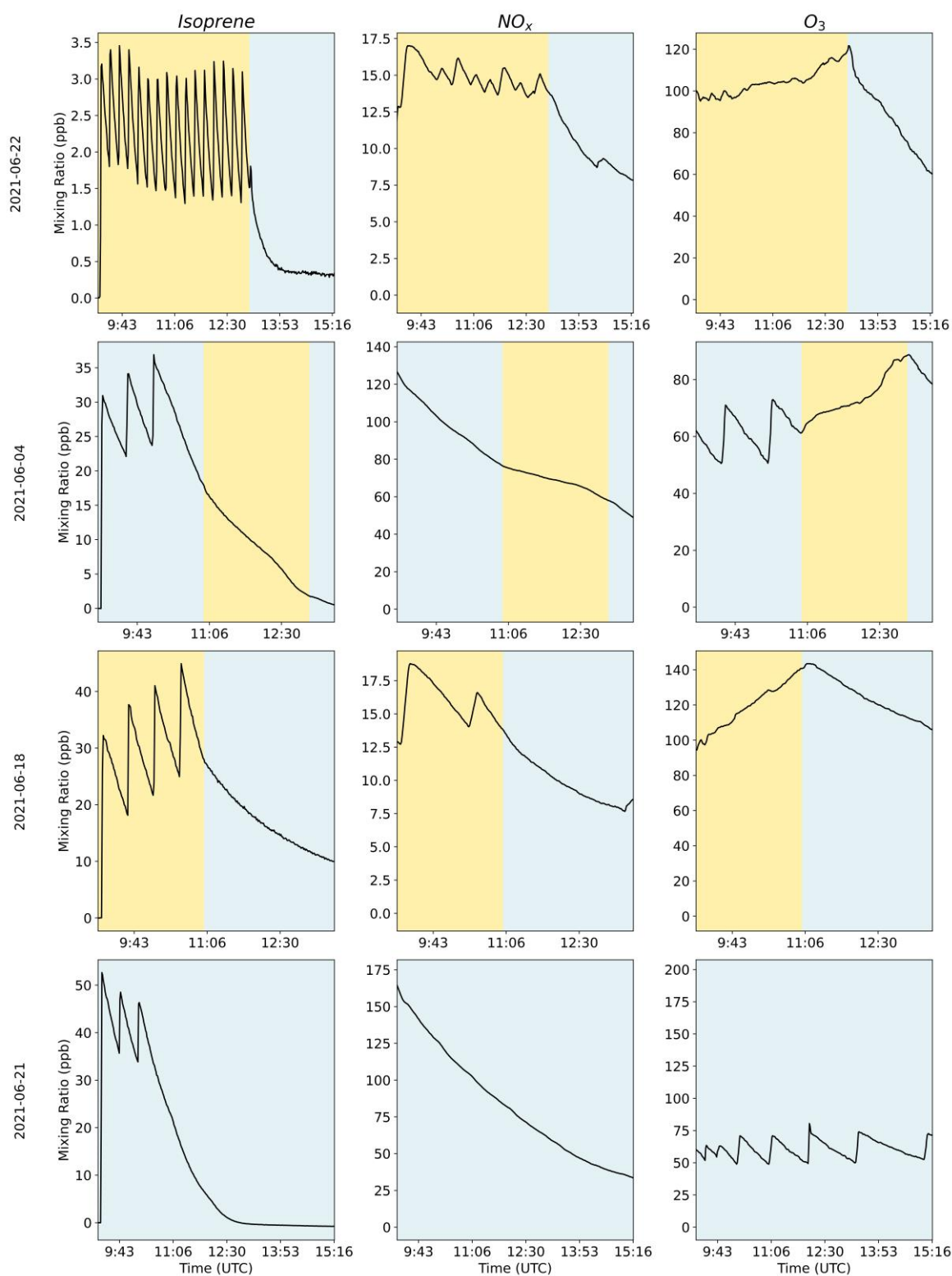
Figure 4.1. Isoprene, NO$_x$, and O$_3$ mixing ratios throughout the experiments performed on 2021-06-22, 2021-06-04, 2021-06-18, and 2021-06-21. The yellow and blue portions of the plots represent periods where the chamber roof was open or closed, respectively.

4.2.3 Filter Analysis

Particle samples were collected at the end of each experiment (with the exception of the 2021-06-28 where two filters were collected, Table 4.1) by drawing air through a quartz filter at a flow rate of 10 L min^{-1} for 60 minutes. The filters were baked prior to use at 500°C. Prior to analysis, the filters were stored at -20°C, wrapped in aluminium foil. The method outlined in Bryant *et al.* was used to extract the organic aerosol from the filters.[21] Briefly, this comprised of ultrasonic extraction into methanol, followed by reducing the sample to dryness and reconstituting in 1mL of 50:50 methanol:water.

The filter extracts were analysed by ultra-high-performance liquid chromatography mass-spectrometry (UHPLC-MS) via an Ultimate 3000 UHPLC (Thermo Scientific, USA) coupled to a Q Exactive Orbitrap MS (Thermo Fisher Scientific, USA) with heated electrospray ionization (HESI), according to the method outlined in Bryant *et al.*[21] The method was adjusted to use a 20μl injection volume, as opposed to 4μl, to ensure sufficient concentrations for the particle-phase analysis.

Isoprene tracers with three formulae were detected and analysed in the filters, using the expected m/z and retention times taken from previous work.[51,193] These masses and retention times are listed in Table 4.2. In the case of $C_5H_{10}N_2O_{11}S$, where multiple isomers are separated and detected, the areas of all of the peaks were added before further analysis to determine the total amount of $C_5H_{10}N_2O_{11}S$. Example chromatograms and mass spectra for each group of species are shown in Figure 4.2, Figure 4.3, and Figure 4.4. Each of the sample chromatograms and spectra are taken from the experiments that showed the highest peak area for each compound.

Table 4.2. m/z and RT values for each of the peaks analysed from the UHPLC-MS data, across the filters collected in each of the chamber experiments. These tracers were selected for analysis based on the reported m/z and RT values in Hamilton et al. 2021.[51]

Formula	Mean [M-H]$^-$ m/z	Min. [M-H]$^-$ m/z	Max. [M-H]$^-$ m/z	Mean RT	Min. RT	Max. RT
C5H11NO9S	260.0085	260.0082	260.0087	0.89	0.83	0.94
C5H9NO10S	273.9878	273.9874	273.9882	0.97	0.94	1.01
C5H10N2O11S	304.9934	304.9924	304.9937	1.61	1.46	1.66
C5H10N2O11S	304.9933	304.9925	304.9940	1.89	1.75	1.99
C5H10N2O11S	304.9935	304.9930	304.9938	2.17	2.07	2.23
C5H10N2O11S	304.9925	304.9923	304.9935	3.68	3.56	3.91
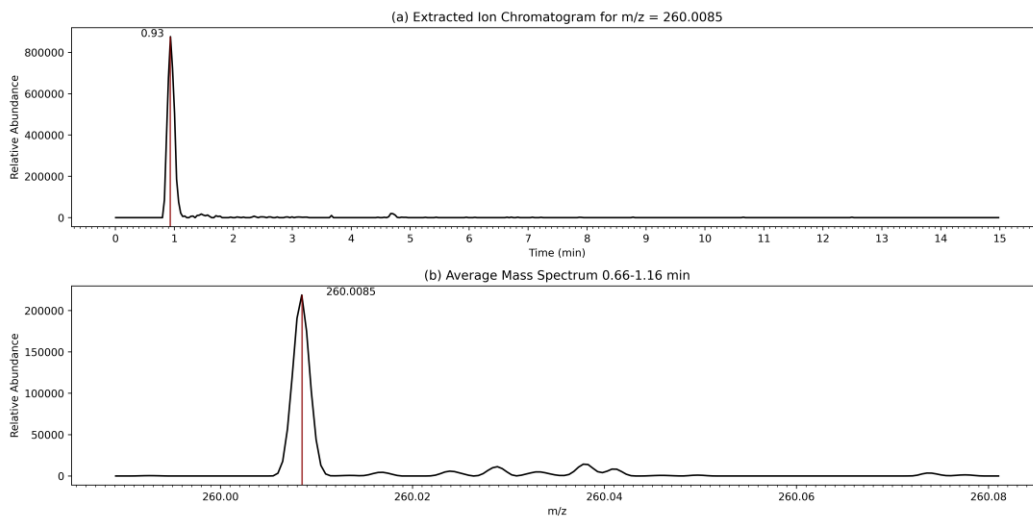
Figure 4.2. Extracted ion chromatogram (a) and average mass spectrum (b) for $C_5H_{10}NO_9S^-$ in the filter collected from the 2021-06-10 experiment, which showed the highest area for the $C_5H_{10}NO_9S^-$ peak.
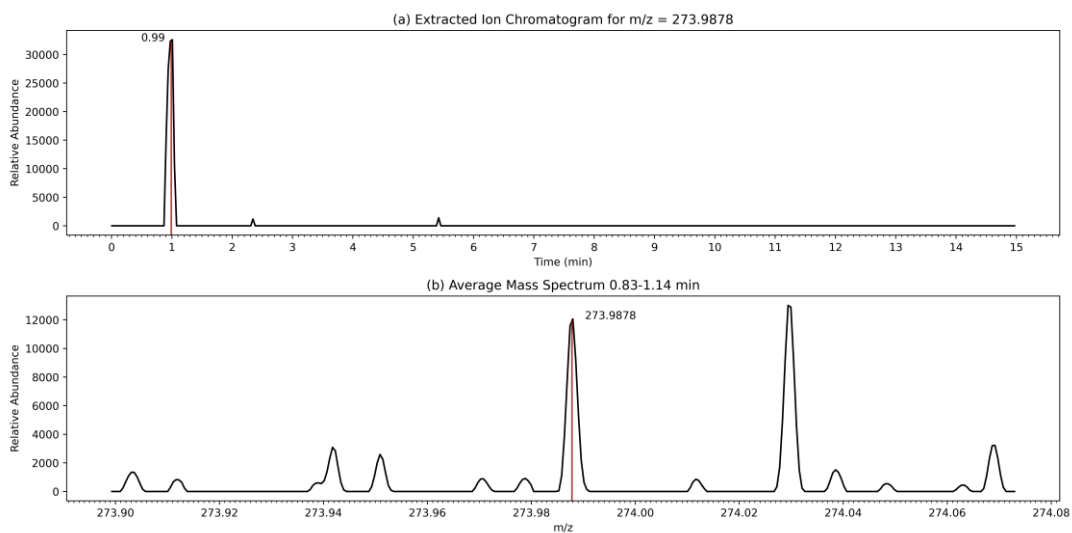
Figure 4.3. Extracted ion chromatogram (a) and average mass spectrum (b) for $C_5H_8NO_{10}S^-$ in the filter collected from the 2021-06-04 experiment, which showed the highest area for the $C_5H_8NO_{10}S^-$ peak.
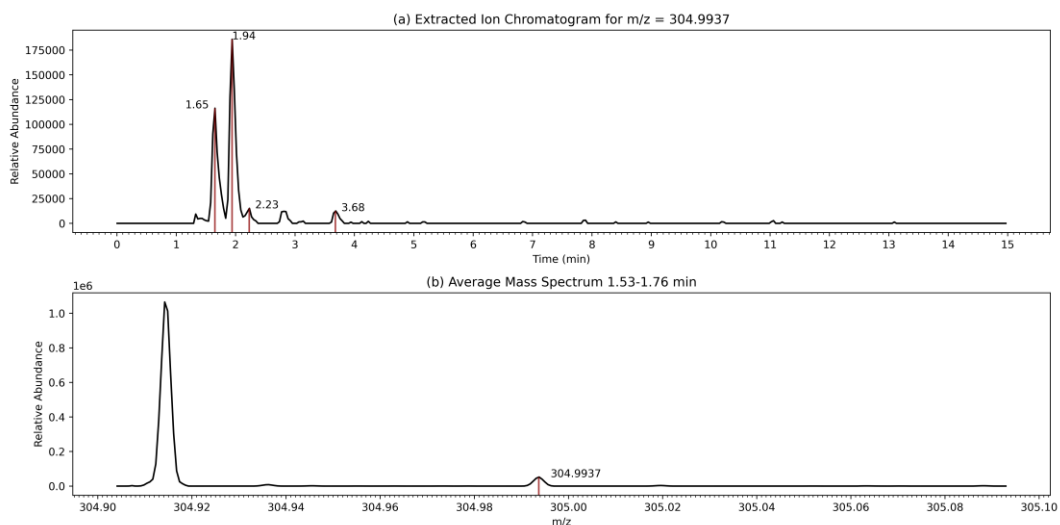
Figure 4.4. Extracted ion chromatogram (a) and average mass spectrum (b) for $C_5H_9N_2O_{11}S^-$ in the filter collected from the 2021-06-17 experiment, which showed the combined highest area for the $C_5H_9N_2O_{11}S^-$ peaks.

4.2.4 Box Modelling

In order to overcome the lack of radical measurements in these experiments, a series of box models were run to predict the losses of isoprene. These models were run using AtChem2, an open-source zero-dimensional box-model.[153] These models were constrained to measured values of temperature, pressure, and RH. The dilution rate of the chamber air was also constrained to the value calculated as described in Section 4.2.1.

Photolysis rates were calculated by AtChem2 according the MCM procedure,[97] based on latitude and longitude values provided to AtChem2. The values of latitude and longitude used here were 39.551° and -0.462° respectively, corresponding to the position of the EUPHORE Chamber. In order to account for changes in photolysis, for example as the result of clouds, all of the calculated photolysis rates were scaled by the ratio of the measured and calculated J_{NO2}. This scaling factor is termed JFAC. Scaling all photolysis rates based on the J_{NO2} attenuation will cause issues when the photolysis occurs as the result of light with very different wavelengths from the light required for NO_2 photolysis. Different wavelengths of light will be blocked to different extents by different materials, which is in contrast to the use of JFAC which assumes that all photolysis rates will be fractionally equally effected by disturbances. Seckemyer et al. showed that shorter wavelengths more easily penetrate clouds, though this effect is small and has also been shown to be statistically insignificant in other studies. [194] This may be important when considering the photolysis of NO_3 in this work, which occurs at wavelengths longer than NO_2.[57] As such, it should be considered that applying JFAC to J_{NO3} may result in an overprediction of the NO_3 photolysis rate, and therefore an underprediction in NO_3 concentrations. However, no NO_3 measurements are available from these experiments to verify this.

Previous work has shown the difficulty of reproducing HO_2 concentrations in isoprene oxidation chamber experiments, and so HO_2 was constrained to the measured values in order to properly represent the RO_2 loss routes.[68,124] Similarly, a good representation of HONO is important for the representation of NO_x in chamber experiments, so this was constrained to measured values. CO was constrained to measured values due to the consistent underprediction of CO formation in the models. Finally, O_3 was constrained due to a tendency for the models to over-predict O_3 formation and the importance of correct ozone concentrations for the calculation of isoprene loss to O_3.

Injections into the chamber were accounted for by replacing the modelled species concentration at each injection time with the measured value before proceeding with the model run. In practice, when using AtChem2, this means running a model up to the first injection, then initialising a new model starting with all of the same conditions as the end of the previous model, with just the injected species concentration changed. Then this new model is run forward to the next injection point, and so on until the end of the experiment is reached.

Section 4.5.2 makes use of model data from the Beijing reproduction experiments described in Chapter 2.[126] This model data is separate from the EUPHORE models used in the rest of this chapter.

4.2.5 Mechanism

The FZJ Isoprene Mechanism outlined in Chapter 3 was used for all of the models presented in this chapter. Additional reactions were added to this mechanism in order to properly represent the effect of chamber walls on the chemistry occurring in the EUPHORE experiments. An auxiliary mechanism has previously been produced for the EUPHORE chamber.[189] This auxiliary mechanism was used as a base and was modified based on the three empty-chamber experiments. In each of these experiments, the chamber air was monitored over the course of the day, and the auxiliary mechanism has been adjusted to best reproduce these observations. The auxiliary mechanism reactions are listed in Table 4.3.

Dewald *et al.* previously characterised the loss of NO_3 and N_2O_5 to the walls of the SAPHIR chamber.[195] Since the EUPHORE experiments did not include measurements of NO_3 or N_2O_5, it is difficult to constrain the magnitude of this effect on the results presented here. Since SAPHIR and EUPHORE are both large, Teflon-walled, outdoor chambers, the wall losses of NO_3 and N_2O_5 have been directly applied as calculated by Dewald *et al.* These reactions are also listed in Table 4.3.

The production of many compounds from the chamber walls is dependent on photolysis conditions, with the production rate often being measured in separate tests with the roof open and closed. Since these experiments involved the chamber roof being open and closed at different times, JFAC was used to scale between the dark and light production rates. JFAC is described in Section 4.2.4. When the roof is closed, JFAC is equal to 0 because J_{NO2} will also be equal to 0.

Table 4.3. Auxiliary mechanism added to the EUPHORE model runs based on rates taken from Zador et al. 2006 and adjusted to match empty chamber experiments performed as part of this campaign.

Rate Constant	Reaction
$(JFAC \times 1.62 \times 10^7) + ((1 - JFAC) \times 1.4 \times 10^7)$ molecules cm^{-3} s^{-1}	HCOOH Production
$((3.1 \times 10^{17}) \times J_{NO2} \times e^{\frac{-5686}{TEMP}}) \times 3$ molecules cm^{-3} s^{-1}	HCHO Production
$((JFAC \times 5.98 \times 10^6) + ((1 - JFAC) \times 1.85 \times 10^6)) \times 1.7$ molecules cm^{-3} s^{-1}	NO Production
1.3×10^{-3} s^{-1} [a]	NO3 Loss
3.3×10^{-4} s^{-1} [a]	N2O5 Loss

[a] Rates taken from Dewald *et al.* 2020.[195]

4.2.6 Correlation Plots

Section 4.6 plots the particle-phase measurements of species against average measurements of gas-phase species in order to investigate potential relationships between the two. These correlation plots only include seeded experiments. Although particle-phase species are often detected in the filters from the unseeded experiments, likely as a result of uptake to particles formed by nucleation

(Section 4.3), there is uncertainty as to the characteristics of the particles formed in these experiments (e.g. particle acidity). The particles in the seeded experiments should be more consistent between experiments than those formed in the unseeded experiments.

Since only one filter was collected for each experiment, correlations with gas-phase measurements require averaging across the experimental time series, to represent the average conditions under which the particle-phase species were formed. Although the median is used in Section 4.6, use of the mean or cumulative sum did not affect the conclusions.

4.3 Particle Nucleation

As noted in Section 4.2.2, repeat experiments were performed with and without the addition of acidified ammonium sulfate seed aerosol in order to enable comparisons between conditions with and without particle-phase processes.

Figure 4.5 shows SMPS number concentration data from the unseeded experiment on 2021-06-10 and the analogous seeded experiment on 2021-06-14. The seeded experiment shows high concentrations of particles with a diameter of around 375 nm after the seed is added at 08:26 to 08:48. The average particle diameter begins to increase after the first isoprene injection at 09:10 to around 550 nm, consistent with growth of the particles due to the uptake of isoprene oxidation products as well as physical processes such as coagulation. The number concentration also decreases over the course of the experiment, illustrating the loss of particles due to dilution and deposition to the chamber walls. The filter sample is collected at 15:30 on 2021-06-14, meaning that much of the initial seed aerosol has already been lost from the chamber air when the sample is taken.

When isoprene injections begin at 09:18 in the non-seeded 2021-06-10 experiment, a series of new particle formation (NPF) events can be seen coinciding with each isoprene injection. The particles produced then increase in diameter over the course of the experiment, until roof closure at 13:08. This NPF can be seen in almost all of the unseeded experiments where isoprene is present while the roof is open, although no NPF is seen in the dark unseeded experiments.

The presence of reasonably high particle concentrations in the unseeded experiments mean that direct comparisons between the seeded and unseeded experiments will not give much information about the impact of particle-phase chemistry, as this chemistry will be occurring in both cases.

In boreal regions, isoprene is often considered to inhibit new particle formation through its interaction with α-pinene.[196-198] This was originally justified by the reactivity of isoprene scavenging OH that would otherwise react with monoterpenes to form low-volatility compounds that would nucleate to form new particles.[196,199,200] However, more recent work has highlighted the potential

role of gas-phase dimerization via RO_2 cross reactions.[87,201,202] In the case of monoterpenes, two C_{10} RO_2 species can react together to form a large, low-volatility C_{20} peroxide dimer. The addition of isoprene to this system results in the formation of mixed oligomers from the reaction of isoprene RO_2 and α-pinene RO_2, which will be C_{15} compounds.

This suppression of monoterpene NPF in the presence of isoprene is not inconsistent with the observations of NPF from isoprene made here for multiple reasons. Firstly, assuming the dimerization explanation for NPF, the higher volatility of isoprene dimers (and isoprene-monoterpene mixed dimers) may reduce NPF in mixed systems but does not preclude any NPF in isoprene-only systems, provided the dimers are still of low-enough volatility. Secondly, the previously cited studies focus on NPF under pristine conditions, where the role of NO_x is minimal. Additional studies investigating NPF under urban conditions are complicated by the interactions of biogenic and non-biogenic VOCs as well as inorganic chemistry, such as the role of H_2SO_4 in NPF.[203-205] The presence of NO_x in these experiments, particularly under the low-NO Beijing-like conditions, may amplify NPF from isoprene by the production of lower volatility organonitrates. An investigation into the composition of ultrafine particles in the Amazon revealed the presence of isoprene tracers as well as demonstrating the role of organic nitrogen species in the formation and growth of ultrafine particles.[206]
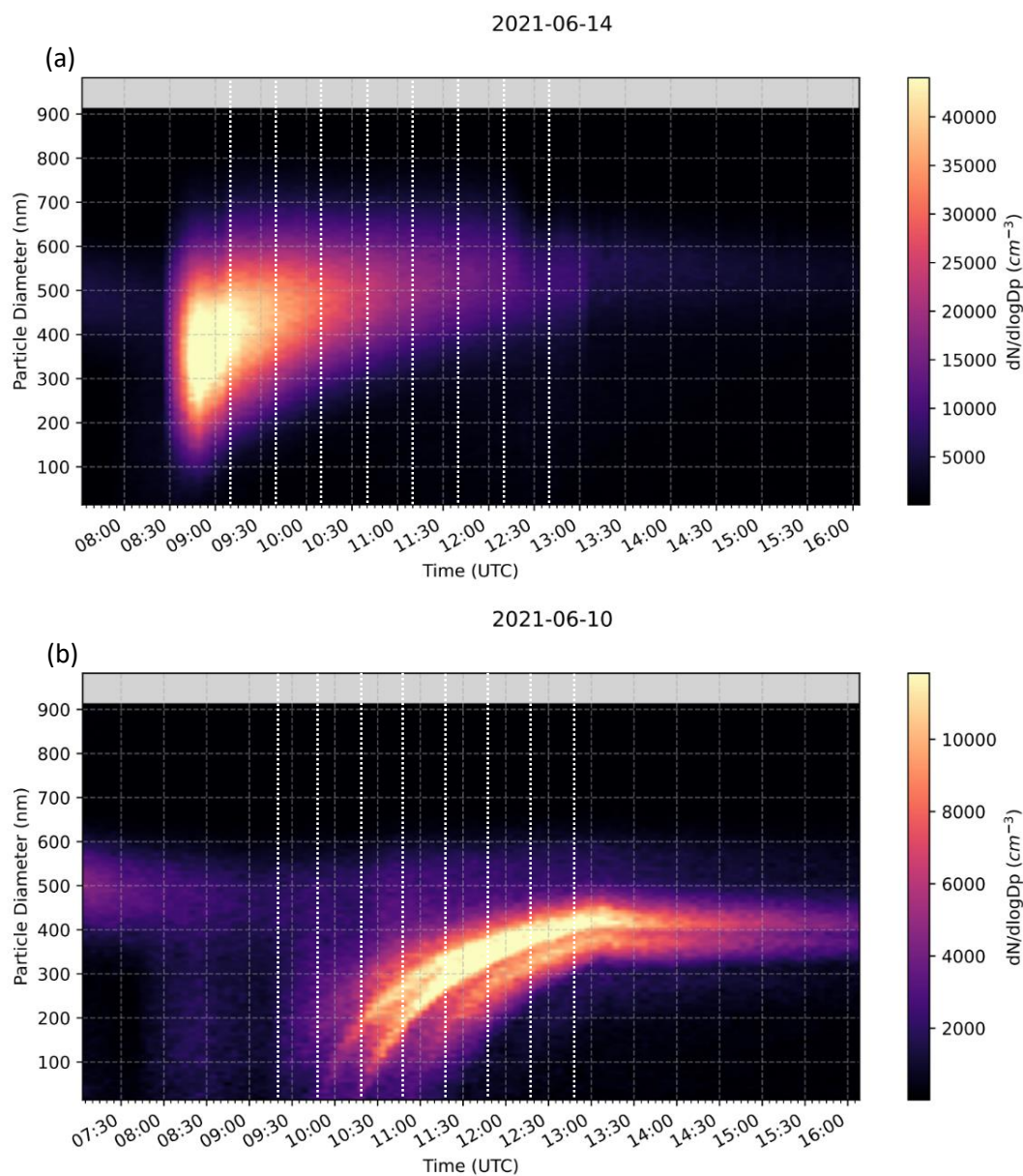
Figure 4.5. SMPS number concentration data from experiments performed on (a) 2021-06-14 and (b) 2021-06-10. (a) is a seeded experiment, whereas (b) is the analogous unseeded experiment. White dotted lines indicate isoprene injections to the chamber. Each SMPS heatmap uses a unique colour scale.

Previous work has indicated that isoprene ozonolysis in the presence of ethene may result in NPF by the oligimerization of stabilised creigee intermediates, however this effect was shown to be substantially supressed under humid conditions, like those used in these experiments, so this pathway may not explain the NPF observed here.[64]

There is likely some role played by wall-effects in these NPF events, as is evidenced by the empty-chamber experiment on 2021-06-07 (Figure 4.6). This experiment shows a clear NPF event at around 09:30 UTC, which does not correspond to any step change in environmental conditions such as temperature, RH, or solar irradiation (represented by the measurement of J_{NO2}). Nothing was added to the chamber during this experiment, aside from water used to humidify the chamber to an RH of around 40%. The observed particle formation does not occur during the humidification of

the chamber so is likely the result of compounds being released from the chamber walls that were deposited in previous experiments. Although the chamber was flushed overnight between experiments with filtered air, the lack of particle formation in the dark experiments suggests that this particular wall-effect is photo-induced, so this dark flushing may not mitigate this issue.

Further evidence of the role of wall effects can be seen in the data from the Beijing reproduction experiment performed on 2021-06-08. Unlike the other Beijing reproduction experiments, this experiment showed no evidence of NPF at the start of the experiment, when isoprene was first introduced. This initial period coincided with particularly low solar irradiance (as evidenced by the J_{NO2} measurements), and NPF begins once the J_{NO2} increases to over 0.006 s^{-1}. The other experiments all show J_{NO2} values of over 0.006 s^{-1} when the roof is open with the exception of the 2021-06-18 light-to-dark experiment, where the average J_{NO2} during the roof-open portion was below 0.005 s^{-1}. This experiment did not show any NPF, despite the injection of isoprene during the roof-open portion. The measurements from the 2017 APHH Beijing campaign show average diurnal J_{NO2} values above 0.006 s^{-1} between 09:20 and 15:30 local time.

The requirement for high solar radiation to initiate the NPF could be a reflection of the requirement for isoprene photochemistry to produce low-volatility products that are able to nucleate, for example through the increased availability of OH. The multiple NPF events observed in the unseeded experiments do highlight the role of isoprene in these NPF events, however it is clear that there is some role played by the release of contaminants from the chamber walls as is seen in the strong NPF event on 2021-06-07 despite the absence of isoprene added to the chamber.
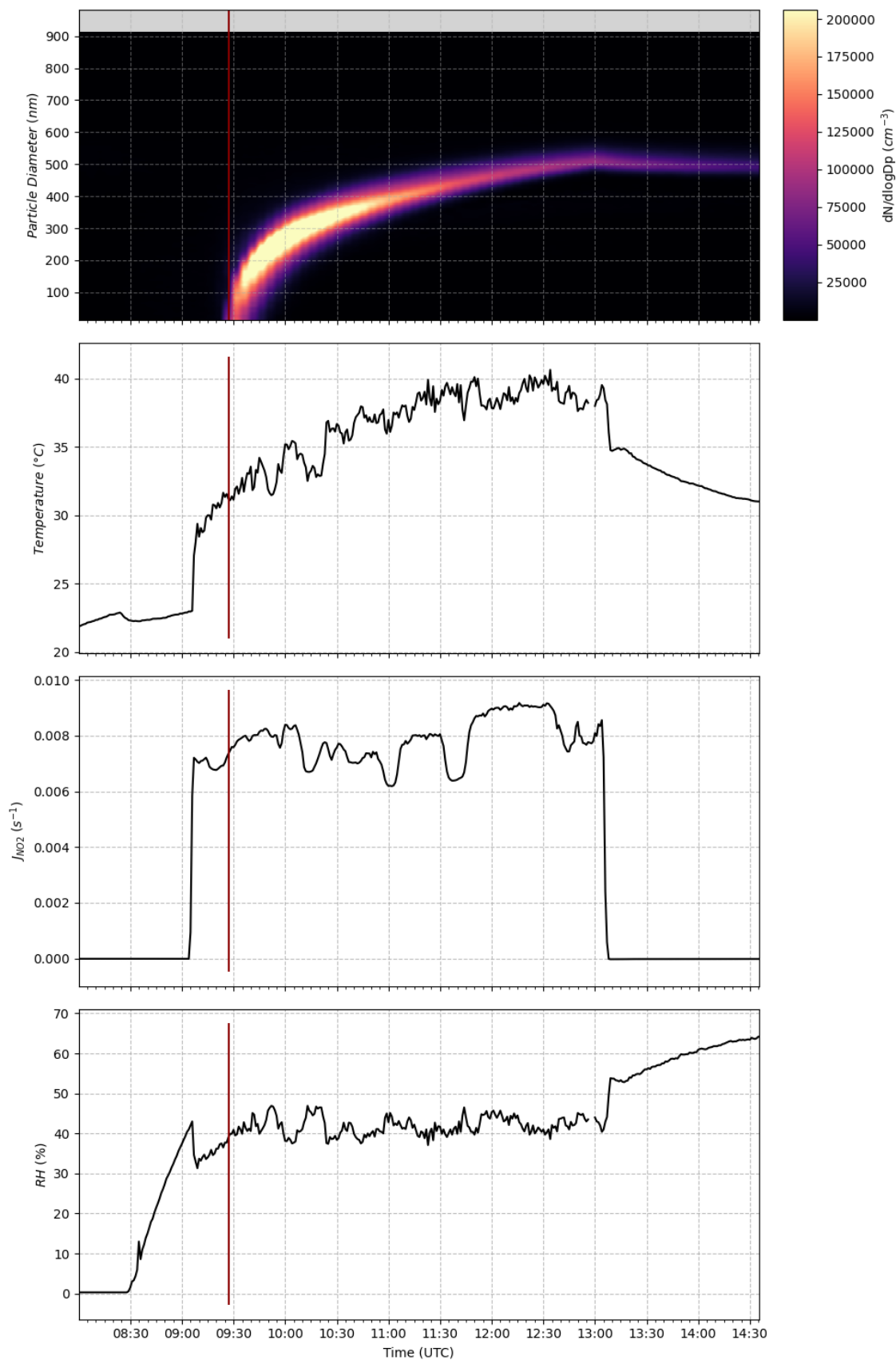
Figure 4.6. Particle number concentrations in the unseeded empty-chamber experiment performed on 2021-06-07, alongside measurements of temperature, J_{NO2}, and RH in the chamber. Each SMPS heatmap uses a unique colour scale.
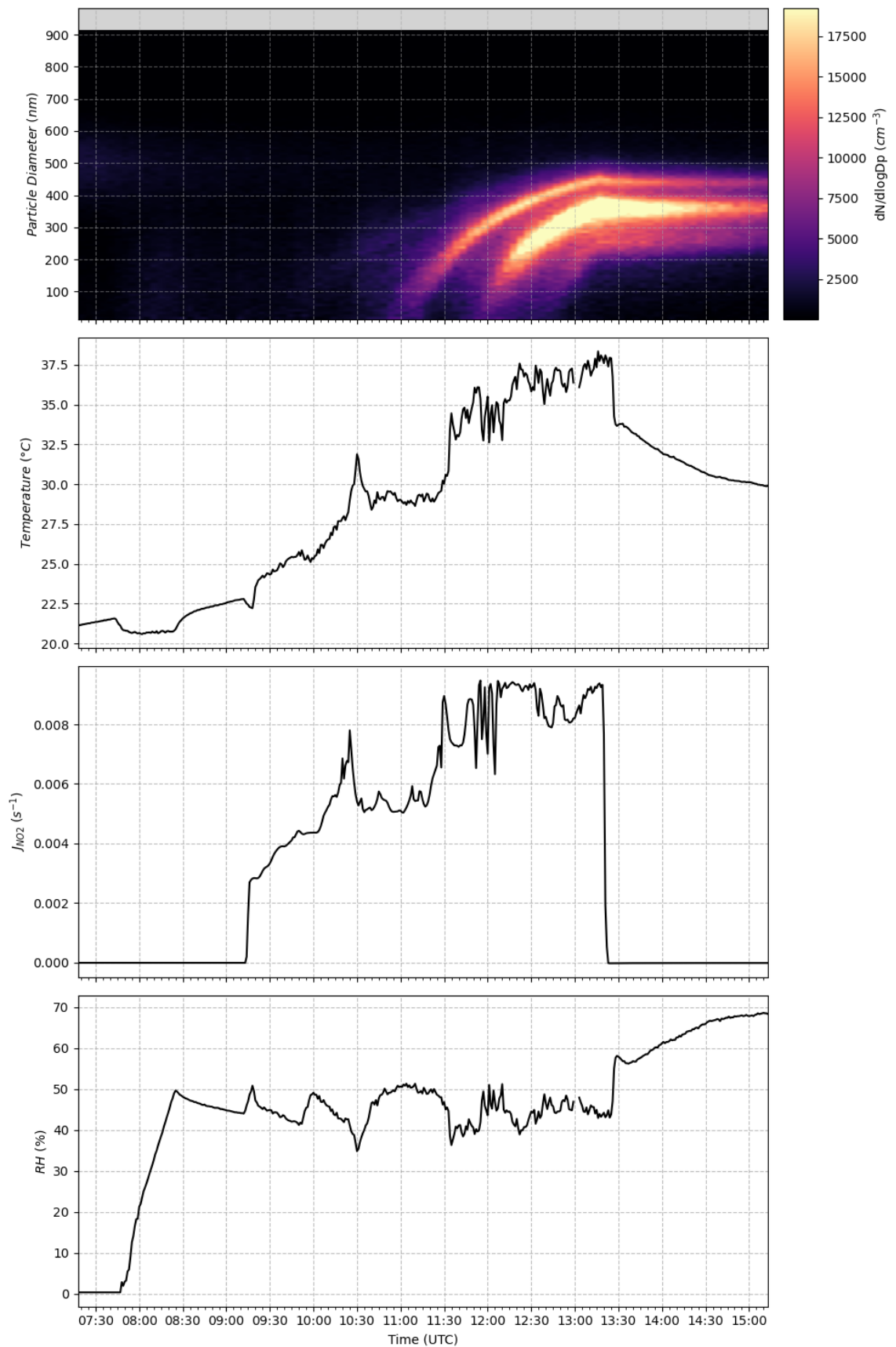
Figure 4.7. Particle number concentrations in the unseeded empty-chamber experiment performed on 2021-06-08, alongside measurements of temperature, JNO2, and RH in the chamber. Each SMPS heatmap uses a unique colour scale.

123

4.4 Evidence for Daytime NO_3 Chemistry

One of the central aims of these experiments was to reproduce the daytime NO_3 chemistry observed in the Beijing 2017 campaign. Figure 4.8 shows the I^--CIMS measurements of ICN and IPN in three Beijing-reproduction experiments. These are unseeded experiments with high-quality I^--CIMS data that represent the range of conditions explored in the Beijing reproduction experiments. The 2021-06-10 experiment is shown in blue and is the extreme case of daytime NO_3 products, as this experiment involved elevated ozone and isoprene concentrations. The 2021-07-05 experiment, shown in orange, also involved elevated isoprene concentrations, but with lower ozone. Finally, the 2021-06-08 experiment shows the case with typical isoprene concentrations but elevated ozone. While ICN is often around 0 during the light portion of the experiments (Figure 4.8a), there is a response to successive isoprene injections into the chamber. The combined signal for IPN and INHE shows a substantial increase during the light portion of the Beijing reproduction experiments, and this is discussed further in Section 4.5.1. These species are only produced via the NO_3-initiated oxidation of isoprene, therefore the increasing concentrations of these compounds during the light portion of these experiments indicates the presence of NO_3 chemistry when O_3 concentrations are high, even when the chamber roof is open.
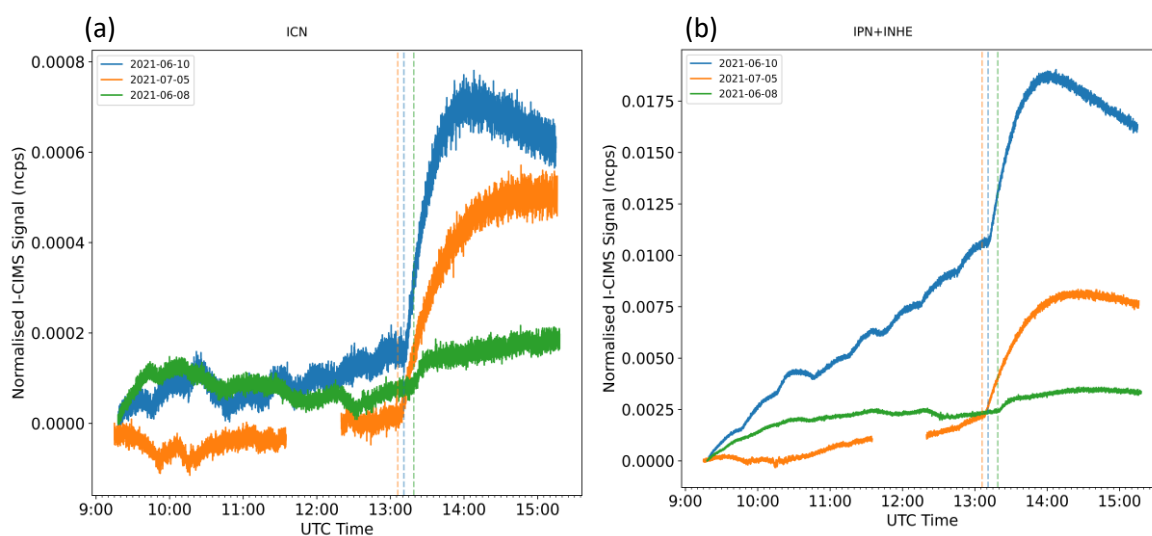
Figure 4.8. I^--CIMS signal for the mass of $C_5H_7NO_4$ and $C_5H_9NO_5$, corresponding to isoprene carbonyl nitrate (ICN) and isoprene hydroperoxy nitrate + isoprene nitrooxyhydroxyepoxide (IPN+INHE) respectively, in three different Beijing reproduction experiments. 2021-06-10 (blue) was a Beijing reproduction experiment with elevated ozone and isoprene concentrations, 2021-07-05 (orange) was a Beijing reproduction experiment with elevated isoprene concentrations, 2021-06-08 (green) was a Beijing reproduction experiment with elevated ozone concentrations. The dashed lines indicate the point at which the roof was closed in each experiment.

The modelling of these experiments also identifies the role of daytime NO_3 chemistry. Figure 4.9 shows the modelled fractional loss of isoprene to OH, O_3, NO_3, and dilution in several of the Beijing reproduction experiments. The results from each experiment are also summarised in Table 4.4. During the light portion of these experiments, although isoprene is predominantly lost to reaction

with OH, up to 20% of the chemical loss of isoprene is comprised of reaction with NO_3. This fraction then increases to comprise 85-95% of the reactivity when the roof is closed in each experiment.

Figure 4.9a shows the modelled isoprene loss for the 2021-07-08 experiment. This experiment involved NO_x, O_3, and isoprene mixing ratios closest to those measured in the Beijing campaign. This resulted in a modelled loss of isoprene to NO_3 of around 2.6% during the light portion, which is consistent with calculations from the Beijing campaign that calculated the loss of isoprene to NO_3 in the afternoon to increase from around 1% at mid-day to around 5% at 17:30.[207]

The fraction of isoprene lost to reaction with NO_3 increased in the 2021-07-05 experiment, where isoprene concentrations are increased to around 10 ppb. This increased loss to NO_3 is the result of the higher O_3 mixing ratios (178 ppb as opposed to the Beijing average of around 100ppb at 16:00) produced by the increased VOC concentration, which increases the production rate of NO_3. As such, the increased NO_3 fractional loss is accompanied by an increase in the fraction of isoprene reacting with O_3 from an average of 4% on 2021-07-08 to 8% on 2021-07-05. This effect of elevated O_3 is further confirmed by Figure 4.9c which shows the model results from 2021-06-08. This experiment used isoprene concentrations similar to those observed in Beijing, but with elevated O_3 concentrations in an attempt to exacerbate the importance of the daytime NO_3 pathway. The model results presented in Figure 4.9c indicate that this attempt was successful, with around 13% of isoprene being lost to reaction with NO_3. However, as with the 2021-07-08 experiment, this also comes with a concurrent increase in the loss of isoprene to O_3, which contributes 11% of the total daytime loss.

Table 4.4. Mean species concentrations and fractional losses of isoprene to NO_3 during the light portion of selected Beijing-reproduction experiments.

Experiment Date	Median Isoprene (ppb)	Median O_3 (ppb)	Median NO_x (ppb)	Median Loss of Isoprene to NO_3 (%)
2021-07-08	3.04	128	14.7	2.64
2021-07-05	11.0	178	14.9	7.60
2021-06-08	5.50	391	16.2	13.3
2021-06-10	27.1	391	14.5	17.1

The extreme case of this high ozonolysis is seen in Figure 4.9d, where high isoprene and O_3 results in ozonolysis accounting for 22% of the isoprene loss in the roof-open portion. Ultimately, Figure 4.9 illustrates that while the Beijing reproduction experiments were successful in reproducing the daytime NO_3 chemistry observed in Beijing, the effects of increased ozonolysis should not be ignored in these very high O_3 conditions.
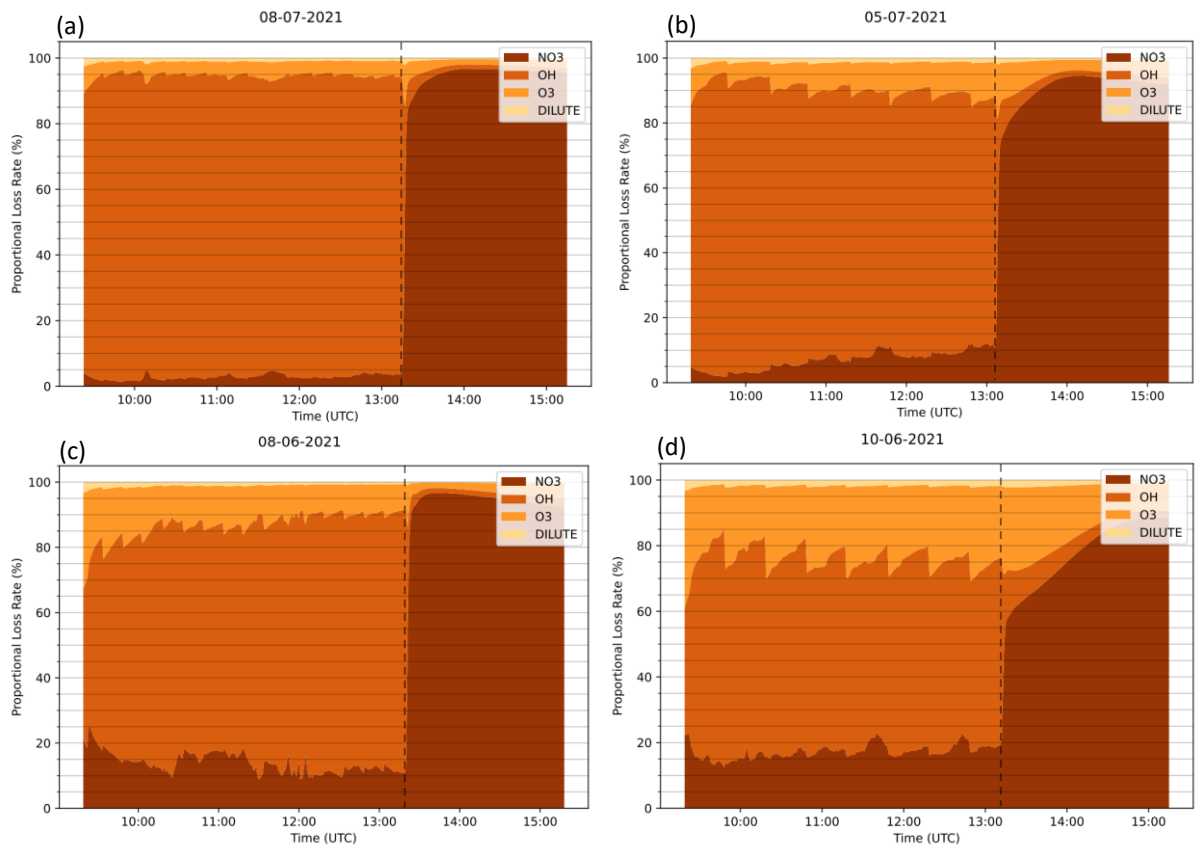
Figure 4.9. Modelled rates of reaction of isoprene with OH, NO$_3$, and O3, and loss to chamber dilution, as a proportion of the total isoprene loss rate. This data is from models of the Beijing Reproduction experiments performed on (a) 2021-07-08, (b) 2021-07-05, (c) 2021-06-08, and (d) 2021-06-10. The dashed line on each plot indicates the point at which the chamber roof is closed.

Figure 4.10a shows the correlation between the fraction of isoprene lost to reaction with NO$_3$ and the measured O$_3$/NO$_x$ ratio. This linear relationship is consistent with findings from Chapter 3, where daytime NO$_3$ concentrations are shown to be almost exclusively dependent on O$_3$ at typical urban NO$_x$ concentrations (Figure 4.10b).
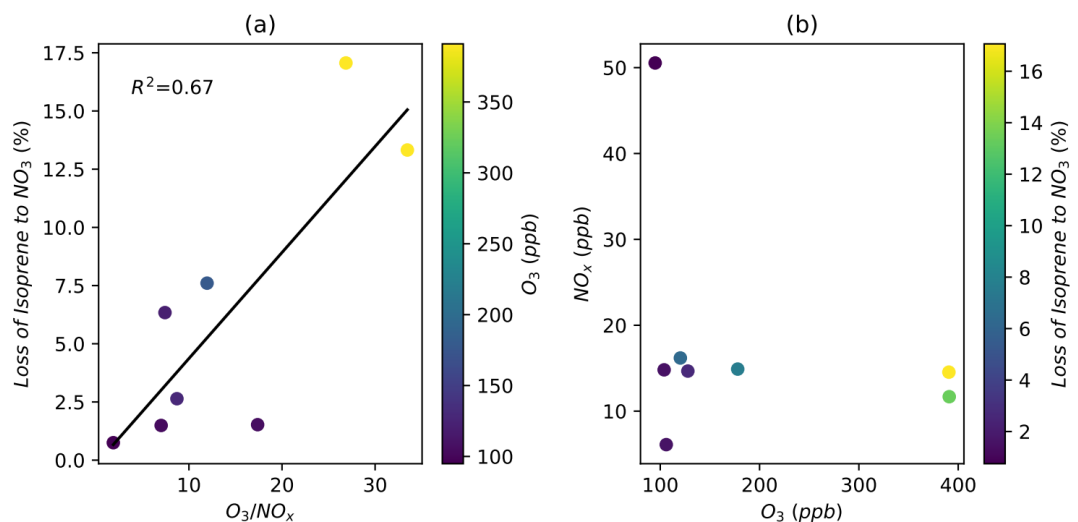
Figure 4.10. (a) Correlation between the average measured O$_3$/NO$_x$ ratio in each experiment and the modelled proportional loss of isoprene to NO$_3$ during the light portion of each experiment. (b) The same proportional loss as a function of average O$_3$ and NO$_x$ concentrations in each experiment.

126

The main deviation from this trend comes from the 2021-06-29 experiment, which has an O_3/NO_x ratio of around 17 and a loss to NO_3 of 1.5%. This experiment involved no addition of NO_x to the chamber, instead relying on the chamber walls to provide low levels of NO_x. This resulted in average NO_x concentrations of 6 ppb alongside the 100 ppb of O_3. The low daytime NO_3 chemistry in this experiment indicates that the formation of NO_3 is limited by the availability of NO_x, as was observed under low NO_x conditions in Chapter 3.

4.4.1 Dinitrate Production from Daytime NO_3 Chemistry

IDN, along with IDNE which is discussed further in Section 4.5.2, represents a special case in the isoprene oxidation products where the formation of the two nitrate groups requires NO_3-initiated oxidation followed by an RO_2 + NO reaction step to form the second nitrate group. The modelling work presented in Chapter 3 illustrated the dependence of IDN formation on daytime NO_3 concentrations and, by extension, ozone concentrations. This same conclusion is supported by Figure 4.11, which shows measured IDN during the selected experiments in Figure 4.8 as well as the high-concentration dark experiment from 2021-06-21, shown in red. This dark experiment shows slow growth in IDN over the course of the experiment because of the low concentrations of NO present, despite the high NO_3 concentrations. In contrast, the high isoprene concentration Beijing-reproduction experiment on 2021-06-10 shows rapid formation of IDN after each isoprene injection in the light portion of the experiment, due to the NO_3 oxidation occurring alongside the presence of moderately low levels of NO. The experiment on 2021-06-08, shown in green, shows an intermediate IDN signal due to the reduced isoprene concentrations used. Similarly, the 2021-07-05 experiment, shown in orange, produces an intermediate IDN signal as the ozone concentrations are lower which reduces the role of daytime NO_3 chemistry. This presents daytime NO_3 chemistry as a potentially important pathway for forming low-volatility dinitrate species in polluted environments similar to Beijing.
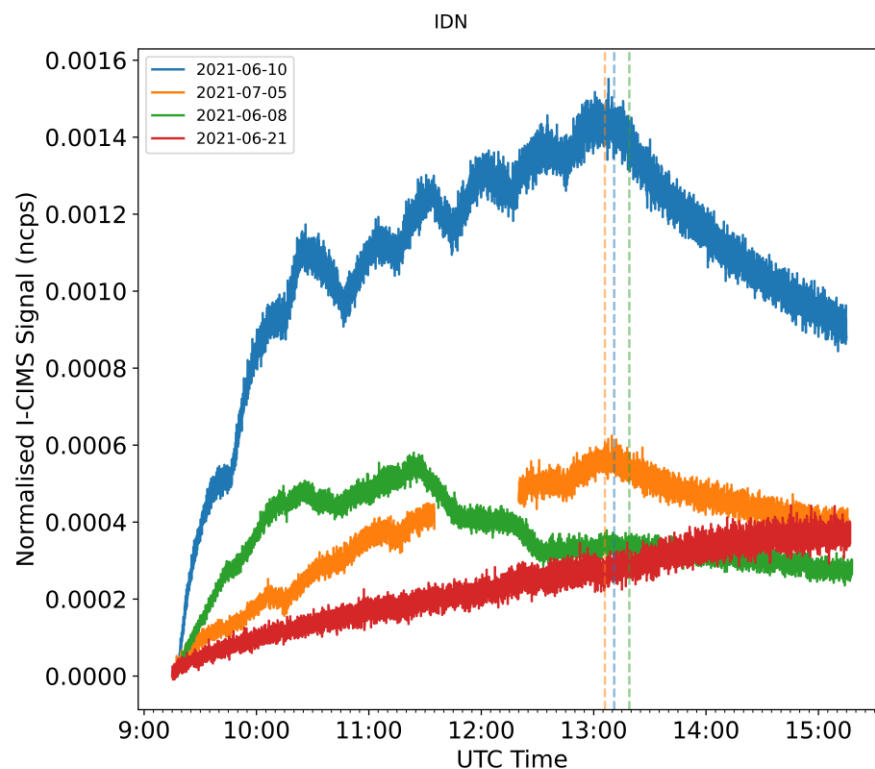
Figure 4.11. I⁻-CIMS signal for the mass of $C_5H_8N_2O_6$, corresponding to isoprene dinitrate (IDN) in four different unseeded EUPHORE experiments. 2021-06-10 (blue) was a Beijing reproduction experiment with elevated ozone and isoprene concentrations, 2021-07-05 (orange) was a Beijing reproduction experiment with elevated isoprene concentrations, 2021-06-08 (green) was a Beijing reproduction experiment with elevated ozone concentrations, 2021-06-21 (red) was a dark experiment with high isoprene concentrations. The dashed lines indicate the point at which the roof was closed in each Beijing reproduction experiment.

4.5 Isoprene Epoxynitrates

As described in Chapter 1, recent studies have proposed a range of nitrated epoxides as products of the oxidation of isoprene by NO_3 (Figure 4.12).[68,124] These include INHE, IDNE, INPE, and INCE, evidence for all of which is seen in the I⁻-CIMS data collected during the EUPHORE experiments.
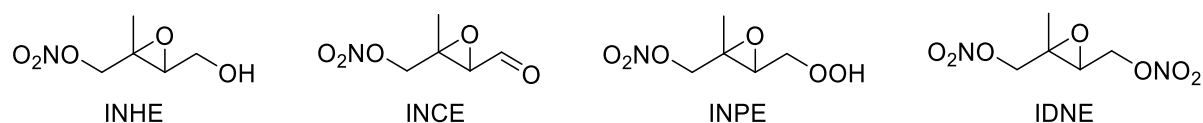
Figure 4.12. Four nitrated epoxides produced via the alkoxy-epoxidation reaction pathway.

4.5.1 INHE

The analysis of INHE by I⁻-CIMS is complicated by the isomeric IPN, meaning that analytical methods such as I⁻-CIMS that differentiate only according to mass, giving information on molecular formula, cannot differentiate these isomeric species. Figure 4.13 shows the measured ΣIPN+INHE from the previously specified Beijing reproduction experiments. This plot illustrates the rapid formation of ΣIPN+INHE from NO_3-initiated chemistry in the dark 2021-06-21 experiment, shown in red. The

Beijing reproduction experiments, show an increase throughout the light portion of the experiments due to the day-time NO_3 chemistry previously explored, followed by a rapid increase in concentrations when the roof is closed, as NO_3 concentrations increase. This is expected based on the known formation routes to IPN and INHE which all rely on the NO_3-initiated oxidation of isoprene.
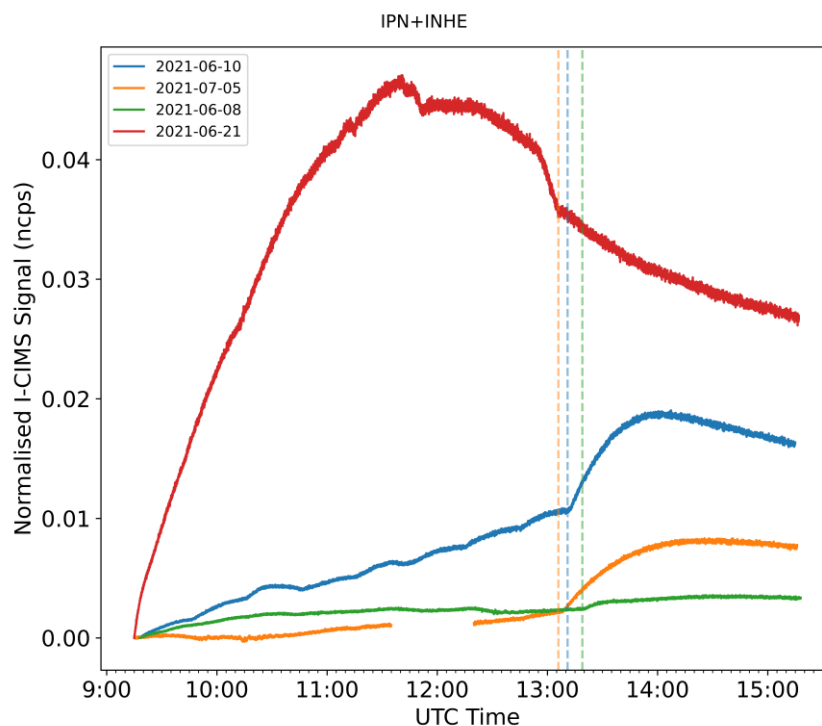
Figure 4.13. I⁻-CIMS signal for the mass of $C_5H_9NO_5$, corresponding to isoprene nitrooxyhydroxyepoxide (INHE) and isoprene hydroperoxynitrate (IPN), in four different EUPHORE experiments. 2021-06-10 (blue) was a Beijing reproduction experiment with elevated ozone and isoprene concentrations, 2021-07-05 (orange) was a Beijing reproduction experiment with elevated isoprene concentrations, 2021-06-08 (green) was a Beijing reproduction experiment with elevated ozone concentrations, 2021-06-21 (red) was a dark experiment with high isoprene concentrations. The dashed lines indicate the point at which the roof was closed in each Beijing reproduction experiment.

Figure 4.14 shows the modelled contribution of INHE, IPN, and other $C_5H_9NO_5$ compounds to the modelled ΣIPN+INHE in the same selection of experiments as Figure 4.13. Figure 4.14b indicates that up to around 20% of the ΣIPN+INHE from isoprene is comprised of INHE during the 2021-07-05 Beijing reproduction experiment. When compared to the results presented in Chapter 1, these models produce a larger proportion of daytime INHE and IPN in the total ΣIPN+INHE.[126] This is the result of a smaller fraction being comprised of C524NO3 and C51NO3. As discussed in Chapter 1, ΣIPN+INHE during the day in the Beijing models is largely comprised of the C524NO3 and C51NO3. However, C524NO3 and C51NO3 both have formation pathways from non-isoprene VOCs that were present in the Beijing models but are not present in the chamber experiments. As such, a higher proportion of C524NO3 and C51NO3 is to be expected in the Beijing models. Both C524NO3 and C51NO3 rely on formation from OH-initiated isoprene oxidation and further reaction with NO, which both require photochemistry to form in large amounts, hence no formation of C524NO3 or C51NO3 is seen in the dark experiment on 2021-06-21 (Figure 4.14d).
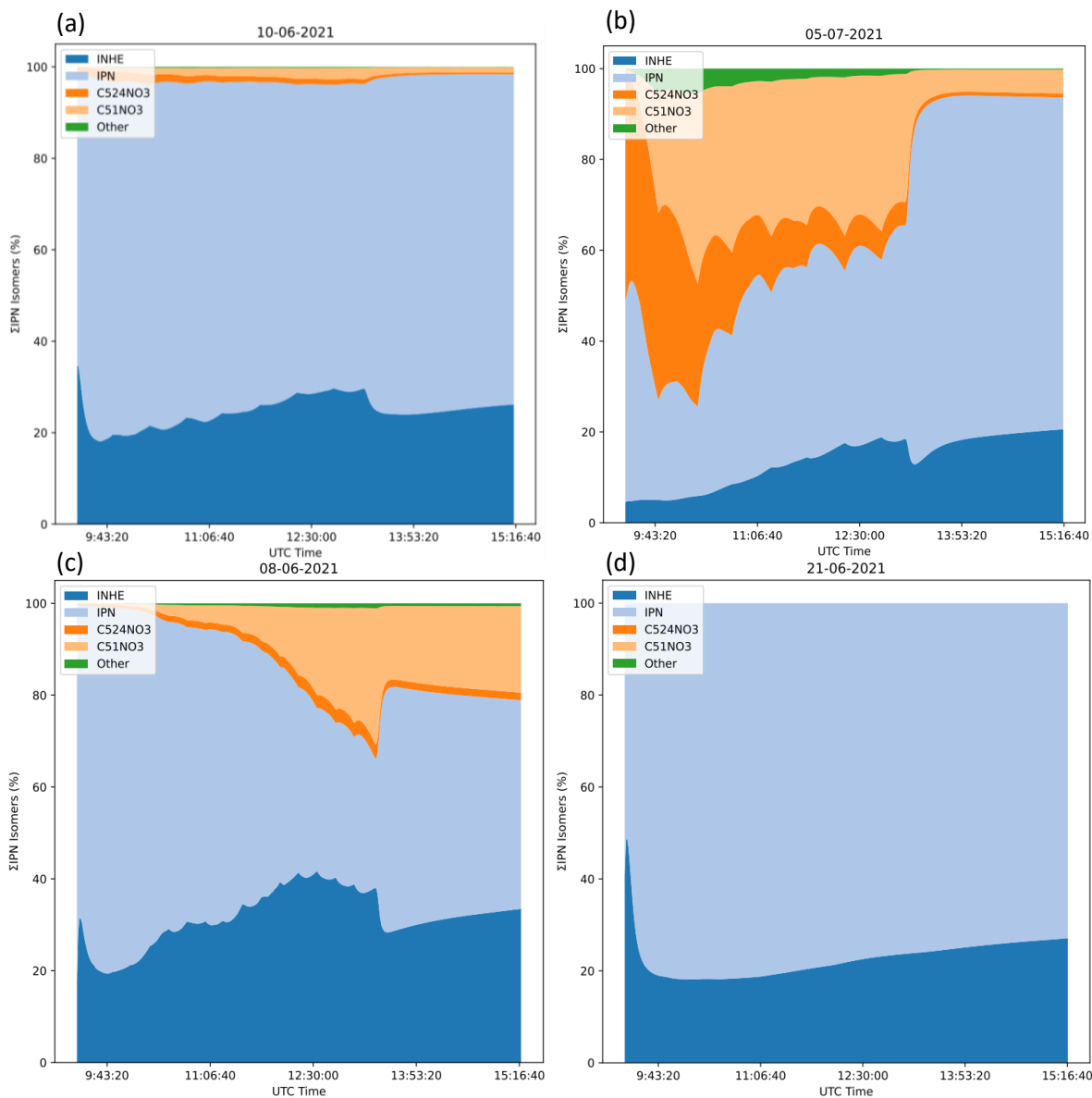
Figure 4.14. Modelled contribution of different groups of $C_5H_9NO_5$ species to the total modelled ΣIPN+INHE.
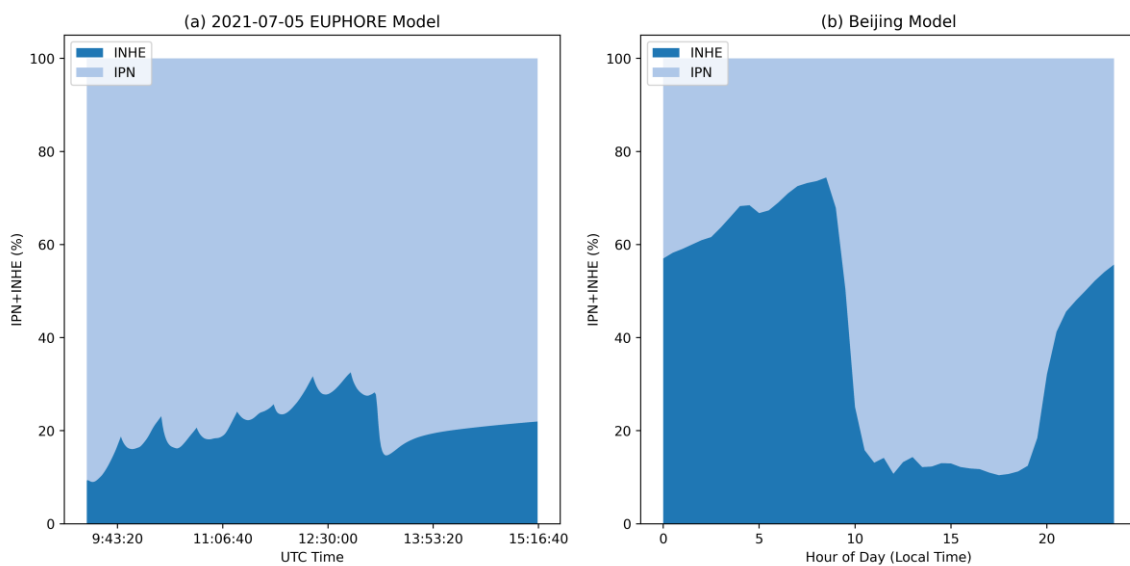
Figure 4.15. Modelled fractions of INHE and IPN. (a) is the output from the model of the 2021-07-05 EUPHORE experiment. (b) shows the diurnal average composition in the Beijing Models described in Chapter 2.

130

In order to directly compare the Beijing model and EUPHORE models, Figure 4.15 shows the fractional contribution of IPN and INHE to the sum of IPN and INHE, without any other isomeric species included. This shows that the daytime portion of the 2021-07-05 experiment has approximately 20% of the IPN+INHE composed of INHE. This is only slightly higher than the daytime diurnal average value in the Beijing model. However, Figure 4.15a doesn't show a large increase in the fraction of IPN+INHE comprised of INHE on roof closure in the Beijing reproduction experiment. This is in contrast to the FZJ Beijing model which shows a much higher contribution from INHE during the night than during the day (Figure 4.15b). This is likely due to the design of the Beijing reproduction experiments which meant that isoprene injections were stopped before the roof was closed, and only a small amount of isoprene underwent primary oxidation in the dark. In the Beijing models, isoprene concentrations were constrained to measured concentrations which were still generally at around 0.5 ppb around sunset, and persisted for longer before reacting away. Even during the night, the measurement would rarely fully reach 0, meaning there was always some isoprene being added to the model and undergoing dark oxidation.

4.5.2 IDNE

Figure 4.16 shows the measured I^--CIMS signal corresponding to IDNE. As discussed in Section 4.4.1 and Chapter 3, the formation of IDNE and IDN require the simultaneous presence of NO_3 and NO, making the Beijing daytime-NO_3 conditions optimal for their formation. As such, the trends between experiments in Figure 4.16 matches the observations in Figure 4.11 for IDN. However, IDNE shows much stronger formation in the Beijing reproduction experiments. The IDNE signal in the 2021-06-10 Beijing reproduction experiment is comparable to the IPN+INHE signal in the dark experiment, indicating potentially large concentrations of IDNE, assuming a consistent response to the I^--CIMS.

IDNE measurements made in the 2017 Beijing Campaign (Figure 4.17) show that IDNE concentrations peak at around mid-day, in contrast to the FZJ Beijing model which shows the highest concentrations at sunset. This indicates that there is either some unrepresented chemistry contributing to the IDNE diurnal profile, or that there is another $C_5H_8N_2O_7$ species contributing to the IDNE I^--CIMS signal. ISOP1N4OH5N, which is formed in the FZJ mechanism through an H-shift reaction of the 1,4-alkoxy nitrate, is the only compound present in any of the mechanisms studied in this thesis that is a positional isomer of IDNE. This compound makes up less than 1% of the total modelled $C_5H_8N_2O_7$ at all times in the Beijing model.

It is not clear what alternative formation route would be available for IDNE or its isomers that would result in a mid-day peak of concentrations, or what the structure of an IDNE isomer that peaks in concentrations at mid-day would be. Furthermore, the modelled IDNE concentrations in the chamber experiments show good agreement with the I^--CIMS IDNE signal (Figure 4.18), so adding

an OH-dependent formation route to an IDNE isomer from isoprene would make this agreement worse. Due to the complex mixture of VOCs present in Beijing air, it is possible that the mid-day peak observed in Beijing results from a precursor other than isoprene.
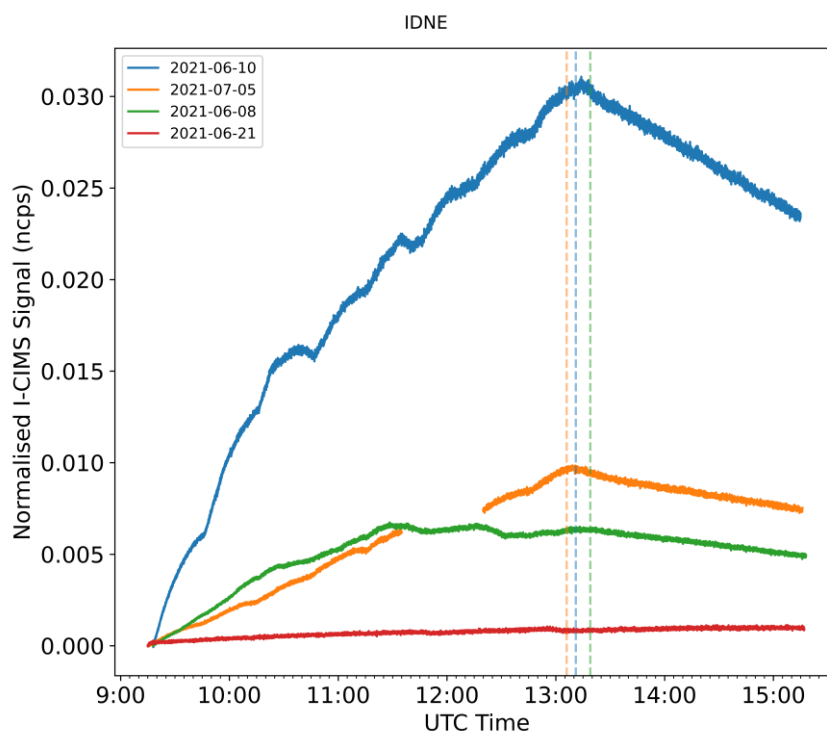
Figure 4.16. I⁻-CIMS signal for the mass of $C_5H_8N_2O_7$, corresponding to isoprene dihydroxynitrooxyepoxide (IDNE), in four different EUPHORE experiments. 2021-06-10 (blue) was a Beijing reproduction experiment with elevated ozone and isoprene concentrations, 2021-07-05 (orange) was a Beijing reproduction experiment with elevated isoprene concentrations, 2021-06-08 (green) was a Beijing reproduction experiment with elevated ozone concentrations, 2021-06-21 (red) was a dark experiment with high isoprene concentrations. The dashed lines indicate the point at which the roof was closed in each Beijing reproduction experiment.
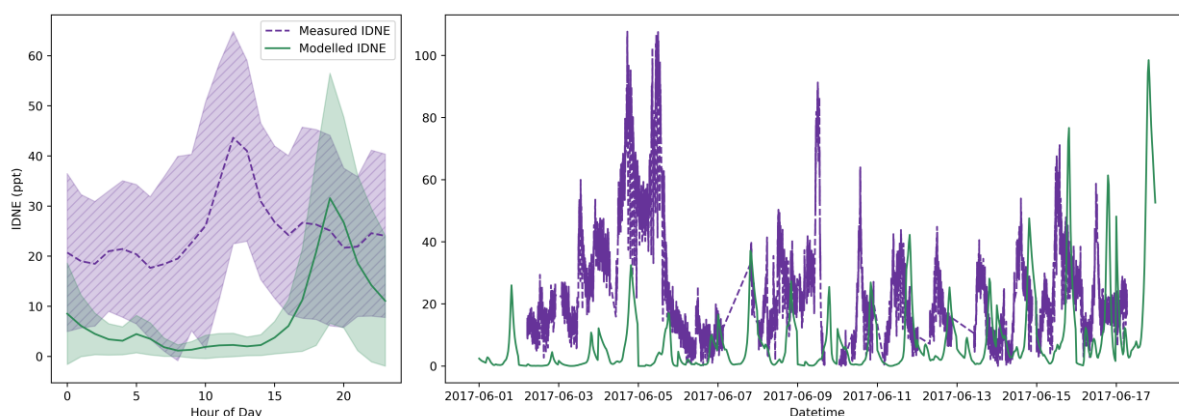
Figure 4.17. Measured and modelled IDNE mixing ratios during the Beijing 2017 campaign, shaded areas in the diurnal plot indicate 1 standard deviation above and below the mean. These plots are similar to those in Mayhew et al. 2022, and use the same model data.[126]
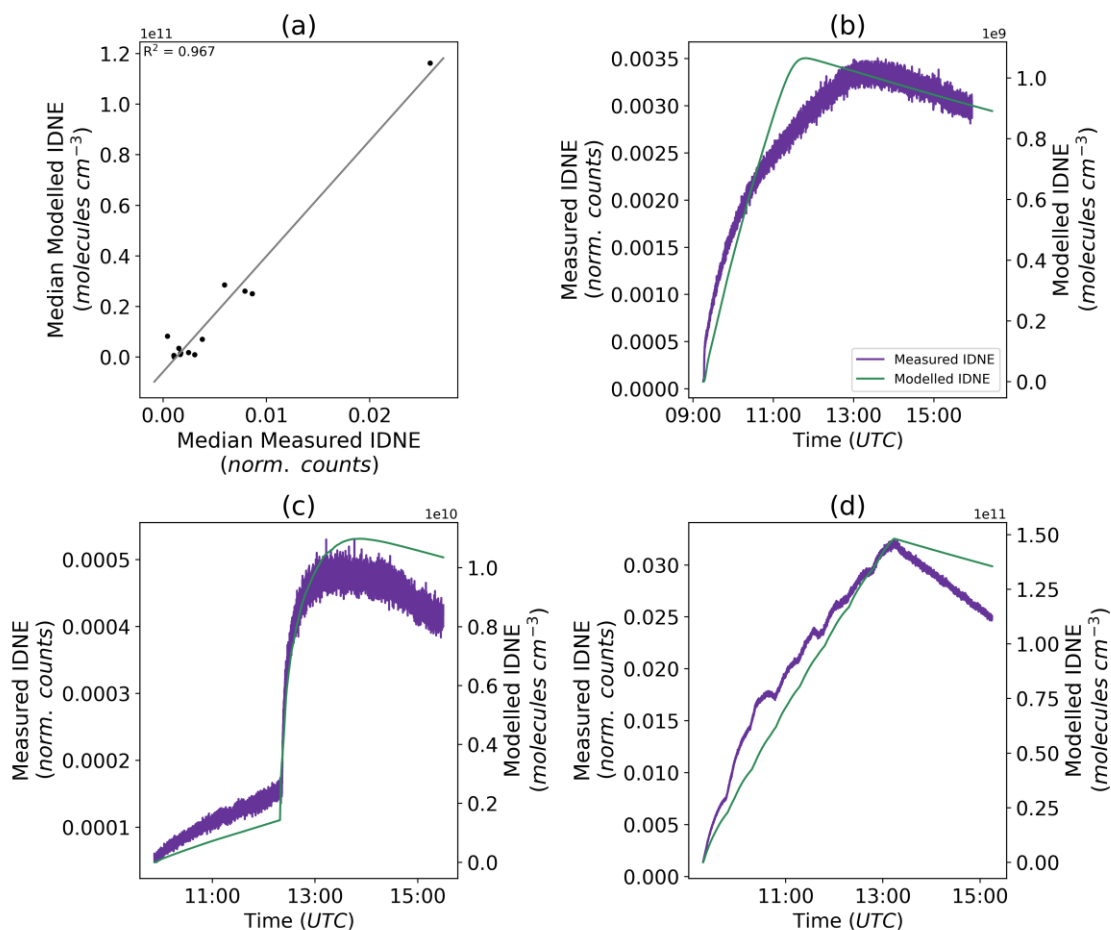
Figure 4.18. A comparison of modelled and measured IDNE in the EUPHORE Chamber experiments. (a) shows the correlation between the modelled and measured median IDNE in each separate experiment. (b-d) show the measured and modelled time series of IDNE in each of the experiments performed on 2021-06-30, 2021-06-03, and 2021-06-10 for (b), (c), and (d), respectively.

4.5.3 INPE and INCE

INPE and INCE both show the highest I^--CIMS signals in the dark experiment on 2021-06-21 (Figure 4.19), as is expected according to the NO_3-initiated formation pathway proposed by Vereecken *et al*.[68] Figure 4.19 also shows that INPE and INCE respond differently to changes in ozone. The experiments performed on 2021-06-10 and 2021-07-05 are performed with 372.6 ppb and 191.4 ppb of ozone, respectively. The 2021-06-10 experiment involves approximately twice the concentration of isoprene. INPE shows similar concentrations in each experiment, whereas INCE shows much lower concentrations in the 2021-07-05 experiment. This is in agreement with the modelling results presented in Chapter 3 which indicate that INCE, like IDN and IDNE, is limited by the availability of daytime NO_3, and so is very sensitive to O_3 concentrations. IPNE is also sensitive to changes in ozone, but to a lesser extent in the absence of a concurrent change in NO_x.
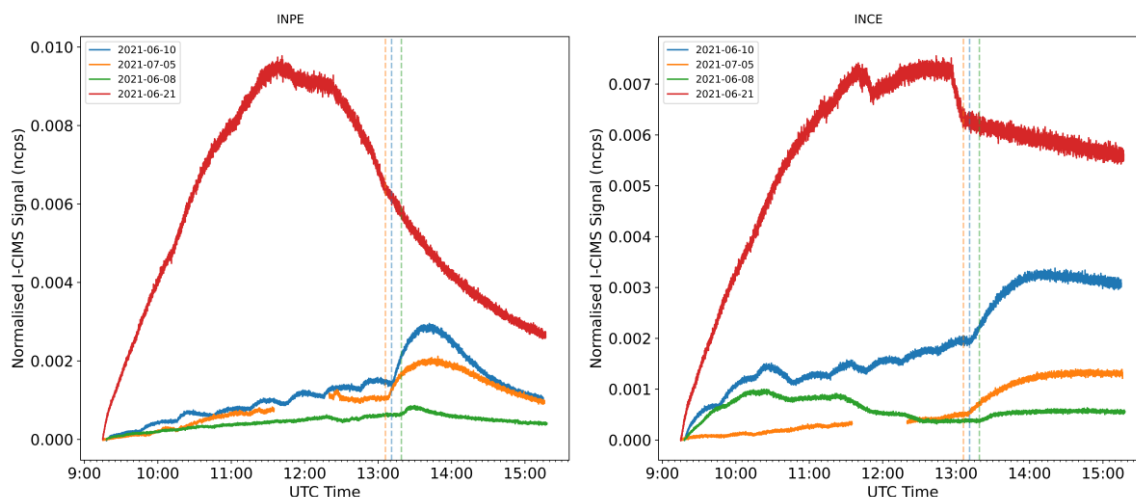
Figure 4.19. I⁻-CIMS signal for the mass of $C_5H_9NO_6$ and $C_5H_7NO_5$, corresponding to isoprene nitrooxyhydroperoxyepoxide (INPE) and isoprene nitrooxycarbonylepoxide (INCE) respectively, in four different EUPHORE experiments. 2021-06-10 (blue) was a Beijing reproduction experiment with elevated ozone and isoprene concentrations, 2021-07-05 (orange) was a Beijing reproduction experiment with elevated isoprene concentrations, 2021-06-08 (green) was a Beijing reproduction experiment with elevated ozone concentrations, 2021-06-21 (red) was a dark experiment with high isoprene concentrations. The dashed lines indicate the point at which the roof was closed in each Beijing reproduction experiment.

4.6 Particle-phase Products

4.6.1 $C_5H_{11}NO_9S$ and $C_5H_{10}N_2O_{11}S$

As discussed in Chapter 1, INHE has been shown to undergo uptake to acidified seed aerosol. In the presence of sulfate ions, this will form products with the formula $C_5H_{11}NO_9S$. This compound is identified in the majority of the filter samples collected in this campaign. Based on the expected formation mechanism, the measured $C_5H_{11}NO_9S$ should be expected to correlate with the average INHE in each experiment. Figure 4.20 shows that there is no correlation with the average measured ΣIPN+INHE (Figure 4.20a) or average modelled INHE (Figure 4.20b) in each experiment.
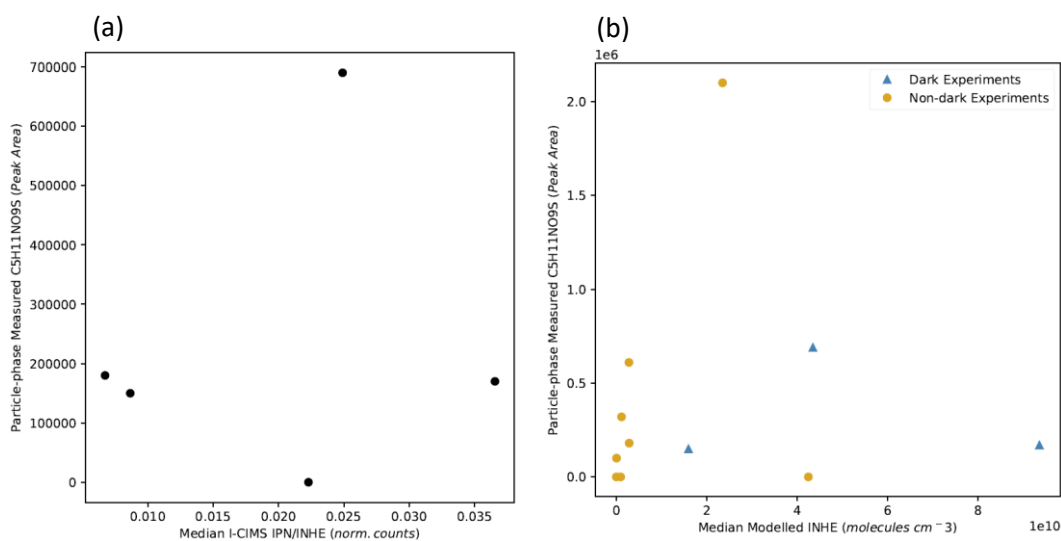
Figure 4.20. Measured $C_5H_{11}NO_9S$ plotted against the median measured ΣIPN+INHE (a) and modelled INHE (b) during each of the seeded experiments. Separate markers are displayed in (b) for the dark experiments (blue triangles), and the non-dark experiments (yellow circles).

As with INHE, IDNE undergoes uptake to acidified seed aerosol and, in the presence of sulfate ions, will form dinitrooxyorganosulfates with the formula $C_5H_{10}N_2O_{11}S$. Based on the I⁻-CIMS data previously presented (Figure 4.16), it should be expected that the highest particle-phase concentrations of $C_5H_{10}N_2O_{11}S$ would be found in the Beijing reproduction experiments. However, the highest concentrations are actually seen in the dark experiments (Figure 4.21). Figure 4.22 illustrates that there is no correlation between the I⁻-CIMS IDNE signal and the LC-MS $C_5H_{10}N_2O_{11}S$ peak area, as may be expected if the two were formed through the same reaction pathway.

The highest concentrations of $C_5H_{10}N_2O_{11}S$ being found in the dark experiments is consistent with findings by Hamilton et al. where this particle-phase dinitrate compound was shown to peak during the night-time in ambient particle-phase measurements from Beijing.[51] Additionally, the experiment performed on 2021-06-28 involved the collection of two filter samples, one before the roof was closed, and one after the roof was closed. Despite the lack of isoprene addition after the roof closure, the 'dark filter' shows 2.7 times more $C_5H_{10}N_2O_{11}S$ than the 'light filter'.
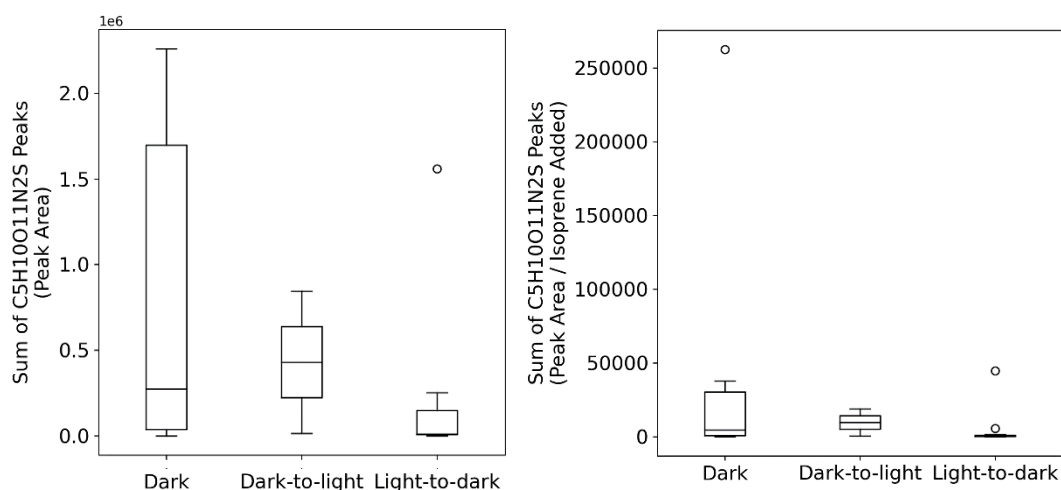
Figure 4.21. The total peak area and normalised peak area of $C_5H_{10}O_{11}N_2S$ in each of the EUPHORE experiments binned by photolysis procedure.

One potential explanation for this discrepancy is particle-phase reactions of $C_5H_{10}N_2O_{11}S$ causing a loss process that dominates the concentration compared to formation from IDNE. A product of the particle-phase reactions of $C_5H_{10}N_2O_{11}S$ could be the mono-nitrated equivalent $C_5H_{11}NO_9S$, which is the expected uptake product of INHE. Figure 4.20b shows that $C_5H_{11}NO_9S$ shows a poor correlation with modelled INHE. Including the modelled IDNE in this plot (Figure 4.23a) improves the R^2 of the correlation, however this is largely driven by a single point with high gas-phase and particle-phase concentrations. $C_5H_{10}N_2O_{11}S$ also shows a poor correlation with modelled INHE + IDNE (Figure 4.23b). Figure 4.23c shows that the sum of $C_5H_{10}N_2O_{11}S$ and $C_5H_{11}NO_9S$ correlates better with the average sum of modelled IDNE and INHE in each experiment, which is consistent with the formation of both $C_5H_{10}N_2O_{11}S$ and $C_5H_{11}NO_9S$ depending on the concentration of both INHE and IDNE. This

could be explained by a set of particle-phase reactions that convert $C_5H_{10}N_2O_{11}S$ to $C_5H_{11}NO_9S$, or vice versa (Figure 4.24).
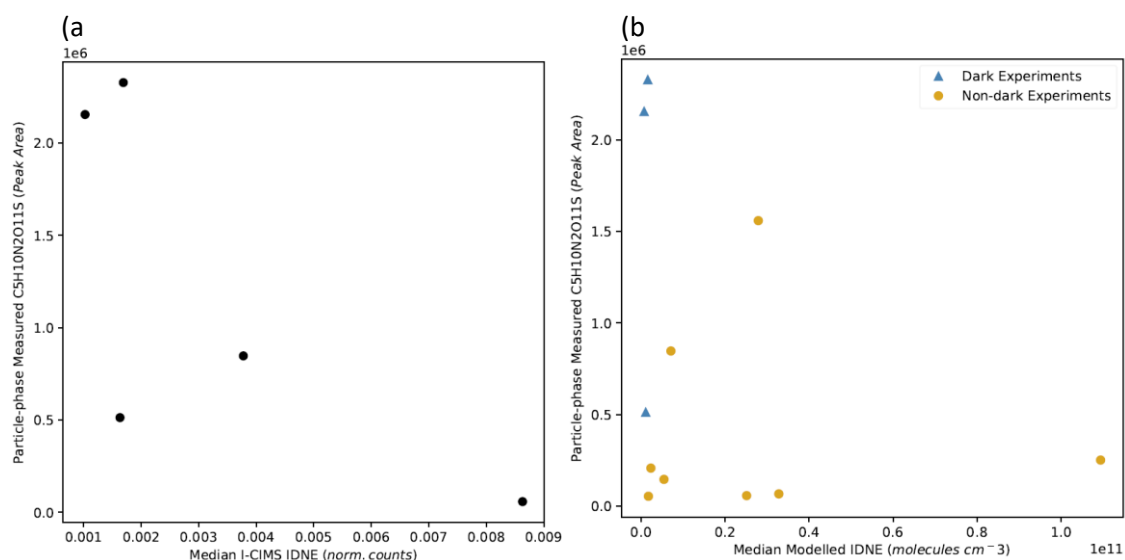
Figure 4.22. Measured $C_5H_{10}O_{11}N_2S$ plotted against the median measured IDNE (a) and modelled IDNE (b) during each of the seeded experiments. Separate markers are displayed in (b) for the dark experiments (blue triangles), and the non-dark experiments (yellow circles).
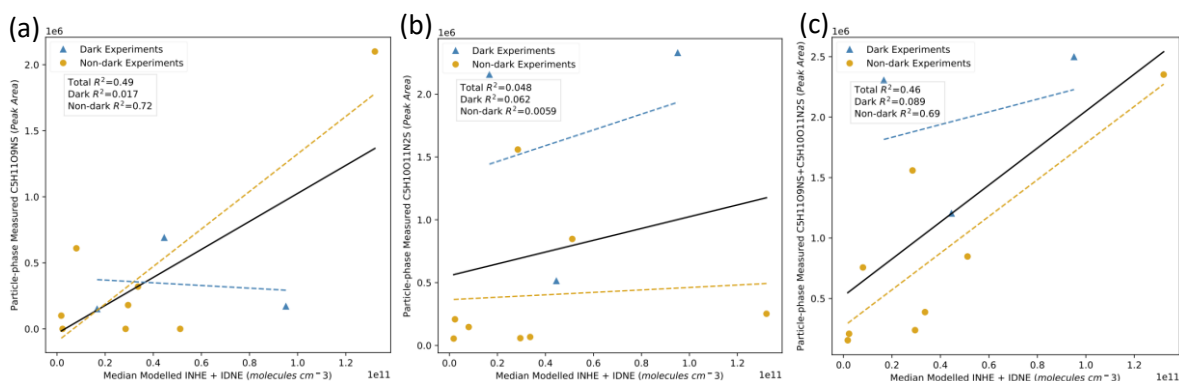
Figure 4.23. Correlations between the modelled sum of INHE and IDNE and measured $C_5H_{11}NO_9S$ (a), $C_5H_{10}N_2O_{11}S$ (b), and $C_5H_{11}NO_9S + C_5H_{10}N_2O_{11}S$ (c).
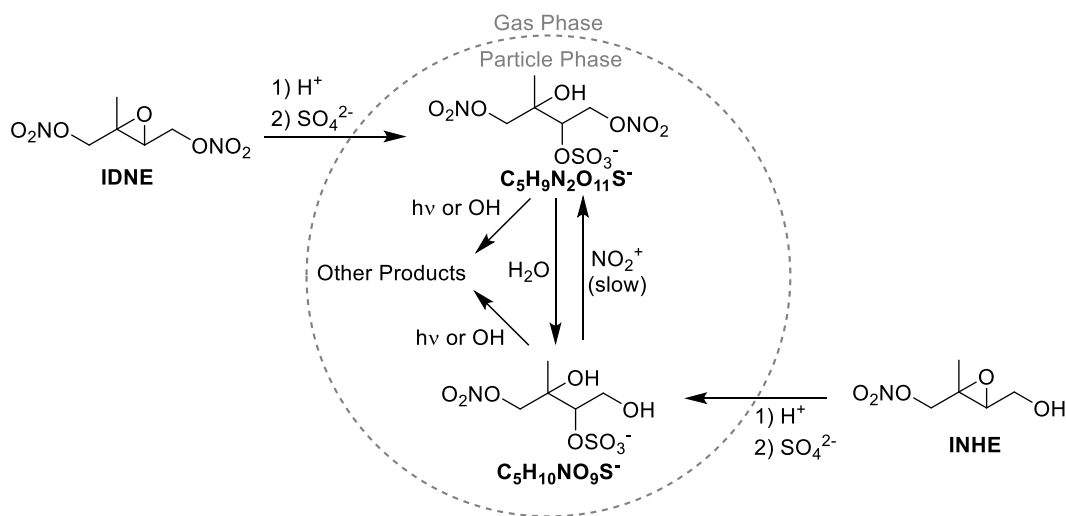
Figure 4.24. Proposed link between IDNE and INHE through particle-phase conversion of $C_5H_{10}N_2O_{11}S$ to $C_5H_{11}NO_9S$.

There is lots of evidence for photo-induced particle-phase degradation of organonitrates, either by direct photolysis of the nitrate group or by reaction with particle-phase OH, which usually dominates the photo-induced loss.[208-213] Photo-induced conversion of $C_5H_{10}N_2O_{11}S$ to $C_5H_{11}NO_9S$ has some potential to explain the high $C_5H_{10}N_2O_{11}S$ concentrations observed in the dark experiments, where this process would be minimised. However, if the conversion process were entirely photo-induced, then a linear relationship should be expected between IDNE and $C_5H_{10}N_2O_{11}S$ in the dark experiments. Although only 3 dark experiments were performed with seed-aerosol present, there is no correlation between IDNE and $C_5H_{10}N_2O_{11}S$ in these three experiments (Figure 4.22b). Additionally, Figure 4.25 shows that there is no correlation between $C_5H_{10}N_2O_{11}S$ and $C_5H_{11}NO_9S$ in the non-dark experiments, as might be expected if $C_5H_{11}NO_9S$ was formed from the large amount of $C_5H_{10}N_2O_{11}S$ anticipated from the gas-phase IDNE concentrations.

There is also no mechanistic basis for the photo-induced conversion of $C_5H_{10}N_2O_{11}S$ to $C_5H_{11}NO_9S$. Direct photolysis of the nitrate group is expected to form an alkoxy radical, which will overwhelmingly be lost by unimolecular decomposition, which does not provide a mechanism for converting $C_5H_{10}N_2O_{11}S$ to $C_5H_{11}NO_9S$.[214] Similarly, OH oxidation in saturated compounds usually proceeds via H-atom abstraction. As such, it is not clear how OH oxidation would provide a conversion route from $C_5H_{10}N_2O_{11}S$ to $C_5H_{11}NO_9S$.
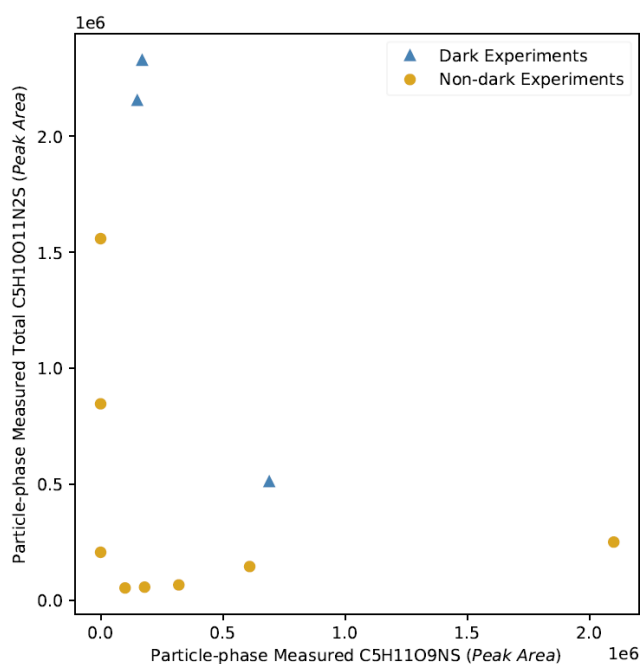
Figure 4.25. Measured $C_5H_{10}O_{11}N_2S$ plotted against the measured $C_5H_{11}NO_9S$ during each of the seeded experiments. Separate markers are displayed for the dark experiments (blue triangles), and the non-dark experiments (yellow circles).

Another established particle-phase degradation mechanism for organonitrates is hydrolysis. The hydrolysis of particle-phase organonitrates has been shown to be rapid, particularly for tertiary nitrates.[131] The hydrolysis process is expected to convert nitrate groups to alcohol groups, which would provide an established route from $C_5H_{10}O_{11}N_2S$ to $C_5H_{11}NO_9S$.[161] However, since all of the

seeded experiments were performed at an RH of over 40%, hydrolysis should play a role in all of the experiments and it is unclear how this would explain the larger-than-expected $C_5H_{10}O_{11}N_2S$ in the dark experiments.

The aerosol-phase conversion of alcohol groups to nitrate groups via reaction with nitronium ions (NO_2^+) has previously been shown to occur in the conversion of methanol to methyl nitrate, but generally at rates too slow to be significant under most atmospheric conditions.[215] However, the reaction rate was shown to be very sensitive to particle acidity as NO_2^+ is formed from HNO_3 under acidic conditions. This provides a potential pathway for the conversion of $C_5H_{11}NO_9S$ to $C_5H_{10}O_{11}N_2S$ in these experiments, where acidified seed particles were used, and the NO_x added to the chamber provides HNO_3 in the particle phase. There is no further work exploring the rate of this reaction for molecules larger or more complex than methanol in atmospheric aerosols. Interestingly, the conversion of alcohols to organonitrates ('O-Nitration' of alcohols) via NO_2^+ is an established method in synthetic organic chemistry, often making use of mixed HNO_3/H_2SO_4 systems or N_2O_5, albeit under very acidic conditions or in the presence of catalysts.[216-218] These reactions are also generally conducted in inorganic solvents, rather than water. As such, while this could be an interesting particle-phase reaction pathway worthy of further scrutiny, it cannot be invoked as an explanation of the particle-phase observations made here.

4.6.2 $C_5H_9NO_9S$ and $C_5H_{11}NO_{10}S$

Based on the uptake of INHE and IDNE to the particle phase, the same process may be expected to occur for INPE and INCE. No compounds with the formulae $C_5H_{11}NO_{10}S$ or $C_5H_9NO_9S$ are observed above the limit of detection of the filter analysis, as might be expected from the reactive uptake of INPE and INCE. The dark experiment on 2021-06-21 shows similar INPE and INCE signals as the ΣIPN+INHE signal scaled by the expected proportion of INHE (Section 4.5.1), so the lack of observations is unlikely to be the result of low INPE and INCE concentrations unless these species are particularly sensitively detected by the I$^-$-CIMS.

The lack of $C_5H_9NO_9S$ and $C_5H_{11}NO_{10}S$ observations could be due to rapid loss in the particle phase. Hydroperoxide groups have been shown to be vulnerable to acid cleavage of the oxygen-oxygen bond, [219] and to undergo heterogeneous decomposition under humid conditions.[220] Despite this reactivity, hydroperoxides are still often observed as major components of SOA, particularly as the result of ozonolysis, although there are no prior observations of organic hydroperoxides that also include the nitrate and sulfate functionalities. Carbonyls have also been proposed as sites of a large array of acid-catalysed particle-phase reactions, potentially accounting for the lack of observation of $C_5H_9NO_9S$ in these experiments.[214,221] One potential loss of $C_5H_9NO_9S$ is described in Section 4.6.3.

Alternatively, these species may be present at similar concentrations to other particle phase species but be less sensitively detected by UHPLC-ESI-MS. Response factors of species to ESI has been

shown to vary by orders of magnitude between similarly-structured compounds, however sensitivities have been shown to be far less variable for organosulfates. [222-224]

4.6.3 $C_5H_9NO_{10}S$

Previous work, including from the 2017 Beijing campaign, has identified $C_5H_9NO_{10}S$ as a major isoprene-derived NOS.[51,225] $C_5H_9NO_{10}S$ was observed in many of the filters collected during these experiments, serving as evidence of this compound as a product of isoprene oxidation under atmospherically-relevant conditions. Hamilton *et al.* 2021 proposes the formation of this species via two pathways (Figure 4.26), either via an isoprenenitrooxy hydroxy-α-lactone (INHL) intermediate or via particle-phase reactions of the $C_5H_{11}NO_9S$ species discussed earlier.
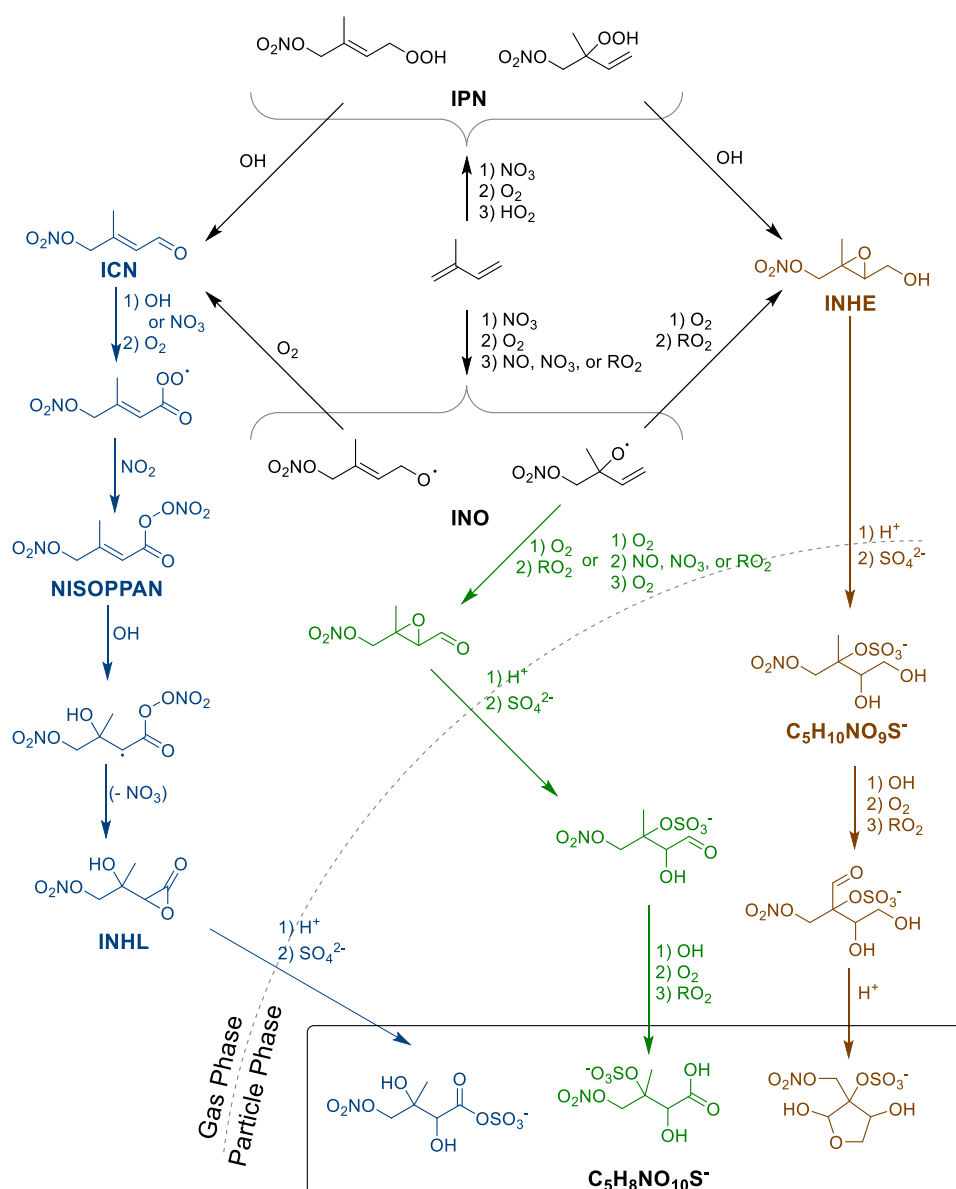
Figure 4.26. Two formation pathways to, and structures of, $C_5H_9NO_{10}S$ (shown here in their deprotonated forms) proposed by Hamilton et al.[51] The first route, shown on the left hand side in blue, proceeds via an isoprenenitrooxy hydroxy-α-lactone (INHL) intermediate, and the second route, shown on the right hand side in brown, proceeds via isoprene nitrooxyhydroxy epoxide (INHE). An extra route is proposed here in green based on the expected reactive uptake of INCE formed via the alkoxy-epoxidation pathway proposed by Vereecken et al.[68] Additional products and reaction pathways are omitted for clarity, including isomers of the key species.

The measured $C_5H_9NO_{10}S$ from the filter samples is generally higher in experiments with higher average measured NO_x concentrations (Figure 4.27), which is not observed for any of the other particle-phase species investigated here. Plotting the particle-phase measurement against the average modelled concentrations of NO and NO_2 show that this correlation with NO_x is driven by a correlation with NO_2, and that there is no such relationship with NO (Figure 4.28). Additionally, a lack of correlation with average modelled NO_3 concentrations indicates that the increased formation under high NO_2 is not the result of increased NO_3 via the NO_2+O_3 reaction.

It is important to consider that this relationship only holds well when including the whole set of unseeded experiments. Taking only the experiments where the roof is open for some period (non-dark experiments) shows a correlation driven by one experiment that shows both high NO_x and $C_5H_9NO_{10}S$. This experiment is the dark-to-light experiment performed on 2021-06-04. Performing Beijing reproduction experiments at a wider range of NO_x values would better demonstrate whether this correlation holds across both light and dark isoprene oxidation.
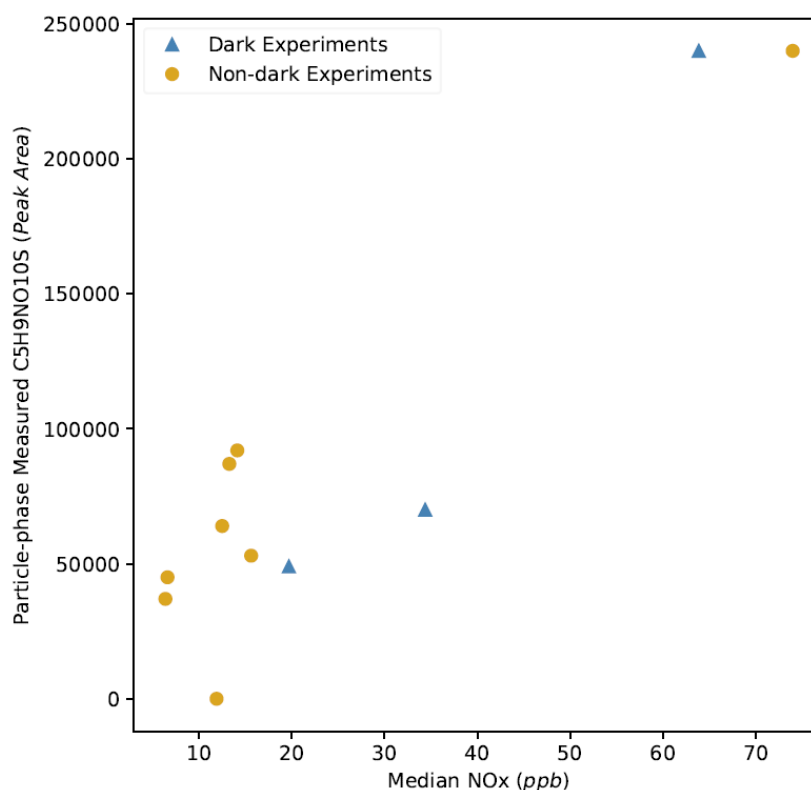
Figure 4.27. Measured $C_5H_9NO_{10}S$ plotted against the median measured NO_x during each of the seeded experiments. Separate markers are displayed for the dark experiments (blue triangles), and the non-dark experiments (yellow circles).
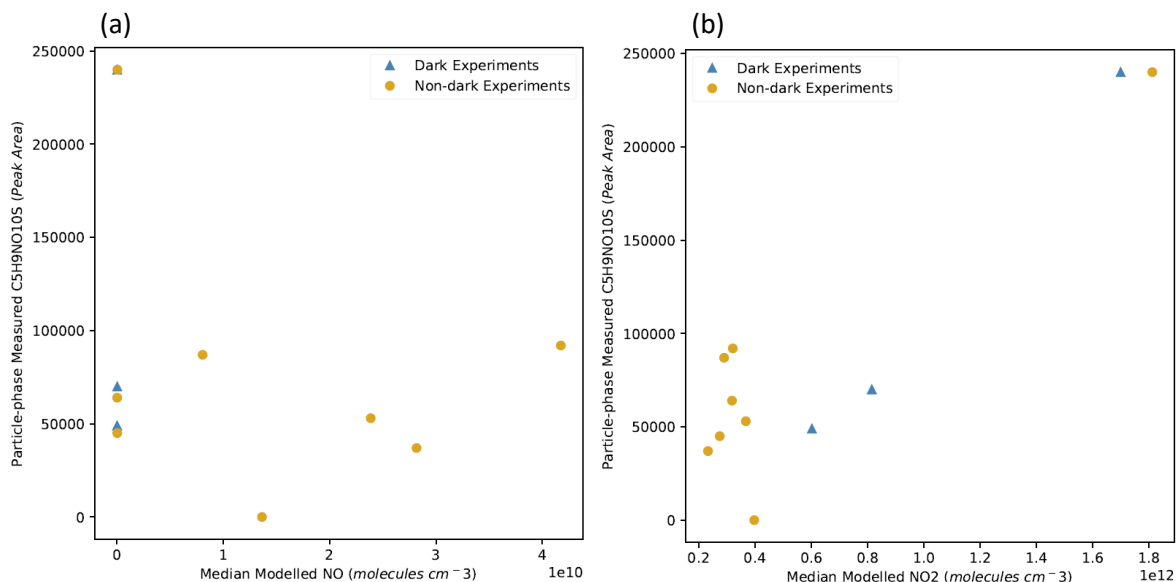
Figure 4.28. Measured $C_5H_9NO_{10}S$ plotted against the median modelled NO (a) and NO_2 (b) during each of the seeded experiments. Separate markers are displayed for the dark experiments (blue triangles), and the non-dark experiments (yellow circles).

The increased formation of $C_5H_9NO_{10}S$ under high NO_2 may support the INHL pathway proposed by Hamilton *et al.*[51] as the major formation route to this compound, as NO_2 is required for reaction with the acyl peroxy radical to form NISOPPAN (Figure 4.26). This is further supported by a similar relationship with measured and modelled NISOPPAN as with NO_2. However, this correlation could simply be a result of the fact that NISOPPAN requires NO_2 for its formation. There is a moderate correlation with measured IPN+INHE, and ICN ($R^2 = 0.70$ and 0.64 for the median measured ICN and IPN+INHE respectively, excluding the unseeded experiments) which lends further weight to the INHL formation route, as both IPN and ICN are proposed precursors of $C_5H_9NO_{10}S$.

Separate correlations of the particle-phase species with modelled IPN and INHE shows a reasonable linear correlation with both ($R^2 = 0.53$ and 0.66 for the median modelled IPN and INHE respectively, excluding the unseeded experiments), which may provide some evidence for the formation via particle-phase reactions of the $C_5H_{11}NO_9S$ species, as INHE is the expected precursor in this case (Figure 4.26). However, there is also a correlation between $C_5H_9NO_{10}S$ and modelled INCE and INPE (Figure 4.29). Since INCE, INPE, and INHE can all form via the same alkoxy-epoxidation route, they will correlate with each other, and so the observed correlation of $C_5H_9NO_{10}S$ with each of these compounds might suggest formation via any subset of the three.
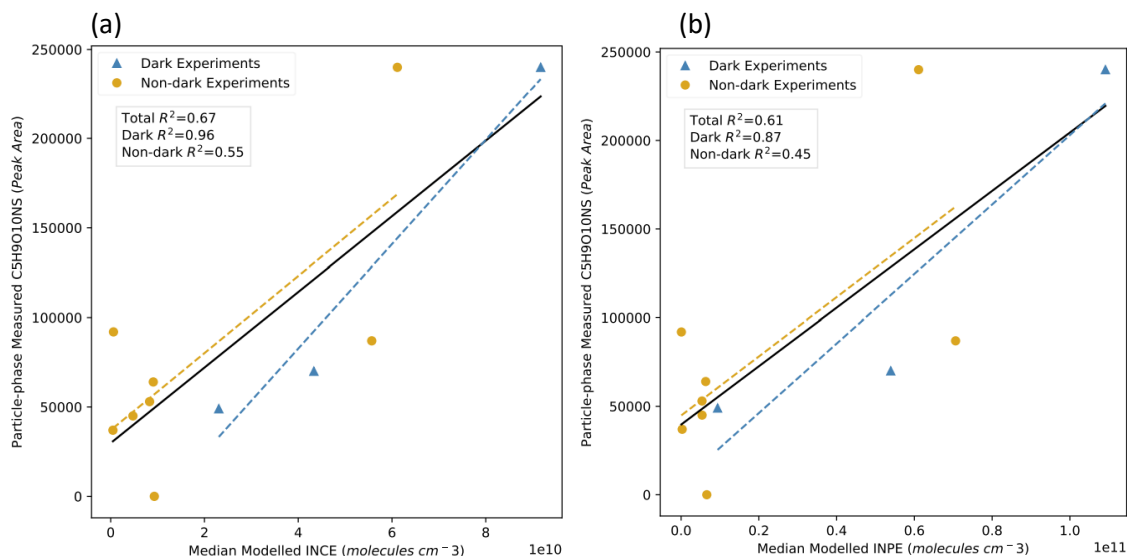
Figure 4.29. Correlation between the measured $C_5H_9NO_{10}S$ and the median modelled INCE (a) and INPE (b) during each of the experiments. Separate regression lines and R^2 values are displayed for when all seeded experiments are included in the linear regression (solid black line), when only the dark experiments are used (dashed blue line), and when the dark experiments are excluded (dashed yellow line).

One potential formation route to $C_5H_9NO_{10}S$ is by the particle-phase reaction of the reactive uptake product from ICNE (Figure 4.30). This proposed particle-phase intermediate is not observed in the filters collected in these experiments, as is discussed in Section 4.6.2. The aldehydic nature of the carbonyl group in two of the three ICNE isomers means that the reaction between OH and the uptake product in the particle-phase could proceed via abstraction of the aldehydic hydrogen to form an acyl peroxy radical. This acyl peroxy radical can then react with RO_2 to form a carboxylic acid group. This explains the good correlation between $C_5H_9NO_{10}S$ and INCE but does not explain the correlation with NO_2.
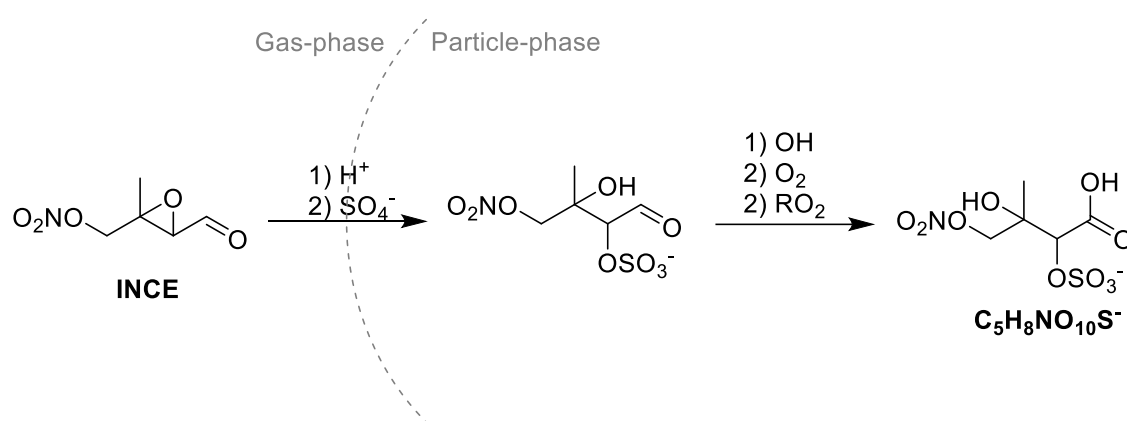
Figure 4.30. Proposed formation pathway to $C_5H_9NO_{10}S$ (shown here in its deprotonated form) from isoprene nitrooxy carbonyl epoxide (INCE).

4.7 Conclusions and Future Work

4.7.1 New Particle Formation

Particle nucleation in these experiments provide a demonstration of the potential impact that chamber walls can have on processes occurring within the chamber. While these experiments provide evidence for particle nucleation from low concentrations of isoprene, the role of species emitted by the chamber walls in this process is uncertain. For example, the nucleation events don't appear to occur under periods of low solar irradiance. This could be a requirement for photochemistry to form low volatility compounds from isoprene or could be the result of photo-initiated emission of compounds from the chamber walls.

While the chamber experiments performed here did involve flushing of the chamber overnight between each experiment, future experiments investigating particle-phase processes under humid environments should ensure better cleaning of the chamber. For example, a period where the chamber roof is opened before each experiment, while flushing the chamber with clean air, might help to avoid this wall-induced NPF. Alternatively, the overnight flushing could be accompanied by artificial irradiation with UV lamps to try and remove as much of the wall contamination.

4.7.2 Daytime NO_3 Chemistry

The EUPHORE experiments clearly demonstrate the potential role of daytime NO_3 chemistry under polluted conditions where high O_3 concentrations are present, which validates the conclusions reached in Chapter 2, Chapter 3, and previous studies into Beijing chemistry.[51,66] Modelling demonstrates that 2.5% of isoprene can be lost to reaction with NO_3 under NO_x and O_3 concentrations typical for the afternoon period in Beijing. This fraction can be increased by increasing the ozone concentration in order to reduce NO concentrations, while total NO_x remains unchanged.

The daytime NO_3 chemistry is also reflected in the day-time formation of gas-phase organonitrates which are typically considered night-time oxidation products of isoprene, such as ICN and IPN. These polluted conditions are demonstrated as efficient conditions for the formation of dinitrate compounds from isoprene, such as IDN and IDNE, where the simultaneous presence of NO and NO_3 is required for the formation of both nitrate groups. This could be further confirmed by more measurements of IDN and IDNE under a range of ambient NO_x and O_3 conditions. While IDN showed lower signal in these experiments, IDNE shows I⁻-CIMS signals on par with those from widely studied isoprene organonitrates such as ΣIPN+INHE. However, IDNE measurements collected during the Beijing 2017 campaign show evidence of an isomeric species that peaks at mid-day which may hamper ambient measurement attempts with techniques that don't include the separation of isomeric species.

4.7.3 Gas-phase Nitrooxyepoxides and Reactive Uptake

The measurements of the gas-phase epoxides investigated in this work provide experimental evidence for their formation from isoprene. Furthermore, the magnitude of the I$^-$-CIMS signals measured indicates that the concentrations of these nitrooxyepoxides could be in the same range as those of more widely studied nitrates. This has implications for SOA formation from isoprene, as reactive uptake of these nitrooxyepoxides has the potential to form low volatility particle-phase species, particularly IDNE which showed the highest concentrations of these novel epoxides and will also form the lowest volatility oxidation products due to the two nitrate groups present in the molecule.

The particle phase analysis showed evidence for a range of isoprene tracers, confirming their formation from isoprene and not from other VOCs present in ambient analyses. Analysis of the particle-phase products expected to result from the reactive uptake of INHE and IDNE indicate that the formation of $C_5H_{11}NO_9S$ and $C_5H_{10}O_{11}N_2S$ in the particle phase is not simply the result of reactive uptake of INHE and IDNE respectively. Instead, there is likely chemical conversion of $C_5H_{10}O_{11}N_2S$ to $C_5H_{11}NO_9S$ in the particle-phase. Hydrolysis reactions provide an established non-photo-induced route from $C_5H_{10}O_{11}N_2S$ to $C_5H_{11}NO_9S$, and there is little evidence that suggests $C_5H_{10}O_{11}N_2S$ may be formed from $C_5H_{11}NO_9S$. A non-photo-induced process like hydrolysis cannot explain the high concentrations of $C_5H_{10}O_{11}N_2S$ observed in the dark experiments (when IDNE concentrations are very low), so it is possible that $C_5H_{10}O_{11}N_2S$ in the particle-phase is also undergoing photolysis and reaction with OH which reduces the concentrations during the non-dark experiments.

No evidence is seen of the INCE and INPE uptake products in the filter analysis, which could be the result of rapid chemical loss in the particle phase as both hydroperoxide groups and carbonyl groups have been shown to be reactive sites for particle-phase processes. The lack of detection could also result from slow reactive uptake of these particular epoxides. Alternatively, a high sensitivity of IDNE and INPE to detection in the I$^-$-CIMS or a low sensitivity of the uptake products to the HPLC-ESI-MS could justify the lack of detection of these compounds when we observe high gas-phase signals.

$C_5H_9NO_{10}S$ was detected in the filter extracts from these experiments, confirming its formation from isoprene, though the mechanism of formation is still uncertain. $C_5H_9NO_{10}S$ shows a correlation with NO$_2$ which may support formation via a PAN species, however this needs to be further supported by more experiments at a wider range of NO$_x$ concentrations. Additional correlations with nitrooxyepoxide species suggests an additional potential formation pathway involving the reactive uptake of INHE or INCE. The formation pathway to this particle phase species could be confirmed by chamber or flow reactor studies directly investigating INHE and IDNE in the absence of other oxidation products that result from this study where oxidation begins from isoprene oxidation. This

would be difficult as it would require the chemical synthesis of the INHE and IDNE species, which are not commercially available.

4.7.4 Improvements for Future Chamber Studies

One of the difficulties when planning these experiments was the ability to cover a wide range of photolysis conditions, NO concentrations, and seed concentrations. With a limited amount of experiment time, there is a trade-off between the breadth of the experiments and the confidence in the results that comes from performing repeats. In light of this, it may have been more useful in these experiments to focus on a smaller number of Beijing reproduction experiments and performed each experiment at least twice. Excluding the non-Beijing reproduction experiments would also allow for a wider range of NO_x and O_3 concentrations to be explored, which was shown to be important in Chapter 3 and Section 4.6.

Similarly, this campaign involved experiments in the presence and absence of acidified seed aerosol in an attempt to identify particle-specific pathways. In hindsight, it is clear that the changes resulting from adding seed to an experiment are complex and will alter the concentration of oxidants as well as oxidation products. For example, adding seed will change the gas-phase concentration of NO_3 due to the uptake of N_2O_5 to the particle phase. This means that it is difficult to attribute differences between oxidation products in the seeded and unseeded experiments to particle-phase processes involving the oxidation product itself or the oxidants required to form those oxidation products. This is especially difficult considering the absence of NO_3 measurements in these experiments. This complexity means that it may have been beneficial to focus on repeating seeded experiments in order to draw firmer conclusions about the particle-phase chemistry described in Section 4.6, as opposed to trying to run each experiment in the presence and absence of seed.

More generally, the analysis of particle-phase species could be improved by performing more chamber experiments in the presence of acidified seed aerosol, these experiments would need to be performed under both dark and light conditions in order to clarify the apparent different behaviour between each group in the correlation plots. Additionally, while an effort was made throughout the analysis to increase the concentration of the filter extracts, the intensity of many of the measured peaks was still low. As such, a better analysis may be performed by conducting experiments with much higher isoprene concentrations. While this would change the chemistry in other ways (for example increasing the rate of RO_2 cross-reactions), these experiments have already demonstrated the formation of these tracers under atmospherically relevant conditions, so higher concentration experiments would allow for better detection in a mechanistic investigation.

Time-resolved aerosol measurements would also help to improve this analysis. Primarily, the use of a Filter Inlet for Gases and AEROsols (FIGAERO) for the I^--CIMS instrument would allow for the

composition of the particle phase organic species to be measured at regular intervals.[147] This would be particularly helpful for identifying the role of photo-induced processes in the formation and loss of particle-phase species as the response of particle phase species concentrations to roof opening or closing could be monitored. An aerosol mass spectrometer (AMS) would also allow time-resolved information on particle composition, though would not provide as high a level of mechanistic detail.[226]

Chapter 5

Summary and Future Work

5.1 Isoprene Oxidation Mechanisms

Recent years have seen great improvements in the understanding of the atmospheric oxidation of isoprene.[42] This is particularly true of isoprene oxidation by NO_3, which has been the subject of lots of recent study due to the potential implications for NO_x budgets and SOA formation.[68] Despite these advances, the work presented in this thesis demonstrates that there are many aspects of the mechanism of isoprene oxidation that require further investigation.

Chapter 2 illustrates that these developments have led to improvements in the predictions made using existing chemical mechanisms of some isoprene nitrate species, particularly ICN. The improvements in ICN predictions result from updated INO chemistry, including fragmentation, autooxidation, and epoxidation reactions of INO, as opposed to only considering the reaction with O_2 to form HO_2 and ICN. The importance of epoxidation reactions is further confirmed by observations of the nitrooxyepoxide products in the EUPHORE experiments from Chapter 4. These measurements suggest that the concentration of these products may be comparable to other commonly-studied isoprene organonitrates. This is particularly true of IDNE which showed large I^--CIMS signal during the Beijing reproduction experiments.

One of the major findings from Chapter 3 is the large impacts of a small number of relatively low concentration, low-volatility HOMs on SOA formation. These HOMs are not currently well represented in explicit chemical mechanisms, in part due to the complexity of their formation. Representation of HOMs in (semi-) explicit chemical mechanisms, such as the MCM, will present a substantial challenge due to the wide array of formation pathways and the potential impact that minor reaction products can have on particle formation. These factors mean that the inclusion of HOM chemistry in chemical mechanisms can result in very large mechanisms which may not be easily implementable in computational models. For example, Draper *et al.* identified 33 potential closed shell HOM species resulting from the intramolecular reactions of a single alkyl radical produced from Δ-3-Carene.[227]

Finally, while showing evidence of several particle-phase isoprene tracers, Chapter 4 illustrates the large uncertainty surrounding particle-phase processes, and the difficulty in assessing chemistry occurring in the particle phase. Further chamber investigations in the presence of seed aerosol may help to elucidate particle-phase processes, particularly in combination with the use of time-resolved aerosol measurement techniques like FIGAERO-CIMS. Furthermore, there would be value to experiments starting from known oxidation products, as opposed to the parent VOC, to reduce the complexity of the system. However, this is often difficult as the oxidation products are rarely commercially available.

5.2 Measurement of Isoprene Oxidation Products

The findings from Chapter 2 demonstrate the difficulty of measuring isoprene nitrates, particularly the large uncertainties in sensitivity of different compounds to I$^-$-CIMS. This also presented challenges in the analysis of I$^-$-CIMS data from the chamber experiments described in Chapter 4, though the constrained nature of the experiments allowed for an easier comparison to modelled species concentrations. A good understanding of instrument responses will be required when investigating the impact of low-concentration HOMs on particle formation, as described in Chapter 3.

Due to the unavailability of authentic standards for many of the isoprene organonitrates of interest, further work should be performed to enable predictions of the responses of different species to I$^-$-CIMS. This is analogous to the highly variable responses of species to electrospray ionisation in HPLC-ESI-MS analysis. Recent work has demonstrated the ability to construct predictive models of ESI response factors.[222,223] While further work is required to apply this technique to a wider range of isoprene tracers, a similar approach could be taken to predict the responses of species in I$^-$-CIMS. On top of the issues with calibration, Chapter 2 and Chapter 4 also demonstrate the potential impact of isobaric interferences on the measurement of isoprene organonitrates. This is particularly true for IPN, where the modelling results from both chapters suggest that the measured ΣIPN signal could be comprised of a large fraction of INHE, as well as other OVOCs. To overcome this issue, future investigations into isoprene nitrates could use alternative measurement techniques that are able to distinguish between isobaric species, such as GC-MS.

Aside from a general model for predicting the response of species to I$^-$-CIMS, the work presented throughout this thesis can be applied to identify key isoprene organonitrates for which improved measurements would help to answer key research questions. Firstly, Chapter 3 highlights that IHN comprises the majority of daytime isoprene nitrates under most NO_x and O_3 concentrations, and Chapter 2 illustrates key differences between the IHN isomers predicted by the Caltech and FZJ mechanisms. Speciated IHN measurements of all of these IHN isomers, particularly 2,1-IHN, would help to improve the calibration of measurements of ΣIHN, as well as allowing a judgement to be made on the rapid 2,1-IHN formation included in the Caltech mechanism. Reeves et al. have previously presented speciated GC-MS measurements of IHN, but were unable to measure all of the relevant IHN isomers.[145]

Secondly, ICN concentrations are very different in each of the three models presented in Chapter 2, due to the representation of INO decomposition in each mechanism. While Chapter 2 shows that the MCM overpredicts ICN, the accuracy of the I$^-$-CIMS calibration prevents a conclusion to be drawn regarding the predictions made using the Caltech and FZJ mechanisms. The formation of ICN from INO means that an accurate I$^-$-CIMS calibration would allow for the assumptions made around

INO decomposition in the Caltech and FZJ mechanisms to be tested, including intramolecular reactions and epoxide formation which could be important for SOA formation.

Additionally, more measurements of the nitrated epoxides will help to assess the theoretical predictions contained in the FZJ mechanism about their formation. Chapter 4 demonstrates that these species can be measured using I^--CIMS, however a calibrated measurement would help to identify the relative importance of these species for SOA formation. Chapter 4 shows that IDNE produces the highest I^--CIMS signal of all of the nitrates epoxides under Beijing-like conditions, and the signal is of a similar magnitude to other commonly-studies isoprene organonitrates. As such, this would make IDNE an interesting target for calibrated analysis to identify its potential role in the formation of SOA under polluted urban conditions.

INHE also forms via the same alkoxy-epoxidation pathway as IDNE in the FZJ mechanism. Chapter 2 highlights the complex mixture of isomers that contribute to ΣIPN, and the difference between the predictions made using each mechanism. The major difference between the Caltech and FZJ mechanisms is the formation of a large proportion of night-time INHE, predominantly ISOP1N23O4OH. As such, measurements of INHE separate from IPN and other ΣIPN isomers could help to further explore the alkoxy-epoxidation chemistry proposed by the FZJ mechanism and determine the role of INHE in SOA formation.

5.3 Daytime NO$_3$ Chemistry

One of the central themes running through the work presented in this thesis is the role of daytime NO$_3$ chemistry in heavily polluted environments. This chemistry which has traditionally been considered "night-time chemistry" becomes important during the day in environments with high concentrations of O$_3$.[46-48,51,54-56]

Chapter 3 demonstrates the strong dependence during the day of many groups of isoprene nitrates on ozone concentrations, particularly those that require NO$_3$ for their formation. Additionally, Chapter 4 presents direct observations of the formation of products of the NO$_3$-initiated oxidation of isoprene under light conditions analogous to those observed in Beijing.

Much of the evidence for day-time NO$_3$ chemistry comes from the measurement of NO$_3$-initiated oxidation products, modelling work, or calculated estimates of NO$_3$ concentrations. Since recent advances have allowed the direct measurement of NO$_3$ mixing ratios,[228-230] more measurements in a range of environments could help to validate the predicted importance of daytime NO$_3$.

5.4 Does Night-time Chemistry of Isoprene Impact Urban Air Quality in Polluted Environments?

In answer to the central question of this thesis, it is clear that night-time chemistry of isoprene does play an important role in urban air quality through impacts on NO$_x$ and the formation of SOA. True

night-time chemistry was shown to be important for the formation of isoprene nitrates in Chapter 2, with the concentrations of many of the species of interest peaking during the night. Subsequent chapters show that NO_3-initiated oxidation produces organonitrates under polluted urban conditions throughout the afternoon and into the night. Chapter 3 highlights the complex interactions between OH-initiated and NO_3-initiated organonitrate formation during the day in polluted environments. It also demonstrates that the presence of day-time NO_3 chemistry can lead to elevated organonitrate concentrations under high ozone concentrations. Chapter 4 provides experimental evidence for many of the conclusions from the previous chapters, as well as demonstrating the role of 'night-time chemistry' on isoprene SOA species.

5.4.1 Policy Implications

Much of the work in this thesis centres around the potential for daytime NO_3 chemistry to form previously unexplored species, or to present alternative formation pathways to species of interest. Chapter 3 illustrates that the formation of organonitrates resulting from daytime NO_3 chemistry under Beijing-like conditions is much more sensitive to changes in O_3 than changes in NO_x. Furthermore, many of the HOM species that may contribute most to SOA due to their low volatility are produced most strongly under high-O_3, low-NO_x conditions. This means that for cities in an O_3 production regime where reductions in NO_x may result in increased O_3 concentrations, the concentration of gas-phase SOA precursors may increase, resulting in increased PM. The non-linear relationships presented in Chapter 3 highlight that organonitrate concentrations should not necessarily be expected to decrease with decreasing NO_x concentrations and may increase for individual species.

The potential to form large amounts of nitrated epoxides under urban conditions, such as the large IDNE signals observed in the chamber experiments presented in Chapter 4, will also have implications for policy to mitigate SOA formation from isoprene. The uptake of epoxides to acidified particles is often considered for IEPOX under less polluted environments. While INHE has been previously investigated as a source of isoprene SOA, the results from modelling in this thesis indicate that the nitrated epoxide species from the alkoxy-epoxidation pathway in the FZJ mechanism could be produced in much larger quantities than previously anticipated. The formation of IDNE through daytime NO_3 chemistry is a further incentive to ensure O_3 concentrations stay low. However, the formation of INHE, INPE, and INCE at night means that NO_x concentrations need to be reduced to reduce night-time NO_3 concentrations.

The work explored throughout this thesis contributes to the understanding of isoprene chemistry in urban environments, but it is clear that isoprene will continue to present challenges to the scientific community for many years to come.

Reference List

1   Loreto, F., Dicke, M., Schnitzler, J.-P. & Turlings, T. C. J. Plant volatiles and the environment. *Plant, Cell & Environment* **37**, 1905-1908 (2014). https://doi.org/10.1111/pce.12369

2   Guenther, A. *et al.* A global model of natural volatile organic compound emissions. *Journal of Geophysical Research* **100** (1995). https://doi.org/10.1029/94jd02950

3   Guenther, A. *et al.* Estimates of global terrestrial isoprene emissions using MEGAN (Model of Emissions of Gases and Aerosols from Nature). *Atmospheric Chemistry and Physics* **6**, 3181-3210 (2006). https://doi.org/10.5194/acp-6-3181-2006

4   Guenther, A. B. *et al.* The Model of Emissions of Gases and Aerosols from Nature version 2.1 (MEGAN2.1): an extended and updated framework for modeling biogenic emissions. *Geoscientific Model Development* **5**, 1471-1492 (2012). https://doi.org/10.5194/gmd-5-1471-2012

5   Sindelarova, K. *et al.* Global data set of biogenic VOC emissions calculated by the MEGAN model over the last 30 years. *Atmospheric Chemistry and Physics* **14**, 9317-9341 (2014). https://doi.org/10.5194/acp-14-9317-2014

6   Sharkey, T. D., Wiberley, A. E. & Donohue, A. R. Isoprene emission from plants: why and how. *Ann Bot* **101**, 5-18 (2008). https://doi.org/10.1093/aob/mcm240

7   Monson, R. K., Jones, R. T., Rosenstiel, T. N. & Schnitzler, J. P. Why only some plants emit isoprene. *Plant Cell Environ* **36**, 503-516 (2013). https://doi.org/10.1111/pce.12015

8   Zeinali, N., Altarawneh, M., Li, D., Al-Nu'airat, J. & Dlugogorski, B. Z. New Mechanistic Insights: Why Do Plants Produce Isoprene? *ACS Omega* **1**, 220-225 (2016). https://doi.org/10.1021/acsomega.6b00025

9   Otu-Larbi, F. *et al.* Modelling the effect of the 2018 summer heatwave and drought on isoprene emissions in a UK woodland. *Glob Chang Biol* (2019). https://doi.org/10.1111/gcb.14963

10   Mo, Z. *et al.* Tower-based measurements of NMHCs and OVOCs in the Pearl River Delta: Vertical distribution, source analysis and chemical reactivity. *Environ Pollut* **292**, 118454 (2022). https://doi.org/10.1016/j.envpol.2021.118454

11   Pfannerstill, E. Y. *et al.* Total OH reactivity over the Amazon rainforest: variability with temperature, wind, rain, altitude, time of day, season, and an overall budget closure. *Atmospheric Chemistry and Physics* **21**, 6231-6256 (2021). https://doi.org/10.5194/acp-21-6231-2021

12   Edwards, P. M. *et al.* Transition from high- to low-NO x control of night-time oxidation in the southeastern US. *Nature Geoscience* **10**, 490-495 (2017). https://doi.org/10.1038/ngeo2976

13   Wang, X. *et al.* Effects of light on the emissions of biogenic isoprene and monoterpenes: A review. *Atmospheric Pollution Research* **13** (2022). https://doi.org/10.1016/j.apr.2022.101397

14   Zou, Y., Deng, X. J., Deng, T., Yin, C. Q. & Li, F. One-Year Characterization and Reactivity of Isoprene and Its Impact on Surface Ozone Formation at A Suburban Site in Guangzhou, China. *Atmosphere* **10**, 201 (2019). https://doi.org/10.3390/atmos10040201

15   Wei, D. *et al.* Investigation of Isoprene Dynamics During the Day-to-Night Transition Period. *Journal of Geophysical Research: Atmospheres* **125** (2020). https://doi.org/10.1029/2020jd032784

16   Wang, J.-L. *et al.* Biogenic isoprene in subtropical urban settings and implications for air quality. *Atmospheric Environment* **79**, 369-379 (2013). https://doi.org/10.1016/j.atmosenv.2013.06.055

17   Panopoulou, A. *et al.* Yearlong measurements of monoterpenes and isoprene in a Mediterranean city (Athens): Natural vs anthropogenic origin. *Atmospheric Environment* **243** (2020). https://doi.org/10.1016/j.atmosenv.2020.117803

18 Cheng, X. *et al.* Atmospheric isoprene and monoterpenes in a typical urban area of Beijing: Pollution characterization, chemical reactivity and source identification. *J Environ Sci (China)* **71**, 150-167 (2018). https://doi.org/10.1016/j.jes.2017.12.017

19 Khan, M. *et al.* A Two-Decade Anthropogenic and Biogenic Isoprene Emissions Study in a London Urban Background and a London Urban Traffic Site. *Atmosphere* **9** (2018). https://doi.org/10.3390/atmos9100387

20 Borbon, A. *et al.* An investigation into the traffic-related fraction of isoprene at an urban location. *Atmospheric Environment* **35**, 3749-3760 (2001). https://doi.org/10.1016/S1352-2310(01)00170-4

21 Bryant, D. J. *et al.* Biogenic and anthropogenic sources of isoprene and monoterpenes and their secondary organic aerosol in Delhi, India. *Atmospheric Chemistry and Physics* **23**, 61-83 (2023). https://doi.org/10.5194/acp-23-61-2023

22 Chang, C.-C. *et al.* Seasonal characteristics of biogenic and anthropogenic isoprene in tropical–subtropical urban environments. *Atmospheric Environment* **99**, 298-308 (2014). https://doi.org/10.1016/j.atmosenv.2014.09.019

23 Hu, L. *et al.* Isoprene emissions and impacts over an ecological transition region in the U.S. Upper Midwest inferred from tall tower measurements. *Journal of Geophysical Research: Atmospheres* **120**, 3553-3571 (2015). https://doi.org/10.1002/2014jd022732

24 Wagner, P. & Kuttler, W. Biogenic and anthropogenic isoprene in the near-surface urban atmosphere--a case study in Essen, Germany. *Sci Total Environ* **475**, 104-115 (2014). https://doi.org/10.1016/j.scitotenv.2013.12.026

25 Kashyap, P., Kumar, A., Kumar, R. P. & Kumar, K. Biogenic and anthropogenic isoprene emissions in the subtropical urban atmosphere of Delhi. *Atmospheric Pollution Research* **10**, 1691-1698 (2019). https://doi.org/10.1016/j.apr.2019.07.004

26 Liakakou, E. *et al.* Isoprene above the Eastern Mediterranean: Seasonal variation and contribution to the oxidation capacity of the atmosphere. *Atmospheric Environment* **41**, 1002-1010 (2007). https://doi.org/10.1016/j.atmosenv.2006.09.034

27 Atkinson, R. & Arey, J. Gas-phase tropospheric chemistry of biogenic volatile organic compounds: a review. *Atmospheric Environment* **37**, 197-219 (2003). https://doi.org/10.1016/s1352-2310(03)00391-1

28 Jenkin, M. E., Young, J. C. & Rickard, A. R. The MCM v3.3.1 degradation scheme for isoprene. *Atmospheric Chemistry and Physics* **15**, 11433-11459 (2015). https://doi.org/10.5194/acp-15-11433-2015

29 Khan, M. A. H. *et al.* Estimation of Daytime NO3 Radical Levels in the UK Urban Atmosphere Using the Steady State Approximation Method. *Advances in Meteorology* **2015**, 1-9 (2015). https://doi.org/10.1155/2015/294069

30 Khan, M. A. H. *et al.* Night-time NO3 and OH radical concentrations in the United Kingdom inferred from hydrocarbon measurements. *Atmospheric Science Letters* **9**, 140-146 (2008). https://doi.org/10.1002/asl.175

31 Seinfeld, J. H. & Pandis, S. N. *Atmospheric Chemistry and Physics: From Air Pollution to Climate Change*. 2nd edn, (John Wiley & Sons, 2006).

32 Sadanaga, Y., Matsumoto, J. & Kajii, Y. Photochemical reactions in the urban air: Recent understandings of radical chemistry. *Journal of Photochemistry and Photobiology C: Photochemistry Reviews* **4**, 85-104 (2003). https://doi.org/10.1016/s1389-5567(03)00006-6

33 Kleffmann, J. Daytime Sources of Nitrous Acid (HONO) in the Atmospheric Boundary Layer. *Chemphyschem* **8**, 1137-1144 (2007). https://doi.org/10.1002/cphc.200700016

34 Xue, C. *et al.* HONO Budget and Its Role in Nitrate Formation in the Rural North China Plain. *Environmental Science & Technology* **54**, 11048-11057 (2020). https://doi.org/10.1021/acs.est.0c01832

35 Long, B., Bao, J. L. & Truhlar, D. G. Atmospheric Chemistry of Criegee Intermediates: Unimolecular Reactions and Reactions with Water. *J Am Chem Soc* **138**, 14409-14422 (2016). https://doi.org/10.1021/jacs.6b08655

36   Comes, F. J. Recycling in the Earth's Atmosphere: The OH Radical—Its Importance for the Chemistry of the Atmosphere and the Determination of Its Concentration. *Angewandte Chemie International Edition in English* **33**, 1816-1826 (1994). https://doi.org/10.1002/anie.199418161

37   Peeters, J. & Muller, J. F. HO(x) radical regeneration in isoprene oxidation via peroxy radical isomerisations. II: experimental evidence and global impact. *Phys Chem Chem Phys* **12**, 14227-14235 (2010). https://doi.org/10.1039/c0cp00811g

38   Medeiros, D. J., Blitz, M. A., Seakins, P. W. & Whalley, L. K. Direct Measurements of Isoprene Autoxidation: Pinpointing Atmospheric Oxidation in Tropical Forests. *JACS Au* **2**, 809-818 (2022). https://doi.org/10.1021/jacsau.1c00525

39   Heard, D. E. Atmospheric field measurements of the hydroxyl radical using laser-induced fluorescence spectroscopy. *Annu Rev Phys Chem* **57**, 191-216 (2006). https://doi.org/10.1146/annurev.physchem.57.032905.104516

40   Peeters, J., Muller, J. F., Stavrakou, T. & Nguyen, V. S. Hydroxyl radical recycling in isoprene oxidation driven by hydrogen bonding and hydrogen tunneling: the upgraded LIM1 mechanism. *J Phys Chem A* **118**, 8625-8643 (2014). https://doi.org/10.1021/jp5033146

41   Novelli, A. *et al.* Importance of isomerization reactions for OH radical regeneration from the photo-oxidation of isoprene investigated in the atmospheric simulation chamber SAPHIR. *Atmospheric Chemistry and Physics* **20**, 3333-3355 (2020). https://doi.org/10.5194/acp-20-3333-2020

42   Wennberg, P. O. *et al.* Gas-Phase Reactions of Isoprene and Its Major Oxidation Products. *Chemical Reviews* **118**, 3337-3390 (2018). https://doi.org/10.1021/acs.chemrev.7b00439

43   Teng, A. P., Crounse, J. D. & Wennberg, P. O. Isoprene Peroxy Radical Dynamics. *J Am Chem Soc* **139**, 5367-5377 (2017). https://doi.org/10.1021/jacs.6b12838

44   Jeon, J., Barker, J. R. & Song, K. OH + Isoprene: A Direct Dynamics Study. *Bulletin of the Korean Chemical Society* **38**, 651-660 (2017). https://doi.org/10.1002/bkcs.11145

45   Brown, S. S. & Stutz, J. Nighttime radical observations and chemistry. *Chem Soc Rev* **41**, 6405-6447 (2012). https://doi.org/10.1039/c2cs35181a

46   Geyer, A. Direct observations of daytime NO3: Implications for urban boundary layer chemistry. *Journal of Geophysical Research* **108** (2003). https://doi.org/10.1029/2002jd002967

47   Xue, L. *et al.* Oxidative capacity and radical chemistry in the polluted atmosphere of Hong Kong and Pearl River Delta region: analysis of a severe photochemical smog episode. *Atmospheric Chemistry and Physics* **16**, 9891-9903 (2016). https://doi.org/10.5194/acp-16-9891-2016

48   Wang, H. *et al.* NO3 and N2O5 chemistry at a suburban site during the EXPLORE-YRD campaign in 2018. *Atmospheric Environment* **224** (2020). https://doi.org/10.1016/j.atmosenv.2019.117180

49   Brown, S. S. *et al.* Aircraft observations of daytime NO3 and N2O5 and their implications for tropospheric chemistry. *Journal of Photochemistry and Photobiology A: Chemistry* **176**, 270-278 (2005). https://doi.org/10.1016/j.jphotochem.2005.10.004

50   Osthoff, H. D. *et al.* Observation of daytime N2O5 in the marine boundary layer during New England Air Quality Study-Intercontinental Transport and Chemical Transformation 2004. *Journal of Geophysical Research: Atmospheres* **111** (2006). https://doi.org/10.1029/2006jd007593

51   Hamilton, J. F. *et al.* Key Role of NO3 Radicals in the Production of Isoprene Nitrates and Nitrooxyorganosulfates in Beijing. *Environ Sci Technol* **55**, 842-853 (2021). https://doi.org/10.1021/acs.est.0c05689

52   Hoyle, C. R., Berntsen, T., Myhre, G. & Isaksen, I. S. A. Secondary organic aerosol in the global aerosol – chemical transport model Oslo CTM2. *Atmos. Chem. Phys* **7**, 5675-5694 (2007). https://doi.org/https://doi.org/10.5194/acp-7-5675-2007

53   Foulds, A. *et al.* Abundance of NO3 Derived Organo-Nitrates and Their Importance in the Atmosphere. *Atmosphere* **12** (2021). https://doi.org/10.3390/atmos12111381

54   Forkel, R. *et al.* Trace gas exchange and gas phase chemistry in a Norway spruce forest: A study with a coupled 1-dimensional canopy atmospheric chemistry emission model. *Atmospheric Environment* **40**, 28-42 (2006). https://doi.org/10.1016/j.atmosenv.2005.11.070

55   Hu, X.-M., Fuentes, J. D., Toohey, D. & Wang, D. Chemical processing within and above a loblolly pine forest in North Carolina, USA. *Journal of Atmospheric Chemistry* **72**, 235-259 (2013). https://doi.org/10.1007/s10874-013-9276-3

56   Mermet, K. *et al.* Atmospheric reactivity of biogenic volatile organic compounds in a maritime pine forest during the LANDEX episode 1 field campaign. *Sci Total Environ* **756**, 144129 (2021). https://doi.org/10.1016/j.scitotenv.2020.144129

57   Atkinson, R. *et al.* IUPAC Task Group on Atmospheric Chemical Kinetic Data Evaluation. *Atmos. Chem. Phys.* **4**, 1461-1738 (2004).

58   Chhantyal-Pun, R. *et al.* Criegee intermediates: production, detection and reactivity. *International Reviews in Physical Chemistry* **39**, 385-424 (2020). https://doi.org/10.1080/0144235x.2020.1792104

59   Osborn, D. L. & Taatjes, C. A. The physical chemistry of Criegee intermediates in the gas phase. *International Reviews in Physical Chemistry* **34**, 309-360 (2015). https://doi.org/10.1080/0144235x.2015.1055676

60   Welz, O. *et al.* Direct Kinetic Measurements of Criegee Intermediate (CH_2OO) Formed by Reaction of CH_2I with O_2. *Science* **335**, 204-207 (2012). https://doi.org/10.1126/science.1213229

61   Taatjes, C. A. *et al.* Direct Measurements of Conformer-Dependent Reactivity of the Criegee Intermediate CH_3CHOO. *Science* **340**, 177-180 (2013). https://doi.org/10.1126/science.1234689

62   Nguyen, T. B. *et al.* Atmospheric fates of Criegee intermediates in the ozonolysis of isoprene. *Physical Chemistry Chemical Physics* **18**, 10241-10254 (2016). https://doi.org/10.1039/c6cp00053c

63   Riva, M., Budisulistiorini, S. H., Zhang, Z., Gold, A. & Surratt, J. D. Chemical characterization of secondary organic aerosol constituents from isoprene ozonolysis in the presence of acidic aerosol. *Atmospheric Environment* **130**, 5-13 (2016). https://doi.org/10.1016/j.atmosenv.2015.06.027

64   Inomata, S., Sato, K., Sakamoto, Y. & Hirokawa, J. Direct observation of new particle formation during ozonolysis of isoprene and ethene competing against the growth of preexisting particles. *Atmospheric Environment* **170**, 149-155 (2017). https://doi.org/10.1016/j.atmosenv.2017.09.053

65   Day, D. A. *et al.* Secondary Organic Aerosol Mass Yields from NO_3 Oxidation of alpha-Pinene and Delta-Carene: Effect of RO_2 Radical Fate. *J Phys Chem A* **126**, 7309-7330 (2022). https://doi.org/10.1021/acs.jpca.2c04419

66   Newland, M. J. *et al.* Low-NO atmospheric oxidation pathways in a polluted megacity. *Atmospheric Chemistry and Physics* **21**, 1613-1625 (2021). https://doi.org/10.5194/acp-21-1613-2021

67   Peeters, J., Nguyen, T. L. & Vereecken, L. HOx radical regeneration in the oxidation of isoprene. *Phys Chem Chem Phys* **11**, 5935-5939 (2009). https://doi.org/10.1039/b908511d

68   Vereecken, L. *et al.* Theoretical and experimental study of peroxy and alkoxy radicals in the NO_3-initiated oxidation of isoprene. *Phys Chem Chem Phys* **23**, 5496-5515 (2021). https://doi.org/10.1039/d0cp06267g

69   Orlando, J. J. & Tyndall, G. S. Laboratory studies of organic peroxy radical chemistry: an overview with emphasis on recent issues of atmospheric significance. *Chem Soc Rev* **41**, 6294-6317 (2012). https://doi.org/10.1039/c2cs35166h

70   Jenkin, M. E., Valorso, R., Aumont, B. & Rickard, A. R. Estimation of rate coefficients and branching ratios for reactions of organic peroxy radicals for use in automated mechanism construction. *Atmospheric Chemistry and Physics* **19**, 7691-7717 (2019). https://doi.org/10.5194/acp-19-7691-2019

71   Carter, W. P. L. & Atkinson, R. Alkyl Nitrate Formation from the Atmospheric Photooxidation of Alkanes; a Revised Estimation Method. *Journal of Atmospheric Chemistry* **8**, 165-173 (1989). https://doi.org/10.1007/BF00053721

72   Arey, J., Aschmann, S. M., Kwok, E. S. C. & Atkinson, R. Alkyl Nitrate, Hydroxyalkyl Nitrate, and Hydroxycarbonyl Formation from the NOx-Air Photooxidations of C5-C8 n-Alkanes. *Journal of Physical Chemistry* **105**, 1020-1027 (2001). https://doi.org/10.1021/jp003292z

73   Teng, A. P. *et al.* Hydroxy nitrate production in the OH-initiated oxidation of alkenes. *Atmospheric Chemistry and Physics* **15**, 4297-4316 (2015). https://doi.org/10.5194/acp-15-4297-2015

74   Wallington, T. J., Dagaut, P. & Kurylo, M. J. Ultraviolet Absorption Cross Sections and Reaction Kinetics and Mechanisms for Peroxy Radicals in the Gas Phase. *Chemical Reviews* **92**, 667-710 (1992). https://doi.org/10.1021/cr00012a008,

75   Warneke, C. *et al.* Isoprene and Its Oxidation Products Methyl Vinyl Ketone, Methacrolein, and Isoprene Related Peroxides Measured Online over the Tropical Rain Forest of Surinam in March 1998. *Journal of Atmospheric Chemistry* **38**, 167-185 (2001). https://doi.org/10.1023/a:1006326802432

76   Liu, Y. *et al.* Isoprene photochemistry over the Amazon rainforest. *Proc Natl Acad Sci U S A* **113**, 6125-6130 (2016). https://doi.org/10.1073/pnas.1524136113

77   Docherty, K. S., Wu, W., Lim, Y. B. & Ziemann, P. J. Contributions of Organic Peroxides to Secondary Aerosol Formed from Reactions of Monoterpenes with O3. *Environmental Science & Technology* **39**, 4049-4059 (2005). https://doi.org/10.1021/es050228s

78   Jackson, A. V. & Hewitt, C. N. Atmosphere Hydrogen Peroxide and Organic Hydroperoxides: A Review. *Critical Reviews in Environmental Science and Technology* **29**, 175-228 (1999). https://doi.org/10.1080/10643389991259209

79   Lee, M., Heikes, B. G. & O'Sullivan, D. W. Hydrogen peroxide and organic hydroperoxide in the troposphere: a review. *Atmospheric Environment* **34**, 3475-3494 (2000). https://doi.org/https://doi.org/10.1016/S1352-2310(99)00432-X

80   Snow, J. A. Winter-spring evolution and variability of HOx reservoir species, hydrogen peroxide, and methyl hydroperoxide, in the northern middle to high latitudes. *Journal of Geophysical Research* **108** (2003). https://doi.org/10.1029/2002jd002172

81   Biggs, P., Canosa-Mas, C. E., Fracheboud, J.-M., Shallcross, D. E. & Wayne, R. P. Rate Constants for the Reactions of C2H5, C2H5O and C2H5O2 Radicals with NO, at 298 K and 2.2 Torr. *Journal of the Chemical Society, Faraday Transactions* **91**, 817-825 (1995). https://doi.org/https://doi.org/10.1039/FT9959100817

82   Hasan, G., Salo, V. T., Valiev, R. R., Kubecka, J. & Kurten, T. Comparing Reaction Routes for (3)(RO...OR') Intermediates Formed in Peroxy Radical Self- and Cross-Reactions. *J Phys Chem A* **124**, 8305-8320 (2020). https://doi.org/10.1021/acs.jpca.0c05960

83   Hasan, G., Valiev, R. R., Salo, V. T. & Kurten, T. Computational Investigation of the Formation of Peroxide (ROOR) Accretion Products in the OH- and NO3-Initiated Oxidation of α-Pinene. *J Phys Chem A* **125**, 10632-10639 (2021). https://doi.org/10.1021/acs.jpca.1c08969

84   Valiev, R. R., Hasan, G., Salo, V. T., Kubecka, J. & Kurten, T. Intersystem Crossings Drive Atmospheric Gas-Phase Dimer Formation. *J Phys Chem A* **123**, 6596-6604 (2019). https://doi.org/10.1021/acs.jpca.9b02559

85   Mellouki, A., Wallington, T. J. & Chen, J. Atmospheric chemistry of oxygenated volatile organic compounds: impacts on air quality and climate. *Chem Rev* **115**, 3984-4014 (2015). https://doi.org/10.1021/cr500549n

86   Murphy, S. E. *et al.* Accretion Product Formation in the Self-Reaction of Ethene-Derived Hydroxy Peroxy Radicals. *Environmental Science: Atmospheres* (2023). https://doi.org/10.1039/d3ea00020f

87   Weber, J. *et al.* CRI-HOM: A novel chemical mechanism for simulating highly oxygenated organic molecules (HOMs) in global chemistry–aerosol–climate models. *Atmospheric Chemistry and Physics* **20**, 10889-10910 (2020). https://doi.org/10.5194/acp-20-10889-2020

88   Lee, S. H. *et al.* New Particle Formation in the Atmosphere: From Molecular Clusters to Global Climate. *Journal of Geophysical Research: Atmospheres* **124**, 7098-7146 (2019). https://doi.org/10.1029/2018jd029356

89   Bianchi, F. *et al.* Highly Oxygenated Organic Molecules (HOM) from Gas-Phase Autoxidation Involving Peroxy Radicals: A Key Contributor to Atmospheric Aerosol. *Chemical Reviews* **119**, 3472-3509 (2019). https://doi.org/10.1021/acs.chemrev.8b00395

90   Zhao, D. *et al.* Highly oxygenated organic molecules (HOM) formation in the isoprene oxidation by NO3 radical. *Atmos. Chem. Phys.* **21**, 9681-9704 (2021). https://doi.org/10.5194/acp-21-9681-2021

91   Jaoui, M. *et al.* Rapid production of highly oxidized molecules in isoprene aerosol via peroxy and alkoxy radical isomerization pathways in low and high NOx environments: Combined laboratory, computational and field studies. *Science of The Total Environment* **775** (2021). https://doi.org/10.1016/j.scitotenv.2021.145592

92   Brean, J. *et al.* Observations of highly oxidized molecules and particle nucleation in the atmosphere of Beijing. *Atmospheric Chemistry and Physics* **19**, 14933-14947 (2019). https://doi.org/10.5194/acp-19-14933-2019

93   Massoli, P. *et al.* Ambient Measurements of Highly Oxidized Gas-Phase Molecules during the Southern Oxidant and Aerosol Study (SOAS) 2013. *ACS Earth and Space Chemistry* **2**, 653-672 (2018). https://doi.org/10.1021/acsearthspacechem.8b00028

94   Ma, F. *et al.* Atmospheric Chemistry of Allylic Radicals from Isoprene: A Successive Cyclization-Driven Autoxidation Mechanism. *Environ Sci Technol* **55**, 4399-4409 (2021). https://doi.org/10.1021/acs.est.0c07925

95   Vereecken, L. & Peeters, J. Decomposition of substituted alkoxy radicals--part I: a generalized structure-activity relationship for reaction barrier heights. *Phys Chem Chem Phys* **11**, 9062-9074 (2009). https://doi.org/10.1039/b909712k

96   Liu, Q. *et al.* Carbonyl compounds in the atmosphere: A review of abundance, source and their contributions to O3 and SOA formation. *Atmospheric Research* **274** (2022). https://doi.org/10.1016/j.atmosres.2022.106184

97   Jenkin, M. E., Saunders, S. M. & Pilling, M. J. The Tropospheric Degradation of Volatile Organic Compounds: A Protocol for Mechanism Development. *Atmospheric Environment*, 81-104 (1997). https://doi.org/10.1016/S1352-2310(96)00105-7

98   Fu, T.-M. *et al.* Global budgets of atmospheric glyoxal and methylglyoxal, and implications for formation of secondary organic aerosols. *Journal of Geophysical Research* **113** (2008). https://doi.org/10.1029/2007jd009505

99   Vereecken, L. & Peeters, J. Nontraditional (Per)oxy Ring-Closure Paths in the Atmospheric Oxidation of Isoprene and Monoterpenes. *Journal of Physical Chemistry* **108**, 5197-5204 (2004). https://doi.org/10.1021/jp049219g

100   Vereecken, L., Müller, J.-F. & Peeters, J. Low-volatility poly-oxygenates in the OH-initiated atmospheric oxidation of α-pinene: impact of non-traditional peroxyl radical chemistry. *Physical Chemistry Chemical Physics* **9**, 5241-5248 (2007). https://doi.org/10.1039/b708023a

101   Wang, L., Wu, R. & Xu, C. Atmospheric oxidation mechanism of benzene. Fates of alkoxy radical intermediates and revised mechanism. *J Phys Chem A* **117**, 14163-14168 (2013). https://doi.org/10.1021/jp4101762

102   Romer Present, P. S., Zare, A. & Cohen, R. C. The changing role of organic nitrates in the removal and transport of NOx. *Atmospheric Chemistry and Physics* **20**, 267-279 (2020). https://doi.org/10.5194/acp-20-267-2020

103   Kim, K. H., Kabir, E. & Kabir, S. A review on the human health impact of airborne particulate matter. *Environ Int* **74**, 136-143 (2015). https://doi.org/10.1016/j.envint.2014.10.005

104   IPCC. *Climate Change 2021: The Physical Science Basis. Contribution of Working Group I to the Sixth Assessment Report of the Intergovernmental Panel on Climate Change*. Vol. In Press (Cambridge University Press, 2021).

105   Hallquist, M. *et al.* The formation, properties and impact of secondary organic aerosol: current and emerging issues. *Atmos. Chem. Phys.* **9**, 5155-5236 (2009). https://doi.org/10.5194/acp-9-5155-2009

106   Zhang, Q. *et al.* Ubiquity and dominance of oxygenated species in organic aerosols in anthropogenically-influenced Northern Hemisphere midlatitudes. *Geophysical Research Letters* **34** (2007). https://doi.org/10.1029/2007gl029979

107   Ziemann, P. J. & Atkinson, R. Kinetics, products, and mechanisms of secondary organic aerosol formation. *Chem Soc Rev* **41**, 6582-6605 (2012). https://doi.org/10.1039/c2cs35122f

108   Gouw, J. D. & Jimenez, J. L. Organic Aerosols in the Earth's Atmosphere. *Environmental Science & Technology* **43**, 7614-7618 (2009). https://doi.org/10.1021/es9006004

109   Jimenez, J. L. *et al.* Evolution of Organic Aerosols in the Atmosphere. *Science* **326**, 1525-1529 (2009). https://doi.org/10.1126/science.1180353

110   Allan, J. D. *et al.* Airborne observations of IEPOX-derived isoprene SOA in the Amazon during SAMBBA. *Atmospheric Chemistry and Physics* **14**, 11393-11407 (2014). https://doi.org/10.5194/acp-14-11393-2014

111   Zhang, Z.-S. *et al.* Determination of isoprene-derived secondary organic aerosol tracers (2-methyltetrols) by HPAEC-PAD: Results from size-resolved aerosols in a tropical rainforest. *Atmospheric Environment* **70**, 468-476 (2013). https://doi.org/10.1016/j.atmosenv.2013.01.020

112   Pöschl, U. *et al.* Rainforest Aerosols as Biogenic Nuclei of Clouds and Precipitation in the Amazon. *Science* **329**, 1513-1516 (2010). https://doi.org/10.1126/science.1191056

113   Xu, Z. N. *et al.* Multifunctional Products of Isoprene Oxidation in Polluted Atmosphere and Their Contribution to SOA. *Geophysical Research Letters* **48** (2021). https://doi.org/10.1029/2020gl089276

114   Zhang, Y. Q. *et al.* Observational Insights into Isoprene Secondary Organic Aerosol Formation through the Epoxide Pathway at Three Urban Sites from Northern to Southern China. *Environ Sci Technol* **56**, 4795-4805 (2022). https://doi.org/10.1021/acs.est.1c06974

115   Fan, W. *et al.* A review of secondary organic aerosols formation focusing on organosulfates and organic nitrates. *J Hazard Mater* **430**, 128406 (2022). https://doi.org/10.1016/j.jhazmat.2022.128406

116   Salvador, C. M. *et al.* Measurements of submicron organonitrate particles: Implications for the impacts of NOx pollution in a subtropical forest. *Atmospheric Research* **245** (2020). https://doi.org/10.1016/j.atmosres.2020.105080

117   Wu, R. *et al.* Molecular composition and volatility of multi-generation products formed from isoprene oxidation by nitrate radical. *Atmospheric Chemistry and Physics* **21**, 10799-10824 (2021). https://doi.org/10.5194/acp-21-10799-2021

118   Paulot, F. *et al.* Unexpected Epoxide Formation in the Gas-Phase Photooxidation of Isoprene. *Science* **325**, 730-733 (2009). https://doi.org/10.1126/science.1172910

119   Surratt, J. D. *et al.* Reactive intermediates revealed in secondary organic aerosol formation from isoprene. *Proceedings of the National Academy of Sciences* **107**, 6640-6645 (2010). https://doi.org/10.1073/pnas.0911114107

120   Claeys, M. *et al.* Formation of Secondary Organic Aerosols Through Photooxidation of Isoprene. *Science* **303**, 1173-1176 (2004). https://doi.org/10.1126/science.109280

121   Claeys, M. & Maenhaut, W. Secondary Organic Aerosol Formation from Isoprene: Selected Research, Historic Account and State of the Art. *Atmosphere* **12** (2021). https://doi.org/10.3390/atmos12060728

122   He, Q. F. *et al.* Secondary Organic Aerosol Formation From Isoprene Epoxides in the Pearl River Delta, South China: IEPOX- and HMML-Derived Tracers. *Journal of Geophysical Research: Atmospheres* **123**, 6999-7012 (2018). https://doi.org/10.1029/2017jd028242

123   Schwantes, R. H. *et al.* Isoprene NO3 Oxidation Products from the RO2 + HO2 Pathway. *Journal of Physical Chemistry A* **119**, 10158-10171 (2015). https://doi.org/10.1021/acs.jpca.5b06355

124   Carlsson, P. T. M. *et al.* Comparison of isoprene chemical mechanisms at atmospheric night-time conditions in chamber experiments: Evidence of hydroperoxy aldehydes and epoxy products from NO3 oxidation. *Atmos. Chem. Phys* (2023). https://doi.org/10.5194/acp-23-3147-2023

125   Shi, Z. *et al.* Introduction to the special issue "In-depth study of air pollution sources and processes within Beijing and its surrounding region (APHH-Beijing)". *Atmospheric Chemistry and Physics* **19**, 7519-7546 (2019). https://doi.org/10.5194/acp-19-7519-2019

126   Mayhew, A. W. *et al.* Evaluation of isoprene nitrate chemistry in detailed chemical mechanisms. *Atmospheric Chemistry and Physics* **22**, 14783-14798 (2022). https://doi.org/10.5194/acp-22-14783-2022

127   Emmerson, K. L. & Evans, M. J. Comparison of tropospheric gas-phase chemistry schemes for use within global models. *Atmos. Chem. Phys* **9**, 1831-1845 (2009). https://doi.org/10.5194/acp-9-1831-2009

128   Bates, K. H. & Jacob, D. J. A new model mechanism for atmospheric oxidation of isoprene: global effects on oxidants, nitrogen oxides, organic products, and secondary organic aerosol. *Atmospheric Chemistry and Physics* **19**, 9613-9640 (2019). https://doi.org/10.5194/acp-19-9613-2019

129   Schwantes, R. H. *et al.* Low-volatility compounds contribute significantly to isoprene secondary organic aerosol (SOA) under high-NOx conditions. *Atmospheric Chemistry and Physics* **19**, 7255-7278 (2019). https://doi.org/10.5194/acp-19-7255-2019

130   Schwantes, R. H. *et al.* Comprehensive isoprene and terpene gas-phase chemistry improves simulated surface ozone in the southeastern US. *Atmospheric Chemistry and Physics* **20**, 3739-3776 (2020). https://doi.org/10.5194/acp-20-3739-2020

131   Vasquez, K. T. *et al.* Rapid hydrolysis of tertiary isoprene nitrate efficiently removes NOx from the atmosphere. *Proceedings of the National Academy of Sciences* **117**, 33011-33016 (2020). https://doi.org/10.1073/pnas.2017442117

132   Palmer, P. I., Marvin, M. R., Siddans, R., Kerridge, B. J. & Moore, D. P. Nocturnal survival of isoprene linked to formation of upper tropospheric organic aerosol. *Science* **375**, 562-566 (2022). https://doi.org/10.1126/science.abg4506

133   Novelli, A. *et al.* Experimental and theoretical study on the impact of a nitrate group on the chemistry of alkoxy radicals. *Phys Chem Chem Phys* **23**, 5474-5495 (2021). https://doi.org/10.1039/d0cp05555g

134   Tsiligiannis, E. *et al.* A Four Carbon Organonitrate as a Significant Product of Secondary Isoprene Chemistry. *Geophysical Research Letters* **49** (2022). https://doi.org/10.1029/2021gl097366

135   Praske, E. *et al.* Atmospheric fate of methyl vinyl ketone: peroxy radical reactions with NO and HO2. *J Phys Chem A* **119**, 4562-4572 (2015). https://doi.org/10.1021/jp5107058

136   Müller, J. F., Peeters, J. & Stavrakou, T. Fast photolysis of carbonyl nitrates from isoprene. *Atmospheric Chemistry and Physics* **14**, 2497-2508 (2014). https://doi.org/10.5194/acp-14-2497-2014

137   Brownwood, B. *et al.* Gas-Particle Partitioning and SOA Yields of Organonitrate Products from NO3-Initiated Oxidation of Isoprene under Varied Chemical Regimes. *ACS Earth Space Chem* **5**, 785-800 (2021). https://doi.org/10.1021/acsearthspacechem.0c00311

138   Ayres, B. R. *et al.* Organic nitrate aerosol formation via NO3 + biogenic volatile organic compounds in the southeastern United States. *Atmospheric Chemistry and Physics* **15**, 13377-13392 (2015). https://doi.org/10.5194/acp-15-13377-2015

139   Zaveri, R. A., Shilling, J. E., Fast, J. D. & Springston, S. R. Efficient Nighttime Biogenic SOA Formation in a Polluted Residual Layer. *Journal of Geophysical Research: Atmospheres* (2020). https://doi.org/10.1029/2019jd031583

140   Pratt, K. A. *et al.* Contributions of individual reactive biogenic volatile organic compounds to organic nitrates above a mixed forest. *Atmospheric Chemistry and Physics* **12**, 10125-10143 (2012). https://doi.org/10.5194/acp-12-10125-2012

141 Xiong, F. *et al.* Observation of isoprene hydroxynitrates in the southeastern United States and implications for the fate of NOx. *Atmospheric Chemistry and Physics* **15**, 11257-11272 (2015). https://doi.org/10.5194/acp-15-11257-2015

142 Romer, P. S. *et al.* The lifetime of nitrogen oxides in an isoprene-dominated forest. *Atmospheric Chemistry and Physics* **16**, 7623-7637 (2016). https://doi.org/10.5194/acp-16-7623-2016

143 Chen, X., Wang, H. & Lu, K. Simulation of organic nitrates in Pearl River Delta in 2006 and the chemical impact on ozone production. *Science China Earth Sciences* **61**, 228-238 (2018). https://doi.org/10.1007/s11430-017-9115-5

144 Zare, A. *et al.* A comprehensive organic nitrate chemistry: insights into the lifetime of atmospheric organic nitrates. *Atmospheric Chemistry and Physics* **18**, 15419-15436 (2018). https://doi.org/10.5194/acp-18-15419-2018

145 Reeves, C. E. *et al.* Observations of speciated isoprene nitrates in Beijing: implications for isoprene chemistry. *Atmospheric Chemistry and Physics* **21**, 6315-6330 (2021). https://doi.org/10.5194/acp-21-6315-2021

146 Whalley, L. K. *et al.* Evaluating the sensitivity of radical chemistry and ozone formation to ambient VOCs and NOx in Beijing. *Atmospheric Chemistry and Physics* **21**, 2125-2147 (2021). https://doi.org/10.5194/acp-21-2125-2021

147 Lopez-Hilfiker, F. D. *et al.* A novel method for online analysis of gas and particle composition: description and evaluation of a Filter Inlet for Gases and AEROsols (FIGAERO). *Atmospheric Measurement Techniques* **7**, 983-1001 (2014). https://doi.org/10.5194/amt-7-983-2014

148 Hopkins, J. R., Jones, C. E. & Lewis, A. C. A dual channel gas chromatograph for atmospheric analysis of volatile organic compounds including oxygenated and monoterpene compounds. *J Environ Monit* **13**, 2268-2276 (2011). https://doi.org/10.1039/c1em10050e

149 Huang, Z., Zhang, Y., Yan, Q., Zhang, Z. & Wang, X. Real-time monitoring of respiratory absorption factors of volatile organic compounds in ambient air by proton transfer reaction time-of-flight mass spectrometry. *J Hazard Mater* **320**, 547-555 (2016). https://doi.org/10.1016/j.jhazmat.2016.08.064

150 Whalley, L. K. *et al.* The chemistry of OH and HO2 radicals in the boundary layer over the tropical Atlantic Ocean. *Atmospheric Chemistry and Physics* **10**, 1555-1576 (2010). https://doi.org/10.5194/acp-10-1555-2010

151 Whalley, L. K. *et al.* Understanding in situ ozone production in the summertime through radical observations and modelling studies during the Clean air for London project (ClearfLo). *Atmospheric Chemistry and Physics* **18**, 2547-2571 (2018). https://doi.org/10.5194/acp-18-2547-2018

152 Zhou, W. *et al.* Production of N2O5 and ClNO2 in summer in urban Beijing, China. *Atmospheric Chemistry and Physics* **18**, 11581-11597 (2018). https://doi.org/10.5194/acp-18-11581-2018

153 Sommariva, R. *et al.* AtChem, an open source box-model for the Master Chemical Mechanism. *Geoscientific Model Development* (2019). https://doi.org/10.5194/gmd-2019-192

154 Nguyen, T. B. *et al.* Rapid deposition of oxidized biogenic compounds to a temperate forest. *Proceedings of the National Academy of Sciences* **112**, E392-E401 (2015). https://doi.org/10.1073/pnas.1418702112

155 Gaston, C. J. *et al.* Reactive Uptake of an Isoprene-Derived Epoxydiol to Submicron Aerosol Particles. *Environmental Science & Technology* **48**, 11178-11186 (2014). https://doi.org/10.1021/es5034266

156 Riedel, T. P. *et al.* Constraining condensed-phase formation kinetics of secondary organic aerosol components from isoprene epoxydiols. *Atmos. Chem. Phys* **16**, 1245-1254 (2016). https://doi.org/10.5194/acpd-15-28289-2015

157 Budisulistiorini, S. H. *et al.* Simulating Aqueous-Phase Isoprene-Epoxydiol (IEPOX) Secondary Organic Aerosol Production During the 2013 Southern Oxidant and Aerosol

Study (SOAS). *Environmental Science & Technology* **51**, 5026-5034 (2017). https://doi.org/10.1021/acs.est.6b05750

158   Rivera-Rios, J. C. *et al.* Conversion of hydroperoxides to carbonyls in field and laboratory instrumentation: Observational bias in diagnosing pristine versus anthropogenically controlled atmospheric chemistry. *Geophysical Research Letters* **41**, 8645-8651 (2014). https://doi.org/10.1002/2014gl061919

159   Nguyen, T. B. *et al.* Organic aerosol formation from the reactive uptake of isoprene epoxydiols (IEPOX) onto non-acidified inorganic seeds. *Atmospheric Chemistry and Physics* **14**, 3497-3510 (2014). https://doi.org/10.5194/acp-14-3497-2014

160   Mohr, C. *et al.* Molecular identification of organic vapors driving atmospheric nanoparticle growth. *Nature Communications* **10** (2019). https://doi.org/10.1038/s41467-019-12473-2

161   Liu, S. *et al.* Hydrolysis of Organonitrate Functional Groups in Aerosol Particles. *Aerosol Science and Technology* **46**, 1359-1369 (2012). https://doi.org/10.1080/02786826.2012.716175

162   Lee, B. H. *et al.* An iodide-adduct high-resolution time-of-flight chemical-ionization mass spectrometer: application to atmospheric inorganic and organic compounds. *Environ Sci Technol* **48**, 6309-6317 (2014). https://doi.org/10.1021/es500362a

163   Riedel, T. P. *et al.* Heterogeneous Reactions of Isoprene-Derived Epoxides: Reaction Probabilities and Molar Secondary Organic Aerosol Yield Estimates. *Environmental Science & Technology Letters* **2**, 38-42 (2015). https://doi.org/10.1021/ez500406f

164   Iyer, S., Lopez-Hilfiker, F., Lee, B. H., Thornton, J. A. & Kurtén, T. Modeling the Detection of Organic and Inorganic Compounds Using Iodide-Based Chemical Ionization. *The Journal of Physical Chemistry A* **120**, 576-587 (2016). https://doi.org/10.1021/acs.jpca.5b09837

165   Mayhew, A. W., Edwards, P. M. & Hamilton, J. F. Daytime Isoprene Nitrates Under Changing NOx and O3. (2023). https://doi.org/10.5194/egusphere-2023-226

166   Daytime Isoprene Nitrates Under Changing NOx and O3 - Reviewer 1 Comment. (2023). https://doi.org/10.5194/egusphere-2023-226-RC1

167   Pye, H. O. *et al.* Modeling the Current and Future Roles of Particulate Organic Nitrates in the Southeastern United States. *Environ Sci Technol* **49**, 14195-14203 (2015). https://doi.org/10.1021/acs.est.5b03738

168   Williams, J. *et al.* Opposite OH reactivity and ozone cycles in the Amazon rainforest and megacity Beijing: Subversion of biospheric oxidant control by anthropogenic emissions. *Atmospheric Environment* **125**, 112-118 (2016). https://doi.org/10.1016/j.atmosenv.2015.11.007

169   Langford, B. *et al.* Seasonality of isoprene emissions and oxidation products above the remote Amazon. *Environmental Science: Atmospheres* **2**, 230-240 (2022). https://doi.org/10.1039/d1ea00057h

170   Topping, D. *et al.* UManSysProp v1.0: an online and open-source facility for molecular property prediction and atmospheric aerosol calculations. *Geoscientific Model Development* **9**, 899-914 (2016). https://doi.org/10.5281/zenodo.45143

171   Barley, M. H. & McFiggans, G. The critical assessment of vapour pressure estimation methods for use in modelling the formation of atmospheric organic aerosol. *Atmospheric Chemistry and Physics* **10**, 749-767 (2010). https://doi.org/10.5194/acp-10-749-2010

172   O'Meara, S., Booth, A. M., Barley, M. H., Topping, D. & McFiggans, G. An assessment of vapour pressure estimation methods. *Phys. Chem. Chem. Phys.* **16**, 19453-19469 (2014). https://doi.org/10.1039/c4cp00857j

173   Vereecken, L. & Nozière, B. H migration in peroxy radicals under atmospheric conditions. *Atmospheric Chemistry and Physics* **20**, 7429-7458 (2020). https://doi.org/10.5194/acp-20-7429-2020

174   Donahue, N. M., Epstein, S. A., Pandis, S. N. & Robinson, A. L. A two-dimensional volatility basis set: 1. organic-aerosol mixing thermodynamics. *Atmospheric Chemistry and Physics* **11**, 3303-3318 (2011). https://doi.org/10.5194/acp-11-3303-2011

175   Shrivastava, M. *et al.* Urban pollution greatly enhances formation of natural aerosols over the Amazon rainforest. *Nature Communications* **10** (2019). https://doi.org/10.1038/s41467-019-08909-4

176   Wei, W., Li, Y., Ren, Y., Cheng, S. & Han, L. Sensitivity of summer ozone to precursor emission change over Beijing during 2010–2015: A WRF-Chem modeling study. *Atmospheric Environment* **218** (2019). https://doi.org/10.1016/j.atmosenv.2019.116984

177   Ren, J., Hao, Y., Simayi, M., Shi, Y. & Xie, S. Spatiotemporal variation of surface ozone and its causes in Beijing, China since 2014. *Atmospheric Environment* **260** (2021). https://doi.org/10.1016/j.atmosenv.2021.118556

178   Hidy, G. M. Atmospheric Chemistry in a Box or a Bag. *Atmosphere* **10** (2019). https://doi.org/10.3390/atmos10070401

179   Charan, S. M., Huang, Y. & Seinfeld, J. H. Computational Simulation of Secondary Organic Aerosol Formation in Laboratory Chambers. *Chem Rev* **119**, 11912-11944 (2019). https://doi.org/10.1021/acs.chemrev.9b00358

180   Zhang, X. *et al.* Influence of vapor wall loss in laboratory chambers on yields of secondary organic aerosol. *Proc Natl Acad Sci U S A* **111**, 5802-5807 (2014). https://doi.org/10.1073/pnas.1404727111

181   Matsunaga, A. & Ziemann ‡, P. J. Gas-Wall Partitioning of Organic Compounds in a Teflon Film Chamber and Potential Effects on Reaction Product and Aerosol Yield Measurements. *Aerosol Science and Technology* **44**, 881-892 (2010). https://doi.org/10.1080/02786826.2010.501044

182   Chu, B. *et al.* Application of smog chambers in atmospheric process studies. *National Science Review* **9** (2022). https://doi.org/10.1093/nsr/nwab103

183   Trump, E. R., Epstein, S. A., Riipinen, I. & Donahue, N. M. Wall effects in smog chamber experiments: A model study. *Aerosol Science and Technology* **50**, 1180-1200 (2016). https://doi.org/10.1080/02786826.2016.1232858

184   Chen, T. *et al.* Differences of the oxidation process and secondary organic aerosol formation at low and high precursor concentrations. *Journal of Environmental Sciences* **79**, 256-263 (2019). https://doi.org/10.1016/j.jes.2018.11.011

185   Crounse, J. D., Paulot, F., Kjaergaard, H. G. & Wennberg, P. O. Peroxy radical isomerization in the oxidation of isoprene. *Physical Chemistry Chemical Physics* **13**, 13607 (2011). https://doi.org/10.1039/c1cp21330j

186   Chen, Y. *et al.* Effect of NO2 on nocturnal chemistry of isoprene: Gaseous oxygenated products and secondary organic aerosol formation. *Sci Total Environ* **842**, 156908 (2022). https://doi.org/10.1016/j.scitotenv.2022.156908

187   Munoz, A., Borras, E., Rodenas, M., Vera, T. & Pedersen, H. A. Atmospheric Oxidation of a Thiocarbamate Herbicide Used in Winter Cereals. *Environmental Science & Technology* **52**, 9136-9144 (2018). https://doi.org/10.1021/acs.est.8b02157

188   Becker, K. H. *Design and Technical Development of the European Photoreactor and First Experimental Results, Final Report of the EC-Project (EV5V-CT92-0059).* (1996).

189   Zádor, J., Turányi, T., Wirtz, K. & Pilling, M. J. Measurement and investigation of chamber radical sources in the European Photoreactor (EUPHORE). *Journal of Atmospheric Chemistry* **55**, 147-166 (2006). https://doi.org/10.1007/s10874-006-9033-y

190   Bloss, W. J. *et al.* Validation of the calibration of a laser-induced fluorescence instrument for the measurement of OH radicals in the atmosphere. *Atmospheric Chemistry and Physics* **4**, 571-583 (2004). https://doi.org/10.5194/acp-4-571-2004

191   Vivanco, M. G. *et al.* SOA formation in a photoreactor from a mixture of organic gases and HONO for different experimental conditions. *Atmospheric Environment* **45**, 708-715 (2011). https://doi.org/10.1016/j.atmosenv.2010.09.059

192   Lee, B. H. *et al.* An Iodide-Adduct High-Resolution Time-of-Flight Chemical-Ionization Mass Spectrometer: Application to Atmospheric Inorganic and Organic Compounds. *Environmental Science & Technology* **48**, 6309-6317 (2014). https://doi.org/10.1021/es500362a

193 Rattanavaraha, W. *et al.* Assessing the impact of anthropogenic pollution on isoprene-derived secondary organic aerosol formation in PM2.5 collected from the Birmingham, Alabama, ground site during the 2013 Southern Oxidant and Aerosol Study. *Atmospheric Chemistry and Physics* **16**, 4897-4914 (2016). https://doi.org/10.5194/acp-16-4897-2016

194 Seckmeyer, G., Erb, R. & Albold, A. Transmittance of a cloud is wavelength-dependent in the UV-range. *Geophys. Res. Lett.* **23**, 2753-2755 (1996). https://doi.org/10.1029/96GL02614

195 Dewald, P. *et al.* Evolution of NO3 reactivity during the oxidation of isoprene. *Atmospheric Chemistry and Physics* **20**, 10459-10475 (2020). https://doi.org/10.5194/acp-20-10459-2020

196 Kiendler-Scharr, A. *et al.* New particle formation in forests inhibited by isoprene emissions. *Nature* **461**, 381-384 (2009). https://doi.org/10.1038/nature08292

197 Lee, S. H. *et al.* Isoprene suppression of new particle formation: Potential mechanisms and implications. *Journal of Geophysical Research: Atmospheres* **121**, 14,621-614,635 (2016). https://doi.org/10.1002/2016jd024844

198 Kanawade, V. P. *et al.* Isoprene suppression of new particle formation in a mixed deciduous forest. *Atmospheric Chemistry and Physics* **11**, 6013-6027 (2011). https://doi.org/10.5194/acp-11-6013-2011

199 Kiendler-Scharr, A. *et al.* Isoprene in poplar emissions: effects on new particle formation and OH concentrations. *Atmospheric Chemistry and Physics* **12**, 1021-1030 (2012). https://doi.org/10.5194/acp-12-1021-2012

200 McFiggans, G. *et al.* Secondary organic aerosol reduced by mixture of atmospheric vapours. *Nature* **565**, 587-593 (2019). https://doi.org/10.1038/s41586-018-0871-y

201 Heinritzi, M. *et al.* Molecular understanding of the suppression of new-particle formation by isoprene. *Atmospheric Chemistry and Physics* **20**, 11809-11821 (2020). https://doi.org/10.5194/acp-20-11809-2020

202 Wang, S. *et al.* Organic Peroxides in Aerosol: Key Reactive Intermediates for Multiphase Processes in the Atmosphere. *Chemical Reviews* (2023). https://doi.org/10.1021/acs.chemrev.2c00430

203 Guo, Y. *et al.* Seasonal variation in oxygenated organic molecules in urban Beijing and their contribution to secondary organic aerosol. *Atmospheric Chemistry and Physics* **22**, 10077-10097 (2022). https://doi.org/10.5194/acp-22-10077-2022

204 Brean, J. *et al.* Molecular insights into new particle formation in Barcelona, Spain. *Atmospheric Chemistry and Physics* **20**, 10029-10045 (2020). https://doi.org/10.5194/acp-20-10029-2020

205 Lyu, X. P., Guo, H., Cheng, H. R. & Wang, D. W. New particle formation and growth at a suburban site and a background site in Hong Kong. *Chemosphere* **193**, 664-674 (2018). https://doi.org/10.1016/j.chemosphere.2017.11.060

206 Glicker, H. S. *et al.* Chemical composition of ultrafine aerosol particles in central Amazonia during the wet season. *Atmospheric Chemistry and Physics* **19**, 13053-13066 (2019). https://doi.org/10.5194/acp-19-13053-2019

207 Bryant, D. J. *et al.* Strong anthropogenic control of secondary organic aerosol formation from isoprene in Beijing. *Atmospheric Chemistry and Physics* **20**, 7531-7552 (2020). https://doi.org/10.5194/acp-20-7531-2020

208 Li, C. *et al.* Laboratory Insights into the Diel Cycle of Optical and Chemical Transformations of Biomass Burning Brown Carbon Aerosols. *Environmental Science & Technology* **54**, 11827-11837 (2020). https://doi.org/10.1021/acs.est.0c04310

209 Romonosky, D. E. *et al.* Absorption spectra and aqueous photochemistry of β-hydroxyalkyl nitrates of atmospheric interest. *Molecular Physics* **113**, 2179-2190 (2015). https://doi.org/10.1080/00268976.2015.1017020

210 González-Sánchez, J. M. *et al. On the importance of multiphase photolysis of organic nitrates on their global atmospheric removal* (Copernicus GmbH, 2023).

211 Romonosky, D. E., Laskin, A., Laskin, J. & Nizkorodov, S. A. High-Resolution Mass Spectrometry and Molecular Characterization of Aqueous Photochemistry Products of

Common Types of Secondary Organic Aerosols. *The Journal of Physical Chemistry A* **119**, 2594-2606 (2015). https://doi.org/10.1021/jp509476r

212   Nguyen, T. B., Laskin, A., Laskin, J. & Nizkorodov, S. A. Direct aqueous photochemistry of isoprene high-NOx secondary organic aerosol. *Physical Chemistry Chemical Physics* **14**, 9702 (2012). https://doi.org/10.1039/c2cp40944e

213   Hu, K. S., Darer, A. I. & Elrod, M. J. Thermodynamics and kinetics of the hydrolysis of atmospherically relevant organonitrates and organosulfates. *Atmospheric Chemistry and Physics* **11**, 8307-8320 (2011). https://doi.org/10.5194/acp-11-8307-2011

214   Bräuer, P. *et al.* Development of a protocol for the auto-generation of explicit aqueous-phase oxidation schemes of organic compounds. *Atmospheric Chemistry and Physics* **19**, 9209-9239 (2019). https://doi.org/10.5194/acp-19-9209-2019

215   Iraci, L. T., Riffel, B. G., Robinson, C. B., Michelsen, R. R. & Stephenson, R. M. The acid catalyzed nitration of methanol: formation of methyl nitrate via aerosol chemistry. *Journal of Atmospheric Chemistry* **58**, 253-266 (2007). https://doi.org/10.1007/s10874-007-9091-9

216   Kuchurov, I. V., Zharkov, M. N., Fershtat, L. L., Makhova, N. N. & Zlotin, S. G. Prospective Symbiosis of Green Chemistry and Energetic Materials. *ChemSusChem* **10**, 3914-3946 (2017). https://doi.org/10.1002/cssc.201701053

217   An, J. *et al.* Practical catalytic nitration directly with commercial nitric acid for the preparation of aliphatic nitroesters. *Organic & Biomolecular Chemistry* **18**, 6612-6616 (2020). https://doi.org/10.1039/d0ob01519a

218   Shen, J., Zhao, Y., Chen, G. & Yuan, Q. Investigation of Nitration Processes of iso-Octanol with Mixed Acid in a Microreactor. *Chinese Journal of Chemical Engineering* **17**, 412-418 (2009). https://doi.org/10.1016/S1004-9541(08)60225-6

219   Liu, Y., Kuwata, M., McKinney, K. A. & Martin, S. T. Uptake and release of gaseous species accompanying the reactions of isoprene photo-oxidation products with sulfate particles. *Phys Chem Chem Phys* **18**, 1595-1600 (2016). https://doi.org/10.1039/c5cp04551g

220   Li, H., Chen, Z., Huang, L. & Huang, D. Organic peroxides' gas-particle partitioning and rapid heterogeneous decomposition on secondary organic aerosol. *Atmospheric Chemistry and Physics* **16**, 1837-1848 (2016). https://doi.org/10.5194/acp-16-1837-2016

221   Jang, M., Czoschke, N. M., Lee, S. & Kamens, R. M. Heterogeneous Atmospheric Aerosol Production by Acid-Catalyzed Particle-Phase Reactions. *Science* **298**, 814-817 (2002). https://doi.org/10.1126/science.1075798

222   Bryant, D. J. *et al.* Overcoming the lack of authentic standards for the quantification of biogenic secondary organic aerosol markers. *Environmental Science: Atmospheres* (2023). https://doi.org/10.1039/d2ea00074a

223   Mayhew, A. W., Topping, D. O. & Hamilton, J. F. New Approach Combining Molecular Fingerprints and Machine Learning to Estimate Relative Ionization Efficiency in Electrospray Ionization. *ACS Omega* **5**, 9510-9516 (2020). https://doi.org/10.1021/acsomega.0c00732

224   Wang, Y., Ren, J., Huang, X. H. H., Tong, R. & Yu, J. Z. Synthesis of Four Monoterpene-Derived Organosulfates and Their Quantification in Atmospheric Aerosol Samples. *Environmental Science & Technology* **51**, 6791-6801 (2017). https://doi.org/10.1021/acs.est.7b01179

225   Nestorowicz, K. *et al.* Chemical composition of isoprene SOA under acidic and non-acidic conditions: effect of relative humidity. *Atmospheric Chemistry and Physics* **18**, 18101-18121 (2018). https://doi.org/10.5194/acp-18-18101-2018

226   Nash, D. G., Baer, T. & Johnston, M. V. Aerosol mass spectrometry: An introductory review. *International Journal of Mass Spectrometry* **258**, 2-12 (2006). https://doi.org/10.1016/j.ijms.2006.09.017

227   Draper, D. C. *et al.* Formation of Highly Oxidized Molecules from NO3 Radical Initiated Oxidation of Δ-3-Carene: A Mechanistic Study. *ACS Earth and Space Chemistry* **3**, 1460-1470 (2019). https://doi.org/10.1021/acsearthspacechem.9b00143

228   Sobanski, N., Schuladen, J., Schuster, G., Lelieveld, J. & Crowley, J. N. A five-channel cavity ring-down spectrometer for the detection of NO$_2$, NO$_3$, N$_2$O$_5$, total peroxy nitrates and total

alkyl nitrates. *Atmospheric Measurement Techniques* **9**, 5103-5118 (2016). https://doi.org/10.5194/amt-9-5103-2016

229   Liebmann, J. M. *et al.* Measurement of ambient NO3 reactivity: design, characterization and first deployment of a new instrument. *Atmospheric Measurement Techniques* **10**, 1241-1258 (2017). https://doi.org/10.5194/amt-10-1241-2017

230   Wang, D. *et al.* Diode laser cavity ring-down spectroscopy for in situ measurement of NO3 radical in ambient air. *Journal of Quantitative Spectroscopy and Radiative Transfer* **166**, 23-29 (2015). https://doi.org/10.1016/j.jqsrt.2015.07.005